THE IMPACT OF MIXING OVER TOPOGRAPHY ON PLANKTON DYNAMICS

Thesis submitted in accordance with the requirements of the University of Liverpool for the degree of Doctor in Philosophy

by

Charlotte E. Smith

September 2018

Department of Earth, Ocean and Ecological Sciences

University of Liverpool

Declaration of Authorship

I declare that this thesis titled, “The impact of mixing over topography on plankton dynamics” and the work presented in it are my own work. The material contained in the thesis has not been presented, nor is currently being presented, either wholly or in part, for any other degree or qualification.

Signed:

Charlotte E. Smith

September 2018

Abstract

The Impact of mixing over topography on plankton dynamics

Charlotte Smith

The subtropical oceans make up ~60% of the global ocean. They are stratified, nutrient limited environments characterised by low phytoplankton biomass dominated by picophytoplankton, and rapid recycling of carbon and nutrients in surface waters. Nutrient supply to support phytoplankton export production in these regions has been questioned for the last two decades. Recently, the RidgeMix project (JR15007) and others have observed that internal tide dissipation over the sharp topography of mid-ocean ridges enhances vertical turbulent mixing and nitrate fluxes into the photic zone compared to adjacent basins. In the ocean, higher turbulence and nutrient regimes are often associated with the dominance of larger phytoplankton. This project was based on the main hypothesis that, over the Mid-Atlantic Ridge (MAR) in the subtropical North Atlantic, there is enhanced primary production and a shift towards larger phytoplankton as a result of the enhanced supply of nutrients to the photic zone.

During RidgeMix, the size-distribution and species composition of phytoplankton were analysed using size-fractionated chlorophyll-*a* (0.2-2 µm, 2-20 µm, > 20 µm), flow cytometry (< 10 µm) and light microscopy (> 10 µm). Higher concentrations of chlorophyll-*a* in the two larger size-fractions (2-20 µm and > 20 µm) and higher abundances of picoeukaryotes (~2.9 µm) and nanoeukaryotes (~4.6 µm) were observed over the ridge. There were no changes in the abundance of > 10 µm cells (diatoms and dinoflagellates) at the chlorophyll-*a* maximum or the standing stock of particulate organic carbon (POC), over the top 500 m of the water column, which might suggest enhanced zooplankton grazing over the ridge. Zooplankton abundance, composition and biomass from 0-200 m were analysed using light microscopy, size-fractionated into 200-500 µm, 500-1000 µm, 1000-2000 µm and > 2000 µm, and analysis of wet and dry weight. Higher abundances of zooplankton were observed over the ridge compared to the adjacent basin. Larger phytoplankton cells and enhanced zooplankton grazing may ultimately result in higher POC export fluxes over the ridge with implications for the higher trophic levels of the benthic and pelagic community in these regions and global biogeochemical cycling.

Finally, three techniques for marine particle collection were compared, namely the Stand Alone Pumps, Marine Snow Catcher and Niskin bottle, during RidgeMix and in the Celtic Shelf Sea (DY026, DY029, DY033). Determination of POC, PN and lipid biomarkers showed that each method collected different quantities (concentrations) and compositions of particles, the latter varying significantly with physical conditions of stations. Consequently, how representative of the water column each sample collected is remains unresolved, but it is important that oceanographers are aware of these issues.

Acknowledgements

Firstly, I would like to thank my supervisors Claire Mahaffey, George Wolff, Jonathan Sharples and Kostas Kiriakoulakis for their continual support, supervision and guidance over the last 4 years. Your insights and feedback have helped develop and improve my quality of science.

I would like to thank my funders NERC for their financial support, without which this project would not be possible. Also, the Department for Environment, Food & Rural Affairs (Defra) who, with NERC, co-funded the SSB project. I would like to thank all those on the NERC EAO DTP for their friendship and support over the years.

A large fraction of this project would not have been possible without external collaborations. I would like to thank Glen Tarran for flow cytometry tuition at Plymouth Marine Laboratry (PML); Corrine Pebody and Sari Giering for guidance on zooplankton analysis at the National Oceanography Centre Southampton (NOC); and Callum Whyte for phytoplankton microscopy advice at the Scottish Association for Marine Science (SAMS).

In Liverpool I would like to give a huge thank you to Anu Thompson for her assistance, guidance and patience in the chemistry lab and Sabena Blackbird for analysing hundreds of my POC samples.

I would like to acknowledge all those I've been to sea with for their friendship. Thank you to all those on AMT25, we had an amazing time on- and off-ship. Thank you for keeping my spirits high. I will never forget the three days we spent on Ascension Island or the Crossing the Line Ceremony at the equator. Thank you to all those on the RidgeMix cruise. A special thank you to Jenny Jardine for analysing size-fractionated chlorophyll-*a* for me and keeping me company long into the night, you kept me sane(ish). Thank you to my bubbly cabin-mate Beth Francis, your positive attitude really inspired me. Thank you Robyn Tuerena for your help throughout both cruises and for the guidance you have given me during my PhD. Finally, I would like to acknowledge the crew and NMF for their assistance with the sampling equipment during both cruises.

To my fellow PhDs. I would like to thank all those I shared an office with over the years. Special mentions got to Mila Mateeva, Nealy Carr, Valerie Le Guennec, Dennis Tuyogon and Eugenio Ruiz. Mila I couldn't have asked for a friendlier, more informed or supportive friend. Nealy and Dennis, thank you for making me laugh, your sense of humour was always very welcome. Valerie for thinking along similar lines and being easy to talk to and Eugenio for help debugging Matlab scripts. Additional thanks go to all the people I've met outside the University over the last few years.

A final thank you goes to my family for all their encouragement and support and for making me laugh. This thesis is dedicated to them.

This study has been conducted using E.U. Copernicus Marine Service Information.

Table of Contents

List of Figures

List of Tables

1 Introduction

1.1 Background

1.1.1 Nutrient dynamics in the subtropical Atlantic Ocean

The subtropical North Atlantic is a stable oligotrophic environment, characterised by a stratified water column, a deep mixed layer and a weak net supply of nutrients to the euphotic zone due to wind-driven downwelling (Williams & Follows, 1998; Heywood et al., 2006). The limited nutrient supply leads to very low levels of phytoplankton biomass with assemblages dominated by picophytoplankton (Olson et al., 1990; Partensky et al., 1999; Marañón et al., 2000; Durand et al., 2001). In addition, phytoplankton production in the surface waters of oligotrophic gyres is thought to be supported by regenerated nutrients, i.e. the 'microbial loop' (Azam et al., 1983; Ducklow & Carlson, 1992). Large cells are relatively scarce and occur when the stable system is perturbed by seasonal and episodic mixing and horizontal transport of nutrients into the euphotic zone of the subtropical ocean (Williams & Follows, 1998; Williams et al., 2006; McGillicuddy et al., 2007).

Understanding nutrient supply to the subtropical North Atlantic is an ongoing research topic. The major sources of nutrient supply into the subtropical gyre are Ekman transfer and convection, eddy upwelling, and nitrogen fixation (Williams & Follows, 2011). However, measured supplies of nitrogen into the euphotic zone in the subtropical North Atlantic are much weaker than required to fuel the proposed primary production calculated from export production (Jenkins, 1982; Jenkins & Goldman, 1985). While the sum of nitrogen sources may be equal or close to nitrogen demand (Table 1.1) uncertainty in the accuracy of fluxes, particularly eddy upwelling, leave the budget open to debate (Jenkins & Doney, 2003).

Table 1.1 Estimates of carbon export and nitrogen sources in the Sargasso Sea. Based upon a table in Williams & Follows 2011.

Export production	**Method**	**Value** (mol N m^{-2} y^{-1})	**Reference**
	O_2 utilisation	0.48 ± 0.10	Jenkins & Wallace (1992)
		0.42 ± 0.09	Jenkins & Goldman (1985)
	O_2 production	0.46 ± 0.09	" "
		0.39 ± 0.16	Spitzer & Jenkins (1989)
		0.51 ± 0.14	" "
	^{3}He flux gauge	0.56 ± 0.16	Jenkins (1988)
Nitrogen demand	mean	0.47 ± 0.12	

Nitrogen sources	**Method**	**Value** (mol N m^{-2} y^{-1})	**Reference**
Atmospheric deposition		0.03	Knap et al. (1986)
Diapycnic diffusion	Microstructure	0.05 ± 0.01	Michaels et al. (1994)

	NO_3^- and velocity	0.05 ± 0.01	" "
Eddy upwelling	Model simulation	0.35 ± 0.10	McGillicuddy & Robinson (1997)
	Satellite data and model	0.19 ± 0.10	Mcgillicuddy. et al. (1998)
	Model simulation	< 0.05	Oschlies (2002)
Nitrogen fixation	N*	0.07	Gruber & Sarmiento (1997)
	Excess nitrate	0.02-0.08	Hansell et al. (2004)
Supply of DON	Model and *in situ* data	0.05 ± 0.02	Roussenov et al. (2006)
Nitrogen supply	Mean using low and high eddy estimates	0.43 to 0.65	

1.1.2 Observations of phytoplankton community, cell size and mixing

Phytoplankton communities can be classified into groups based on environmental conditions and productivity (Margalef, 1978; Latasa et al., 2010). Both phytoplankton size-structure and species composition change with physical forcing and nutrient availability. Cell size is a key trait in phytoplankton as many fundamental ecophysiological processes are directly related to cell size (Acevedo-Trejos et al., 2013). Cell size influences resource acquisition and storage, metabolic rate, maximum growth rate, sinking rate (Stokes Law) and grazing susceptibility (Finkel et al., 2016). In general, nutrient-poor, highly stratified waters are dominated by small cells that have low sinking rates and an intrinsic advantage to nutrient uptake. Nutrient-rich waters tend to be dominated by larger cells and associated with rapid growth and high biomass (Margalef, 1978; Chisholm, 1992; Cullen et al., 2002; Irwin et al., 2006; Sharples et al., 2009). Upon nutrient addition larger cells may bloom due to the lag in growth of their larger predators (mesozooplankton, 200- 2000 µm), whereas smaller cells are limited by their grazers (microzooplankton, 20-200 µm) which have similar growth rates (Azam et al., 1983; Rassoulzadegan, 1993; Legendre & Rassoulzadegan, 1995; Legendre & Rivkin, 2002; Acevedo-Trejos et al., 2015; Finkel et al., 2016).

As the subtropical ocean's oligotrophic surface waters are dominated by small cells, nutrient addition can initiate a large response in the phytoplankton community. In the subtropical North Pacific gyre the addition of nutrient-rich deep seawater to the nutrient-limited surface waters saw an 18-fold increase in chlorophyll-*a* and a shift away from a small-cell community dominated by *Prochlorooccus* towards a community with a higher proportion of larger cells – dominated by diatoms and *Synechococcus* (Mahaffey et al., 2012). Diatoms in particular, are associated with highly turbulent and nutrient-rich environments (Margalef, 1978). During an eddy-driven nutrient upwelling event, McGuillicuddy *et* al., (2007) saw a shift towards a diatom dominated community where diatom concentrations were estimated to be 4 to 5x the background concentrations.

Increased turbulent mixing due to breaking of the internal tide on the shelf edge in the Celtic Sea has been associated with a stronger nitrate flux into the base of the thermocline and larger phytoplankton cells (Sharples et al., 2009). Sharples *et al*. (2009) found no increase in phytoplankton biomass at the shelf edge but a larger proportion of biomass in larger cells. On-shelf at intermediate nitrate fluxes higher abundances of small eukaryotes (picoeukaryotes) were observed in the thermocline. Sharples *et al*. suggest internal tide impact on phytoplankton community size structure could be an underlying reason behind spawning fish distribution along the shelf edge.

1.1.3 Why do we care about phytoplankton community structure?

Phytoplankton are the base of the food chain that supports the microbial loop and the marine food web. The microbial loop is the consumption of phytoplankton by bacteria and conversion of particulate organic carbon (POC) into dissolved organic carbon (DOC). Bacteria are thought to consume the equivalent of up to 50% of phytoplankton carbon daily (Azam et al., 1983; Ducklow & Carlson, 1992; Caron et al., 1995).

Phytoplankton are also food for higher trophic levels where the traditional view is that they are consumed by zooplankton (e.g. copepods and krill) which are consumed by larger fish and animals (Pomeroy, 1974). Zooplankton are made up of a diverse range of herbivorous, omnivorous and carnivorous species (Castellani & Edwards, 2017). Microzooplankton (20-200 μm), key grazers of small phytoplankton, are involved in the microbial loop and rapid cycling of carbon. Mesozooplankton (200-2000 μm) graze on larger phytoplankton and microzooplankton and are associated with increased export of particulate organic material and transfer to higher trophic levels (Pomeroy, 1974; Azam et al., 1983; Irwin et al., 2006; Finkel et al., 2010). Phytoplankton and zooplankton production both support fish production, despite plasticity in trophic interactions. Annual fishery yields in the north-east Pacific and north-west Atlantic are observed to be strongly correlated ($R^2 > 0.69$) with annual mean chlorophyll-*a* concentration (Ware & Thomson, 2005; Frank et al., 2006).

Phytoplankton community structure also plays a large role in the export of POC to the deep ocean. The transfer of POC to depth via living cells, their remains and associated organic compounds is important for global biogeochemical cycles and the climate system (De La Rocha & Passow, 2007). Larger cells and phytoplankton that contain biominerals such as opal and calcium carbonate are denser, so sink faster through the water column contributing substantially to carbon export, particularly following blooms (De La Rocha & Passow, 2007; Turner, 2015). The grazing and repackaging of larger phytoplankton by zooplankton into dense faecal pellets, which rapidly sink out of the euphotic zone, along with transport of

organic matter to depth by diel vertical migration play a major role in carbon export, along with sinking of marine aggregates (marine snow) and phytodetritus (Turner, 2002, 2015).

Phytoplankton proliferation is beneficial for commercial fisheries. However, in some cases phytoplankton blooms can have a negative impact associated with harmful algal blooms (HABs). This negative bloom impact can be by one of three mechanisms 1) phytoplankton densities result in oxygen depletion zones that kill fish and other animals 2) phytoplankton species produce harmful toxins that pass through the food-chain to fish, animals and humans 3) phytoplankton species damage and block the gills of fish, starving them of oxygen (Hallegraeff, 2004).

1.1.4 The Mid-Ocean Ridge and other areas of abrupt topography enhance local mixing

The Mid-Ocean Ridge is an interconnected mountain chain system which runs along the tectonic plate boundaries along the sea floor (Figure 1.1a). The section in the Atlantic Ocean, the Mid-Atlantic ridge, rises 2-3 km from the seafloor and travels for ~16,000 km. Away from ocean boundary currents and located in the middle of ocean basins, mid-ocean ridges receive most energy from the tide (Figure 1.1b). Internal tide dissipation against the sharp topography of ocean ridges has been observed to enhance vertical turbulent mixing (Polzin et al., 1997; Waterhouse et al., 2014), a process that has been observed globally across topographic features including seamounts and the continental shelf edge (Rippeth et al., 2005; Sharples et al., 2009; Bashmachnikov et al., 2013; Waterman et al., 2013; Waterman, 2014). During RidgeMix, Vic *et al.*, observed concentrated internal tide energy, that was available for diapycnal mixing, over the Mid-Atlantic Ridge (Vic et al., 2018). At the shelf edge during the summer in the Celtic Sea, a time period when the shelf seas are stratified like the open ocean, the internal tide causes mixing in the thermocline, driving nutrient supply to the surface waters and altering the local ecosystem (Sharples et al., 2001, 2009; Rippeth et al., 2005).

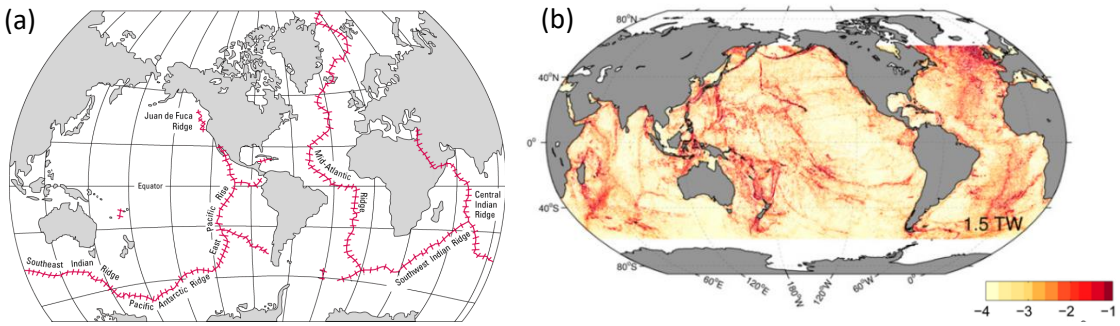

Figure 1.1 (a) Global distribution of mid-ocean ridges (USGS, 1999). *(b) Internal wave generation by the tides ($log_{10}(W\ m^{-2})$), figure 2a from Waterhouse et al., 2014.*

The role of the Mid-Atlantic Ridge in enhancing biomass and diversity has been questioned before. In 2013, Priede *et al*. used satellite images to measure primary production and particle export over the ridge. They observed no differences over the ridge, but this may be due to the depth limitations of satellite observations which can only look at the top ~30 m. In the subtropical Atlantic gyre, phytoplankton are present down to the deep chlorophyll-*a* maximum (DCM) at 67 to 126 m depth (Pérez et al., 2006) – beyond the reach of satellite sensors.

Recent observations from 36°N in the Atlantic Ocean have shown evidence for enhanced vertical mixing as well as dissolved organic carbon drawdown over the Mid-Atlantic ridge (Figure 1.2). In light of these observations it has been hypothesised that physical mixing over topography, specifically over the Mid-Atlantic Ridge, may be an important yet overlooked nutrient supply mechanism in the subtropical North Atlantic gyre. This hypothesis was tested during a 3-year NERC funded project called Ridgemix. The project, which started in 2015, set out to quantify the mechanism through measurements of physical mixing (turbulence), nutrient fluxes (nitrate) and dissolved organic carbon. The fieldwork associated with the Ridgemix project formed the basis of the research carried out for this thesis.

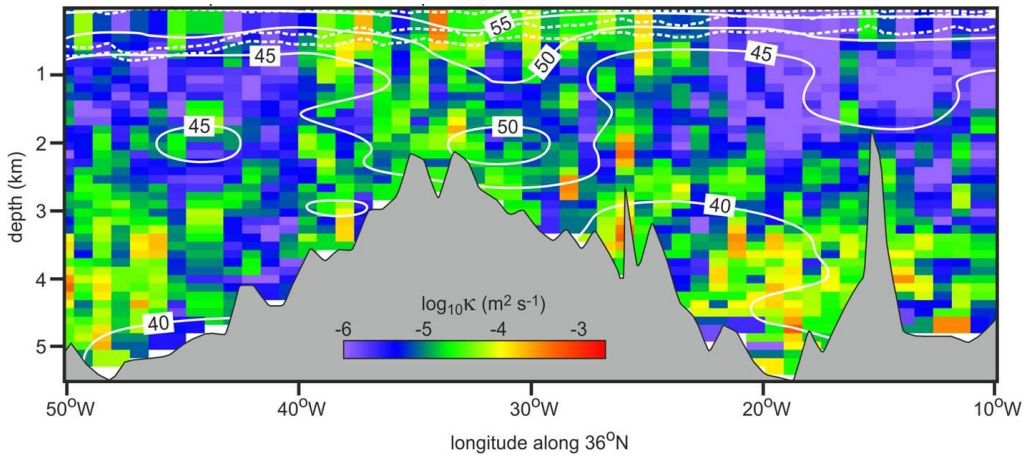

Figure 1.2 Vertical eddy diffusivity (κ, colours) and dissolved organic carbon (DOC, µM, solid line contours) along 36°N in the Atlantic. Source: RidgeMix Proposal.

1.2 Aims and hypotheses

It is suspected that the implications of a nutrient supply mechanism over the Mid-Atlantic ridge will be widespread, affecting ecosystem components and nutrient cycles. This study focuses on the local impact of enhanced mixing over the ridge on plankton community structure. The aims are to assess ridge signals in a) phytoplankton cell size structure and

community composition b) particulate organic material biomass and composition and c) zooplankton size-structure, composition and biomass. Stations and sampling are recorded in Appendix Table I.I.

The hypotheses tested are:

H1) Vertical turbulent mixing enhances nutrient fluxes over the Mid-Atlantic Ridge and is associated with increased local phytoplankton biomass.

H2) Over the site of enhanced nutrient fluxes over the Mid-Atlantic Ridge, the phytoplankton community shifts from a small-cell to a large-cell dominated community, characterised by diatoms.

H3) There is higher zooplankton abundance and biomass over the Mid-Atlantic Ridge.

H4) A larger standing stock of particulate organic carbon is found over the Mid-Atlantic Ridge.

1.3 Thesis structure

This thesis is split into three sections. Chapter 2 is a comparison of three marine particle collection techniques (Niskin bottles, the Marine Snow Catcher, and Stand-Alone Pumps) in terms of the quantity and composition of particles collected. Chapter 3 is an analysis of the controls on phytoplankton dynamics and the influence of abrupt topography in the subtropical North Atlantic. Chapter 4 is an assessment of suspended marine particles and zooplankton dynamics, and the influence of abrupt topography in the subtropical North Atlantic. The major findings, wider implications and suggestions for future research are presented in the Chapter 5, the synthesis.

1.4 References

Acevedo-Trejos, E., Brandt, G., Bruggeman, J., & Merico, A. (2015). Mechanisms shaping size structure and functional diversity of phytoplankton communities in the ocean. *Scientific Reports*, *5*(8918). https://doi.org/10.1038/srep08918

Acevedo-Trejos, E., Brandt, G., Merico, A., & Smith, S. L. (2013). Biogeographical patterns of phytoplankton community size structure in the oceans. *Global Ecology and Biogeography*, *22*(9), 1060–1070. https://doi.org/10.1111/geb.12071

Azam, F., Fenchel, T., Field, J., Gray, J., Meyer-Reil, L., & Thingstad, F. (1983). The Ecological Role of Water-Column Microbes in the Sea. *Marine Ecology Progress Series*, *10*, 257–263. https://doi.org/10.3354/meps010257

Bashmachnikov, I., Loureiro, C. M., & Martins, A. (2013). Topographically induced circulation patterns and mixing over Condor seamount. *Deep Sea Research Part II: Topical Studies in Oceanography*, *98*, 38–51. https://doi.org/10.1016/j.dsr2.2013.09.014

Caron, D. A., Dam, H. G., Kremer, P., Lessard, E. J., Madin, L. P., Malone, T. C., … Youngbluth, M. J. (1995). The contribution of microorganisms to particulate carbon and nitrogen in surface waters of the Sargasso Sea near Bermuda. *Deep-Sea Research Part I*, *42*(6), 943–972. https://doi.org/10.1016/0967-0637(95)00027-4

Castellani, C., & Edwards, M. (Eds.). (2017). *Marine Plankton: A Practical Guide to Ecology, Methodology, and Taxonomy* (1st ed.). Oxford: Oxford University Press.

Chisholm, S. W. (1992). What limits phytoplankton growth? *Oceanus*, *35*(3), 36–46.

Cullen, J. J., Franks, P. J. S., Karl, D. M., & Longhurst, A. (2002). Physical influences on marine ecosystem dynamics. In A. R. Robinson, J. J. McCarthy, & B. J. Rothschild (Eds.), *The Sea* (Vol. 12, pp. 297–336). New York: John Wiley and Sons Inc.

De La Rocha, C. L., & Passow, U. (2007). Factors influencing the sinking of POC and the efficiency of the biological carbon pump. *Deep-Sea Research Part II: Topical Studies in Oceanography*, *54*, 639–658. https://doi.org/10.1016/j.dsr2.2007.01.004

Ducklow, H. W., & Carlson, C. A. (1992). Oceanic Bacterial Production. In K. C. Marshal (Ed.), *Advances in Microbial Ecology: Volume 12* (pp. 113–181). New York: Plenum Press. https://doi.org/10.1007/978-1-4684-7609-5_3

Durand, M. D., Olson, R. J., & Chisholm, S. W. (2001). Phytoplankton population dynamics at the Bermuda Atlantic Time-series station in the Sargasso Sea. *Deep-Sea Research Part II: Topical Studies in Oceanography*, *48*(8–9), 1983–2003. https://doi.org/10.1016/S0967-0645(00)00166-1

Finkel, Z. V., Beardall, J., Flynn, K. J., Quigg, A., Rees, T. A. V, & Raven, J. A. (2010). Phytoplankton in a changing world: Cell size and elemental stoichiometry. *Journal of Plankton Research*, *32*(1), 119–137. https://doi.org/10.1093/plankt/fbp098

Finkel, Z. V., Follows, M. J., & Irwin, A. J. (2016). Size-scaling of macromolecules and chemical energy content in the eukaryotic microalgae. *Journal of Plankton Research*, *38*(5), 1151–1162. https://doi.org/10.1093/plankt/fbw057

Frank, K. T., Petrie, B., Shackell, N. L., & Choi, J. S. (2006). Reconciling differences in trophic control in mid-latitude marine ecosystems. *Ecology Letters*, *9*(10), 1096–1105. https://doi.org/10.1111/j.1461-0248.2006.00961.x

Gruber, N., & Sarmiento, J. L. (1997). Global patterns of marine nitrogen fixation and denitrification. *Global Biogeochemical Cycles*. https://doi.org/10.1029/97GB00077

Hallegraeff, G. M. (2004). Harmful algal blooms: a global overview. In G. M. Hallegraeff, D. M. Anderson, & A. D. Cembella (Eds.), *Manual on Harmful Marine Microalgae* (2nd ed., pp.

25–50). Paris: UNESCO Publishing. Retrieved from http://unesdoc.unesco.org/images/0013/001317/131711e.pdf

Hansell, D. A., Bates, N. R., & Olson, D. B. (2004). Excess nitrate and nitrogen fixation in the North Atlantic Ocean. *Marine Chemistry*. https://doi.org/10.1016/j.marchem.2003.08.004

Heywood, J. L., Zubkov, M. V., Tarran, G. A., Fuchs, B. M., & Holligan, P. M. (2006). Prokaryoplankton standing stocks in oligotrophic gyre and equatorial provinces of the Atlantic Ocean: Evaluation of inter-annual variability. *Deep Sea Research Part II: Topical Studies in Oceanography*, *53*(14–16), 1530–1547. https://doi.org/10.1016/j.dsr2.2006.05.005

Irwin, A. J., Finkel, Z. V., Schofield, O. M. E., & Falkowski, P. G. (2006). Scaling-up from nutrient physiology to the size-structure of phytoplankton communities. *Journal of Plankton Research*, *28*(5), 459–471. https://doi.org/10.1093/plankt/fbi148

Jenkins, W. J. (1982). Oxygen utilization rates in North Atlantic subtropical gyre and primary production in oligotrophic systems. *Nature*, *300*, 246–248. Retrieved from http://scholar.google.com/scholar?hl=en&btnG=Search&q=intitle:No+Title#0

Jenkins, W. J. (1988). Nitrate flux into the euphotic zone near Bermuda. *Nature*, *331*, 521–523.

Jenkins, W. J., & Doney, S. C. (2003). The subtropical nutrient spiral. *Global Biogeochemical Cycles*, *17*(4), n/a-n/a. https://doi.org/10.1029/2003GB002085

Jenkins, W. J., & Goldman, J. C. (1985). Seasonal oxygen cycling and primary production in the Sargasso Sea. *Journal of Marine Research*, *43*(2), 465–491. https://doi.org/10.1357/002224085788438702

Jenkins, W. J., & Wallace, D. W. R. (1992). *Tracer Based Inferences of New Primary Production in teh Sea*. (P. G. Falkowski, A. D. Woodhead, & K. Vivirito, Eds.). Boston, MA: Springer US. https://doi.org/10.1007/978-1-4899-0762-2

Knap, A., Jickells, T., Pszenny, A., & Galloway, J. (1986). Significance of atmospheric-derived fixed nitrogen on productivity of the Sargasso Sea. *Nature*, *320*(6058), 158–160. https://doi.org/10.1038/320158a0

Latasa, M., Scharek, R., Vidal, M., Vila-Reixach, G., Gutiérrez-Rodríguez, A., Emelianov, M., & Gasol, J. M. (2010). Preferences of phytoplankton groups for waters of different trophic status in the northwestern Mediterranean sea. *Marine Ecology Progress Series*, *407*, 27–42. https://doi.org/10.3354/meps08559

Legendre, L., & Rassoulzadegan, F. (1995). Plankton and nutrient dynamics in marine waters. *Ophelia*, 41(1), 153-172.

Legendre, L., & Rivkin, R. B. (2002). Fluxes of carbon in the upper ocean: Regulation by food-web control nodes. *Marine Ecology Progress Series*, *242*, 95–109. https://doi.org/10.3354/meps242095

Mahaffey, C., Björkman, K., & Karl, D. (2012). Phytoplankton response to deep seawater nutrient addition in the North Pacific Subtropical Gyre. *Marine Ecology Progress Series*, *460*, 13–34. https://doi.org/10.3354/meps09699

Marañón, E., Holligan, P. M., Varela, M., Mouriño, B., & Bale, A. J. (2000). Basin-scale variability of phytoplankton biomass, production and growth in the Atlantic Ocean. *Deep Sea Research Part I: Oceanographic Research Papers*, *47*(5), 825–857. https://doi.org/10.1016/S0967-0637(99)00087-4

Margalef, R. (1978). Life-forms of phytoplankton as survival alternatives in an unstable environment. *Oceanologica Acta*, *1*, 493–509. https://doi.org/10.1007/BF00202661

Mcgillicuddy., D. J., Johnsonk, R., & Knapk, A. H. (1998). New Evidence for the impact of

mesoscale eddies on biogeochemical cycling in the Sargasso Seain the Sargasso Sea. *Nature*, *394*(1977), 263–266. https://doi.org/10.1038/28367

McGillicuddy, D. J., Anderson, L. a, Bates, N. R., Bibby, T., Buesseler, K. O., Carlson, C. a, … Steinberg, D. K. (2007). Eddy/wind interactions stimulate extraordinary mid-ocean plankton blooms. *Science*, *316*(5827), 1021–1026. https://doi.org/10.1126/science.1136256

McGillicuddy, D. J., & Robinson, A. R. (1997). Eddy-induced nutrient supply and new production in the Sargasso Sea. *Deep-Sea Research Part I: Oceanographic Research Papers*, *44*(8), 1427–1450. https://doi.org/10.1016/S0967-0637(97)00024-1

Michaels, A. F., Knap, A. H., Dow, R. L., Gundersen, K., Johnson, R. J., Sorensen, J., … Bidigare, R. (1994). Seasonal patterns of ocean biogeochemistry at the U.S. JGOFS Bermuda Atlantic time-series study site. *Deep Sea Research Part I: Oceanographic Research Papers*, *41*(7), 1013–1038. https://doi.org/10.1016/0967-0637(94)90016-7

Olson, R. J., Chisholm, S. W., Zettler, E. R., Altabet, M. A., & Dusenberry, J. A. (1990). Spatial and temporal distributions of prochlorophyte picoplankton in the North Atlantic Ocean. *Deep Sea Research*, *37*(6), 1033–1051. https://doi.org/10.1016/0198-0149(90)90109-9

Oschlies, A. (2002). Nutrient supply to the surface waters of the North Atlantic: A model study. *Journal of Geophysical Research*. https://doi.org/10.1029/2000JC000275

Partensky, F., Blanchot, J., & Vaulot, D. (1999). Differential distribution and ecology of Prochlorococcus and Synechococcus in oceanic waters : a review. *Bulletin de l'Institut Océanographique - Special Issue: Marine Cyanobacteria*, *19*, 457–476.

Pérez, V., Fernández, E., Marañón, E., Morán, X. A. G., & Zubkov, M. V. (2006). Vertical distribution of phytoplankton biomass, production and growth in the Atlantic subtropical gyres. *Deep Sea Research Part I: Oceanographic Research Papers*, *53*(10), 1616–1634. https://doi.org/10.1016/j.dsr.2006.07.008

Polzin, K. L., Toole, J. M., Ledwell, J. R., & Schmitt, R. W. (1997). Spatial Variability of Turbulent Mixing in the Abyssal Ocean. *Science*, *276*(5309), 93–96. https://doi.org/10.1126/science.276.5309.93

Pomeroy, L. R. (1974). The Ocean's Food Web, A Changing Paradigm. *BioScience*, *24*(9), 499–504. https://doi.org/10.2307/1296885

Rassoulzadegan, F. (1993). Protozoan patterns in the Azam-Ammerman's bacteria-phytoplankton mutualism. In R. Guerrero & C. Perdos-Alio (Eds.), *Trends in microbial ecology* (pp. 435-439). Barcelona: Spanish Society for Microbiology.

Rippeth, T. P., Palmer, M. R., Simpson, J. H., Fisher, N. R., & Sharples, J. (2005). Thermocline mixing in summer stratified continental shelf seas. *Geophysical Research Letters*, *32*(5), L05602. https://doi.org/10.1029/2004GL022104

Roussenov, V., Williams, R. G., Mahaffey, C., & Wolff, G. A. (2006). Does the transport of dissolved organic nutrients affect export production in the Atlantic Ocean? *Global Biogeochemical Cycles*, *20*(3). https://doi.org/10.1029/2005GB002510

Sharples, J., Moore, C. M., Hickman, A. E., Holligan, P. M., Tweddle, J. F., Palmer, M. R., & Simpson, J. H. (2009). Internal tidal mixing as a control on continental margin ecosystems. *Geophysical Research Letters*, *36*(23). https://doi.org/10.1029/2009GL040683

Sharples, J., Moore, C. M., Rippeth, T. P., Holligan, P. M., Hydes, D. J., Fisher, N. R., & Simpson, J. H. (2001). Phytoplankton distribution and survival in the thermocline. *Limnology and Oceanography*, *46*(3), 486–496. https://doi.org/10.4319/lo.2001.46.3.0486

Spitzer, W. S., & Jenkins, W. J. (1989). Rates of vertical mixing, gas exchange and new production: Estimates from seasonal gas cycles in the upper ocean near Bermuda. *Journal*

of Marine Research. https://doi.org/10.1357/002224089785076370

Turner, J. T. (2002). Zooplankton fecal pellets, mrine snow and sinking phytoplankton blooms. *Aquatic Microbial Ecology*, *27*, 57–102. https://doi.org/Doi 10.3354/Ame027057

Turner, J. T. (2015). Zooplankton fecal pellets, marine snow, phytodetritus and the ocean's biological pump. *Progress in Oceanography*, *130*, 205–248. https://doi.org/10.1016/j.pocean.2014.08.005

USGS. (1999). Mid-ocean ridge, like baseball seam [This Dynamic Earth, USGS]. Retrieved May 1, 2015, from http://pubs.usgs.gov/gip/dynamic/baseball.html

Vic, C., Naveira Garabato, A. C., Green, J. A. M., Spingys, C., Forryan, A., Zhao, Z., … Sharples, J. (2018). The Lifecycle of Semidiurnal Internal Tides over the Northern Mid-Atlantic Ridge. *Journal of Physical Oceanography*, *48*(1), 61–80. https://doi.org/10.1175/JPO-D-17-0121.1

Ware, D. M., & Thomson, R. E. (2005). Bottom-Up ecoststem trophic dynamics determine fish production in the Northeast Pacific. *Science*, *308*(May), 1280–1284. https://doi.org/10.1126/science.1109049

Waterhouse, A. F., MacKinnon, J. A., Nash, J. D., Alford, M. H., Kunze, E., Simmons, H. L., … Lee, C. M. (2014). Global Patterns of Diapycnal Mixing from Measurements of the Turbulent Dissipation Rate. *Journal of Physical Oceanography*, *44*(7), 1854–1872. https://doi.org/10.1175/JPO-D-13-0104.1

Waterman, S. (2014). Oceans Finescale parameterizations of turbulent dissipation. *Journal of Geophysical Research: Oceans*, 1383–1419. https://doi.org/10.1002/2013JC008979.Received

Waterman, S., Naveira Garabato, A. C., & Polzin, K. L. (2013). Internal Waves and Turbulence in the Antarctic Circumpolar Current. *Journal of Physical Oceanography*, *43*(2), 259–282. https://doi.org/10.1175/JPO-D-11-0194.1

Williams, R. G., & Follows, M. J. (1998). *The Ekman transfer of nutrients and maintenance of new production over the North Atlantic*. *Deep-Sea Research I* (Vol. 45). Retrieved from http://citeseerx.ist.psu.edu/viewdoc/download?doi=10.1.1.538.8325&rep=rep1&type=pdf

Williams, R. G., & Follows, M. J. (2011). *Ocean Dynamics and the Carbon Cycle: Principles and Mechanisms*. Cambridge University Press. Retrieved from http://books.google.co.uk/books/about/Ocean_Dynamics_and_the_Carbon_Cycle.html?id=dfTJdgZg260C&pgis=1

Williams, R. G., Roussenov, V., & Follows, M. J. (2006). Nutrient streams and their induction into the mixed layer. *Global Biogeochemical Cycles*, *20*(1), n/a-n/a. https://doi.org/10.1029/2005GB002586

2 Comparison of marine particle collection techniques using elemental and lipid biomarkers

2.1 Introduction

2.1.1 Marine particles

Marine particles consist of organic and inorganic material that is suspended or sinking in the water column. The primary source of carbon fixed is the production of organic (biosynthesis) and inorganic (biomineralisation) material *de-novo* by phytoplankton. Particles can also originate from allochthonous sources, including atmospheric deposition of dust, re-suspension of sediments and river and groundwater inputs, the latter two being more important in near-coastal regions. Once produced, organic material (OM) undergoes a variety of processes in the water column that modify its size, composition and character (De La Rocha & Passow, 2007). Particles are consumed, fragmented and released by other organisms. They physically interact with each other through aggregation and disaggregation mechanisms, and are constantly influenced by the chemical composition of the surrounding water (e.g. mineral scavenging; Figure 2.1). The resulting concoction is highly heterogeneous, composed of living cells (phytoplankton, zooplankton, bacterial and viruses) but primarily their remains (phytodetritus) and associated components (marine aggregates/snow, faecal pellets, dissolved organic material; Yanada & Maita, 1995; Volkman & Tanoue, 2002; De La Rocha & Passow, 2007; Sanders et al., 2014; Turner, 2015).

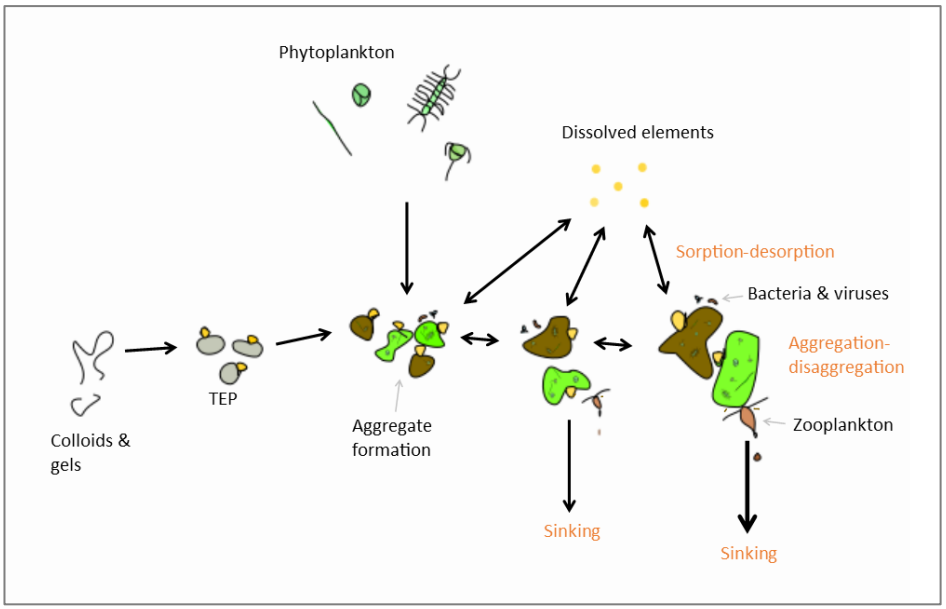

Figure 2.1 Interaction of particles in the water column. Marine aggregate formation from live and dead phytoplankton, colloids & gels and transparent exopolymer particles (TEP), and the consequent physical, chemical and biological aggregation-disaggregation of small, medium and large aggregates, and sorption-desorption of dissolved elements such as trace metals. Re-drawn and adapted figure from Jackson & Burd (2015).

OM is composed of three major classes of compound: carbohydrates, proteins and lipids (Lee et al., 2004). Carbohydrates and lipids are carbon-rich compounds that provide cell structure (membrane control) and energy-storage components. Proteins are nitrogen rich compounds responsible for structure, metabolism and cell growth. In the 1930s, the average elemental composition of marine organisms and inorganic nutrients was discovered to be globally uniform with an elemental ratio for C:N:P of 106:16:1 (Redfield, 1958). Since then many studies have investigated the ratio of C:N:P and causes for deviations from it (see Geider and Roche 2002). Recently, it was discovered that the composition of macromolecules (carbohydrates, proteins and lipids) play a large role in the stoichiometry of organic material in the ocean (Geider & Roche, 2002; Arrigo, 2005). High C:N and N:P ratios relative to the Redfield ratio, carbon-enriched material, are found where accumulation of carbohydrate and neutral lipid storage compounds occurs under nutrient limitation (Geider & Roche, 2002). Low C:N and N:P ratios relative to Redfield, nitrogen-enriched material, is associated with high protein concentrations related to high nutrients, high growth rates, and light limitation (Mei et al., 2005; Martiny et al., 2013). It is now thought that changes in C:N are due to cell phylogenetics and the relative proportions of detritus and dead phytoplankton material (Martiny et al., 2013).

2.1.2 Global significance

Marine particles are important tracers for the global nutrient and trace metal cycles in the ocean. In addition to C, N and P there are three other abundant elements that make up OM: oxygen, hydrogen, and sulphur. There are also other key nutritional elements, present in much smaller concentrations, including silica, major ions (calcium, potassium, sodium, magnesium and chloride), and trace metals (manganese, iron, cobalt, copper and zinc). The main mechanism by which these elements are transported from the surface to the deep ocean is thought to be through the sinking of particles. This process is termed the Biological Carbon Pump (BCP; Figure 2.2). The pump starts in the surface waters where phytoplankton photosynthesis transforms atmospheric CO_2 into OM using sunlight and nutrients. The fixed OM then cycles through the food web and is either exported to depth or returned to the atmosphere. The main pathways for particle export are thought to be the sinking of faecal pellets, marine aggregates and phytodetritus (Riley et al., 2012; Turner, 2015). Particle sinking velocities or transfer efficiencies are controlled by size, shape, porosity, density, permeability, mineral content, phytoplankton species and physiological cell state (Laurenceau-Cornec et al., 2015). For example, large and dense faecal pellets of repackaged phytoplankton material sink quickly and mineral ballast of certain phytoplankton species (coccolithophores and diatoms) can cause sedimentation of blooms. The global distribution of organic biomass and its composition, is thus important for understanding global nutrient, ion and trace metal cycles.

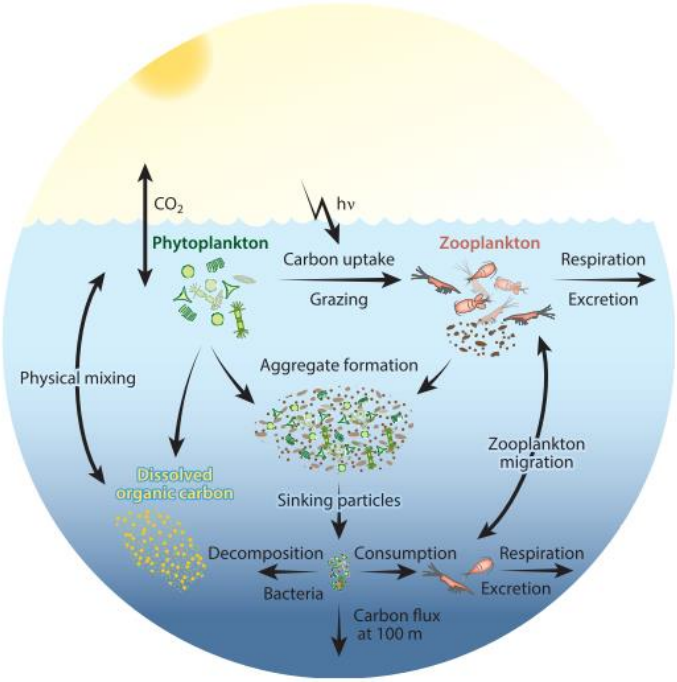

Figure 2.2 The Biological Carbon Pump (BCP). Figure 1b from Benner & Amon (2014).

The strength of the marine biological pump is set, in the surface ocean, by the biological, physical and chemical conditions which control phytoplankton growth and abundance and drive downward vertical flux of particles (Buesseler & Boyd, 2009). The biological carbon pump varies in strength. For example, at high latitudes the ocean is comparatively more dynamic than at low latitudes with higher turbulence, and nitrate concentrations which support higher rates of new production and support large phytoplankton blooms (Buesseler & Boyd, 2009). Being able to accurately collect and quantify the characteristics of marine particles in the surface ocean in different environments is therefore important for our understanding of the BCP.

2.1.3 Marine particle collection

To measure particulate OM (POM), either the bulk pool is quantified to give a concentration or the POM is characterised by analysing lipids, pigments and amino acid biomarkers or DNA. The bulk pool measurements give a biomass standing stock measurement of organic compounds (particulate organic carbon (POC): carbohydrates and lipids; particulate nitrogen (PN): proteins and amino acids). The ratio of these compounds (POC:PN) can then be used to help determine the quality and source of the material. Characterisation of the material involves either identification of major organic compound classes or quantification of specific compounds, such as hydrocarbons, hopanes, steranes and isoprenoids (Philp & Lewis, 1987). These measurements are designed to evaluate the source and function, as well as the quality and composition of organic material.

A variety of techniques can be used to collect samples for suspended material (McDonnell et al., 2015). *In-situ* filtration pumps, bottle collection (large and small volume), and underway and towed sampling systems are used for bulk pool measurements. Bottle collection, plankton nets, flow cytometry and SCUBA collection of particles >500 μm are used to characterise sub-populations of particles. Bulk pool measurements, for practical purposes, are mechanically split into material that does or does not pass through a given filter i.e. dissolved organic matter (DOM), and POM, respectively. The filter pore size used varies between 0.2 and 0.8 μm (Altabet et al., 1992; Moran et al., 1999; Volkman & Tanoue, 2002; Gardner et al., 2003; Turnewitsch et al., 2007; Liu et al., 2009; Bishop et al., 2012; Riley et al., 2012; Edwards et al., 2015; Steinberg & Landry, 2017). POM includes zooplankton, phytoplankton, bacteria, macrogels and transparent exopolymer particles (TEP) whereas, DOM includes, viruses, macromolecules, microgels and colloidal nanogels (Verdugo et al., 2004). It is important to note that it is an operational separation and that the two groups are tightly coupled through interconnected aggregation-disaggregation mechanisms (Lee et al., 2004).

Quantifying particle fluxes and processes in the ocean is important if we wish to further our understanding of cycling of C, N, P, but also minerals and trace metals. Since the first attempts at particle collection, considerable effort has been made to develop particle collection methodologies to improve their accuracy and precision (Lampitt et al., 1993; Hunter et al., 1996; Bishop & Wood, 2008; Bishop et al., 2012; Planquette & Sherrell, 2012; Riley et al., 2012; McDonnell et al., 2015). The result is the variety of different methods that are commonly used. If we wish to understand the biogeochemical roles and cycling of marine particles, it is important that we question which particles the techniques collect and with what efficiency. Having a clear understanding of whether and how this differs between methods is crucial.

Here three particle collection techniques are compared: *in-situ* pumps (Challenger Oceanic Stand Alone Pumps; SAPs), small-volume bottles (Niskin bottles, commonly referred to as the CTD or rosette) and large-volume bottles (Marine Snow Catchers; MSC). The aim is to elucidate the quantity and composition of particles collected using each technique and to infer whether they all collect the same pool of POM. Samples were analysed for POC, PN and lipid composition. Lipids are informative and stable biomarkers that impart information about the source of organic material and act as tracers of biological processes and organic matter quality (*e.g.* Parrish 2013, Table 2.1).

Table 2.1 Abundant lipid biomarkers found in the Celtic Sea and their major sources.

Lipid biomarker	Source/indicator	See references in
Polyunsaturated fatty acids		
C_{16}, C_{16} PUFA's and $C_{20:5\omega3}$	Particularly abundant in diatoms and prymnesiophytes	(Volkman et al., 1989; Dalsgaard et al., 2003; Tolosa et al., 2004; Parrish, 2013)
C_{18}, C_{18} PUFA's and $C_{22:6\omega3}$	Indicative of (dino)flagellates	(Dalsgaard et al., 2003; Tolosa et al., 2004; Volkman, 2006; Parrish, 2013)
$C_{16:4\omega3}$, $C_{18:3\omega3}$, $C_{18:2\omega3}$, $C_{18:2\omega6}$	Indicative of chlorophytes	(Dalsgaard et al., 2003)
Monounsaturated fatty acids		
$C_{16:1\omega7}$	Typical of diatoms	(Volkman et al., 1989; Dalsgaard et al., 2003; Tolosa et al., 2004; Parrish, 2013)
$C_{18:1\omega9 \text{ and } \omega11}$, $C_{20:1}$, $C_{22:1}$	Crustaceous zooplankton	(Sheridan et al., 2002; Tolosa et al., 2004)
Fatty alcohols: C_{14}, C_{16} and C_{18}	Copepod remains from carnivore feeding/microzooplankton	(Sheridan et al., 2002; Dalsgaard et al., 2003)
Branched *iso* and *anteiso* chain fatty acids and **odd chain saturated fatty acids**	Bacteria	(Sheridan et al., 2002; Dalsgaard et al., 2003; Parrish, 2013)
Sterols		
Cholesterol and Cholesta-5,22-dien-3β-ol	Zooplankton derived material	(Sheridan et al., 2002)
Brassicasterol	Diatoms. Indicative of autotrophy	(Sheridan et al., 2002)
Unsaturated fatty acids/saturated fatty acids	Indicator of the lability of OM	(Hayakawa et al., 1996)

2.2 Method

2.2.1 Study locations

Samples were collected during four cruises, three in the coastal Celtic Sea (DY026, DY029, DY033) and the subtropical North Atlantic Ocean (JR15007; Figure 2.3, Table 2.2).

Samples were collected using the three particle collection techniques during a cruise to the Celtic Sea in August 2014 (DY026, RRS Discovery), from 20 m and 60 m water depth at the Central Celtic Sea station (CCS, 150 m water depth), 50 m at the Celtic Sea 2 station (CS2, 203 m water depth), and 50 m at the Celtic Deep station (CD) (Figure 2.3). Niskin bottles were collected pre-dawn (05:00-07:30), MSC just after dawn 06:45-08:30, and SAPs throughout the day (09:00, 11:00, 14:00 and 00:00). Temperature and chlorophyll-*a* concentrations (fluorescence) were determined using sensors attached to the CTD frame mounted with Niskin bottles.

Samples collected on RRS Discovery at station CCS during cruises DY029 (April 2015) and DY033 (July 2015) were used for further comparison of the MSC and Niskin bottle. During these cruises, samples were collected at 10 m and 70 m, termed "the surface mixed layer" and

"beneath the mixed layer". During DY029 samples were collected under three different biogeochemical conditions termed "pre-bloom" (11th April), "peak-bloom" (15th April), and "post-bloom" (20th April). Niskin bottles were collected pre-dawn (01:26-02:14), and MSC in the afternoon/early evening (14:00-21:30). All samples from the Celtic Sea were collected during the *UK Shelf Sea Biogeochemistry* (SSB) research program by Clare Davis.

Samples from the oligotrophic subtropical North Atlantic (24-36°N, 32-50°W) were collected on the RRS *James Clark* Ross (JR15007, June 2016). Marine particles were collected using SAPs and Niskin bottle from three depths (the chlorophyll-*a* maximum, 100 m below the chlorophyll-*a* maximum, and 500 m) at 10 stations. Samples were collected at night (Niskin bottle between 19:00 and midnight, SAPs between 21:30 and 04:00).

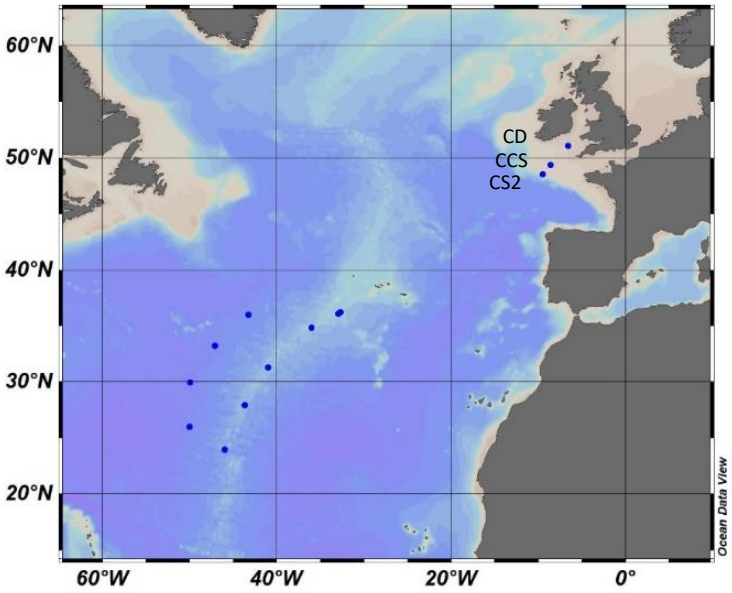

Figure 2.3 Station locations. Three stations in the European continental shelf sea (Celtic Sea): the Celtic Deep (CD), Central Celtic Sea (CCS), and Celtic Sea 2 (CS2) on the shelf edge. Ten stations in the oligotrophic subtropical North Atlantic (Sargasso Sea).

Table 2.2 Cruise details and sample collection.

Location	Cruise	Date	Technique	Analyses	Comparisons
Celtic Sea	DY026	August 2014	SAP, MSC, Niskin bottle	POC, PN, Lipids	4
	DY029	April 2015	MSC, Niskin bottle	POC, PN	6
	DY033	July 2015	MSC, Niskin bottle	POC, PN	2
Subtropical North Atlantic Ocean	JR15007	June 2016	SAP, Niskin bottle	POC, PN	33

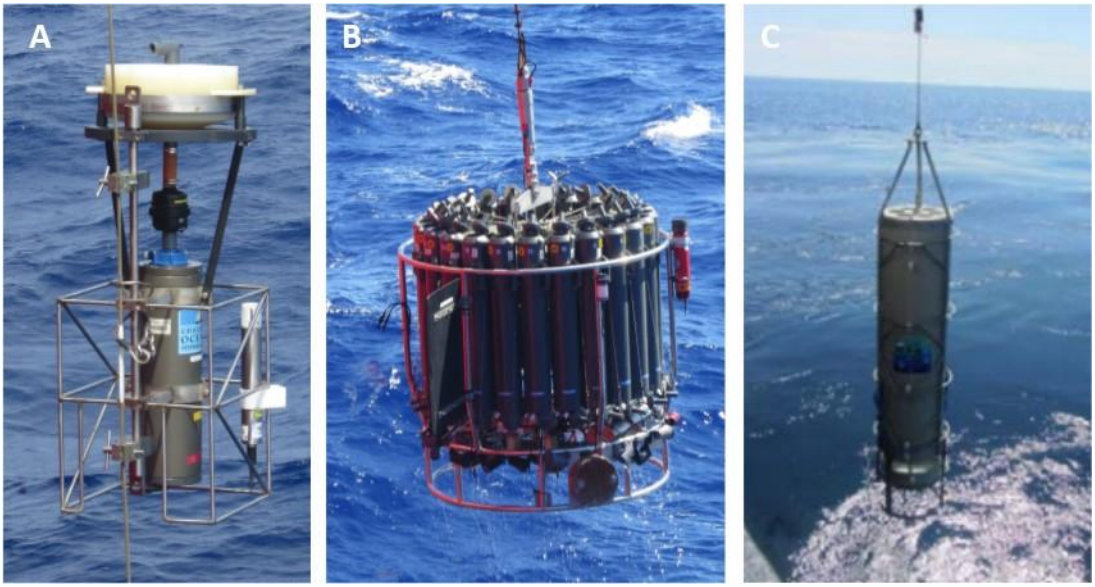

Figure 2.4 Particle collection techniques used in this study. (a) Challenger Oceanic Stand-Alone Pump (SAP). (b) 24 Niskin bottles mounted on a rosette (CTD). (c) Marine Snow Catcher (MSC). The last picture was copied from the DY026 cruise report.

2.2.2 Particle collection

2.2.2.1 Stand Alone Pumps

The Stand Alone Pump (SAP) is a large-volume *in-situ* pump that collects particles by pumping water through filters (mesh and GFF). They were initially designed to collect 'rare' marine particles. There are three models of pump: Challenger Oceanic's Stand Alone Pumps (SAPs, used in this study; Figure 2.4a), the McLane Large Volume Water Transfer System ("McLane pumps"), and the Multiple Unit Large Volume *in-situ* Filtration System (MUL-VFS). There are also a large variety of pump modifications available, which mainly involve varying filter house designs (see Bishop et al., 2012). The filter housing of the SAP can be set up to accommodate multiple filters allowing for size-fractionation. The pump is pre-programmed to start pumping once it reaches a pre-specified depth in the water column. The pump will then operate for a pre-programmed length of time, filtering hundreds to thousands of litres of water. The volume pumped depends on the particle density. Depth profiles are achieved by attaching multiple pumps onto a single wire.

Four SAPs were deployed in the Celtic Sea during DY026 and 33 SAPs were deployed in the subtropical North Atlantic during JR15007. The SAPs were set up to collect two particle size-fractions, >53 µm and 0.7-53 µm, using a 53 µm nylon mesh and stacked 0.7 µm 293 mm GFFs (Whatman, combusted 400°C, 12 h). The SAPs in the oligotrophic North Atlantic were set to pump for 90 minutes. 3/33 pumped for less (55, 57 and 79 minutes). The volume of water pumped varied between 210 and 1,290 L with an average of 974±262 L. The SAPs in the Celtic Sea were set to pump for a shorter period of 60 minutes, due to higher particulate

concentrations. The photic zone sample filtered 383 L, and those in the mixed layer filtered 480 L, 525 L and 597 L of water. Once on deck, the two stacked GFFs (sample + DOM correction) were stored in pre-combusted (400°C, 12 h) aluminium foil at -80°C. The 53 µm mesh was washed down onto a 47 mm GFF filter (Whatman, 0.7 µm pore size, combusted) using a plastic filtration rig and was stored in pre-combusted foil at -80°C.

2.2.2.2 Niskin bottles

Niskin bottles are the most universally used method of water collection for chemical analysis in oceanography (Figure 2.4b). They were introduced in 1966 as an improvement on the Nansen bottle, designed in 1894; bottles vary in size from 1-2 L, 10 L or 20 L and are usually arranged in a rosette of 12, 24 or 36 bottles on a stainless-steel frame upon which other instruments/sensors can be attached (typically conductivity, temperature and depth; CTD). The Niskin bottle operates as a cylinder with two tensioned lids that can be closed remotely via an electronic signal. For analysis, either a sub-sample is taken or the entire Niskin bottle is filtered.

During DY026, DY029 and DY033 cruises, 24 x 10 L Niskin bottles were used on a rosette on a stainless-steel frame. Sub-samples of 3 L of water were filtered using a plastic filtration rig through 0.7 µm 25 mm GFFs (Whatman, combusted at 400°C, 12 h) under <12 kPa vacuum pressure.

Samples were collected using 20 L Niskin bottles in the oligotrophic North Atlantic on a 24-bottle rosette. Sub-samples of 2-4 L were filtered depending on sample depth. Niskin bottle sub-samples were filtered through a 25 mm GFF (Whatman, nominal pore size 0.7 µm, combusted at 400°C, 12 h) using a glass and stainless steel filtration rig.

2.2.2.3 Marine Snow Catcher

Marine Snow Catchers (MSCs) are a large-volume bottle (Figure 2.4c). They have recently been used as an important part of the Shelf Seas Biogeochemistry program where they were used to collect particles in three operationally defined sinking fractions: "suspended" (f1), "slow-sinking" (f2) and "fast-sinking" (f3) particles (McDonnell et al., 2015; Riley et al., 2012), in this study referred to as MSC_{susp}, MSC_{slow} and MSC_{fast} respectively. The MSC comes in two sizes, 'small' 100 L and 'large' 300 L. They consist of a cylinder with removable lids at each end. The cylinder is lowered into the water with its lids held open with tensioned elastic, and when the pre-specified depth is reached a messenger is fired that releases the tension and snaps shut the two lids - trapping water within the cylinder.

During DY026, three samples were collected using the 'large' 300 L marine snow catcher. After collection they were left to settle on deck for 2 h then 2-3 L subsamples were collected from the top (MSC_{susp}) and bottom (MSC_{slow}) sections of the marine snow catcher and the bottom tray (MSC_{fast}; particles were picked from the bottom lid with a Pasteur pipette; Figure

2.5). All three subsamples were filtered through 0.7 µm 45 mm GFFs (Whatman, combusted) and stored in the freezer. To calculate total MSC concentration the MSC_{slow} and MSC_{fast} fractions were summed, based on the MSC_{slow} fraction containing both "suspended" and "slow-sinking" particles (Riley et al., 2012). For the station in the mixed layer at CCS, 20 m, we also included the sum of the MSC_{susp} and MSC_{fast} fractions, as at this station MSC_{susp} POC and lipids concentrations were higher than MSC_{slow} (Table 2.5).

During DY029 and DY033, six and two samples were collected, respectively, using 'small' 100 L marine snow catchers. Following deployment, a settling time of 1 h 20 minutes was used. MSC_{susp} particles were siphoned from the top tap, MSC_{slow} from the bottom tap, and MSC_{fast} collected from the bottom tray (Figure 2.5). 2 L were filtered onto a 25 mm GFF (Whatman, pore size 0.7 µm, combusted) on a plastic filter rig under < 12 kPa vacuum pressure and stored at -80°C (DY026, DY029) and -20°C (DY033).

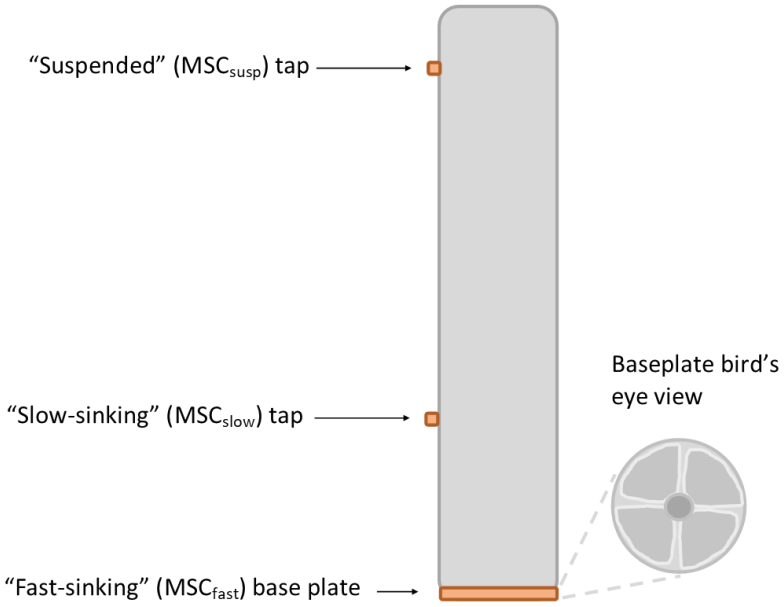

Figure 2.5 Schematic of the Marine Snow Catcher (MSC). Highlighting the location of the taps and a bird's eye view showing the four segments of the 300 L MSC baseplate.

2.2.3 POC and PN analyses

Freeze-dried samples (DY026 SAPs and MSC_{fast} particles, and samples from the subtropical North Atlantic) were placed in a desiccator with HCl overnight to remove the inorganic carbon using the vapour phase de-carbonation method of Yamamuro and Kayanne (1995). All samples were analysed by Sabena Blackbird (University of Liverpool) in duplicate using a Thermo Scientific Flash 2000 Organic Elemental Analyser or a Thermo Scientific Flash Smart. Samples were combusted instantaneously using the Dynamic Flash Combustion method

(helium carrier gas 130 mL min^{-1} enriched with high purity oxygen, platinized Alumina oxidation column 950°C, copper wire reduction column 750°C, Magnesium Perchlorate water absorption trap). A two-point calibration was performed using High Organic Sediment Standard OAS (Elemental Microanalysis Ltd, NIST certified values). The results were always within uncertainty limits of the certified value, which are 7.17 ± 0.09% carbon and 0.57 ± 0.02% nitrogen, with detection limits of 100 ppm for both C and N.

Punches for analysis were taken from the SAPs and MSC_{fast} GFFs. Four 4 mm punches were taken from the SAPs mesh GFF and four 1 mm punches were taken from the SAPs and MSC_{fast} GFF. For the SAPs GFF filters, care was taken to remove punches from homogenous areas of the filter. For filters from the Celtic Sea, two punches were taken from the centre and two from the outside of the filter (duplicates) to reduce the effects of possible heterogeneity across the filter. For the Atlantic Ocean SAPs, the bottom-stacked filter was subtracted from the top as a blank. On all filters, care was taken to avoid large zooplankton that would skew the results.

Niskin bottle, MSC_{susp} and MSC_{slow} POC and PN for the Celtic Sea Cruises were provided by the UK Shelf Sea Biogeochemistry programme.

2.2.4 Lipid extraction, identification and quantification

After freeze-drying, filters were cut into small pieces and placed in a test tube using scissors and tweezers. $1/8^{th}$ of the 293 mm diameter SAPs GFF was cut up while the entire 47 mm diameter filter papers were cut up for the SAPs mesh, MSC and Niskin bottle. Lipids were extracted using ~15 mL of 9:1 dichloromethane:methanol. An internal standard, 100 µL of 5α(H)-cholestane (100.96 ng μL^{-1} in cyclohexane), was added to the samples and a blank which were then sonicated (30 minutes) and centrifuged (5 minutes, 2500 rpm, 17 °C). The liquid (superlative) was pipetted into a round bottom flask. To ensure all the lipids were extracted this process was repeated twice more, each time adding ~5 mL of 9:1 dichloromethane:methanol. The solvent was then evaporated under vacuum and the residue passed through an anhydrous sodium sulphate column. Samples were methylated using methanol and acetyl chloride (6 mL for 5 samples, < 10:1) and warmed overnight (12 h; 45°C; Christie 1982). Samples were then neutralised by filtering through potassium carbonate. All the glassware was pre-cleaned (overnight in Decon), oven dried (2-4 h; 70°C) and combusted (24 h; 400°C).

Prior to GC-MS analysis samples were derivatised using bis-trimethylsilyltrifluoroacetamide (25 µL; 60°C; 45 mins). The samples were first analysed using an Agilent 6890 series Gas Chromatograph to check their quality, then using a Thermo Quest EC Instruments Trace 2000 series GC (on-column injector, 60 m x 0.25 mm, 0.1 µm film, DB-5MS; J&W; Helium carrier gas 1.6 mL min^{-1}, oven 60°C for 1 min, 60°C to 170°C at 6°C min^{-1}, 170°C to 315°C at 2.5°C min^{-1} and held for 10 minutes) coupled with a Thermo Quest Finnigan TSQ7000 mass

spectrometer (source temperature 230°C, 70eV electron beam, trap current 300 μA, m/z 50-600 every 1s). Compounds were identified using X-Calibur (Finnigan Corporation, version 1.0) by comparison of their mass spectra and relative retention indices with those in the literature. Quantitative data was calculated using peak areas and comparison of the internal standard peak area with those of the compounds of interest. The relative response factors of the analytes were determined individually for 36 representative fatty acids, sterols and alkenones using authentic standards. Response factors for analytes where standards were unavailable were assumed to be identical to those of available compounds of the same class.

2.2.5 Statistical analyses

Paired-sample t-tests were used to compare the concentration of POC and PN collected by each of the techniques. Non-normal distributed variables were log-transformed prior to analysis (Kolmogorov-Smirnov test for normality). Data outliers were identified as values higher and lower than the mean ± (interquartile range * 1.5).

To highlight similarities between techniques and stations, multivariate analyses of elemental and key absolute (semi quantitative) lipid concentrations were carried out in RStudio. Hierarchical cluster analysis was performed using Euclidean distance and Ward's clustering criterion ("ward.d2" dissimilarity method). The results were viewed as a dendrogram with the ggplot2, ggdendro and dendextend packages. The optimal number of clusters (10) was chosen using the gap statistic. Principle component analysis (PCA) was performed using the FactoMineR package in RStudio. Data was standardised to variance. The factoextra package was used for visualisation.

2.3 Results

2.3.1 North Atlantic Ocean

2.3.1.1 Water column properties

The subtropical North Atlantic is a stratified oligotrophic ocean although RidgeMix sampled the boundary between the temperate waters to the north and tropical waters to the south (refer to Chapter 3 section 3.4.2). Mixed layer depth varied between 13 and 51 m during RidgeMix with a sea surface temperature ranging from 20 to 27°C, with warmer waters to the south (Figure 2.6a). A subsurface chlorophyll-*a* maximum was observed at depths between 55 and 155 m, occurring deeper in the water column in the south of the transect (Figure 2.6b). The concentrations at the chlorophyll-*a* maximum reached up to 0.60 mg m^{-3} in the north; lower concentrations were observed to the south (0.16-0.19 mg m^{-3}). Surface chlorophyll-*a* concentrations were low, 0.01-0.07 mg m^{-3}.

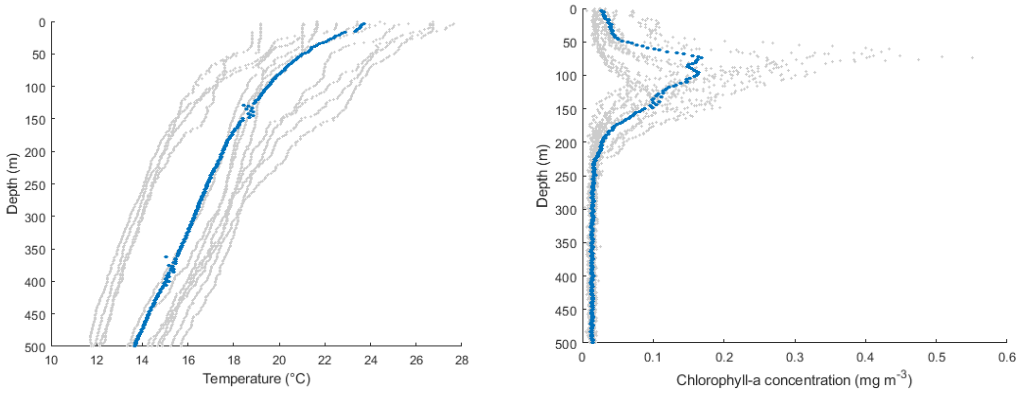

Figure 2.6 Depth profiles of (a) Temperature and (b) chlorophyll-a fluorescence. Grey dots are all stations. Blue profile is 2 m depth average.

2.3.1.2 POC and PN

2.3.1.3 Stand Alone Pumps in the North Atlantic Ocean

In the subtropical North Atlantic, total Stand Alone Pumps (SAPs) POC concentration varied between 0.03 and 6.9 µM and PN between 0.02 and 0.7 µM (Figure 2.6 and Appendix Table 2.1). Concentrations were highest at the DCM and decreased with depth. At 100 m below the DCM, POC concentrations were < 0.5 µM and PN < 0.1 µM. At 500 m, POC was < 0.3 µM and PN < 0.1 µM. The C:N varied between 2.4 and 28 with an average of 5.6 ± 1.4 (outliers removed). The ratio was highest at the DCM with a ratio near Redfield (6.5 ± 0.6) and decreased with depth. At a depth of 100 m below the DCM the average ratio was 5.5 ± 0.9, at 500 m the ratio was 4.2 ± 1.2 (after removing an outlier with C:N 28).

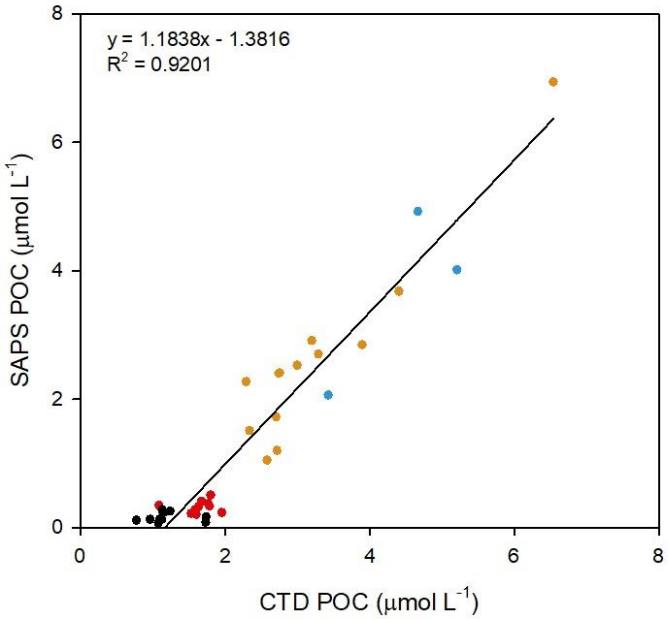

Figure 2.7 Comparison of Niskin bottles (CTD) and in-situ pumps (SAPs) POC. Samples from the Celtic Sea station are in blue (from below the mixed layer, the surface sample was considered an outlier and excluded). The other samples are from the oligotrophic subtropical North Atlantic gyre: orange are samples from the surface (15 m) and chlorophyll-a maximum; red from 100 m below the chlorophyll-a maximum and black from 500 m.

2.3.1.4 Niskin bottle in the North Atlantic Ocean

Niskin bottle POC and PN concentrations are significantly higher than SAPs (paired t-test, $p < 0.001$; Figure 2.7, Table 2.3). At the DCM, POC and PN concentrations were 41 ± 30% and 41 ± 14% higher than total SAPs, 100 m below the DCM they were 81 ± 10% and 76 ± 9% higher, and at 500 m they were 89 ± 8% and 79 ± 14% higher than total SAPs (Table 2.3). Niskin bottle POC concentrations varied between 4 and 9.5 µM and PN between 0.1 and 0.8 µM (Figure 2.7 and Appendix Table 2.1). Like the SAPs, concentrations were highest at the DCM and decreased with increasing depth. The DCM had the highest concentrations of POC ranging from 2.3 to 3.9 µM and PN ranging from 0.3 to 0.8 µM. 100 m below the DCM concentrations ranged from 1.1 to 2.0 µM POC and 0.2 to 0.3 µM PN and at 500 m 0.8 to 1.7 µM POC and 0.1 to 0.4 µM PN.

C:N varied between 4 and 9.5 with an average of 5.7 ± 1.2 (with outliers removed), similar to the SAPs (5.6 ± 1.4). In contrast, the lowest ratio was at the DCM and was lower than the pumps (5.1 ± 0.5 with outlier removed *vs.* 6.5 ± 0.6). The C:N ratio 100 m below the DCM was 6.1 ± 1.4 and at 500 m 5.7 ± 1.3 (outlier removed).

Table 2.3 Comparison of mean ± standard deviation POC and PN concentrations for SAPs and Niskin bottle in the subtropical Atlantic Ocean at the DCM, 100 below the DCM and 500 m. t-test, df = 18, p < 0.05, p < 0.001**.*

Depth	POC (µM)			PN (µM)		
	Niskin bottle	SAPs	t	Niskin bottle	SAPs	t
DCM	2.88 ± 0.48	1.76 ± 1.03	3.1*	0.55 ± 0.15	0.32 ± 0.11	3.8*
DCM-100 m	1.64 ± 0.23	0.27 ± 0.15	15.8**	0.27 ± 0.06	0.06 ± 0.02	11.4**
500 m	1.21 ± 0.31	0.13 ± 0.09	10.6**	0.21 ± 0.08	0.04 ± 0.03	6.3**

In summary, in the North Atlantic we found that Niskin bottle POC concentrations were 68 ± 31% higher than SAPs (2.2 ± 1.2 µM vs 0.1 ± 1.5 µM, paired t-test, $n = 3$, $p < 0.01$) and Niskin bottle PN concentrations were 63 ± 28% higher than SAPs (0.4 ± 0.2 µM vs 0.2 ± 0.2 µM; paired t-test, $n = 33$, $p < 0.01$). We also observed a decrease in the C:N ratio with depth, with slightly higher average Niskin bottle ratios than SAPs, apart from at the DCM where the Niskin bottle ratios were lower than the SAPs and lower than Niskin bottle ratios below the DCM and at 500 m.

2.3.2 Celtic Sea

2.3.2.1 Water column properties

The Celtic Sea is well mixed during autumn and winter. However, during spring and summer, when solar irradiance increases, the deeper regions and areas with weak tidal currents become thermally stratified (Sharples, 2007). The mixed layer depth was < 50 m for all stations sampled. The temperature below the mixed layer was fairly uniform at ~10°C, above the mixed layer the temperature rose to 11°C during spring and 16 to 18°C during summer (Figure 2.8). The highest productivity in shelf sea occurs during spring when the onset of stratification initiates the spring-bloom (Davis et al., 2018; Sharples, 2007; Tweddle et al., 2013). Chlorophyll-*a* concentrations reached 8 mg m^{-3} in the surface mixed layer during peak-bloom during DY029 (Davis et al., 2018; Poulton et al., 2018), at the station in this study chlorophyll-*a* concentrations reached 2 mg m^{-3} (Figure 2.8b). Chlorophyll-*a* concentrations were lower (< 2 mg m^{-3}) during the summer, apart from at the Celtic Deep station in August 2014 (CD; 4.2 mg m^{-3}) and presented subsurface maxima close to the mixed layer depth (Figure 2.8a, c).

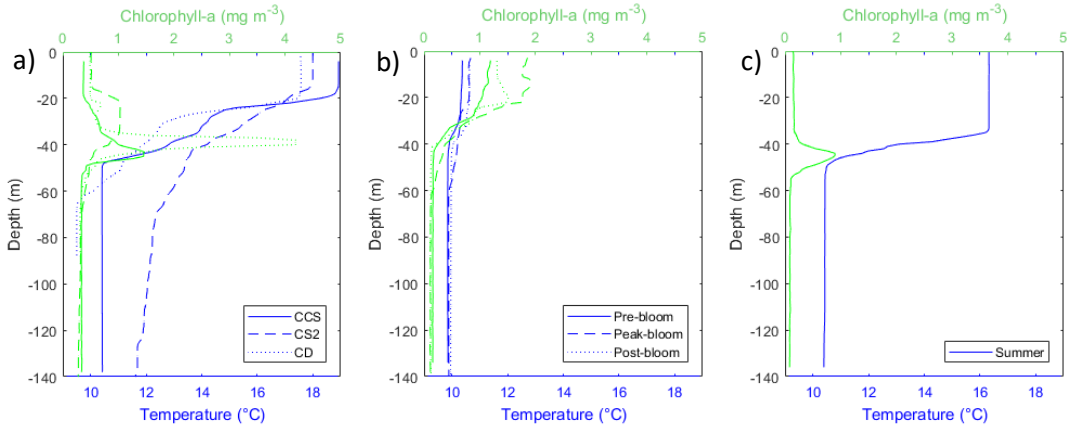

Figure 2.8 Depth profiles of temperature (blue) and fluorescence (green) for (a) August 2014, DY026 (b) April 2015, DY029 and (c) July 2015, DY033. Samples were collected in August 2014 were from the Central Celtic Sea (CCS), Celtic Sea 2 (CS2), and Celtic Deep (CD) stations, see Figure 2.3. During April and July 2015 samples were collected from the CCS station, with sampling pre-, peak- and post-bloom during April.

2.3.2.2 POC and PN

2.3.2.2.1 Stand Alone Pumps in the Celtic Sea

In the Celtic Sea during summer 2014, four samples were collected from three locations: one in the mixed layer (20 m at CCS) and three below the mixed layer (60 m at CCS and 50 m at CS2 and CD, Figure 2.3). POC concentrations varied between 2.2 and 5.0 µM and PN between 0.2 and 0.6 µM (Table 2.4). The POC concentration was highest closest to the coast (CD station, 5.0 µM), lower in the Central Celtic Sea (CCS, 3.6 µM at 20 m and 4.5 µM at 60 m) and the lowest at the shelf edge (CS2, 3.6 µM). However, PN was highest in the Central Celtic Sea (CCS, 0.6 µM at 60 m, 0.3 µM at 20 m), then the coast (CD, 0.5 µM) and lowest at the shelf edge (CS2, 0.2 µM). This results in CCS mixed layer having the highest C:N ratio (10.6), then CD (10.3), CS2 (9.9), and finally CCS below the mixed layer (7.9).

Table 2.4 Comparison of POC, PN, C:N, total lipids and the relative lipid contribution for Stand Alone Pumps (SAPs: 0.7-53 µm and > 53 µm), Marine Snow Catchers (MSC: slow sinking + fast sinking or suspended (susp) + fast sinking particles) and Niskin bottles, collected in the Celtic Sea during summer 2014 (DY026). Samples are from three locations in Celtic Sea: the Central Celtic Sea (CCS 20 m and CCS 60 m), Celtic Sea 2 (CS2 50 m) and the Celtic Deep (CD 50 m). The sample at 20 m is in the mixed layer (ML), the three other locations are below the mixed layer.

Station	Technique	POC (µM)	PN (µM)	C:N	Total Lipids (ng L^{-1})	Lipid contribution to POC (%)
CCS 20 m (ML)	SAPs	3.6	0.3	10.6	4723	11
	MSC (slow + fast)	11.0	0.7	14.7	4082	3
	MSC (susp + fast)	16.2	0.9	19.0	28563	15
	Niskin bottle	9.9	1.1	8.6	27706	23
CCS 60 m	SAPs	4.5	0.6	7.9	5352	10
	MSC (slow + fast)	12.2	1.0	12.4	3782	3
	Niskin bottle	5.2	1.3	4.0	4695	8
CS2 50 m	SAPs	2.2	0.2	9.9	6159	23
	MSC (slow + fast)	9.0	1.2	7.3	7827	7
	Niskin bottle	3.4	0.6	6.1	1941	5
CD 50 m	SAPs	5.0	0.5	10.3	2398	4
	Niskin bottle	4.7	0.5	9.2	1555	3

2.3.2.2.2 Niskin bottle in the Celtic Sea

Niskin bottle samples were collected during all four Celtic Sea Cruises. During summer 2014, POC and PN concentrations varied between 3.4 and 9.9 µM POC and 0.5 and 1.3 µM PN (Table 2.4). Concentrations were higher than the SAPs but this was not statistically significant (paired t-test, $p = 0.138$). This was likely due to Niskin bottle POC and PN concentrations at the Celtic Deep station being very similar to those collected by the SAPs (Table 2.4). If this station is removed, there was a 23 to 67% increase in POC and PN collected by the Niskin bottle relative to SAPs. PN concentrations, in particular, were 2 to 3 times higher for the Niskin bottle compared to the SAPs, resulting in lower C:N ratios (4 to 9.2).

At CCS during spring and summer 2015, Niskin bottle POC and PN concentrations were variable (Table 2.5). The lowest concentrations were observed during the summer particularly below the mixed layer (2.4 µM POC and 0.3 µM PN) and the highest at peak-bloom in the surface waters (28.1 µM POC and 3.8 µM PN). For all stations concentrations were higher in the surface waters than below the mixed layer at 70 m (t-test, $p < 0.05$). The C:N ratio was highest at 10 m for all stations apart from pre-bloom. The ratio was consistently between 5.7 and 6.8, apart from at 10 m during the summer when it increased to 8.7.

Table 2.5 Comparison of Marine Snow Catcher (MSC) and small-volume Niskin bottle (Nisk.) samples from the Central Celtic Sea (CCS) station during cruises DY029 and DY033 (spring and summer 2015). Pre-bloom 11th May, peak-bloom 15th May, post-bloom 20th May, and summer 29th July. MSC susp "suspended" particles, MSC slow "slow-sinking" particles, and MSC fast "fast-sinking" particles.

			POC (µM)				PN (µM)				POC:PN			
	Timing	Depth (m)	Nisk.	MSC susp	MSC slow	MSC fast	Nisk.	MSC susp	MSC slow	MSC fast	Nisk.	MSC susp	MSC slow	MSC fast
DY029	Pre-bloom	10	13.9	15.6	15.5	1.3	2.4	2.7	2.4	0.0	5.7	5.8	6.5	
		70	3.7	5.0	5.5	0.5	0.6	1.0	0.9	0.1	6.3	5.1	6.0	4.6
	Peak-bloom	10	28.1	21.6	15.2	0.4	4.1	3.8	3.7	0.0	6.8	5.7	4.1	7.6
		70	3.1	10.9	5.1	0.0	0.5	0.9	1.1	0.0	6.2	12.5	4.7	
	Post-bloom	10	17.8	25.1	26.7	0.3	3.0	4.3	4.8	0.1	6.0	5.8	5.6	3.2
		70	5.0	5.1	5.0	0.0	0.9	1.0	1.0	0.0	5.8	5.1	5.0	
DY033	Summer	10	6.3	6.8	6.2	0.0	0.7	1.3	0.9	0.0	8.7	5.2	7.2	
		70	2.4	8.6	5.4	0.2	0.3	1.3	1.0	0.1	6.8	6.5	5.6	3.6

2.3.2.2.3 Marine Snow Catcher in the Celtic Sea

The Marine Snow Catcher (MSC) was deployed during all four Celtic Sea cruises. The MSC was split into three fractions for analysis: MSC_{susp}, MSC_{slow} and MSC_{fast} particles. Of these, POC and PN concentration ranges were most similar for MSC_{susp} and MSC_{slow}. MSC_{susp} concentrations varied between 5 and 25.1 µM POC and 0.9 and 4.3 µM PN, and MSC_{slow} concentrations varied between 5 and 26.7 µM POC and 0.9 and 4.8 µM (Table 2.5, 2.6). Both fractions were higher compared to those collected using the Niskin bottle (paired t-test, $p < 0.05$), apart from MSC_{slow}'s PN concentration, which was not statistically different. By comparison, MSC_{fast} concentrations were lower with POC varying between 0.06 and 0.09 µM and PN between 0.005 and 0.010 µM, more closely resembling the SAPs > 53 µm (Table 2.6).

C:N ratios were variable within and below the mixed layer over the time period studied. During summer 2014, C:N ratios of all fractions were higher than Redfield (6.8-19.1) and higher than the Niskin bottle (apart from MSC_{fast} in the surface at CCS, Table 2.6). During 2015 most C:N ratios were below Redfield and had similar ratios to the Niskin bottle (Table 2.5). MSC_{fast} had the lowest ratios, apart from below the mixed layer in summer 2014 and at peak-bloom in the surface waters during 2015 where MSC_{fast} had the highest ratios.

As with the Niskin bottle data, the seasonal cycle of the Celtic Sea is apparent in the MSC POC and PN concentrations; at CCS during 2015, these were highest at peak- and post-bloom and lowest in the summer (Table 2.5). Concentrations were highest in the surface waters, apart from at the summer station where MSC_{susp} and MSC_{fast} POC and MSC_{slow} and MSC_{fast} PN were higher below the mixed layer. MSC_{fast} PN was also higher below the mixed layer pre-bloom.

Table 2.6 Comparison of POC, PN, C:N, total lipids and the relative lipid contribution for three techniques, in-situ pumps (SAPs 0.7-53 µm and SAPs > 53 µm), large-volume bottles (MSC susp "suspended", MSC slow " slow-sinking" and MSC fast "fast-sinking" particles) and small-volume Niskin bottles, used in the Celtic Sea during summer 2014 (DY026). Samples are from three locations in Celtic Sea: Central Celtic Sea (CCS 60 m and CCS 20 m), Celtic Sea 2 (CS2) and the Celtic Deep (CD). The sample at 20 m is in the mixed layer (ML), the three other locations are below the mixed layer.

Station	Technique	POC (µM)	PN (µM)	C:N	Lipids (ng L^{-1})	Lipids (%)[a]
CCS 20 m (ML)	SAPs (0.7-53 µm)	3.4	0.3	10.5	3135	8
	SAPs (> 53 µm)	0.5	0.1	13.4	1588	24
	MSC susp	16.1	0.8	19.1	28561	15
	MSC slow	10.9	0.7	14.8	4080	3
	MSC fast	0.1	10*	6.8	2	0.2
	Niskin bottle	9.9	1.1	8.6	27706	23
CCS 60 m	SAPs (0.7-53 µm)	3.9	0.5	8.2	5191	11
	SAPs (> 53 µm)	0.1	8*	6.3	161	12
	MSC susp	6.6	0.8	7.8	5547	7
	MSC slow	12.1	1.0	12.4	3623	2
	MSC fast	0.1	7*	13.5	159	16
	Niskin bottle	5.2	1.3	4.0	4695	8
CS2 50 m	SAPs (0.7-53 µm)	1.8	0.2	11.4	5702	29
	SAPs (> 53 µm)	0.4	0.1	6.2	457	10
	MSC susp	8.6	1.3	6.8	8013	8
	MSC slow	8.9	1.2	7.3	7826	7
	MSC fast	0.1	5*	11.1	1	0.1
	Niskin bottle	3.4	0.6	6.1	1941	5
CD 50 m	SAPs (0.7-53 µm)	4.9	0.5	10.4	2360	4
	SAPs (> 53 µm)	0.1	15*	6.9	38	6
	Niskin bottle	4.7	0.5	9.2	155	0.3

[a] % of POC
*nmol L^{-1}

2.3.2.2.3.1 Comparison of MSC_{susp} and MSC_{slow} in the Celtic Sea

The MSC_{susp} and MSC_{slow} particle fractions had similar POC and PN concentrations and C:N ratios during the sampling period; there was no consistent difference between the two fractions (Table 2.5, 2.6). However, changes between the two fractions were noticeable seasonally and varied with sample depth. In the photic zone (10-20 m), POC and PN are higher for MSC_{susp} compared to MSC_{slow} for all samples apart from post-bloom in spring 2015 (Figure 2.9a, b circled). C:N ratios were similar for MSC_{susp} and MSC_{slow} during spring and summer 2015 but higher during summer 2014 where MSC_{susp} was more carbon-enriched than MSC_{slow} (Figure 2.9c). Below the mixed layer, at 50-70 m, POC and PN concentrations were more variable. For POC, before the spring bloom MSC_{slow} was higher (CCS and CS2 during

summer 2014 and CCS pre-bloom in 2015), but after the onset of the spring bloom MSC_{susp} was higher (Figure 2.9d). For PN, MSC_{susp} was higher at CS2 in summer 2014, pre-bloom and in summer 2015; MSC_{slow} was higher for CCS in summer 2014 and peak-bloom in 2015; and post bloom MSC_{susp} and MSC_{slow} are equal (Figure 2.9e). Like the POC concentrations, C:N was higher and so particles more carbon-enriched for MSC_{slow} before the spring bloom and MSC_{susp} after the spring bloom (Figure 2.9f).

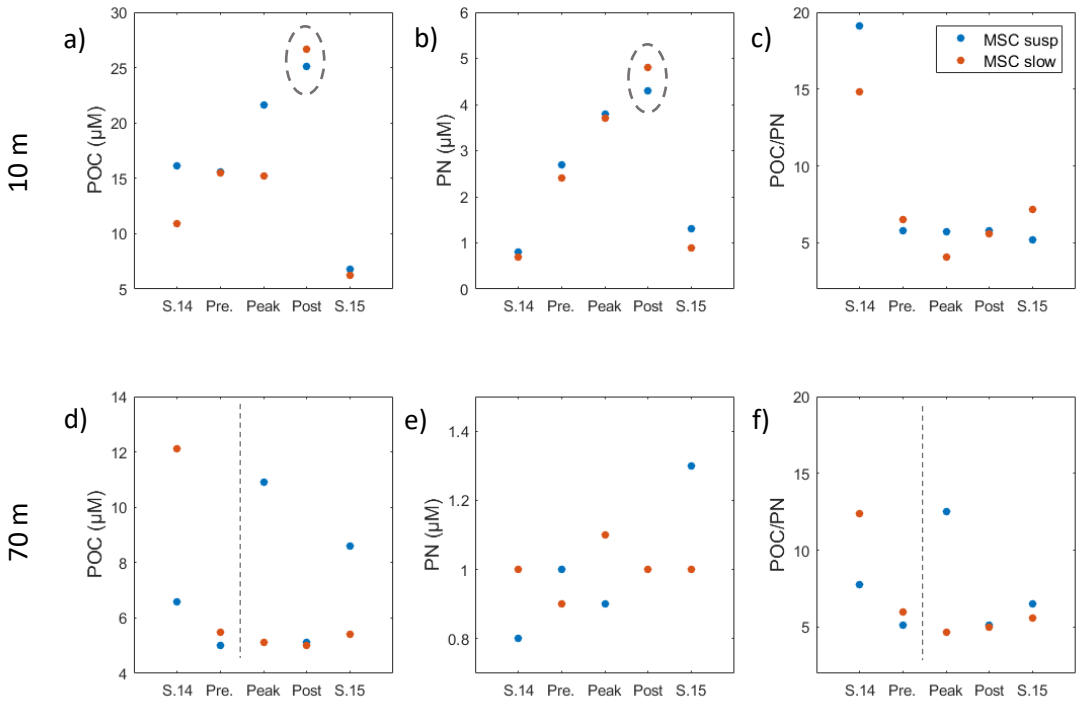

Figure 2.9 POC (a, d), PN (b, e) and POC:PN ratios (c, f) at Celtic Sea station CCS at 10 m (a, b, c) and 70 m (d, e, f). For MSC susp ("suspended" particle MSC fraction) and MSC slow ("slow sinking" particle MSC fraction). Plotted against time of year: summer 2014, spring pre-bloom, peak-bloom, post bloom 2015 and summer 2015.

In summary, we found that in the Celtic Sea MSC_{susp} and MSC_{slow} POC concentrations (10.8 ± 6.4 µM and 7.0 ± 8.6 µM) were 34 ± 25% and 30 ± 23% higher than Niskin bottles (7.1 ± 5.2 µM, paired t-test, n = 10, $p < 0.05$) and Niskin bottle POC (5.8 ± 2.8 µM) and PN (0.9 ± 0.4 µM) concentrations were 26 ± 26% and 48 ± 29% higher than SAPs (3.8 ± 1.1 µM POC and 0.4 ± 0.2 µM PN; paired t-test, n = 4, p = 0.1). We also observe seasonal and depth variation in the composition of particles (C:N) collected by each technique.

2.3.2.3 Lipids in the Celtic Sea during summer 2014 (DY026)

To further characterise variation in particle composition between techniques, lipid analysis was undertaken at the four stations in the Celtic Sea during summer 2014 (DY026). The main

groups of lipids present were fatty acids (saturated (sFA), polyunsaturated (PUFA) and monounsaturated (MUFA) compounds, fatty alcohols (OH) and sterols (Table 2.1, 2.7, Appendix Figure 2.1, Appendix Table 2.2, 2.3). Unsaturated alcohols and branched fatty acids were also present in low concentrations. Phytoplankton markers were the predominant form of lipid biomarker, including the essential fatty acids 20:5ω3 (EPA), 22:6ω3 (DHA) and 18:3ω3 (ALA; Lang et al., 2011; Parrish, 2009; Volkman, 2006; Appendix Table 2.3). Other notably predominant biomarkers include the ubiquitous saturated fatty acids C_{16} and C_{18}. Biomarkers for zooplankton (OH, long-chain MUFAs) and bacterially-associated material (bFA, odd-chain FA) were present, but in low concentrations (see Table 2.7 and Appendix Figure 2.1).

Total lipid concentrations varied between techniques and stations (1,555-28,563 ng L^{-1}, Table 2.6), making up 3-23% of POC. Concentrations were highest at Central Celtic Sea (CCS) and lowest at CD (Table 2.6).

2.3.2.3.1 Stand Alone Pumps in the Celtic Sea

Total lipid concentrations, for the sum of both size-fractions, varied between 2398 and 6159 ng L^{-1} (Table 2.4). Separately, the lipid concentrations were higher for the 0.7-53 µm fraction (2360-5702 ng L^{-1}) than > 53 µm fraction (38-1588 ng L^{-1}), although both contributed in a similar way to POC (4-29% and 6-24%, Table 2.6). sFA and PUFAs dominated stations CCS and CS2 for the 0.7-53 µm fraction (34-62% and 9-43%) and OH, sterols and PUFAs dominated station CD (50%, 20% and 18% (Table 2.7). The > 53 µm fraction was dominated by PUFAs (13-80%), FAs (3-77%), and MUFAs (2-55%; Table 2.7). In comparison the composition of the 0.7-53 µm fraction was more variable (Appendix Figure 2.1).

2.3.2.3.2 Niskin bottle in the Celtic Sea

Total Niskin bottle lipid concentrations are slightly more variable than the SAPs, ranging from 155 to 27,706 ng L^{-1} with lipids making up 3-23% of POC (Table 2.6). sFA make up the largest proportion of lipids (51-94%) making the semi-labile pool the largest particle pool at all stations (C_{16} and C_{18}; Table 2.7; Figure 2.10). In addition to sFA, CS2 had high contributions of MUFAs (20%) and bacterial FA (59%) and the CD of PUFAs (28%).

2.3.2.3.3 Marine Snow Catcher in the Celtic Sea

For fraction MSC_{susp}, lipid concentrations were 5547 to 28,561 ng L^{-1}. Lipids made up 7-15% of POC (Table 2.6). MSC_{susp} was dominated by semi-labile sFA (29-100%), as for the Niskin bottle. Like the Niskin bottle the dominant biomarkers are C_{16} and C_{18} (Appendix Figure 2.1). At CS2, PUFAs also made up a large proportion of lipids (48%) indicating that the particles were more labile (labile pool was the largest), particularly abundant biomarkers at CS2 were C_{16}, $C_{18:3\omega3}$ and $C_{22:6\omega6}$ (Table 2.7, Figure 2.10, Appendix Figure 2.1).

Table 2.7 Comparison of percentage contribution of major lipid groups to total lipid concentration (%), for Stand Alone Pumps (SAPs 0.7-53 µm and SAPs > 53 µm), Marine Snow Catchers (MSC susp "suspended", MSC slow " slow-sinking" and MSC fast "fast-sinking" particles) and Niskin bottles, collected in the Celtic Sea during summer 2014 (DY026). Samples are from three locations in Celtic Sea: Central Celtic Sea (CCS 60 m and CCS 20 m), Celtic Sea 2 (CS2) and the Celtic Deep (CD). The sample at 20 m is in the mixed layer (ML), the three other locations are below the mixed layer.

Station	Technique	Lipids (ng L^{-1})	sFA[a] (%)	PUFA[a] (%)	MUFA[a] (%)	Ster[a] (%)	fOH[a] (%)	baFA[a] (%)
CCS 20 m (ML)	SAPs (0.7-53 µm)	3135	61.7	8.6	5.5	2.0	3.3	0.6
	SAPs (> 53 µm)	1588	3.3	28.1	54.7	2.5	11.3	0.1
	MSC susp	28561	99.5	0.5	0.0	0.0	0.0	0.0
	MSC slow	4080	54.4	22.1	10.3	12.1	1.1	0.0
	MSC fast	2	80.5	8.9	2.9	6.4	1.4	0.0
	Niskin bottle	27706	89.1	6.3	1.1	3.0	0.1	0.1
CCS 60 m	SAPs (0.7-53 µm)	5191	43.3	43.1	6.6	2.9	0.2	0.7
	SAPs (> 53 µm)	161	21.5	53.1	16.8	1.5	7.0	0.4
	MSC susp	5547	80.2	8.2	3.7	3.0	1.8	0.8
	MSC slow	3623	58.7	15.5	11.4	1.5	12.7	0.0
	MSC fast	159	11.4	31.0	13.8	0.5	43.2	0.5
	Niskin bottle	4695	94.6	2.1	1.1	0.4	0.4	0.1
CS2 50 m	SAPs (0.7-53 µm)	5702	34.1	14.4	7.2	6.9	2.6	0.8
	SAPs (> 53 µm)	457	8.7	79.7	2.6	7.1	1.9	0.5
	MSC susp	8013	28.7	48.3	12.3	9.0	1.4	0.2
	MSC slow	7826	25.6	49.8	12.3	10.3	1.8	0.5
	MSC fast	1	86.7	0.0	8.6	2.0	2.3	0.0
	Niskin bottle	1941	51.1	2.1	19.7	0.0	0.6	58.7
CD 50 m	SAPs (0.7-53 µm)	2360	8.1	17.5	0.7	20.2	49.4	0.2
	SAPs (> 53 µm)	38	76.6	12.9	2.2	4.1	1.2	2.3
	Niskin bottle	155	52.6	28.3	8.5	4.3	1.8	0.0

[a] sFA: saturated fatty acids, PUFA: polyunsaturated fatty acids, MUFA: monounsaturated fatty acids, Ster: sterols, fOH: fatty alcohols (saturated and unsaturated), baFA: bacterial fatty acids (branched + odd-number saturated fatty acids)

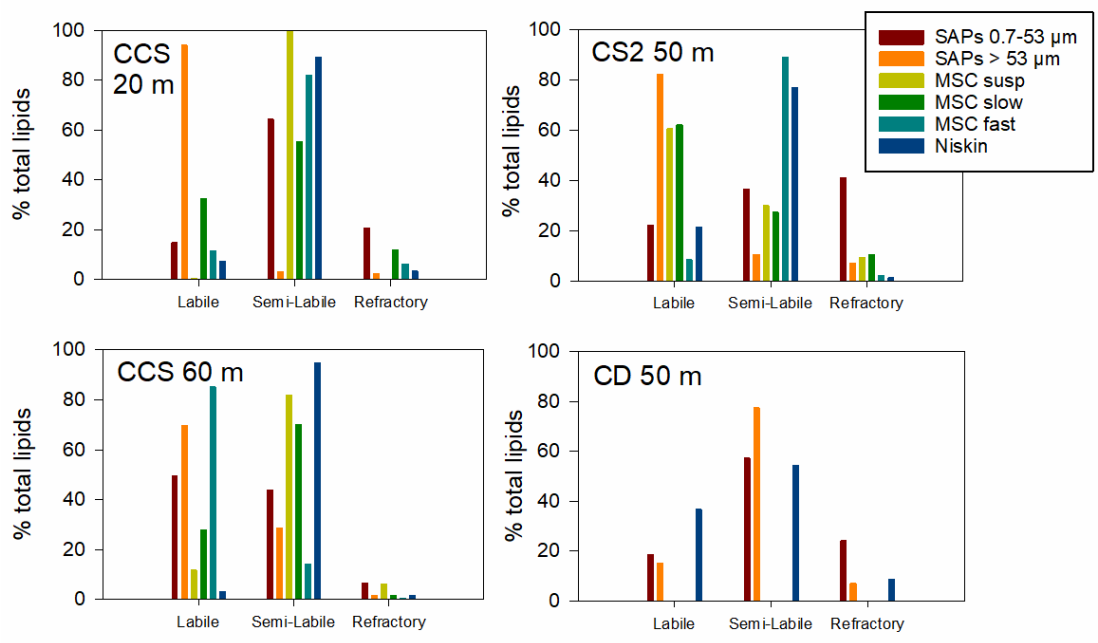

Figure 2.10 Particle lability for each of the collection techniques during DY026 in the Celtic Sea. Labelled SAPs and Sm (Stand-Alone Pump System 0.7-53 µm and >53 µm), MSC (Marine Snow Catcher), and CTD (Niskin bottle). MSC susp "suspended" particles, MSC slow "slow-sinking" particles, and MSC fast "fast-sinking" particles.

For fraction MSC_{slow}, lipid concentrations were in the range 3623 to 7826 ng L^{-1}. Lipids in this fraction contributed less to POC than MSC_{susp} (2-7%). MSC_{slow} lipids, like MSC_{susp}, were dominated by sFA (26-59%) but also PUFAs (16-50%), MUFAs (10-12%) and sterols (2-12%; Table 2.7). At CCS, below the mixed layer, fatty alcohols make up 13% of lipids. Like MSC_{susp}, the semi-labile pool was the largest particle pool at CCS and the labile pool was higher at CS2 - where MSC_{slow} has almost identical biomarker signature to MSC_{susp} (Figure 2.10, Appendix Figure 2.1). The main differences between MSC_{susp} and MSC_{slow} at CCS are that MSC_{slow} has lower concentrations of saturated fatty acids (C_{16} and C_{18}) but higher concentrations of PUFAs and MUFAs (Table 2.7, Appendix Figure 2.1).

Fraction MSC_{fast} lipid concentrations were lower than MSC_{susp} and MSC_{slow} at 2 to 533 ng L^{-1} with lipids making up 0.1-16% of POC (Table 2.6). Like the other fractions and the Niskin bottle, lipids for CCS 20 m and CS2 (50 m) are dominated by semi-labile sFA (81-87%). However, below the mixed layer lipids at CCS are dominated by fatty alcohols (43%) and PUFAs (31%) resulting in a larger labile pool of material (Figure 2.10).

In summary, the techniques collected different quality particles of somewhat different lipid composition, depending on location and depth. In the mixed layer at CCS, SAPs > 53 µm collected a high proportion of labile particles (> 90%) and all other techniques collected high proportions of semi-labile particles (> 50%, Figure 2.10). Below the mixed layer, at CCS, SAPS (0.7-53 and > 53 µm) and MSC_{fast} collected high proportions of labile material (> 70%) whilst the other techniques collected more semi-labile particles. In comparison, at CS2 whilst SAPs > 53 µm, MSC_{susp} and MSC_{slow} collect higher proportions of labile material SAPs 0.7-53 µm collected high proportions of refractory material, and MSC_{fast} and Niskin bottle high proportions of semi-labile material. At CD all techniques collected high proportions of semi-labile material.

2.3.3 Multivariate Analyses for the Celtic Sea during summer 2014 (DY026)

In the previous sections we reported differences in physics between locations in the Celtic Sea during DY026 (section 2.3.2.1) and differences in the particle quantity and composition collected by the three techniques (SAPs, MSC and Niskin bottle; sections 2.3.2.2 and 2.3.2.3). In this section we conduct metric multidimensional scaling (mMDS), principle component analysis (PCA), with POC, PN and lipid concentrations to visualise variation between techniques. Principal component analysis of lipid biomarker concentrations, POC and PN was carried out to determine which samples were most alike and showed that the first two components explained 56% of the total variance among samples (Figure 2.11). The first component (PC1), for which the greatest loadings were labile MUFAs (22:1, 20:1 and 18:1), PUFAs (18:3ω9 and 20:5), and brassicasterol contributes 29%. The second component (PC2) which had greatest loadings from labile PUFAs (18:5ω3, 18:4ω3, 22:6 ω3 and 20:5 ω3), semi-labile sFA C_{14} and branched sFA i-C_{15}, and refractory sterols ($C27\Delta^{5,22}$) contributes 28%.

The dendrogram clusters further highlight similarities between samples (Figure 2.12). There are two large clusters, one containing five samples and the other seven. The MSC_{fast} fractions and the SAPs > 53 µm from CCS 60 m and CD 50 m group were in one cluster. The other large cluster was Niskin bottles below the mixed layer, the MSC_{susp} fraction at CCS 60 m, SAPs 0.7-53 µm at CCS 20 m and CD, and SAPs > 53 µm at CS2. All the other clusters contained one sample except for one cluster containing MSC_{susp} and MSC_{slow} fractions from CS2 (numbers 15 and 16 in Figure 2.11).

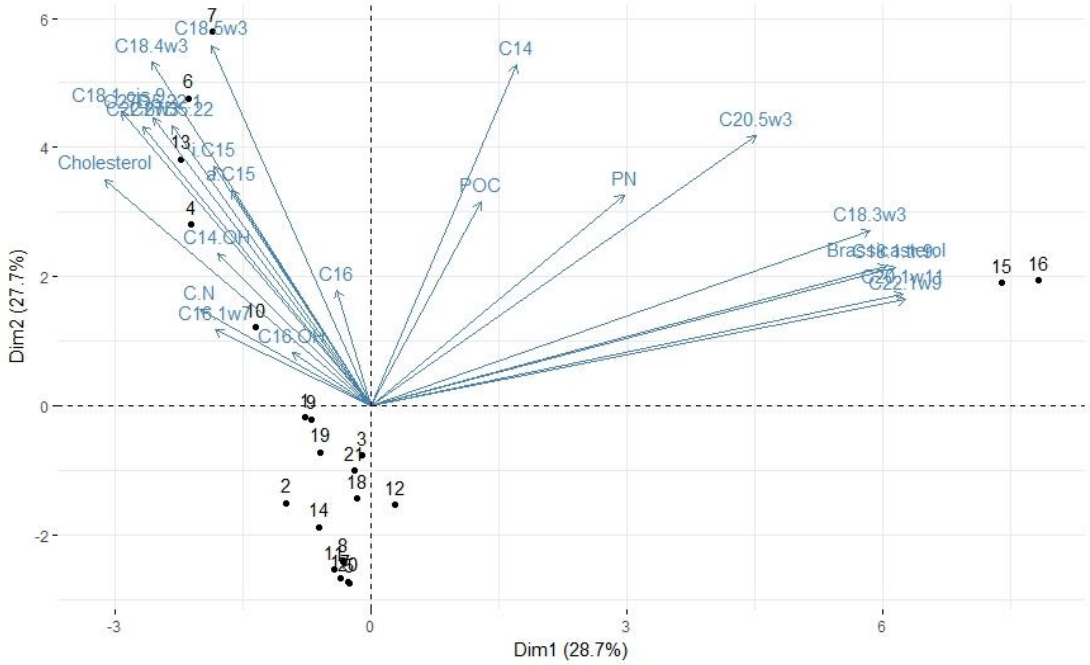

Figure 2.11 Multivariate analysis of techniques. Principle component analysis (PCA). Numbers are the sample numbers, in the order of Table 2.7 e.g. 1 is SAPs 0.7-53 µm from CCS 20 m.

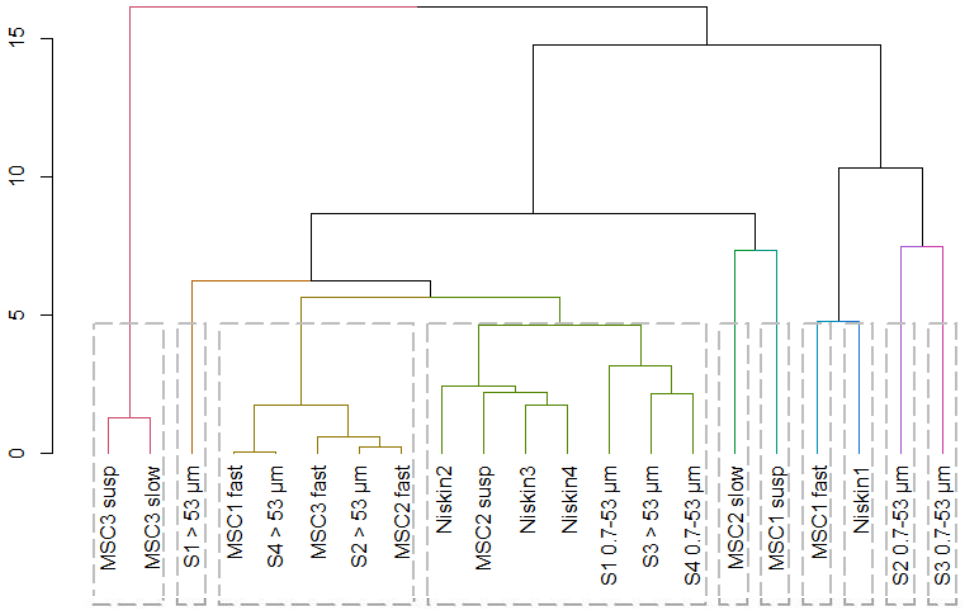

Figure 2.12 Multivariate analysis of techniques. Dendrogram. Techniques are Stand Alone Pumps (SAPs labelled S "size fraction"), Marine Snow Catcher (MSC "sinking fraction"), and Niskin bottles (Niskin). MSC susp "suspended" particles, MSC slow "slow-sinking" particles, and MSC fast "fast-sinking" particles. The number after the technique name symbolises the station number: 1. Central Celtic Sea (CCS) 20 m. 2. Central Celtic Sea (CCS) 60 m. 3. Celtic Sea two (CS2) 50 m. 4. Celtic Deep (CD) 50 m.

2.4 Discussion

2.4.1 Comparison of the bulk particles

The MSC collected the largest standing stock of POC and PN followed by the small-volume Niskin bottles and then the *in-situ* pumps. In this study, the Niskin bottle POC (2.2 ± 1.2 µM) and PN (0.4 ± 0.2 µM) were 68 ± 31% and 63 ± 28% higher than SAPs (0.1 ± 1.5 µM POC and 0.2 ± 0.2 µM PN) in the subtropical Atlantic (n = 33) and 26 ± 26% and 48 ± 29% higher for the Niskin bottle (5.8 ± 2.8 µM POC and 0.9 ± 0.4 µM PN) than the SAPs (3.8 ± 1.1 µM POC and 0.4 ± 0.2 µM PN; n = 4) in the Celtic Sea. In addition, we find that the MSC_{susp} and MSC_{slow} POC (10.8 ± 6.4 µM and 10.1 ± 6.8 µM) was on average 34 ± 26% and 30 ± 24 % higher than the Niskin bottle (7.1 ± 5.2 µM; n = 10). Differences between MSC and Niskin bottle were calculated after removal of peak-bloom 10 m samples where Niskin bottle concentrations were higher than MSC.

It is well recognised in the literature that Niskin bottles collect consistently higher POC than *in-situ* pumps. Many hypotheses have been proposed and tested. Initial studies investigated the mechanical differences between the two techniques e.g. filter type efficiency, volume filtered, filtration pressure, sorption of DOM onto filters (Moran et al., 1999; Gardner et al., 2003; Turnewitsch et al., 2007). However, they and subsequent studies concluded, the

differences observed were not large enough to explain the consistent offset (Altabet et al., 1992; Moran et al., 1999; Liu et al., 2005).

DOM sorption by the glass fibre filters is a known phenomemon (Moran et al., 1999). In this study, *in-situ* pumps had a filter "blank" subtracted to account for the effect of the larger filter area and increased DOM absorption. However, the Niskin bottles were not corrected for DOM sorption. On a previous cruise to the subtropical Atlantic, AMT25 (2015), Niskin bottle samples were filtered through double-stacked filters at one station, see section 4.2.2.1. The percentage of POC that the bottom filter collected relative to the top filter was used as a measure of DOC sorption. At the DCM this DOC sorption was 36%, at 100 m below the DCM ~50%, and at 500 m 74%. Taking this data into account, for samples in this study, we observe higher POC concentrations from the Niskin bottle. This was not true for six samples at the DCM in the northern half of the Atlantic cruise track, where the Niskin bottle concentrations were lower than SAPs after taking DOC sorption into account. Hence, the results concur with the thorough studies performed by others where DOM sorption by filters does not adequately explain the consistent offset between techniques. (Turnewitsch et al., 2007). However, it is important to consider DOM sorption and although not possible here, it would be beneficial to measure DOM sorption at multiple depths in future studies with Niskin bottles (and MSC).

The latest hypotheses for the differences between Niskin bottles and *in-situ* pumps are that the differences may be caused by particle formation in the Niskin bottles and additionally particle washout and zooplankton avoidance of the pumps (Liu et al., 2009, 2005). Liu *et* al. (2009) found that zooplankton contribute 1 to 2 μM POC to the difference between pump and Niskin bottles, where the Niskin bottles collected more zooplankton relative to the SAPs, similar to the difference observed in this study (1.2 ± 0.6 μM POC). They suggest that particle collection is influenced by filter inlet design where specific types of filter holder are more prone to particle loss in the pumps. The filter holder design used in this study (a sealed filter holder with a narrow right angled tubular opening; Figure 2.4a) was found to be the most efficient for catching and retaining zooplankton and reducing particle washout compared to other housing designs (Liu et al., 2009). The relative abundance of zooplankton biomarkers identified in samples collected by the different techniques will be discussed in the following section (2.4.2).

POC and PN concentrations were higher for the MSC (MSC_{susp} and MSC_{slow}) than Niskin bottles and more than double the concentrations of the SAPs. One concern that has previously been raised is that the Niskin bottle sampling may miss large fast-sinking particles that sink below the spigot during particle collection (Gardner, 1977; Planquette & Sherrell, 2012). This could help explain why MSC collects higher POC and PN than the Niskin bottles. However, adding the MSC_{fast} fraction from the MSC to the Niskin bottle concentration does little to change POC - due to the small contribution of "fast-sinking" particles to the total particle pool

(Table 2.6). Another explanation could be that the difference between the small-volume bottle and the pump is exaggerated when we increase bottle size. It has been noted that the type of *in*-situ pump filter housing design used in this study is not the most efficient at catching passive non-zooplankton particles (Liu et al., 2009). Perhaps it is the case that the bottles capture suspended and slow-sinking particles that are eluding the pumps. It could be that these particles are rarer and so the difference gets larger with bottle size.

Comparison of the C:N ratios between techniques highlighted some large differences between Niskin bottle and *in*-situ pumps, depending on POC concentration. Where POC concentrations were higher, in the Celtic Sea and at the chlorophyll-*a* maximum in the Atlantic (Niskin bottle > 2 µM POC), the total SAPs C:N ratio was higher than the Niskin bottle; but for waters with lower POC concentrations (Niskin bottle < 2 µM POC), 100 m below the DCM and 500 m in the Atlantic ocean, total SAPs C:N was lower than Niskin bottle (see Figure 2.7 and Table 2.8). In waters with higher POC concentrations the SAPs collected more C enriched material and the Niskin bottle collected more N-enriched, whereas in waters with lower POC concentrations SAPs collects more N-enriched material.

Table 2.8 Average (± standard deviation) C:N ratios for SAPs and Niskin bottle from the Celtic Sea (DY026) and subtropical North Atlantic. Paired t-test (degrees of freedom) with significance level, p < 0.1, p < 0.05**, p < 0.01***.*

	Niskin bottle	SAPs	t
Celtic Sea	6.0 ± 2.0	9.6 ± 3.3	2.088 (3)
Subtropical North Atlantic DCM	4.4 ± 0.6[1]	5.6 ± 0.6[1]	3.678 (7)***
Subtropical North Atlantic DCM-100 m	5.4 ± 1.1	3.8 ± 1.5	2.444 (9)**
Subtropical North Atlantic 500 m	5.2 ± 1.3	2.8 ± 1.5	1.955 (9)*

[1]excluding two stations were the SAPs ratio was less than one

The second observation is that during 2014 and 2015 in the Celtic Sea, the C:N ratio for MSC and Niskin bottle appears to highlight a change in the particles collected by each technique. The change occurs at the onset of the spring bloom (peak-bloom). Before the bloom (summer 2014 and pre-bloom) MSC has higher ratios than the Niskin bottle, but after the onset of the bloom (peak-bloom, post-bloom and summer 15) MSC has lower ratios (apart from 70 m during pre-bloom and peak-bloom, Table 2.5). This change in ratio is due to MSC collecting more POC but equal PN than the Niskin bottle before the bloom. After the bloom there is no clear trend. A change at the onset of the spring bloom is also observed in the MSC_{susp} and MSC_{slow} fractions. Below the mixed layer (50-70 m), POC and C:N is higher for MSC_{susp} than MSC_{slow} after the bloom onset. These results suggest that as the particle composition of the water column evolves, due to changing ocean dynamics, the devices are exposed to a different particle fields but also collect different particles.

2.4.2 Comparison of particle characteristics

The lipid composition of POM collected at four stations in the Celtic Sea during summer 2014 were characterised, namely the Central Celtic Sea (CCS) at 20 m and 60 m, the Celtic Sea 2 station (CS2 50 m) and the Celtic Deep (CD 50 m; Figure 2.3). Lipid concentrations varied with station and technique making up 0.3-29% of POC, which is comparable to those previously reported (Kiriakoulakis et al., 2009; Gašparović et al., 2014). Lipids can constitute up to 30% of POC in living cells during a bloom (Kattner et al., 1983). Two samples at CCS 20 m, MSC_{susp} and Niskin bottle, had much higher lipid concentrations (28,561 ng L^{-1} and 27,706 ng L^{-1}) and contributed more to POC (24 and 23%). The rest of the samples had lipid concentrations averaging 4669 ± 1694 ng L^{-1}, excluding MSC_{fast} and Niskin bottle. The fraction of lipids relative to POC varied depending on location. Generally, SAPs had the highest lipid content, apart from in the mixed layer at CCS where Niskin bottle was higher.

Specific lipid biomarkers can be used as indicators of the organic material source (Table 2.1). The dominant lipid biomarkers in the samples were C_{16} and C_{18} which are ubiquitous biomarkers and not source specific (Tolosa et al., 2004). However, other more specific biomarkers were also present including the essential fatty acids, $C_{20:5\omega3}$ (EPA), $C_{22:6\omega3}$ (DHA) and $C_{18:3\omega3}$ (ALA; and see Table 2.1). Essential fatty acids play a crucial role in organism health and functioning; many animals cannot synthesise these *de novo* so must obtained them from their diet (Bell & Tocher, 2009). Of these essential dietary nutrients, the most important are believed to be PUFAs EPA, DHA and $C_{20:4\omega6}$ (ARA; see refs in Parrish, 2009). Other essential fatty acids include $C_{18:2\omega6}$ (LIN) and ALA, although this depends on the precursors organisms contain and their concentrations (Parrish, 2009). These fatty acids, synthesised by phytoplankton, are the most common lipid biomarkers in marine phytoplankton (Lang et al., 2011). EPA along with C_{16} PUFAs and $C_{16:1\omega7}$ are typical of diatoms, DHA and C_{18} PUFAs of dinoflagellates and flagellates, whilst ALA is indicative of chlorophytes or terrestrial input in marine ecosystems (Volkman et al. 1989; Tolosa et al. 2004; Parrish 2013). The most abundant biomarkers collected by the SAPs at CCS and CS2 are all indictors of dinoflagellates and flagellates: C_{18}, $C_{18:5\ \omega\ 3}$, $C_{18:4\ \omega3}$, and DHA. Biomarkers of the other major groups of phytoplankton are present but at lower abundance (diatoms and prymnesiophytes; C_{16}, $C_{16:1\omega7}$ and EPA). The same is true for the Niskin bottles, which although dominated by sFAs also had abundant PUFAs and sterols indicative of dinoflagellates/prymnesiophytes and autotrophy. The Niskin bottle surface sample had a wider range of biomarkers than those below the mixed layer which were dominated by C_{16} and C_{18} sFAs (Appendix Figure 2.1). For CD SAPs sample, $C_{26}\Delta^{5,22}$ was the most abundant biomarker, indicative of zooplankton derived material (Sheridan et al., 2002).

Lipids can also be used to identify the presence of bacteria and zooplankton. Bacteria are identified by the presence of odd-numbered and branched-chain fatty acids (C_{15}–$C_{19;}$ Parrish,

1988; Sheridan et al., 2002; Tolosa et al., 2004). Zooplankton are identified by the presence of MUFAs and unsaturated alcohols (18:1, 20:1 and 22:1) and C_{14}, C_{16} and C_{18} fatty alcohols (Sargent et al., 1977; Sheridan et al., 2002; Dalsgaard et al., 2003; Lee et al., 2006). The sterols cholesterol and $C_{26}\Delta^{5,22}$ are also markers of zooplankton derived material (Harvey et al., 1987; Sheridan et al., 2002). Bacterial biomarkers were present in all samples at very low concentrations (0.1-2.3% of lipids; Table 2.7) apart from CS2 Niskin bottle where they made up to 59% of lipids. Summing the zooplankton marker relative concentrations the Niskin bottles had the highest concentrations for CCS 20 m and CD 50 m agreeing with the "swimmer hypothesis" that Niskin bottles collect more zooplankton than pumps (Figure 2.13). However, at stations CCS 60 m and CS2 50 m MSC_{susp} and MSC_{slow} and SAPs collected higher concentrations than Niskin bottle (Figure 2.13). This doesn't follow the "swimmer hypothesis" that zooplankton are capable of avoiding the pumps relative to the Niskin bottle (Liu et al., 2009).

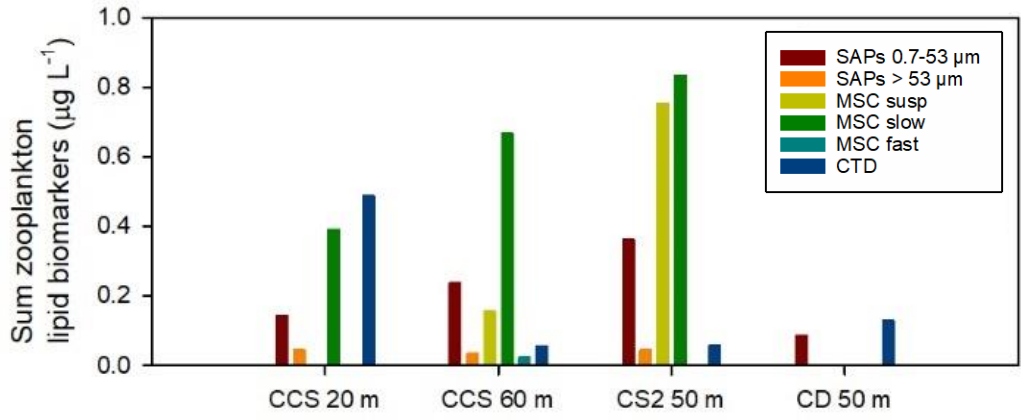

Figure 2.13 Zooplankton lipid biomarker concentrations.

Lipids can be used to investigate the source and freshness of the organic material and its lability (Table 2.1, Figure 2.10; Harvey et al., 1987; Wakeham & Lee, 1989). Unsaturated fatty acids and alcohols (PUFAs, MUFAs and unsat-OH) biosynthesised by phytoplankton and zooplankton and are somewhat labile (Iverson, 2009). The other lipid groups - sFA, OH, sterols and other - are termed semi-labile and refractory following Wolff et al. (2011). To investigate the lability of the organic matter present, a simple indicator, the ratio of saturated to unsaturated fatty acids (USFA/sFA) can be used, where a ratio >1 is indicative of more labile material. At CCS in the surface the most labile material is found in the SAPs >53 µm fraction, all other techniques collect a high proportion of semi-labile material (> 50%, Figure 2.10). Below the mixed layer both SAPs fractions and the MSC_{fast} fraction contain the most unsaturated material; MSC_{susp}, MSC_{slow} and Niskin bottles contain higher proportions of semi-labile material (>70%; Figure 2.10). Below the mixed layer at CS2 the SAPs > 53 µm fraction

and MSC_{susp} and MSC_{slow} collected more unsaturated material; MSC_{fast} and Niskin bottle contain even higher proportions of semi-labile material (Figure 2.10). At CD SAPs 0.7-53 µm and Niskin bottles collected the most unsaturated material but semi-labile material is dominant (> 50%) for all techniques. From this, we can conclude that each technique collects particles of different labilities and this varies between stations and depth and with phytoplankton patchiness.

2.4.3 Multivariate analyses

The main similarities and differences between the particle compositions collected by the different techniques were summarised by the multivariate cluster analysis. The analysis groups the samples into ten clusters, three of which contain more than one sample. The cluster with the closest related samples contains the three MSC_{fast} fractions and the > 53 µm SAPs fractions for CCS 60 m and CD. The clustering of the SAPs mesh (> 53 µm fraction) and MSC_{fast} fraction is consistent with the theory that fast-sinking particles are the larger, denser particles (marine aggregates and faecal pellets; De La Rocha & Passow, 2007). The clustering occurs as these two fractions collect the most similar concentrations of POC, PN and the most labile lipids of all the techniques. The MSC_{susp} and MSC_{slow} fractions from CS2 also cluster together, this due to their near identical elemental and lipid signature. The third, and largest cluster contains two sub-clusters: the Niskin bottle's from below the mixed layer with the MSC_{susp} fraction from CCS 60 m, and the 0.7-53 µm SAPs fractions from CCS 20 m and CD with the > 53 µm SAPs fraction from CS2. The fact that each technique's size fractions do not all group together at all stations suggests that there is high particle heterogeneity in the water.

Some of the variation in POM composition collected by different methods and between stations may be due to phytoplankton patchiness in the water and the dynamics of the tidal cycle in the Celtic Sea. During DY026, 4-9 hours passed between sampling with different techniques; during DY029 12-17 hours; DY033 12-20 hours; and in the subtropical Atlantic Ocean 0.5-2 hours typically passed between technique collection times (see section 2.2.1 for timings). The concentration of particulate material can vary throughout the day, in the oligotrophic ocean particle abundance can vary by 25% diurnally (Bishop & Wood, 2008). Although, previous studies have noted that spatial and temporal variability of particles is not likely to be a main problem given that Niskin bottle POC and PN concentrations are consistently higher than pumps regardless of season or time (Liu et al., 2005), however, patchiness could still be an important factor. Between and within Niskin bottle variability for the subtropical North Atlantic is covered in sections 3.2.3.2 for chlorophyll-*a*, and within Niskin bottle variability in sections 3.3.4.2 for picophytoplankton and 4.2.2.2 for POC. The variation between techniques may also be due to variation in phytoplankton community composition and so particle composition between locations and seasons.

2.5 Summary, limitations and recommendations

Our results show that the bottle techniques (MSC and Niskin bottle) collected more POC than the pumps, with the large-volume MSC collecting the highest concentrations. We can surmise that the SAPs GFF (0.7-53 μm) does not necessarily collect similar particles to the "suspended" and "slow-sinking" Marine Snow Catcher fractions (MSC_{susp} and MSC_{slow}) and the Niskin bottle in terms of both quantity and composition. The bottle techniques (MSC and Niskin bottle) collect particles of a similar, but not identical composition, which is highlighted by the higher POC collected by the MSC and the changes in C:N with time of year. From these observations we can say that we do not understand particle pool dynamics well enough to explain the differences between the techniques.

Whilst this study helps to shed light on the composition of the organic matter collected by different techniques, due to the number of samples (3 to 4, one of which is in the surface and 3 below the mixed layer in different locations) we cannot readily identify differences, in terms of composition and quality of the organic matter. Thus, the compositional variation between stations in this study limits our interpretation and understanding of the causes of differences in POC and PN collection by the different techniques. Ideally a larger number of samples and complimentary techniques would be used, for example, particle imaging. It is rare that oceanographic sampling takes place using more than one collection method at a time, due to time and money constraints. In this study we took advantage of the rare collection of samples using three methods at several stations in the Celtic Sea. However, now that we are placing more and more focus on biogeochemical modelling I would recommend that we take more time to consider what particle pools the different techniques collect under different conditions. Understanding what material is collected in relation to the wider pool is key when making inferences about the broader marine environment. Particle collection is a continually evolving field in marine science and it is important to retain a clear understanding of the limitations and benefits of the techniques in use.

2.6 References

Altabet, M. a., Bishop, J. K. B., & McCarthy, J. J. (1992). Differences in particulate nitrogen concentration and isotopic composition for samples collected by bottles and large-volume pumps in Gulf Stream warm-core rings and the Sargasso Sea. *Deep Sea Research Part A. Oceanographic Research Papers*, *39*, S405–S417. https://doi.org/10.1016/S0198-0149(11)80022-1

Arrigo, K. R. (2005). Marine microorganisms and global nutrient cycles. *Nature*, *437*(7057), 349–355. https://doi.org/10.1038/nature04158

Bell, M. V., & Tocher, D. R. (2009). Biosynthesis of polyunsaturated fatty acids in aquatic ecosystems: general pathways and new directions. In *Lipids in Aquatic Ecosystems* (pp. 211–236). New York, NY: Springer New York. https://doi.org/10.1007/978-0-387-89366-2_9

Benner, R., & Amon, R. M. W. (2015). The Size-Reactivity Continuum of Major Bioelements in the Ocean. *Annual Review of Marine Science*, *7*, 185–205. https://doi.org/10.1146/annurev-marine-010213-135126

Bishop, J. K. B., Lam, P. J., & Wood, T. J. (2012). Getting good particles: Accurate sampling of particles by large volume in-situ filtration. *Limnology and Oceanography: Methods*, *10*, 681–710. https://doi.org/10.4319/lom.2012.10.681

Bishop, J. K. B., & Wood, T. J. (2008). Particulate matter chemistry and dynamics in the twilight zone at VERTIGO ALOHA and K2 sites. *Deep Sea Research Part I: Oceanographic Research Papers*, *55*(12), 1684–1706. https://doi.org/10.1016/j.dsr.2008.07.012

Buesseler, K. O., & Boyd, P. W. (2009). Shedding light on processes that control particle export and flux attenuation in the twilight zone of the open ocean. *Limnology and Oceanography*, *54*(4), 1210–1232. https://doi.org/10.4319/lo.2009.54.4.1210

Christie, W. W. (1982). Esterification of Fatty-Acids in Adipose-Tissue. In *Advances in Lipid Methodology - Two* (pp. 69–111).

Dalsgaard, J., St. John, M., Kattner, G., Muller-Navarra, D., & Hagen, W. (2003). Fatty Acids As Trophic Markers In The Pelagic Marine Environment. *Advances In Marine Biology*, *46*, 225–340.

Davis, C. E., Blackbird, S., Wolff, G., Woodward, M., & Mahaffey, C. (2018). Seasonal organic matter dynamics in a temperate shelf sea. *Progress in Oceanography*. https://doi.org/10.1016/j.pocean.2018.02.021

De La Rocha, C. L., & Passow, U. (2007). Factors influencing the sinking of POC and the efficiency of the biological carbon pump. *Deep-Sea Research Part II: Topical Studies in Oceanography*, *54*, 639–658. https://doi.org/10.1016/j.dsr2.2007.01.004

Edwards, B. R., Bidle, K. D., & Van Mooy, B. a. S. (2015). Dose-dependent regulation of microbial activity on sinking particles by polyunsaturated aldehydes: Implications for the carbon cycle. *Proceedings of the National Academy of Sciences*, *112*(19), 5909–5914. https://doi.org/10.1073/pnas.1422664112

Gardner, W. D. (1977). Incomplete extraction of rapidly settling particles from water samplers. *Limnology and Oceanography*, *22*(4), 764–768.

Gardner, W. D., Richardson, M. J., Carlson, C. a., Hansell, D., & Mishonov, A. V. (2003). Determining true particulate organic carbon: Bottles, pumps and methodologies. *Deep-Sea Research Part II: Topical Studies in Oceanography*, *50*, 655–674. https://doi.org/10.1016/S0967-0645(02)00589-1

Gašparović, B., Frka, S., Koch, B. P., Zhu, Z. Y., Bracher, a., Lechtenfeld, O. J., … Kattner, G.

(2014). Factors influencing particulate lipid production in the East Atlantic Ocean. *Deep Sea Research Part I: Oceanographic Research Papers*, *89*, 56–67. https://doi.org/10.1016/j.dsr.2014.04.005

Geider, R., & Roche, J. La. (2002). Redfield revisited: variability of C:N:P in marine microalgae and its biochemical basis. *European Journal of Phycology*, *37*, 37–41. https://doi.org/10.1017/S0967026201003456

Harvey, H. R., Eglinton, G., O'Hara, S. C. M., & Corner, E. D. S. (1987). Biotransformation and assimilation of dietary lipids by Calanus feeding on a dinoflagellate. *Geochimica et Cosmochimica Acta*, *51*, 3031–3034.

Hayakawa, K., Handa, N., & Wong, C. S. (1996). Changes in the composition of fatty acids in sinking matter during a diatom bloom in a controlled experimental ecosystem. *Journal of Experimental Marine Biology and Ecology*, *208*(1–2), 29–43. https://doi.org/10.1016/0022-0981(95)00158-1

Hunter, C. N., Gordon, R. M., Fitzwater, S. E., & Coale, K. H. (1996). A Rosette system for the collection of trace metal clean water. *Limnol. Oceangr.*, *41*(6), 1367–1372.

Iverson, S. J. (2009). Tracing aquatic food webs using fatty acids: from qualitative indicators to quantitative determination. In T. Arts, Michael, M. J. Kainz, & M. T. Brett (Eds.), *Lipids in Aquatic Ecosystems* (1st ed., pp. 281–308). New York: Springer.

Jackson, G. A., & Burd, A. B. (2015). Simulating aggregate dynamics in ocean biogeochemical models. *Progress in Oceanography*, *133*, 55–65. https://doi.org/10.1016/j.pocean.2014.08.014

Kattner, G., Gercken, G., & Eberlein, K. (1983). Development of lipids during a spring plankton bloom in the northern North Sea. I. Particulate fatty acids. *Marine Chemistry*, *14*(2), 149–162. https://doi.org/10.1016/0304-4203(83)90038-5

Kiriakoulakis, K., Vilas, J. C., Blackbird, S. J., Arístegui, J., & Wolff, G. a. (2009). Seamounts and organic matter—Is there an effect? The case of Sedlo and Seine seamounts, Part 2. Composition of suspended particulate organic matter. *Deep Sea Research Part II: Topical Studies in Oceanography*, *56*(25), 2631–2645. https://doi.org/10.1016/j.dsr2.2008.12.024

Lampitt, R. S., Wishner, K. F., Turley, C. M., & Angel, M. V. (1993). Marine snow studies in the Northeast Atlantic Ocean: distribution, composition and role as a food source for migrating plankton. *Marine Biology: International Journal on Life in Oceans and Coastal Waters*, *116*(4), 689–702. https://doi.org/10.1007/BF00355486

Lang, I., Hodac, L., Friedl, T., & Feussner, I. (2011). Fatty acid profiles and their distribution patterns in microalgae: a comprehensive analysis of more than 2000 strains from the SAG culture collection. *BMC Plant Biology*, *11*, 124. https://doi.org/10.1186/1471-2229-11-124

Laurenceau-Cornec, E. C., Trull, T. W., Davies, D. M., De La Rocha, C. L., & Blain, S. (2015). Phytoplankton morphology controls on marine snow sinking velocity. *Marine Ecology Progress Series*, *520*, 35–56. https://doi.org/10.3354/meps11116

Lee, C., Wakeham, S., & Arnosti, C. (2004). Particulate Organic Matter in the Sea: The Composition Conundrum. *Source: AMBIO: A Journal of the Human Environment Published By: Royal Swedish Academy of Sciences Ambio*, *33*(8), 565–575. https://doi.org/10.1579/0044-7447-33.8.565

Lee, R. F., Hagen, W., & Kattner, G. (2006). Lipid storage in marine zooplankton. *Marine Ecology Progress Series*, *307*(1863), 273–306. https://doi.org/Doi 10.3354/Meps307273

Liu, Z., Cochran, J. K., Lee, C., Gasser, B., Miquel, J. C., & Wakeham, S. G. (2009). Further investigations on why POC concentrations differ in samples collected by Niskin bottle and in situ pump. *Deep-Sea Research Part II: Topical Studies in Oceanography*, *56*(18),

1558–1567. https://doi.org/10.1016/j.dsr2.2008.12.019

Liu, Z., Stewart, G., Cochran, J. K., Lee, C., Armstrong, R. a., Hirschberg, D. J., … Miquel, J. C. (2005). Why do POC concentrations measured using Niskin bottle collections sometimes differ from those using in-situ pumps? *Deep-Sea Research Part I: Oceanographic Research Papers*, *52*, 1324–1344. https://doi.org/10.1016/j.dsr.2005.02.005

Martiny, A. C., Vrugt, J. A., Primeau, F. W., & Lomas, M. W. (2013). Regional variation in the particulate organic carbon to nitrogen ratio in the surface ocean. *Global Biogeochemical Cycles*, *27*(3), 723–731. https://doi.org/10.1002/gbc.20061

McDonnell, A. M. P., Lam, P. J., Lamborg, C. H., Buesseler, K. O., Sanders, R., Riley, J. S., … Bishop, J. K. B. (2015). The oceanographic toolbox for the collection of sinking and suspended marine particles. *Progress in Oceanography*. https://doi.org/10.1016/j.pocean.2015.01.007

Mei, Z. P., Legendre, L., Tremblay, J. É., Miller, L. A., Gratton, Y., Lovejoy, C., … Gosselin, M. (2005). Carbon to nitrogen (C:N) stoichiometry of the spring-summer phytoplankton bloom in the North Water Polynya (NOW). *Deep-Sea Research Part I: Oceanographic Research Papers*, *52*(12), 2301–2314. https://doi.org/10.1016/j.dsr.2005.07.001

Moran, S. B., Charette, M. a., Pike, S. M., & Wicklund, C. a. (1999). Differences in seawater particulate organic carbon concentration in samples collected using small- and large-volume methods: The importance of DOC adsorption to the filter blank. *Marine Chemistry*, *67*(1–2), 33–42. https://doi.org/10.1016/S0304-4203(99)00047-X

Parrish, C. C. (1988). Dissolved and Particulate Marine Lipid Classes: A Review. *Marine Chemistry*, *23*, 17–40.

Parrish, C. C. (2009). Essential fatty acids in aquatic food webs. In *Lipids in Aquatic Ecosystems* (pp. 309–326). New York, NY: Springer New York. https://doi.org/10.1007/978-0-387-89366-2_13

Parrish, C. C. (2013). Lipids in Marine Ecosystems. *ISRN Oceanography*, *2013*, 1–16. https://doi.org/10.5402/2013/604045

Philp, R. P., & Lewis, C. A. (1987). Organic Geochemistry of biomarkers. *Annual Review of Earth and Planetary Sciences*, *15*, 363–395. https://doi.org/10.1007/978-1-4615-2890-6

Planquette, H., & Sherrell, R. M. (2012). Sampling for particulate trace element determination using water sampling bottles: Methodology and comparison to in situ pumps. *Limnology and Oceanography: Methods*, *10*(5), 367–388. https://doi.org/10.4319/lom.2012.10.367

Poulton, A. J., Davis, C. E., Daniels, C. J., Mayers, K. M. J., Harris, C., Tarran, G. A., … Woodward, E. M. S. (2018). Seasonal phosphorus and carbon dynamics in a temperate shelf sea (Celtic Sea). *Progress in Oceanography*. https://doi.org/10.1016/j.pocean.2017.11.001

Redfield, A. C. (1958). The biological control of chemical factors in the environment. *Aquatic Ecology*, *46*, 19–29. https://doi.org/10.5194/bg-11-1599-2014

Riley, J. S., Sanders, R., Marsay, C., Le Moigne, F. a C., Achterberg, E. P., & Poulton, a. J. (2012). The relative contribution of fast and slow sinking particles to ocean carbon export. *Global Biogeochemical Cycles*, *26*, 1–10. https://doi.org/10.1029/2011GB004085

Sanders, R., Henson, S. a., Koski, M., De La Rocha, C. L., Painter, S. C., Poulton, A. J., … Martin, A. P. (2014). The Biological Carbon Pump in the North Atlantic. *Progress in Oceanography*, *129*, 200–218. https://doi.org/10.1016/j.pocean.2014.05.005

Sargent, J. R., Gatten, R. R., & McIntosh, R. (1977). Wax esters in the marine environment - their occurrence, formation, transformation and ultimate fates. *Marine Chemistry*, *5*(4–6), 573–584. https://doi.org/10.1016/0304-4203(77)90043-3

Sharples, J. (2007). Potential impacts of the spring-neap tidal cycle on shelf sea primary production. *Journal of Plankton Research*, *30*(2), 183–197. https://doi.org/10.1093/plankt/fbm088

Sheridan, C. ., Lee, C., Wakeham, S. ., & Bishop, J. K. . (2002). Suspended particle organic composition and cycling in surface and midwaters of the equatorial Pacific Ocean. *Deep Sea Research Part I: Oceanographic Research Papers*, *49*(11), 1983–2008. https://doi.org/10.1016/S0967-0637(02)00118-8

Steinberg, D. K., & Landry, M. R. (2017). Zooplankton and the Ocean Carbon Cycle. *Annual Review of Marine Science*, *9*(1), 413–444. https://doi.org/10.1146/annurev-marine-010814-015924

Tolosa, I., Vescovali, I., LeBlond, N., Marty, J.-C., de Mora, S., & Prieur, L. (2004). Distribution of pigments and fatty acid biomarkers in particulate matter from the frontal structure of the Alboran Sea (SW Mediterranean Sea). *Marine Chemistry*, *88*(3–4), 103–125. https://doi.org/10.1016/j.marchem.2004.03.005

Turner, J. T. (2015). Zooplankton fecal pellets, marine snow, phytodetritus and the ocean's biological pump. *Progress in Oceanography*, *130*, 205–248. https://doi.org/10.1016/j.pocean.2014.08.005

Turnewitsch, R., Springer, B. M., Kiriakoulakis, K., Vilas, J. C., Arístegui, J., Wolff, G., … Waniek, J. J. (2007). Determination of particulate organic carbon (POC) in seawater: The relative methodological importance of artificial gains and losses in two glass-fiber-filter-based techniques. *Marine Chemistry*, *105*(3–4), 208–228. https://doi.org/10.1016/j.marchem.2007.01.017

Tweddle, J. F., Sharples, J., Palmer, M. R., Davidson, K., & McNeill, S. (2013). Enhanced nutrient fluxes at the shelf sea seasonal thermocline caused by stratified flow over a bank. *Progress in Oceanography*, *117*, 37–47. https://doi.org/10.1016/j.pocean.2013.06.018

Verdugo, P., Alldredge, A. L., Azam, F., Kirchman, D. L., Passow, U., & Santschi, P. H. (2004). The oceanic gel phase: A bridge in the DOM-POM continuum. *Marine Chemistry*, *92*(1–4), 67–85. https://doi.org/10.1016/j.marchem.2004.06.017

Volkman, J. K. (2006). Lipid Markers for Marine Organic Matter. In J. K. Volkman (Ed.), *Marine Organic Matter: Biomarkers, Isotopes and DNA* (pp. 27–70). Berlin/Heidelberg: Springer-Verlag. https://doi.org/10.1007/698_2_002

Volkman, J. K., Jeffrey, S. W., Nichols, P. D., Rogers, G. I., & Garland, C. D. (1989). Fatty acid and lipid composition of 10 species of microalgae used in mariculture. *Journal of Experimental Marine Biology and Ecology*, *128*(3), 219–240. https://doi.org/10.1016/0022-0981(89)90029-4

Volkman, J. K., & Tanoue, E. (2002). Chemical and Biological Studies of Particulate Organic Matter in the Ocean. *Journal of Oceanography*. https://doi.org/10.1023/A:1015809708632

Wakeham, S. G., & Lee, C. (1989). Organic geochemistry of particulate matter in the ocean: The role of particles in oceanic sedimentary cycles. *Org. Geochem*, *14*(1), 83–96.

Wolff, G. A., Billett, D. S. M., Bett, B. J., Holtvoeth, J., FitzGeorge-Balfour, T., Fisher, E. H., … Chaillan, F. (2011). The effects of natural iron fertilisation on deep-sea ecology: The Crozet Plateau, southern Indian ocean. *PLoS ONE*, *6*(6). https://doi.org/10.1371/journal.pone.0020697

Yamamuro, M., & Kayanne, H. (1995). Rapid direct determination of organic carbon and nitrogen in carbonate-bearing sediments with a Yanaco MT-5 CHN analyzer. *Limnology and Oceanography*, *40*(5), 1001–1005. https://doi.org/10.4319/lo.1995.40.5.1001

Yanada, M., & Maita, Y. (1995). Regional and seasonal variations of biomass and bio-mediated materials in the North Pacific Ocean. In H. Sakai & Y. Nozaki (Eds.), *Biogeochemical*

Processes and Ocean Flux in the Western Pacific (pp. 293–306). Tokyo: Terra Scientific Publishing Company (TERRAPUB).

3 What controls the distribution of phytoplankton in the subtropical North Atlantic?

3.1 Introduction

Phytoplankton are the primary producers of the ocean; single-celled photosynthetic organisms that provide energy and carbon to the marine ecosystem. Phytoplankton come in a staggering array of sizes and forms, ranging over four orders of magnitude from 0.2 μm to 2000 μm (Sieburth et al., 1978; Finkel et al., 2010). The classic size classification of plankton, the Sieburth-scale, splits phytoplankton into 0.2-2 μm (picopyhytoplankton), 2-20 μm (nanophytoplankton) and >20 μm (microphytoplankton). Small cells tend to out-perform larger cells in the subtropical oligotrophic regions as their larger surface area to volume ratio provides an advantage for light and resource acquisition (Raven, 1998; Marañón et al., 2001; Finkel et al., 2010). Thus phytoplankton tend to be dominated by picophytoplankton in the oligotrophic ocean (Zubkov et al., 1998, 2000; Marañón et al., 2001; Cáceres et al., 2016; Heywood et al., 2006; Poulton et al., 2006; Tarran et al., 2006).

There are two types of phytoplankton cell, prokaryotes and eukaryotes. The main difference between the two is the former lacks a nucleus and organelles (Gould et al., 2008; Massana & Logares, 2013; Ku et al., 2014; Zimorski et al., 2014). In addition, prokaryotes and eukaryotes contain different light harvesting antennas for photosynthesis, prokaryotes have phycobilisome-based antenna whereas, eukaryotes contain light harvesting complexes in thylakoid membranes (Neilson and Durnford, 2010). Prokaryotes include heterotrophic bacteria and the photosynthesising cyanobacteria *Prochlorococcus* and *Synechococcus*. In oligotrophic waters, *Prochlorococcus* followed by *Synechococcus* are the most numerous phytoplankton species (Campbell & Vaulot, 1993; Buck et al., 1996; Campbell et al., 1997; Zubkov et al., 1998, 2000; Heywood et al., 2006; Latasa et al., 2010). Eukaryotes are highly diverse and include all other phytoplankton (Parker et al., 2008). The major groups of open ocean eukaryotic phytoplankton are Bacillariophyceae (diatoms) and Dinophyceae (dinoflagellates). Other phytoplankton are grouped into a generic 'flagellate' category which includes Prymnesiophyceae (e.g. coccolithophores), Prasinophyceae, Raphidophyceae, Dictochophyceae (silicoflagellates), Cryptophyceae, Euglenophyceae, Pelagophyceae, and Chrysophyceae (Hoppenrath et al., 2009; Kraberg et al., 2010; Latasa et al., 2010; Treusch et al., 2012; Estrada et al., 2016). Eukaryotes vary in their evolutionary history, mode of life, cell composition and structure. Individual phytoplankton cells are normally solitary, but some form chains and colonies. Therefore, phytoplankton can also be classified by size, ecological traits and ecological function.

3.1.1 Measuring phytoplankton

Scientists use a variety of techniques to study phytoplankton. The first observations of phytoplankton were through light microscopes or using basic colourmetric analysis to characterise the community (red, green, brown, diatomaceous algae). Today, advances in technology have improved these approaches. We now use electron and fluorescence microscopy, fluorometers, high-performance liquid chromatography (HPLC), flow cytometry, and imaging cytometry to help characterise the phytoplankton community (Johnson & Martiny, 2014). Most of these techniques involve the measurement of chlorophyll-*a*. Chlorophyll-*a* is a universal pigment found in all photosynthesising cells, except anoxygenic photosynthetic bacteria (Hanada, 2016). The fact that chlorophyll-*a* has high intercellular content and chlorophyll-*a* fluorescence is an easy measurement to take means it is used globally as a proxy of phytoplankton abundance and biomass (Martin, 2004). In addition, a wide range of techniques have been developed to help study phytoplankton communities including molecular analyses (e.g. DNA and RNA sequencing), elemental analyses (dissolved and particulate C, N, P), isotopic analyses (N,^{14}C), biomarker analyses (amino acids, lipids), primary production and carbon fixation rate measurement, and remote sensing of ocean colour via satellites. These techniques used in conjunction with nutrient and oxygen data provide insight into the distribution and controls on the phytoplankton community.

3.1.2 Results from RidgeMix and aims of this study

This study aims to investigate the distribution of phytoplankton in the subtropical North Atlantic Ocean and assess whether abrupt topography influences phytoplankton dynamics. During RidgeMix, Tuerena *et al.*, (submitted) observed diapycnal nitrate fluxes into the base of the deep chlorophyll-*a* maximum (DCM) that were an order of magnitude higher over the Mid-Atlantic Ridge (0.033 ± 0.026 mol N m^{-2} y^{-1}) compared to the adjacent basin (0.002 ± 0.002 mol N m^{-2} y^{-1}; Figure 3.1b) due to an order of magnitude increase in vertical turbulent mixing

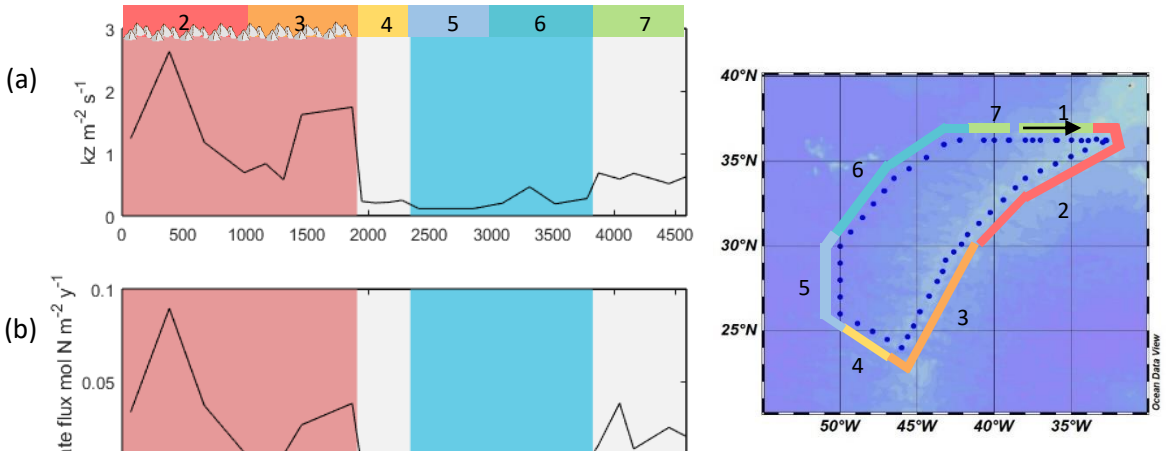

Figure 3.1 Vertical diffusivity (a) and nitrate flux (b) at the base of the DCM (from 500 m to the base of the DCM). Data from over the ridge is highlighted in red and over the basin, blue. Data is replotted from Tuerena et al (submitted).

over the ridge ($1.3 \times 10^{-5} \pm 6.7 \times 10^{-6}$ m^{-2} s^{-1}) versus basin ($2.3 \times 10^{-6} \pm 1.3 \times 10^{-6}$ m^{-2} s^{-1}; Figure 3.1a) and a steeper nitricline.

I hypothesise that increased vertical turbulent mixing and nutrient fluxes over the Mid-Atlantic Ridge will enhance biomass and shift the phytoplankton community towards larger cells, such as diatoms, in the subtropical North Atlantic Ocean. Two approaches were used: community size structure and species identification. The phytoplankton community size-structure was assessed using size-fractionated chlorophyll-*a* (0.2-2 µm (pico), 2-20 µm (nano), and > 20 µm (micro)) and the main phytoplankton groups were quantified using flow cytometry, for species < 10 µm, and light/phase microscopy, for species > 10 µm. Firstly, the distribution, size characteristics and species of phytoplankton were assessed in terms of their vertical, horizontal and temporal distribution. Secondly, I investigated whether the abrupt topography of the Mid-Atlantic ridge and seamounts influence phytoplankton dynamics. Initially, results from laboratory tests on chlorophyll-*a* extraction time, precision of collection of chlorophyll-*a* and phytoplankton, and cell size within flow cytometric analysis will be presented.

3.2 Method

3.2.1 Location

Samples were collected during two cruises aboard the RRS James Clark Ross; (1) the 25th annual Atlantic Meridional Transect (AMT25) from Immingham (UK) to Port Stanley, Falklands, 15th September – 3rd November 2015 and (2) RidgeMix (JR15007), from Trinidad & Tobago to Immingham (UK), 25th May – 10th July 2016. AMT25 sampling focused on the subtropical North Atlantic just south of the Azores, over the Sierra Leone Rise and Rio Grande Rise (Figure 3.2a, b and c). RidgeMix focused on the subtropical North Atlantic (Figure 3.2d).

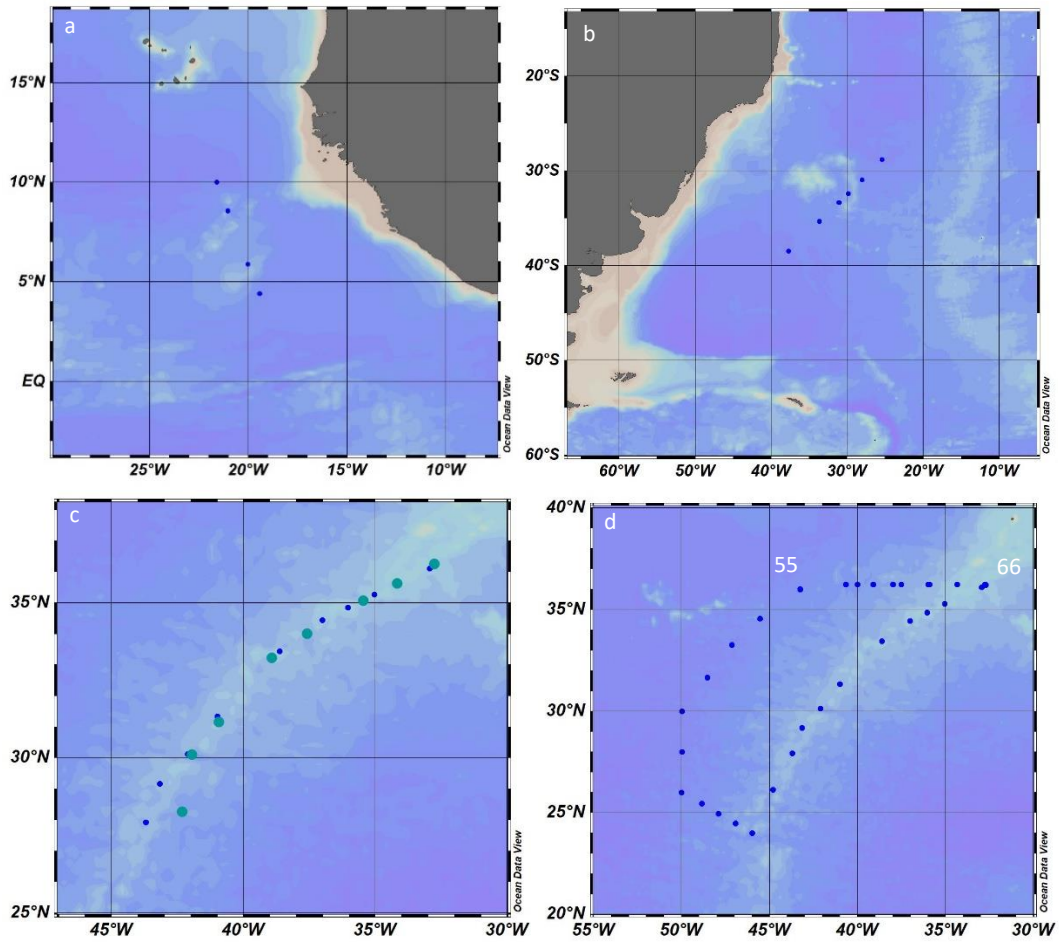

Figure 3.2 CTD sample collection stations for (a) over the Sierra Leone Rise during AMT25 (b) over the Rio Grande Rise during AMT25, (c) seasonal comparison between November 2015 (AMT25, turquoise dots) and June 2016 (RidgeMix, dark blue dots), and (d) RidgeMix, June 2016. CTDs 55 and 66 are labelled on the RidgeMix cruise track.

3.2.2 Sample collection

Water samples were collected using 20 L Niskin bottles in a 24-bottle rosette mounted on a stainless-steel frame (CTD). Sensors to measure temperature, conductivity, pressure, fluorescence, PAR, dissolved oxygen and transmission were attached to the frame. Sensors for fluorescence and oxygen were calibrated for each cast using samples from 5 depths.

From the sensor measurements density, mixed layer depth, buoyancy frequency and 1% light level were calculated. Density was calculated following Fofonoff & Millard (1983) using a Toolbox developed by Phil Morgan in MatLab. The mixed layer depth was calculated as where the density was 0.03 kg m^{-3} greater than the density at 10 m (Mignot et al., 2014). The buoyancy frequency (Brundt Väisällä frequency, N) was calculated using equation 3.1, where g is gravitational acceleration, ρref is potential density at a reference point, δρ is the change in density and δz the change in depth.

Equation 3.1 $$N = \sqrt{\frac{g}{\rho ref}\frac{\delta\rho}{\delta z}}$$

The depth of the euphotic zone was defined as 1% of the surface PAR (Ryther 1956; Letelier et al., 2004) and was only calculated for CTDs deployed around midday (10:20-15:43, n = 12). The slope of the nitracline was calculated from 500 m to 0 µM nitrate (defined as the nitrate gradient or slope), apart from on the northern transect where the nitrate intercept was identified manually due to an abrupt change to a shallow nitracline slope around 50 to 100 m.

CTD Niskin bottles were subsampled for dissolved oxygen, nutrients (nitrite, nitrate, phosphate, silicate), picophytoplankton, size-fractionated chlorophyll-*a* and phytoplankton microscopy. Samples for size-fractionated chlorophyll-*a* and picophytoplankton were collected from the top 300 m with the aim of characterising the chlorophyll-*a* profile. To that effect, 8-14 samples were collected in a depth profile at each station based on the downcast fluorometer profile. Microscopy samples were collected from 10 m and the chlorophyll-*a* maximum (deep chlorophyll-*a* maximum; DCM).

3.2.3 Size-fractionated chlorophyll-*a*

Seawater samples for size-fractionated chlorophyll-*a* were collected by transferring 1L of seawater from the Niskin bottle into 1 L brown bottles, which were triple rinsed with milli-Q and seawater. Analysis was performed on-board by filtering between 0.25 and 1L through sequential filters of pore size 20 µm, 2 µm and 0.2 µm (45 mm polycarbonate filters) in a size-fractionated chlorophyll-*a* 'rig'. After filtration samples were folded and transferred into labelled glass tubes with screw-cap lids. 5 ml of 90% acetone was added in the fume cupboard and samples were stored at 4°C in the fridge for 24 hours. Sample raw fluorescence (RFU) was measured using a Turner Trilogy Fluorometer and chlorophyll-*a* concentrations calculated by calibrating fluorescence with chlorophyll-*a* standards of known concentration. Prior to sample fluorescence measurement, three blanks and two solid standards were measured to confirm instrument stability. The fluorometer cuvette was triple acetone rinsed between samples.

3.2.3.1 Chlorophyll-a extraction experiment

This experiment was to define the efficiency of chlorophyll-*a* extraction with time (hours) after 90% acetone addition, to determine whether a minimum chlorophyll-*a* extraction time was required and whether chlorophyll-*a* concentration decreased with time due to chlorophyll degradation. To assess whether chlorophyll-*a* extraction time affects concentration, 5 L of ship underway water was collected at 05:18 on 26th October 2015 at 30°18.7397'S 27°21.1087'W. The bottle was inverted 3 times and 250 ml were filtered through twenty 0.2 µm polycarbonate membrane filters. 5 ml of 90% acetone was added to extract the chlorophyll-*a* and samples were stored in the fridge at 4°C. Samples were then removed from the fridge and analysed in the fluorometer at 0, 2, 4, 6, 8, 12, 17, 20, 23, 26, 34, and 38 hours. Three samples were analysed at 4, 12, 26, and 38 hours, where we find 11%, 16%, 16% and 1% variation (CV) respectively. Chlorophyll-*a* concentrations were low < 0.1 µg L^{-1}. After the initial 5-10 hours the

chlorophyll-*a* concentration become constant (Figure 3.3). This supports previous studies where chlorophyll-*a* was extracted overnight at -20°C (Marañón et al., 2001; Pérez et al., 2006; Poulton et al., 2006; Teira et al., 2005). Holm-Hansen and Riemann report no loss in chlorophyll-*a* after 3 weeks storage at -20°C (1978). In this study, for convenience, an extraction time of 24 hours was used. RFU precision was tested by taking triplicate measurements for 7 samples. The variation in RFU caused 3.3 ± 1.5% variation in chlorophyll-*a* concentrations.

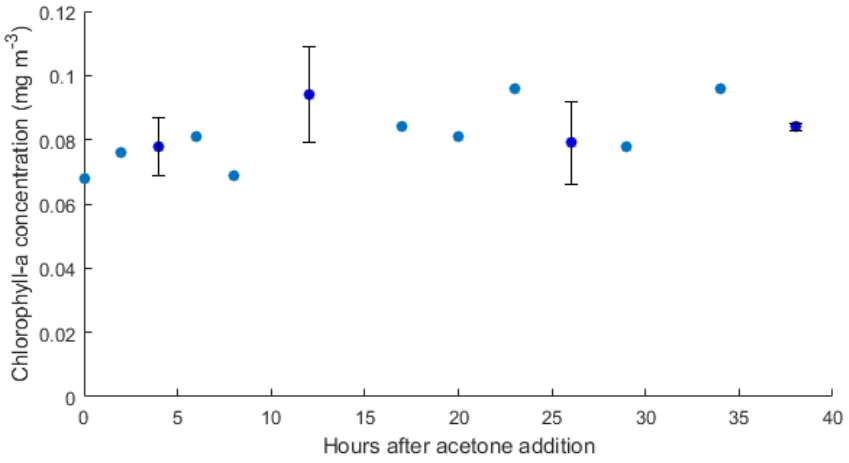

Figure 3.3 Chlorophyll-a extraction experiment. Chlorophyll-a concentration x hours after acetone addition.

3.2.3.2 Sample replication (sample error)

Phytoplankton patchiness occurs at all scales, from the microscale to the mesoscale (Durham et al., 2013; Mahadevan, 2016). To assess how variable size-fractionated chlorophyll-*a* concentrations were and before assessing daily and seasonal variability we first investigated size-fractionated chlorophyll-*a* precision within and between Niskin bottles. During AMT, we collected samples from three Niskin bottles at 130 m at CTD 17. Chlorophyll-*a* concentrations averaged 0.19 ± 0.08 mg m^{-3} varying by 41% between bottles (Appendix Table 3.1). During RidgeMix we collected replicate samples from the surface, the DCM and 300 m to test within Niskin bottle variation (Appendix Table 3.1). Intra-Niskin bottle variation was lower but ranged between 5 and 22%.

3.2.4 Picophytoplankton analysis

Samples for picophytoplankton analysis were collected using 125 ml polycarbonate bottles. Samples were collected straight from the spigot after triple rinsing with Milli-Q and seawater. In the fume hood 1.9 ml of seawater sample was pipetted into 2 ml cryovials containing 20 µL of 50% Glutaraldehyde Solution (0.5% glutaraldehyde). The vials were inverted slowly ten

times and stored in the fridge at 4°C. After 1 hour, samples were flash-frozen using liquid nitrogen and stored in the freezer at -80°C until transport back to the UK on dry ice.

Samples were analysed using a flow cytometer (FACSort™ BØØ43), on-ship by Glen Tarran during AMT25, and at Plymouth Marine Laboratory after RidgeMix. Picophytoplankton cells were identified using side scatter (90° to laser beam, 488nm), chlorophyll fluorescence (red, 650nm) and phycoerythrin fluorescence (orange, 585nm). Six groups of picophytoplankton were identified and enumerated: *Prochlorococcus*, *Synechococcus*, picoeukaryotes, nanoeukaryotes, coccolithophores and cryptophytes. Total heterotrophic bacteria (high and low nucleic acid groups) were also enumerated using SybrGreenI DNA-stain mixed with kcitrate (300 µM) and 500 µL pipetted into each 2 ml sample. Prokaryotes (*Prochlorococcus*, *Synechococcus*, heterotrophic bacteria) were identified using side scatter and red fluorescence. Eukaryotes (picoeukaryotes, nanoeukaryotes, coccolithophores and cryptophytes) using red and orange fluorescence. *Prochlorococcus* cells in surface waters contain very low levels of chlorophyll, we validated these surface cell counts with comparison to DNA stained counts of *Prochlorococcus*.

Cell abundance was calculated using equation 3.3 where the flow rate was calculated using equation 3.2. Flow rates were calibrated using a known concentration (1.03418 x 10^6 ml^{-1}) of 3.6 µm diameter beads (Beckman Coulter™ Flowset™ fluorospheres, Lot #7524034), diluted by ten.

Equation 3.2
$$Flow\ rate\ (\mu L\ min^{-1}) = \frac{\frac{Total\ count}{Diluted\ bead\ concentration} x1000}{2}$$

Equation 3.3
$$Cells/ml = cell\ count\ x \frac{1000}{flow\ rate\ x\ analysis\ time\ (mins)}\ x\ \frac{2240}{2000}$$

3.2.4.1 Picophytoplankton cell sizing

To compare size-fractionated chlorophyll-*a* to picophytoplankton groups identified by the flow cytometer the median cell size of each group was calculated. To find the median cell size for each group of picophytoplankton, 2 ml samples from the chlorophyll-*a* maximum at two stations were filtered through 0.2, 0.4, 0.6, 0.8, 1, 2, 3, 5, 8, and 10 µm polycarbonate filters. The filtered 2 ml samples were then run through the flow cytometer and the six picophytoplankton groups identified and enumerated. The cell count per filter was then plotted against % of unfiltered sample and the size at 50% of unfiltered sample recorded (Figure 3.4). A variety of filter types were used: Whatman Nuclepore Track-Etch membrane for 0.2, 0.8, 2, 8, and 10 µm; Osmonics Inc. Poretics polycarbonate filers for 0.4 and 5 µm; Millipore for 0.6 and 3 µm; and Whatman cyclopore Track Etched membrane for 1 µm. Filters were mounted in a Fisher M1650BB holder and filtered by gravity.

The two CTDs sampled for cell size were CTD 55 and 66 (Figure 3.2d). Cell sizes, shown in Table 3.1, are similar to previous studies (Campbell et al., 1994; Morel et al., 1993; Veldhuis & Kraay, 2000; Wei et al., 2018). *Prochlorococcus* is the smallest of the picophytoplankton followed by *Synechococcus* and then picoeukaryotes. Heterotrophic bacteria are the smallest picoplankton. Cell size (side scatter) was observed to increase with depth. Although we were unable to quantify this, others have observed similar patterns (Chen et al., 2011; Zubkov et al., 1998).

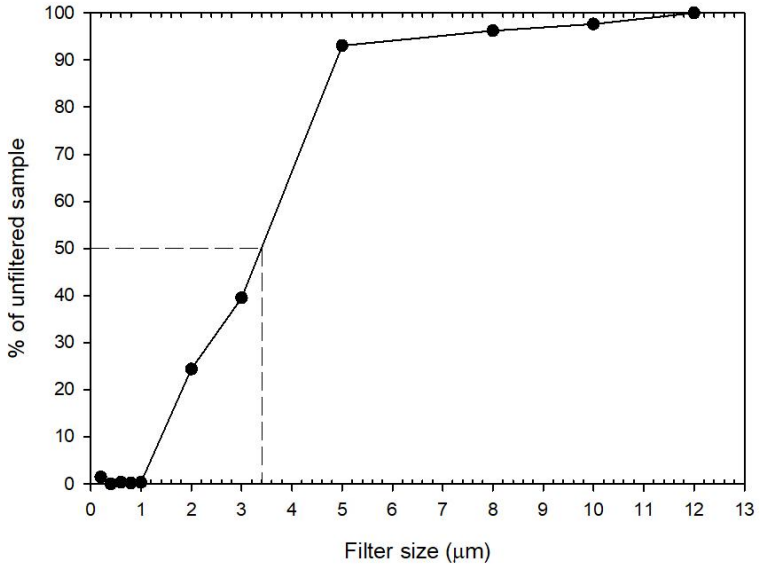

Figure 3.4 Example showing how average cell size was calculated for the picophytoplankton groups. The example is CTD 66, picoeukaryotes. On the x axis is filter pore-size (µm), on the y axis is the % cell count of the unfiltered sample. The unfiltered sample is filter size 12 - which is 100% of the cell count. The dashed line shows median cell size of 3.38 µm.

Table 3.1 Picophytoplankton group average cell size (µm) for two stations CTD 55-73 m and 66-102 m during RidgeMix. Listed in size order.

Group	CTD 55 (µm)	CTD 66 (µm)
Heterotrophic bacteria	0.52	0.55
Prochlorococcus	0.92	0.93
Synechococcus	1.08	2.08
Picoeukaryotes	2.36	3.38
Nanoeukaryotes	4.39	4.9
Coccolithophores	10.3	8.64
Cryptophytes	-	-

3.2.4.2 Sample replication (sample error)

To assess how variable picophytoplankton cell counts were and before we conducted daily and seasonal variability analyses we investigated cell count precision within Niskin bottles. Microscale picoplankton variability was tested at four depths: the DCM at CTD 55 (northwest

corner); and the surface, DCM and 300 m at CTD 66 (northeast corner; Figure 3.2d). Samples from 300 m had a low mean picophytoplankton cell count of 38 cells ml^{-1} (n = 3). Samples from 10 m had a mean cell count of 1.4 x 10^4 cells ml^{-1} and the DCM 6.3 x 10^4 cells ml^{-1} and 6.9 x 10^4 cells ml^{-1} (n = 3). All picophytoplankton groups show high variability (Table 3.2). Mean *Prochlorococcus* variation was 32 ± 34%, *Synechococcus* 6 ± 5%, picoeukaryotes 22 ± 23%, nanoeukaryotes 44 ± 30%, coccolithophores 57 ± 64%, cryptophytes 19 ± 23%, and heterotrophic bacteria 27 ± 45%. Depth and station appears to influence the degree of variability of each group, see Table 3.2. For example, the two samples from the DCM show similar variation per group for all picophytoplankton groups, yet heterotrophic bacteria counts are far more variable at CTD 66 than 55 (94% compared to 11%). More data would be required to determine in-bottle variability.

Table 3.2 Replicate samples from the same Niskin bottle analysed for picophytoplankton: heterotrophic bacteria (Hbac), Prochlorococcus (Pro), Synechococcus (Syn), picoeukaryotes (Peuk), nanoeukaryotes (Neuk), coccolithophores (Cocco) and cryptophytes (Crypt). Cell counts (cells ml^{-1}) are presented as mean ± standard deviation (n = 3, 3, 2, 3). The coefficient of variation (CV; % variance) is recorded.

CTD - depth (m)	Hbact (x 10^4 cells ml^{-1})	Pro (x10^3 cells ml^{-1})	Syn (x 10^2 cells ml^{-1})	Peuk (x 10^2 cells ml^{-1})	Neuk (cells ml^{-1})	Cocco (cells ml^{-1})	Crypt (cells ml^{-1})
CTD 55 - 73 m	38 ± 4.5	53 ± 4.8	49 ± 4.8	40 ± 14	344 ± 126	19 ± 10	13 ± 4
CV (%)	11	10	9	35	37	52	30
CTD 66 – 10 m	57 ± 0.68	11 ± 4.0	23 ± 2.4	8.36 ± 0.35	216 ± 49	5 ± 8	0
CV (%)	1	37	11	4	23	148	0
CTD 66 – 102 m	140 ± 140	66 ± 1.2	5.11 ± 0.14	15.04 ± 7.19	409 ± 110	12 ± 3	2 ± 1
CV (%)	94	2	3	48	27	28	47
CTD 66 – 300 m	14 ± 0.16	0.026 ± 0.021	0.09 ± 0	0.02 ± 0	1 ± 1	0	0
CV (%)	1	78	0	1	87	0	0

3.2.5 Nano and microphytoplankton analysis

Seawater samples were collected in 5 L bottles from the Niskin bottle after triple rinsing with Milli-Q and seawater. 2 L's of seawater were filtered under vacuum through 10 µm pore size polycarbonate filters (47mm diameter). The filters were transferred to 125 ml amber jars, with a PTFE lined white caps, using tweezers and 1l ml of 2% Lugol's solution was added to preserve the samples. Jars were wrapped in foil and stored in the dark for transport back to the UK. Samples were analysed 1 year after the cruise.

The Utermöhl method was used to ID and count phytoplankton (Edler & Elbrächter, 2010; Lund et al., 1958). The sample jar was mixed to homogenise the sample and the filter washed down with ~1% Lugol's solution into the amber jar. The sample was then poured into a 25 ml Utermöhl combined plate settling chamber (Hydro-Bios), the jar rinsed, and the column topped up to 25 ml. The cover slip was then placed on top of the chamber, being careful not to trap any air bubbles. The chamber was left overnight (16-23 hours) in a plastic tray in the dark

(Brierley et al., 2007; Lund et al., 1958). The cover slip was then slid across to remove the settling cylinder and the bottom-plate chamber was checked for random distribution.

An inverted-microscope (GXMXDS-3) with both brightfield and phase contrast was used to identify and count phytoplankton. Magnification was x100, x200 and x400 with 10x binocular eyepieces and power objectives of 10x, 20x and 40x. A digital camera (Lumenera Infinity 1) was attached to the microscope side camera port with a 0.5x CCD adapter. To count the cells three methods of analysis were used. For cells larger than 20 µm the entire chamber was counted at x100 magnification. Intermediate-sized cells, 10-20 µm, were counted in three transects at x200 magnification, one vertical, one horizontal and one diagonal. For one station, where a phytoplankton bloom was observed (CTD 55, Figure 3.2d), the whole chamber was counted at x100 magnification for dinoflagellates > 20 µm and diatoms > 100 µm, then 10 fields of view were counted at x200 magnification for dinoflagellates 10-20 µm and diatoms < 100 µm.

To calculate cell concentration (cells L^{-1}), the number of cells counted at x100 magnification were divided by two as the chamber represents 2 L of water. The cells counted at x200 magnification were calculated using equation 3.4, where A is the percent of the chamber covered by the three transects and V is the number of litres that the base chamber represents. For the cells counted at x200 magnification A is 15.8 (%), for the 10 field of views A is 1.79 (%).

Equation 3.4

$$Cells\ L^{-1} = \frac{\frac{number\ of\ cells\ counted}{A}\ x100}{V}$$

Phytoplankton were identified using identification books (Delgado & Fortuño, 1991; Hoppenrath et al., 2009; Kraberg et al., 2010; Tomas, 1997), literature (Gárate-Lizárraga et al., 2014; Gómez et al., 2008; Gul & Nawaz, 2014; Iwataki, 2008; Latasa et al., 2016; Licea et al., 2004; Meave-del Castillo et al., 2012; Muciño-Márquez et al., 2015; Okolodkov, 2014; Salas et al., 2014; Santos et al., 2013), and online databases such as AlgaeBase and Planktonnet. Light microscopy is limited, as many species lack clear morphological features particularly species < 20 µm (Le Bescot et al., 2016). Here unidentifiable species were grouped into: unknown diatom species, unknown dinoflagellates species, unknown flagellate species, and unknown species for two size-fractions >20 µm and 10-20 µm. Due to the scaling relationship between cell size and abundance, a high portion of species are classified as unknown. Pictures of unidentifiable taxa with prominent features were sent to experienced taxonomists at the Scottish Association for Marine Science (SAMS) for help with identification.

We observe predominantly diatoms and dinoflagellates in samples and little presence of other groups. One of the disadvantages of filtering seawater through a 10 µm membrane is that filtration can distort and destroy delicate, fragile species such as Haptophytes (inc. coccolithophores) and Chrysophytes; filtration favours the more robust diatoms and thecate dinoflagellates (Edler & Elbrächter, 2010). We did not observe coccolithophores in the

microscopy samples. This may be due to their small size or lack of preservation in Lugol's solution as coccolithophores were identified in the flow cytometry analysis. Coccolithophore's have also been observed to decline dramatically over time when preserved in Lugol's (Williams et al., 2015).

3.2.5.1 Sample error

For phytoplankton microscopy, confidence limits are derived from cell counts as random error comprises by far the largest part of total standard error which is comprised of: sampling and subsampling, counting, and colonial forms (Lund et al., 1958). If randomness is achieved the degree of accuracy can be attained with 0.95 confidence limits (Table 3.3). Therefore, it is rarely worthwhile counting more than 400 units to achieve an accuracy of ~10% (Lund et al., 1958). The general rule-of-thumb to maintain an acceptable level of precision is to count at least 500 units for an entire sample and 50 units of the dominant species, giving a 0.95 confidence limit of 28% (Edler & Elbrächter, 2010). In this study I counted 497-3131 cells per sample giving a precision of 3.57-8.97% (equation 3.5.)

Equation 3.5

$$Precision\ (\%) = \frac{2\ x\ 100}{\sqrt{number\ of\ cells\ counted}}$$

Table 3.3 Table copied from Lund et al. *(1958), and added to, shows the percentage accuracy associated with each cell count for approximate 0.95 confidence limits. Highlighted are the suggested total cell counts of 400 and 500 units and their associated accuracy.*

Number of organisms counted	Expressed as percentage of count	Range
4	± 100%	0-8
16	± 50%	8-24
100	± 20%	80-120
400	± 10%	360-440
5,00	± 9%	455-545
1,000	± 6%	940-1060
1,600	± 5%	1,520-1,680
10,000	± 2%	9,800-10,200
40,000	± 1%	39,600-40,400

3.2.6 Satellite data

Altimetry and surface chlorophyll-*a* data were downloaded for the subtropical North Atlantic, 20-40°N 30-55°W, from Copernicus Marine Environment Monitoring Service (European Commission) and plotted in Matlab.

The altimetry data, 'sealevel_GLO_PHY_L4_REP_observations_008_047', consisted of daily L4 sea surface heights and derived variables at a resolution of 0.25 x 0.25 degree. The variables downloaded were sea level anomaly (SLA), absolute dynamic topography (ADT), and the north- and east-ward geostrophic sea water velocities. ADT, the elevation difference caused by flow, is used to determine the net flow of water - the ocean currents (Rio, 2010). The north- and east-ward geostrophic sea water velocities are used to calculate the current direction and velocity.

The chlorophyll-*a* data, 'oceancolour_GLO_CHL_L4_REP_observations_009_082', was downloaded at 4 km resolution for the month of June 2016. The product merges sensor observations from MERIS, MODIS/AQUA, VIIRS and SeaWiFS using the GSM model (Maritorena & Siegel, 2005).

3.2.7 Statistical Analyses

Regression analysis was used to test relationships between variables. To test the strength of linear and non-linear correlations between variables the Pearsons product moment correlation coefficient and Spearmans Rank correlation were used. To assess whether there were significant differences between phytoplankton populations Independent and Pairwise t-tests and ANOVA tests were employed. Non-metric multivariate scaling (NMDS) analyses to visualise dissimilarity between stations were conducted in RStudio using the vegan and factoextra packages, and the squared correlation coefficient used to fit environmental variables to data.

3.3 Results

3.3.1 Subtropical North Atlantic

3.3.1.1 Physical and biogeochemical characteristics

The RidgeMix cruise track is split into 7 regions, based on whether stations are over the Mid-Atlantic Ridge (sections 2-3), abyssal basin (sections 5-6), on the northern (sections 1 & 7) or southern transects (section 4), and, whether they are in the 'north' (sections 1-2, 6-7) or 'south' (sections 3-5). All section plots proceed from section 1 clockwise, travelling southward over the ridge and then northward over the abyssal basin, around to section 7. The water column is stratified, typical of the oligotrophic ocean (Figure 3.5a). The mixed layer depth was deepest in sections 1 & 7 (35 ± 17 m), 2 (46 ± 15 m) and 3 (25 ± 12 m) and shallowest in sections 4 (16 ± 4 m), 5 (19 ± 5 m) and 6 (16 ± 3 m). Surface temperatures were higher and salinity lower in the north (21.5 ± 1.8°C, 36.5 ± 0.2 PSU) than the south (25.8 ± 0.1°C, 37.2 ± 0.1 PSU; Figure 3.5b); sections 3-5 have warmer and denser waters, for a given depth, and so the isopycnals deepen towards the south (Figure 3.5c, section 4). The T-S diagram for the top 300 m shows a

separation in the surface water properties that occurs at 31°N, splitting the cruise transect into north and south (Figure 3.6), herein referred to as a front.

The surface waters were depleted in both nitrate and chlorophyll-*a* (Figure 3.7). Nitrate concentrations gradually increased below 50 m to 8 µM at 300 m. The nitracline deepens to the south roughly following the pycnocline (Figure 3.7a). Surface chlorophyll-*a* concentrations, ranged from 0.01 to 0.16 mg m^{-3}, with higher concentrations to the north, sections 1 & 7 (0.066 ± 0.038 mg m^{-3}), 2 (0.038 ± 0.009 mg m^{-3}) and 6 (0.032 ± 0.020 mg m^{-3}), than south, sections 3 (0.017 ± 0.004 mg m^{-3}), 4 (0.017 ± 0.005 mg m^{-3}), and 5 (0.016 ± 0.001 mg m^{-3}; Figure 3.7b). A pronounced deep chlorophyll-*a* maximum (DCM) was present at all stations but at shallower depths to the north of 31°N, 83 ± 22 m, compared to the south of 31°N, 143 ± 15 m (t-test, $p < 0.001$). Chlorophyll-*a* maximum concentrations were also significantly higher north of 31°N, 0.41 ± 0.16 mg m^{-3} compared to south of 31°N, 0.19 ± 0.03 mg m^{-3} (t-test, $p < 0.001$).

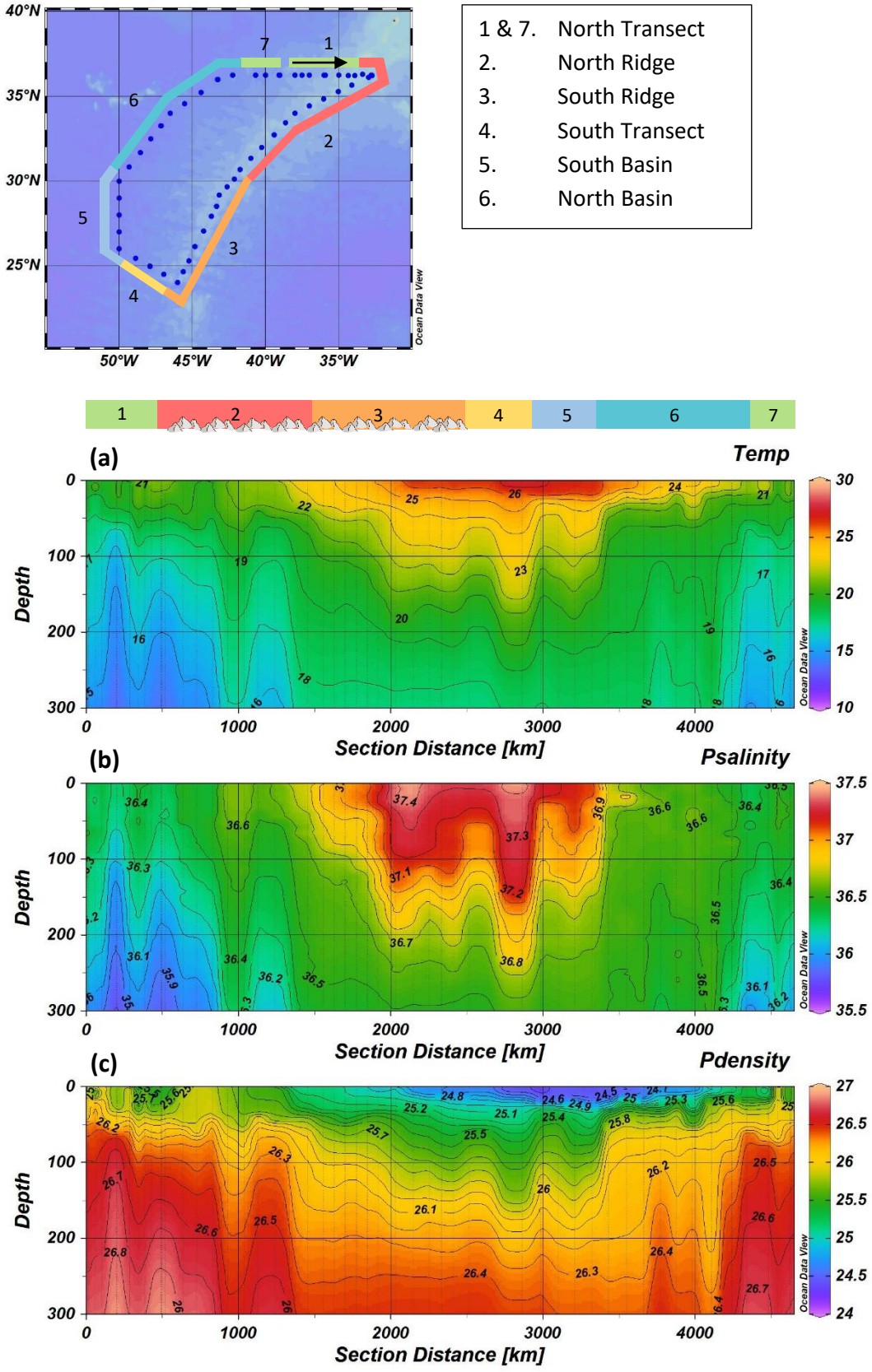

Figure 3.5 (a) Temperature (°C), (b) salinity (PSU), and (c) density (kg m^{-3}) section plots for the top 300 m of the water column. The section plot starts in the middle of the north transect (from section 1) and progresses clockwise. Sections are labelled in the key.

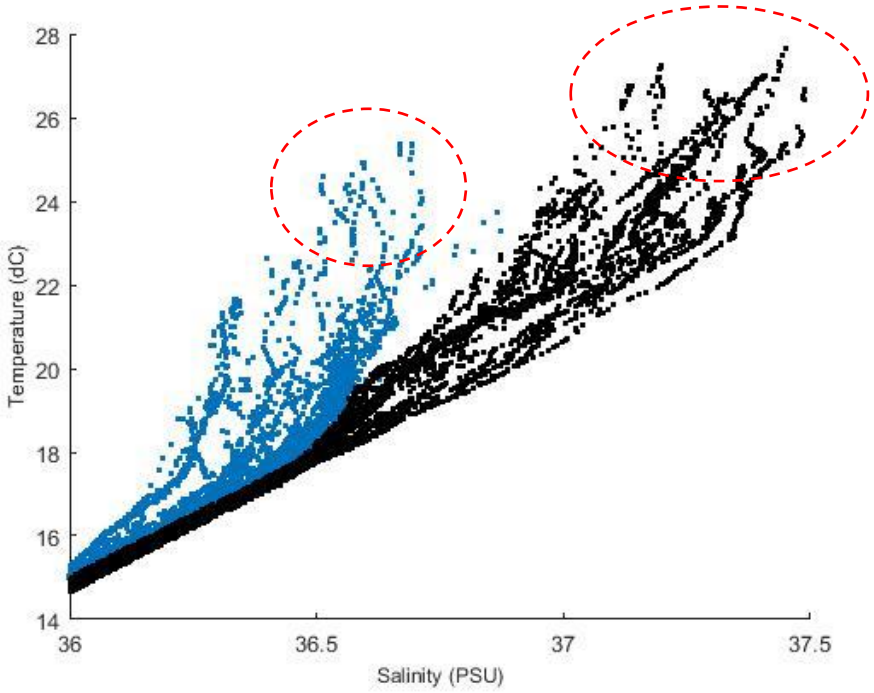

Figure 3.6 Temperature-Salinity plot for the top 300 m of the water column. Stations north of 31°N are blue and those south of 31°N are black. Surface waters are circled in red.

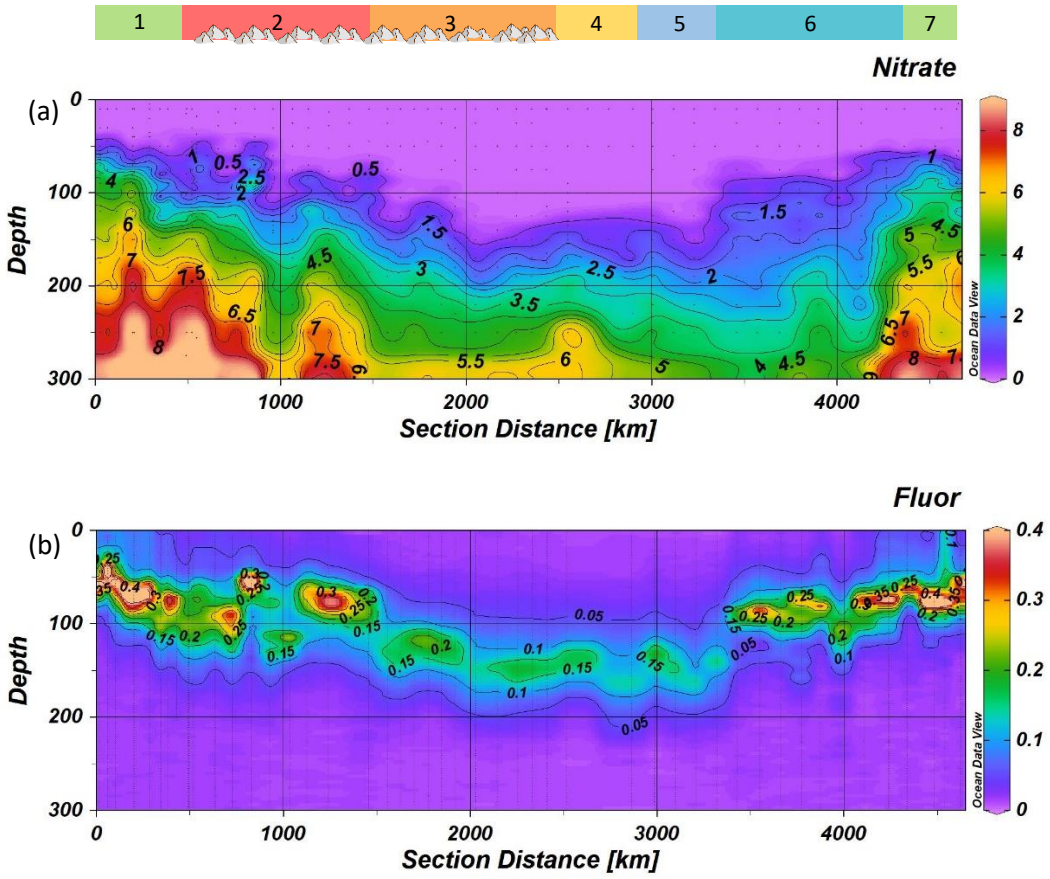

Figure 3.7 Section plots of (a) nitrate (µM) and (b) CTD chlorophyll-a (mg m $^{-3}$).

The ocean currents are quite dynamic in the study area (Figure 3.8). ADT and current velocity are most variable in the northwest of the study area. Areas of high and low ADT surrounded by rotating currents highlight multiple eddies in the northern part of the cruise track. These eddies can be seen in the vertical displacement of density, nitrate and chlorophyll-*a* where they coincide with CTD stations (Figure 3.5c and 3.7a, b). The current velocities and ADT also highlight a current flowing from the northwest corner (40°N-55°W) to north east (32°N-30°W). Surface chlorophyll-*a* concentrations appear to follow these northern surface currents and eddies (Figure 3.9).

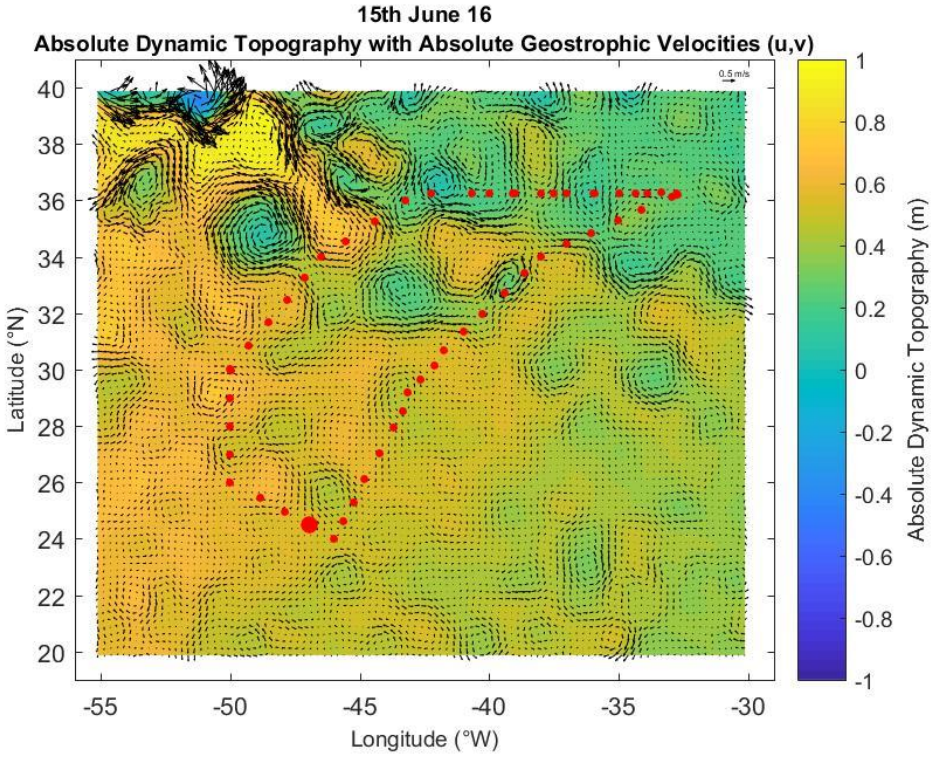

Figure 3.8 Absolute Dynamic Topography with geostrophic current velocities for 15th June. Red dots mark station locations, the larger red dot marks the station sampled on 15th June.

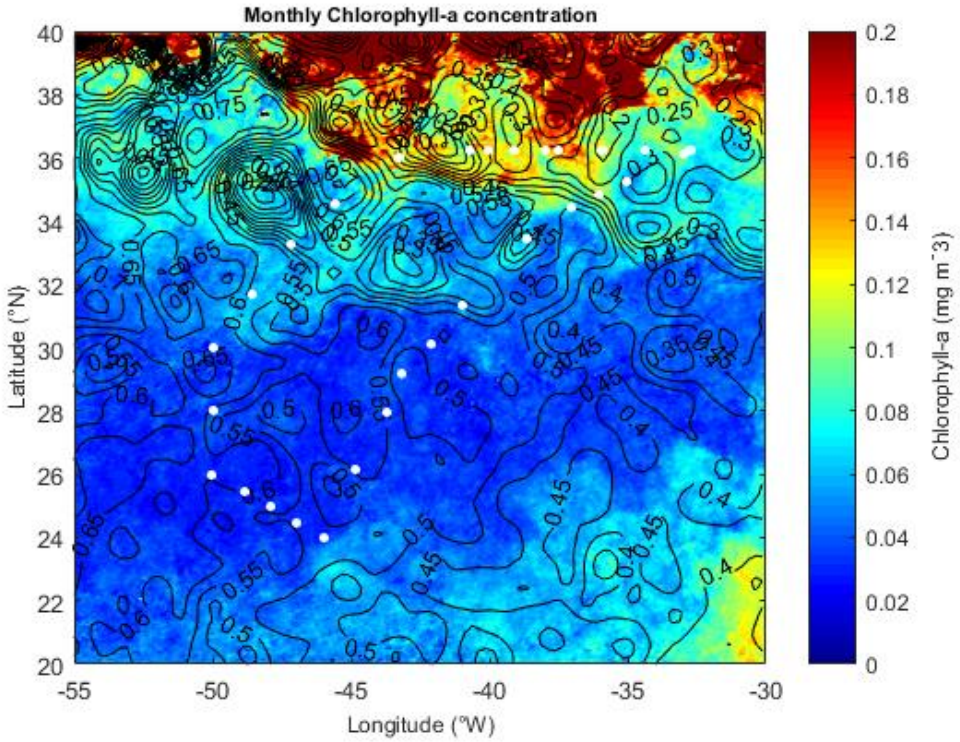

Figure 3.9 Satellite chlorophyll-a concentrations for the month of June 2016 overlaid with ADT (black contours) and stations sampled for phytoplankton (white dots).

Buoyancy frequency (BF), indicative of water column stability, is concurrent with the dynamics of the surface ocean currents seen in Figure 3.8. The depth of the maximum BF is deeper at higher latitudes in this study where the stronger surface currents exist and therefore deeper mixed layers (Figure 3.10a). The depth of the maximum BF varies between 3 and 80 m and positively correlates with the ML depth (Pearson's correlation coefficient, $r = 0.828$, $p < 0.001$; Figure 3.10a). The stability of the surface waters was assessed by looking at the sum squared BF of the top 200 m (Figure 3.10b). The sum of BF^2 over the top 200 m is similar at all latitudes but higher to the west, and so the water column more stable, over the basin than the ridge.

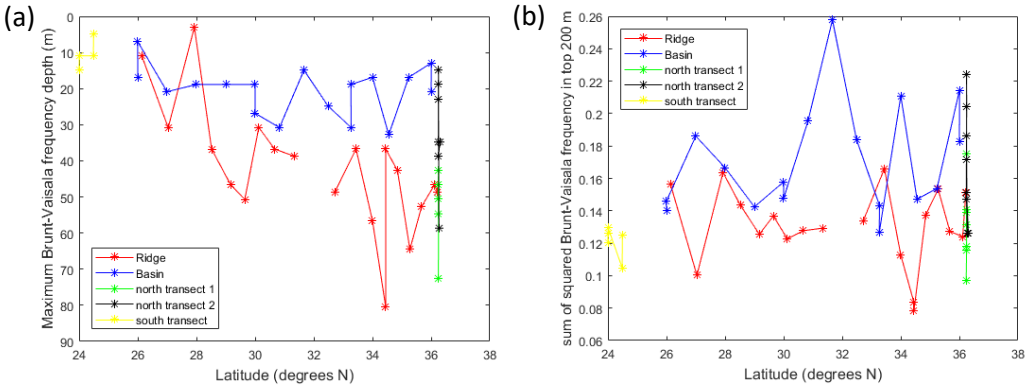

Figure 3.10 (a) the depth of maximum buoyancy frequency, (b) sum squared buoyancy frequency of the top 200 m of the water column.

3.3.1.2 *Controls on the depth of the DCM*

The vertical profile of chlorophyll-*a* in the subtropical North Atlantic was highly variable between stations during the Ridgemix cruise (Figure 3.11). The DCM occured at depths between 43 m and 155 m with maximum concentrations of 0.16 to 0.85 mg m^{-3}. There was a strong negative exponential correlation between DCM depth and DCM concentration, the deeper the DCM the lower the chlorophyll-*a* concentration (ρ = -0.913, $p < 0.001$). There was also a positive exponential correlation between chlorophyll-*a* concentration and total picophytoplankton cell abundance at the DCM (ρ = 0.737, $p < 0.01$; Appendix Figure 3.1), particularly for nanoeukaryotes, which had a linear relationship with chlorophyll-*a* concentrations at the DCM (R = 0.69 and 0.767 respectively, $p < 0.01$; Appendix Figure 3.1). The depth of the euphotic zone (1% light level) was also variable. For the noon CTDs (Figure 3.12a) the euphotic zone depth varied between 60 and 170 m and was correlated to the DCM depth (R^2 = 0.7792, $p < 0.001$; Figure 3.12b), and concentration (R^2 = 0.6561, $p < 0.01$; Figure 3.12c). Light at the DCM varied between 0.13 and 4% with an average of 1.5 ± 1.3% (Figure 3.13). Light at the DCM was not significantly correlated with either DCM depth or concentration.

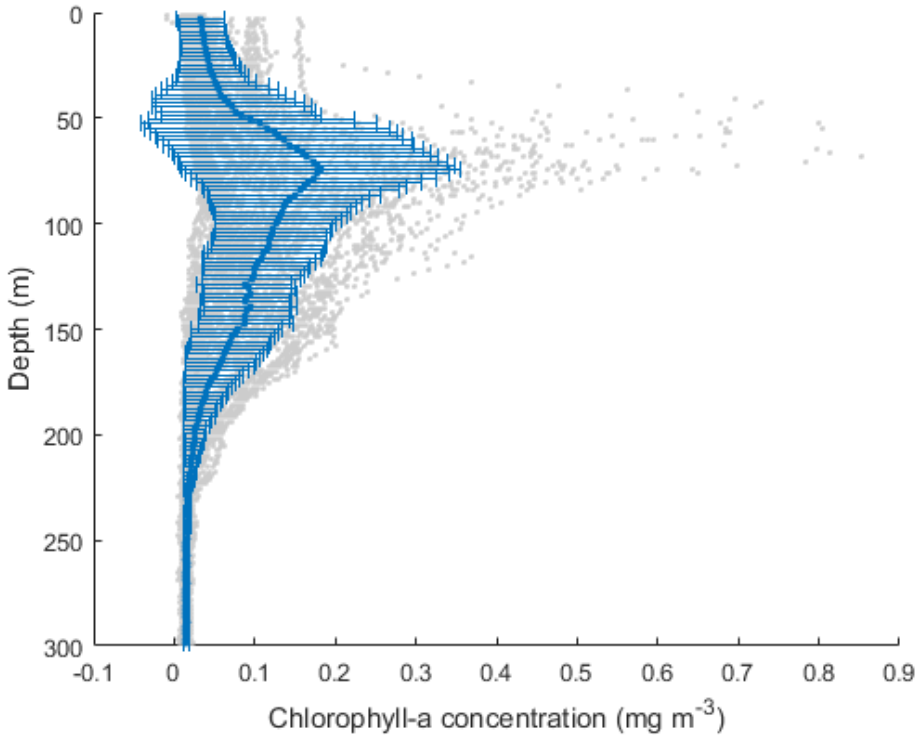

Figure 3.11 Depth profiles of chlorophyll-a concentration for all the stations on RidgeMix (grey dots). The blue dots and error bars are the mean ± standard deviation at 2 m intervals.

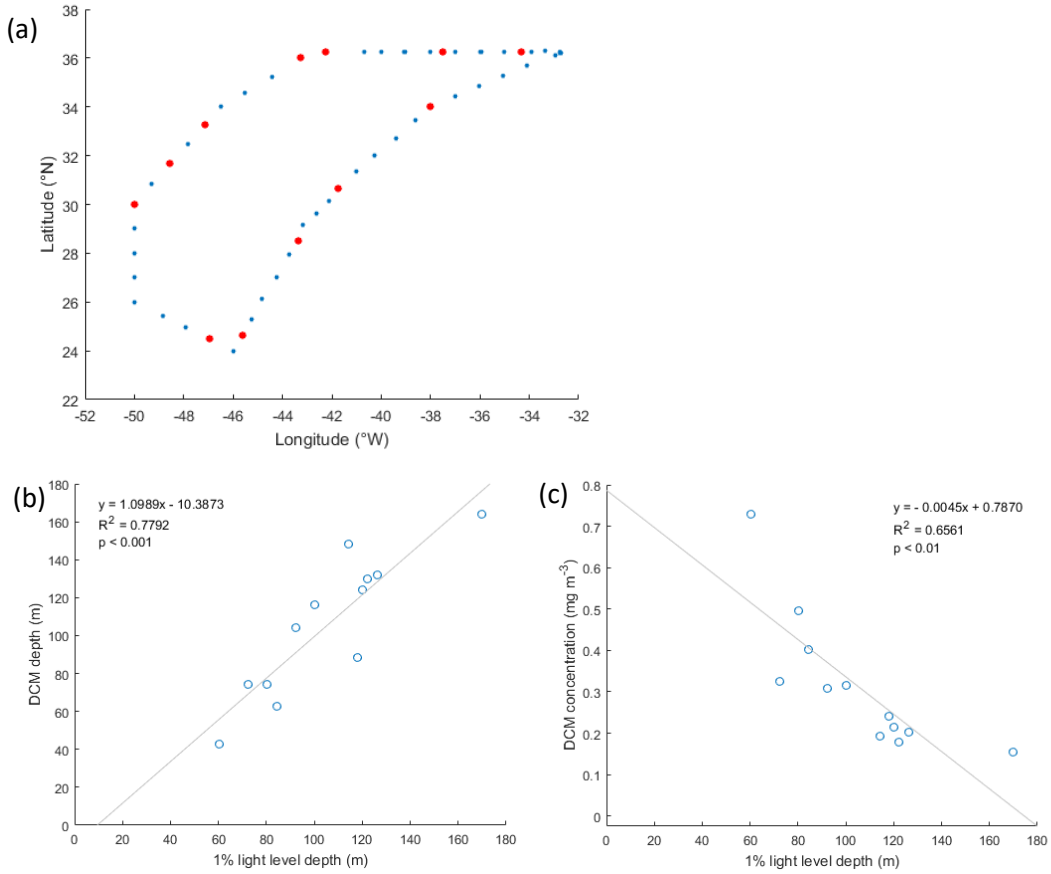

Figure 3.12 Noon CTD 1% light level vs. (b) DCM depth and (c) DCM concentration (linear regression $p < 0.001$). Noon stations are highlighted red on the cruise track (a).

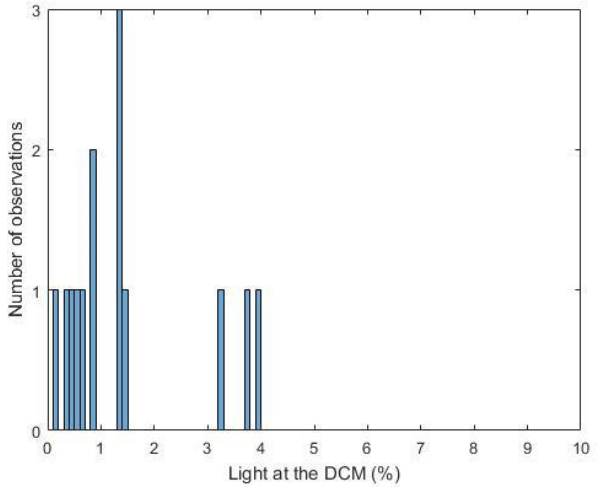

Figure 3.13 Histogram of the percent light at the DCM for all noon stations.

The depth of the nitracline was also highly variable (Figure 3.14b). The depth at which nitrate concentrations decreased to 0 µM, the nitrate intercept, varied between 11 m (in section 1) and 151 m (in section 5) and the slope of the nitracline varied from 6 µmol m^{-1} (in section 1) to 52 µmol m^{-1} (in section 6). The slope was not significantly correlated with DCM depth but the

NO_3 intercept was correlated with the DCM depth (R^2 = 0.7324, p < 0.001; Figure 3.14b), indicating the co-occurrence of the nitracline and DCM.

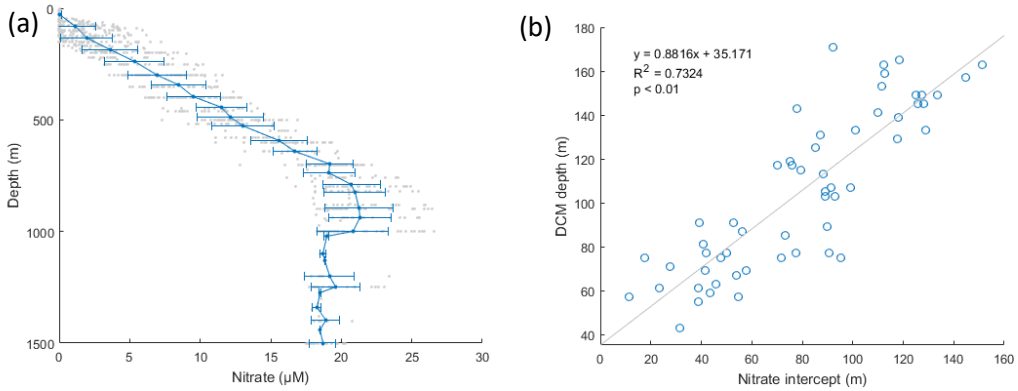

Figure 3.14 Depth profile of (a) nitrate for all stations sampled (grey dots). Blue dots and bars are the average±standard deviation at the sampling resolution of 50 m. (b) Plot of nitrate intercept against DCM depth.

The physical structure of the water column also influences the depth of the DCM. The depth of the DCM was correlated with sea surface temperature (R^2 = 0.6617, p < 0.001), sea surface salinity (R^2 = 0.8103, p < 0.001, Figure 3.15b), surface density (R^2 = 0.4723, p < 0.001) and density at the DCM (R^2 = 0.582, p < 0.001). Where surface measurements were from 10 m, the top depth sampled. The depth of the DCM was only weakly correlated to Buoyancy Frequency (BF; sum BF_{200m} R^2 = 0.336, p < 0.001 and maximum BF R^2 = 0.2129, p < 0.001) and mixed layer depth (R^2 = 0.0885; p < 0.05). The relationship between chlorophyll fluorescence and density shows that in the northern regions, 1 & 7, chlorophyll-*a* concentrations strongly follow isopycnals 26-26.3 kg m^{-3} (Figure 3.16).

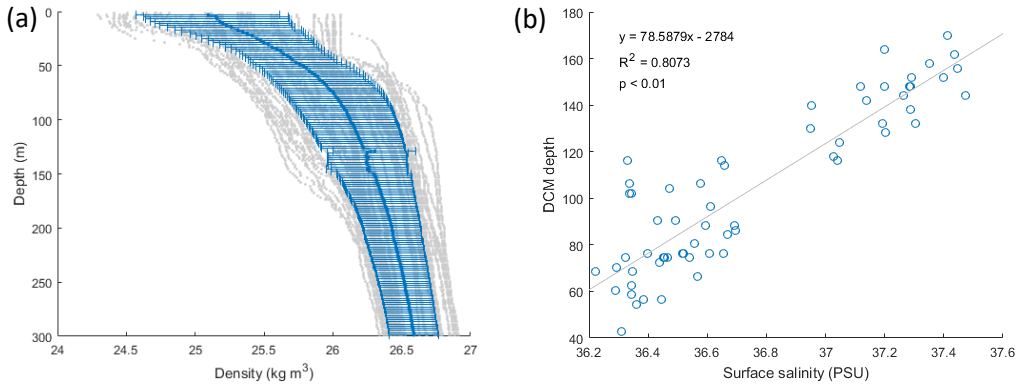

Figure 3.15 (a) Density depth profiles (grey dots) with average ± standard deviation (blue) at 2 m intervals. (b) Surface salinity plotted against DCM depth.

Non-metric multidimensional scaling (NMDS) plots of DCM depth, maximum BF, sum BF_{200m}, surface temperature, salinity and density, density at the DCM, euphotic zone depth, light at

the DCM, nitrate slope and nitrate intercept support the findings reported so far. It is a combination of factors that control the DCM depth in the subtropical North Atlantic, primarily euphotic zone depth, nitrate intercept, density at the DCM and surface salinity (Figure 3.17).

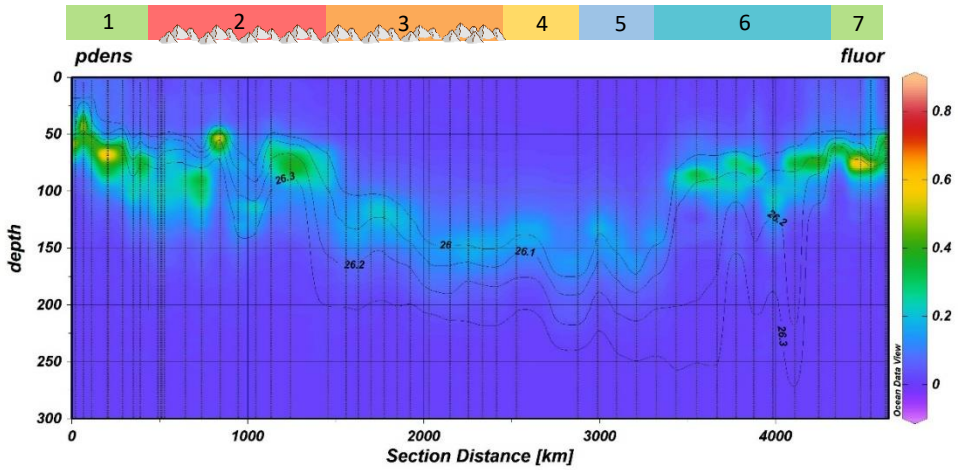

Figure 3.16 Fluorescence section plot with isopycnals 26-26.4 kg m^{-3} (black lines).

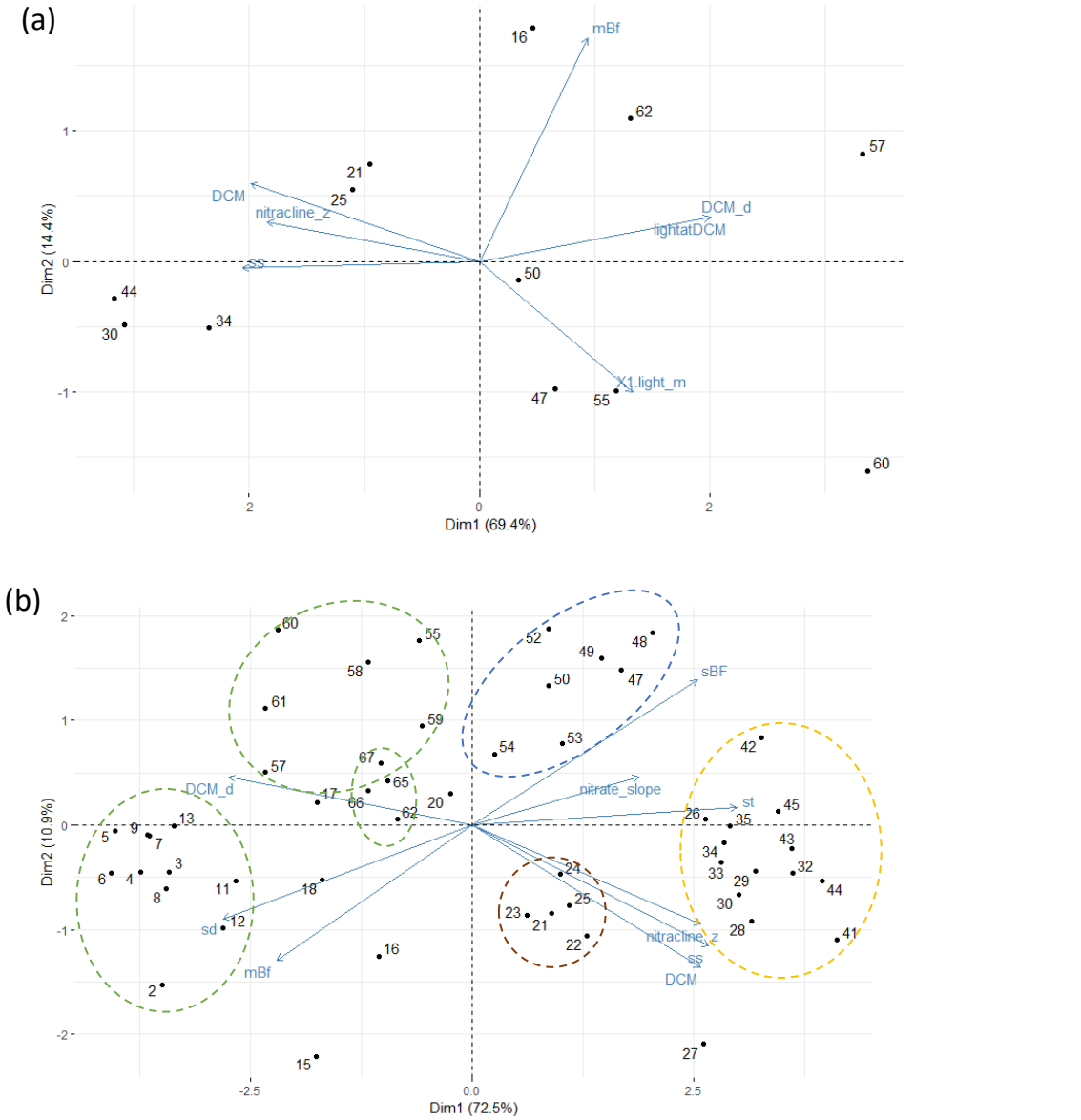

Figure 3.17 Non-metric multidimensional scaling (NMDS). (a) Similarity of noon (n = 12) and (b) all (n = 52) stations based on their physical characteristics. Arrows represent the significant environmental forcings (p < 0.01). Arrows in the same direction or opposite are most strongly related. DCM depth (DCM), surface salinity (ss), surface temperature (st), surface density (sd), nitrate intercept (nitracline_z), nitrate gradient (nitrate_slope), maximum buoyancy frequency (mBF), sum buoyancy frequency of the top 200 m (sBF), density at the DCM (DCM_d), and euphotic zone depth (X1_light_m). Station clusters were visually selected and circled in green = north transect (sections 1 and 7), blue = north basin (section 6), yellow = south transect and basin (sections 4 and 5), brown = south ridge (section 3).

The plot of all stations shows two distinct clusters in the bottom right (Figure 3.17b). These clusters are the stations from the southern half of the cruise track, with CTD 21-25 located in section 3 (circled red) and the other cluster in sections 4 and 5 (circled yellow; Figure 3.17). Stations to the north of the cruise track fall in the top left of figure 3.17 (circled green) and those in section 6 to the top right (circled blue).

3.3.1.3 Spatial variation of phytoplankton community: influence of Mid-Atlantic Ridge versus frontal feature

To test the hypothesis that phytoplankton size structure and composition will change in response to an increase in nutrient flux over the ridge, we now assess spatial distributions of size-fractionated chlorophyll-*a*, picophytoplankton (< 10 µm) analysed by flow cytometry and nano- and microphytoplankton (> 10 µm) analysed by light microscopy. However, we cannot ignore the presence of the front at 31°N or the occurrence of eddies at ~34-36°N.

3.3.1.3.1 Size-fractionated chlorophyll-*a*

For the whole water column and transect, the picophytoplankton size fraction (0.2-2 µm) constitutes 52 ± 20% of total chlorophyll-*a*, with nanophytoplankton (2-20 µm) and microphytoplankton (>20 µm) accounting for 40 ± 16% and 8 ± 7%, respectively. At the DCM, 69 ± 13% of chlorophyll-*a* is represented in the picophytoplankton size-fraction, with nanophytoplankton and microphytoplankton accounting for up 28 ± 11% and 3 ± 3%. Chlorophyll-*a* concentrations in the 2-20 µm size fraction were higher north of 31°N (position of the front; t-test, $p < 0.05$) compared to south of 31°N (Figure 3.18b, sections 1, 2, 6, 7). Concentrations of nano and microphytoplankton were highest at the northernmost station in section 6 (CTD 55, 36°N) and high in sections 1 and 2 for microphytoplankton and at 36°N for nanophytoplankton (Figure 3.18b and c, sections 1 and 7). Nanophytoplankton were also distributed throughout a broader depth range over the ridge in the north (section 2), compared to the basin, (Figure 3.18b, section 6).

3.3.1.3.2 Picophytoplankton (< 10 µm)

In a similar manner to chlorophyll-*a*, there was a subsurface maximum in all picophytoplankton groups which deepened to the south (Figures 3.19 and 3.20). At all stations eukaryotes (picoeukaryotes + nanoeukaryotes + coccolithophores + cryptophytes) had the deepest peak cell abundance in the water column followed by *Prochlorococcus* and then *Synechococcus*. Eukaryotes were found in the deeper layers of the DCM (~0.4 m deeper than the DCM, $R^2 = 0.9431$, $p < 0.01$) and *Prochlorococcus* just above the DCM (~12 m above the DCM, $R^2 = 0.7178$, $p < 0.01$; Figure 3.21).

The cyanobacteria *Prochlorococcus* were the most abundant picophytoplankton observed, with cell densities reaching 10^5 cells ml^{-1}, with maximum abundances reaching < 2.5 x 10^5 cells ml^{-1} they dominated the picophytoplankton (Figure 3.19a). The cyanobacteria *Synechococcus* was the second most abundant, at 10^4 cells ml^{-1}, and with maximum abundances of up to < 6 x 10^4 cells ml^{-1} (Figure 3.19b). Picoeukaryotes were an order of magnitude lower at 10^3 cells ml^{-1}, < 7 x 10^3 cells ml^{-1} (Figure 3.19c), followed by nanoeukaryotes (10^2, < 900 cells ml^{-1}, Figure 3.19d), then coccolithophores (10^1, < 30 cells ml^{-1}, Figure 3.20a) and cryptophytes (10^1, < 50 cells ml^{-1}, Figure 3.20b). Heterotrophic bacteria occurred at the same order of magnitude as

Prochlorococcus, 10^5, but their higher concentrations ranged from 4 x 10 ^{5} cells ml^{-1} to 7 x 10^5 cells ml^{-1} (Figure 3.20c). Integrated heterotrophic bacteria (0-300 m) was 10 ± 5-fold higher than *Prochlorococcus*.

Spatially the abundance of *Synechococcus*, picoeukaryotes, nanoeukaryotes, coccolithophores, cryptophytes and heterotrophic bacteria was lower to the south of 31°N (Figure 3.19 and 3.20; sections 3-5). The highest abundances of *Synechococcus*, picoeukaryote, coccolithophores and cryptophytes were in section 6 at CTD 55 (36°N), in sections 1 and 7 on the northern transect and in the north over the ridge (section 2). Picoeukaryotes, nanoeukaryotes, coccolithophores and cryptophytes appear to cover a broader depth range in the north over the ridge (section 2) compared to the basin (section 6).

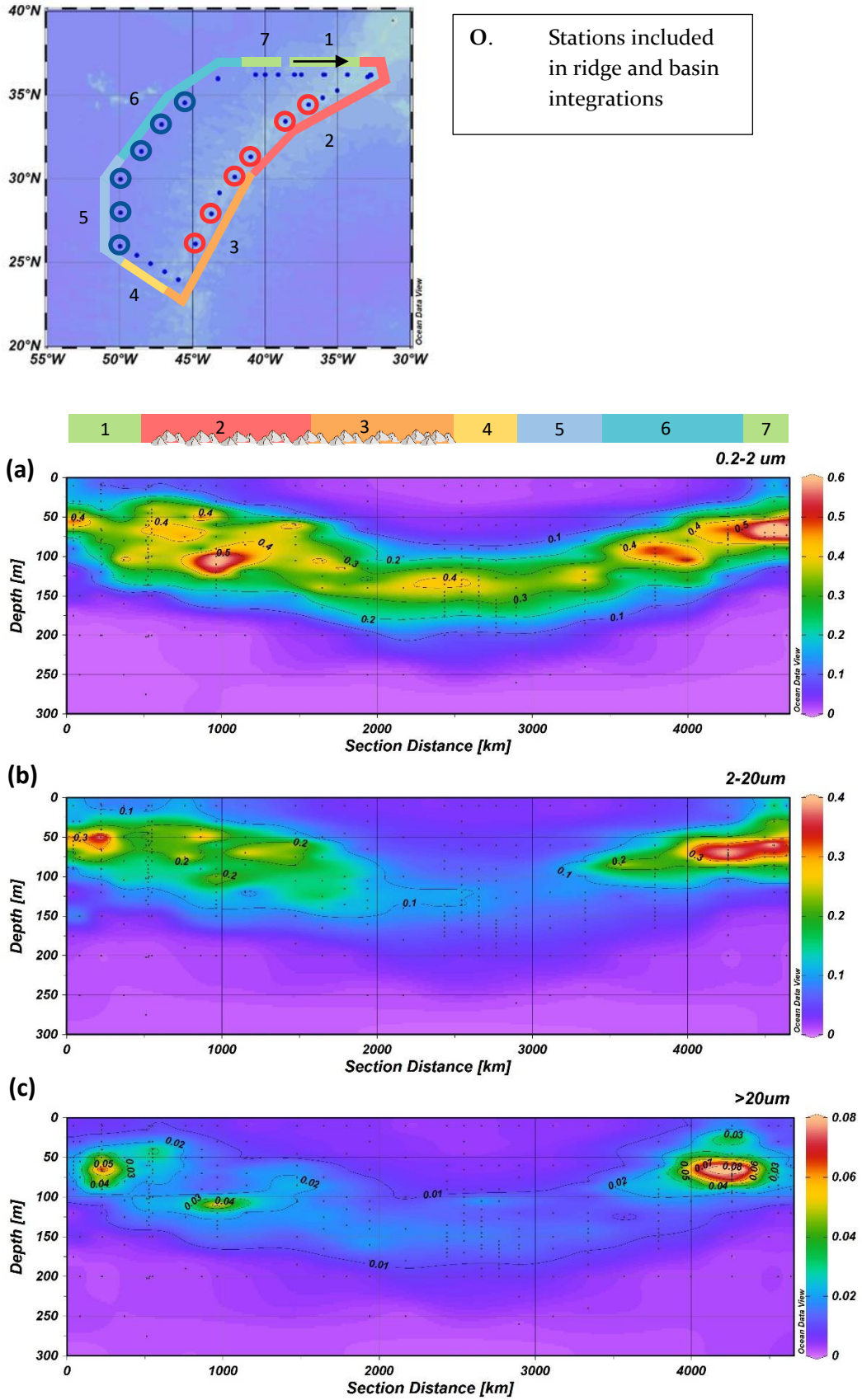

Figure 3.18 Size-fractionated chlorophyll-a (mg m^{-3}) distribution in the top 300 m of the water column. (a) pico (0.2-2 µm), (b) nano (2-20 µm) and (c) micro (> 20 µm) size-fractions. The section starts from the middle of the north transect (section 1) and proceeds clockwise. Stations circled on the map are those chosen for ridge-basin comparison.

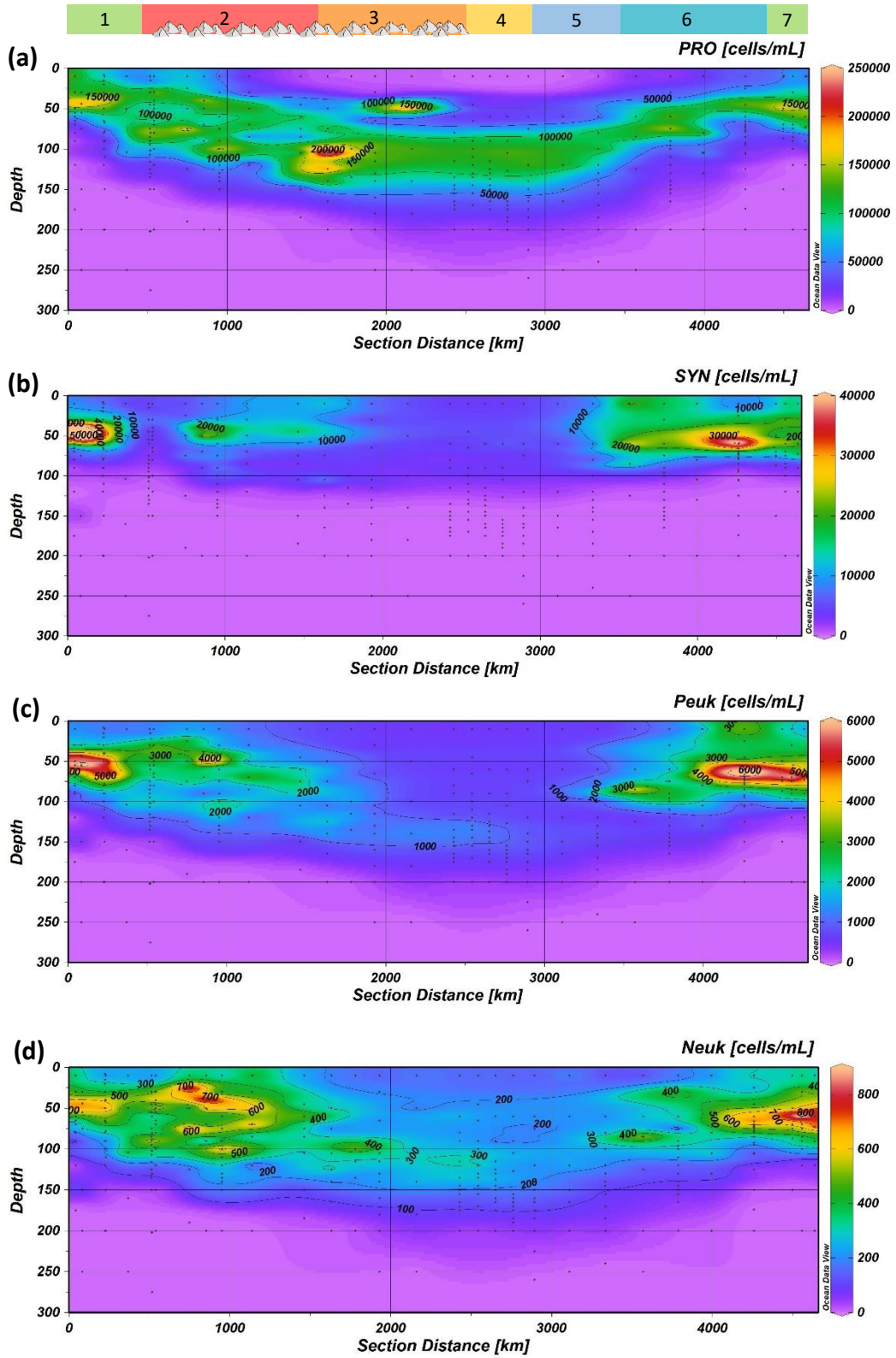

Figure 3.19 Picophytoplankton cell abundance (cells ml^{-1}) for the top 300 m of the water column. (a) Prochlorococcus (Pro), (b) Synechococcus (Syn), (c) picoeukaryotes (Peuk) and (d) nanoeukaryotes (Neuk).

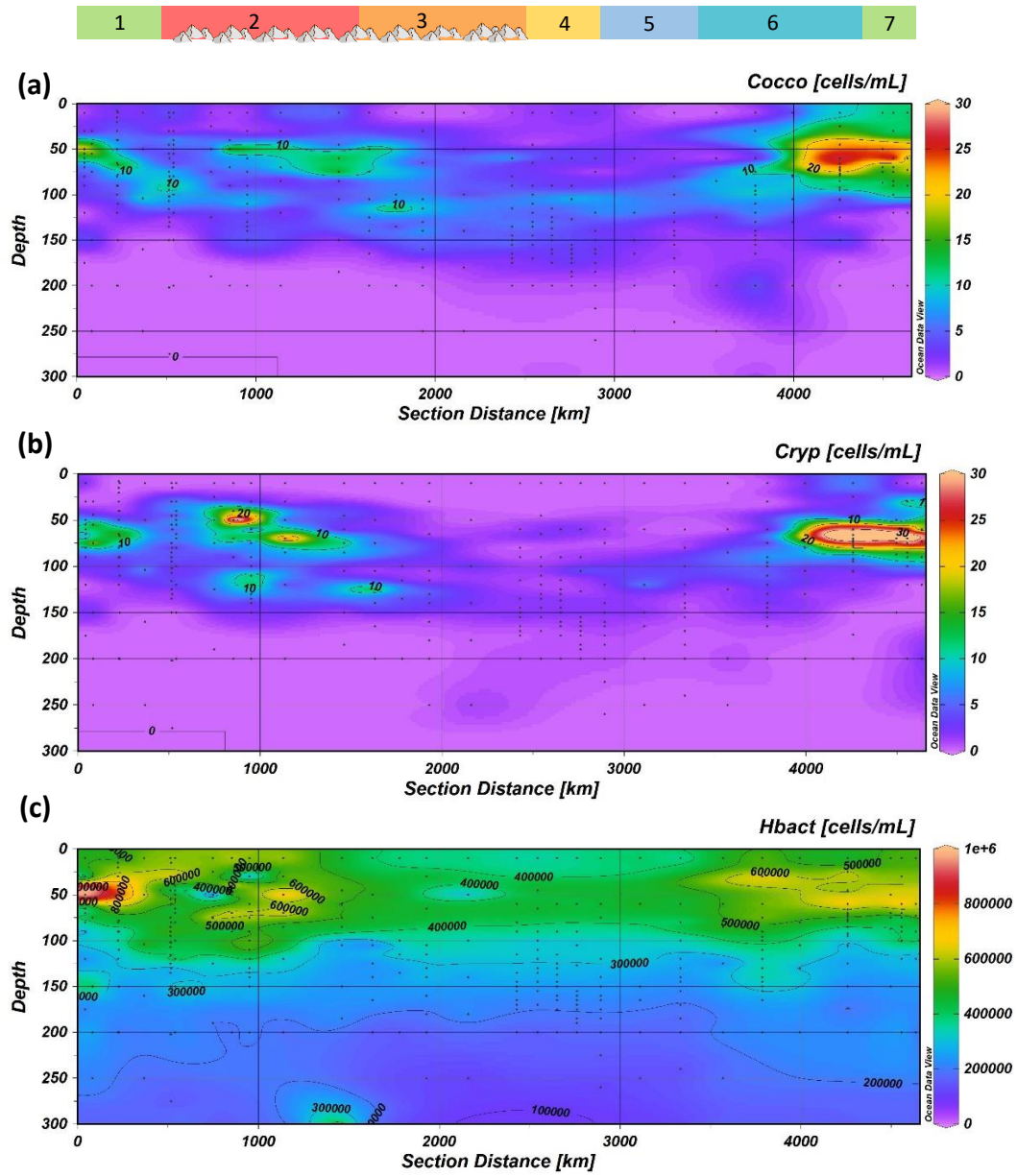

Figure 3.20 Picophytoplankton cell abundance in the top 300 m of the water column. (a) coccolithophores (Cocco), (b) cryptophytes (Crypt) and (c) heterotrophic bacteria (Hbact).

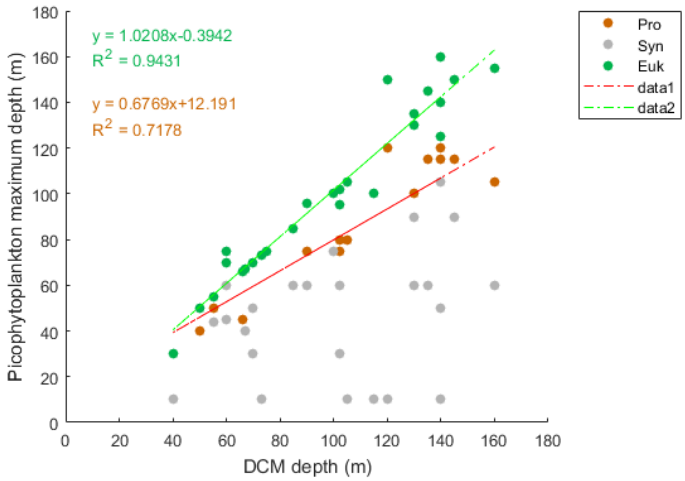

Figure 3.21 Depth of maximum picophytoplankton cell abundance against depth of the DCM. Cyanobacteria Prochlorococcus (Pro) and Synechococcus (Syn) and Eukaryotes (Peuk+Neuk+Cocco+Crypt).

3.3.1.3.3 Nano- and microphytoplankton (> 10 μm)

Phytoplankton cells abundance averaged 1073 ± 492 cells L^{-1}, with the exception of one station in section 6 where a phytoplankton bloom was observed where phytoplankton cell abundance increased to 42,098 cells L^{-1} at 10 m and 2095 cells L^{-1} at the DCM (Figure 3.22b, c). There was a significant difference between phytoplankton cell abundance at 10 m and the depth of the DCM (paired t-test, $p < 0.01$): ignoring the bloom station, cell concentrations were 1222 ± 434 cells L^{-1} at 10 m compared to 940 ± 320 cells L^{-1} at the DCM. At a depth of 10 m, 64 ± 9% of the phytoplankton community consisted of dinoflagellates, except at the bloom station, where diatoms represented 80% of the > 10 μm phytoplankton community (Figure 3.22b). At the DCM, there as an equal contribution of diatoms (34 ± 10%), dinoflagellates (30 ± 9%) and unknown species (25 ± 5%) to the > 10μm phytoplankton community (Figure 3.22c). Non-metric multidimensional scaling (NMDS) plots, based on the species list in Appendix Table 3.2, do not show statistically significant separation of the stations at the 0.05 significance level in terms of north-south of front or ridge-basin, based on phytoplankton species > 10 μm (Figure 3.23a, b), bloom station removed. However, at the 0.1 significance level the DCM phytoplankton composition is significantly different to the north and south (ANOSIM, r^2 = 0.3614, p = 0.051) and over the ridge and basin (r^2 = 0.3484, p = 0.052).

Unidentified dinoflagellate species in the size range of ~10-20 μm dominated the > 10 μm phytoplankton community, representing > 5% of total phytoplankton in all samples. At 10 m, *Heterocapsa* spp. dominated all samples. Unidentified cells in the size range of 10 to 20 μm dominated at the DCM.

3.3.1.3.4 Mesoscale eddies

At CTD 55 in section 6 (36°N) we observed a phytoplankton bloom dominated by diatoms in the > 10 μm size fraction (refer to previous section 3.3.1.3.3). Whilst there was no change in the pycnocline at CTD 55 compared to adjacent stations the nitracline was shallower with a nitrate intercept of 18 m compared to 80 ± 21 m in the rest of section 6 and 56 ± 14 m in section 7. Adjacent stations were 262 and 233 km away. Chlorophyll-*a* concentrations of nano- and microphytoplankton (2-20 μm and > 20 μm) and the abundance of all groups of picophytoplankton apart from *Prochlorococcus* were also higher at CTD 55 compared to most of the stations during RidgeMix (see Figure 3.18b, c; Figure 3.19b, c, d; Figure 3.20a, b).

Eddy signals can be seen north of 31°N in the ADT plot (Figure 3.8) and in the displacement of the thermocline, pycnocline and nitricline in the top 300 m of the water column (Figure 3.5a, c and Figure 3.7a). Several stations within sections 1, 2 and 7 had high concentrations of nano- and microphytoplankton (2-20 μm and > 20 μm; Figure 3.18b, c) and/or *Synechococcus*, picoeukaryotes, and nanoeukaryotes and were thought to be related to eddies (Figure 3.19b, c, d).

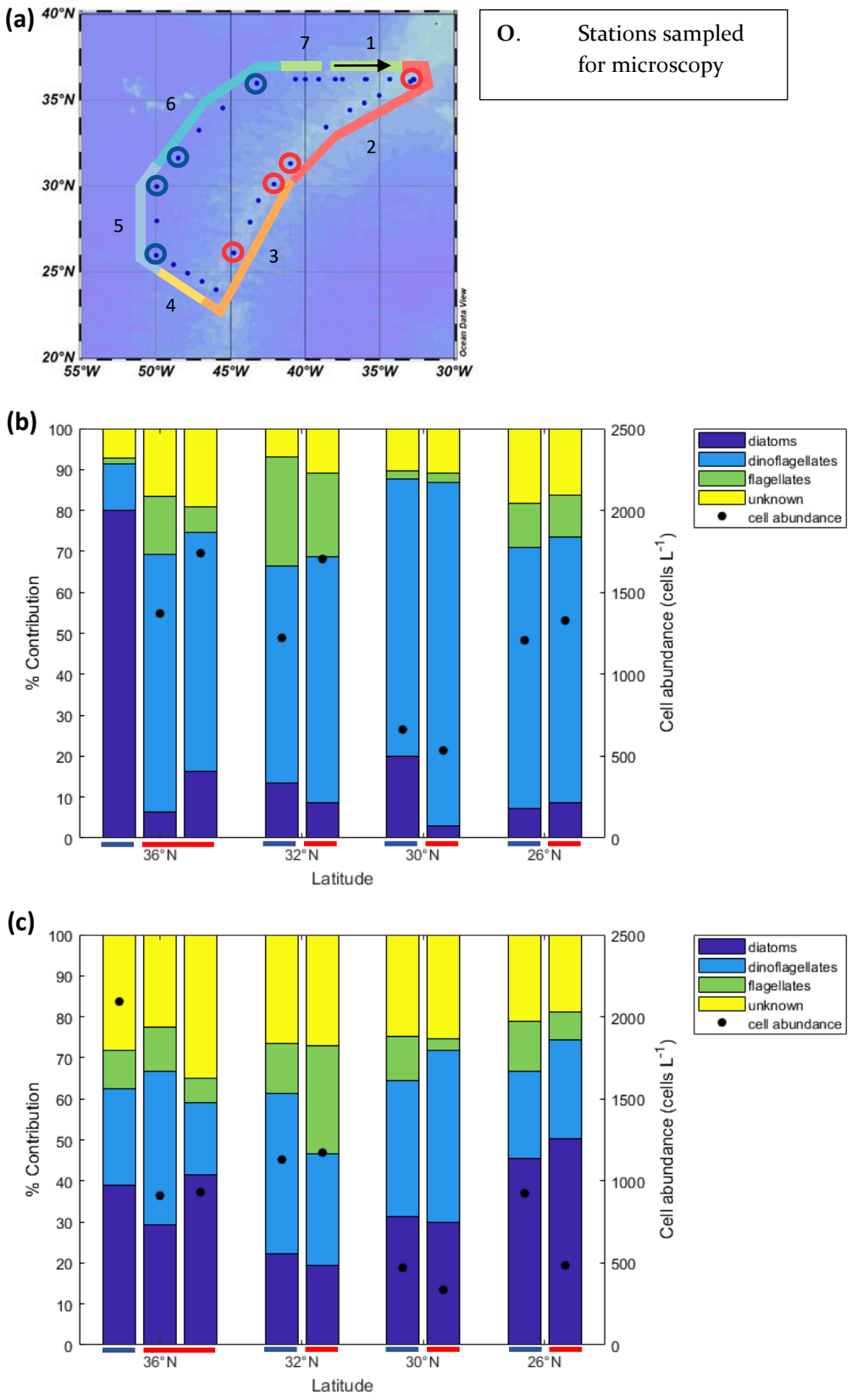

Figure 3.22 Composition and abundance of phytoplankton >10 µm at (b) 10 m and (c) the DCM. Latitude is on the x-axis with blue being basin stations and red ridge stations, see location plot (a). At 10 m the basin station at 36°N had a cell abundance of 42,098 cells L^{-1}.

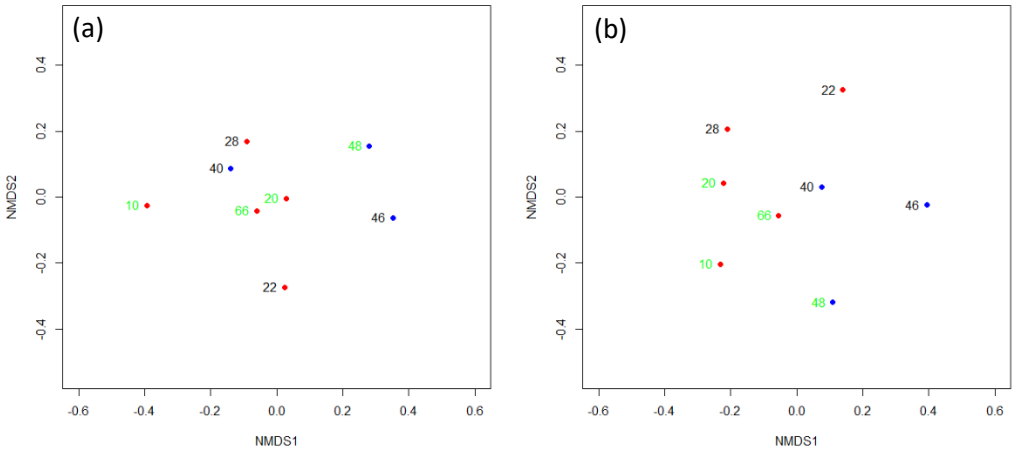

Figure 3.23 Non-metric Multidimensional scaling (NMDS) plots of stations sampled for > 10 µm phytoplankton. Red dots = ridge, blue dots = basin, green numbers = north, black numbers = south. (a) 10 m samples and (b) the DCM. Numbers are CTD numbers.

3.3.1.4 Statistical analysis of the phytoplankton community over the Mid-Atlantic Ridge versus adjacent basin

To test whether the Mid-Atlantic Ridge affects water column concentrations of phytoplankton we integrated water column concentrations over the top 300 m and combined stations within sections, with sections 2 and 3 representing over the ridge, and sections 5 and 6 over the adjacent basin, sections 2 and 6 representing to the north of the front and sections 3 and 5 to the south of the front (Figure 3.24 and 3.25). Nanophytoplankton (2-20 µm) were significantly higher over the ridge in the north (t-test, p = 0.035) and microphytoplankton (> 20 µm) were significantly higher over the ridge in the south (t-test, p = 0.032; Figure 3.24b, c). Pairwise comparison of all stations finds that both nano- and microphytoplankton chlorophyll-*a* size-fractions were significantly higher over the ridge (paired t-test, p = 0.017 and 0.022). For picophytoplankton cell abundances, it is the larger cells (eukaryotes) that appear to be affected by the ridge (Figure 3.25c, d). Picoeukaryotes (~2.8 µm) had higher abundances over the ridge in the south, and pairwise comparison finds nanoeukaryotes (~4.6 µm) have higher abundances over the ridge (paired t-test, p = 0.55 and 0.53).

The abundance and composition of > 10 µm phytoplankton are statistically similar on and off ridge, apart from the bloom station (Figure 3.26). The cell abundance at 10 m at the bloom station was 42,098 cells L^{-1} and was composed of 80% diatoms whereas the comparison ridge stations was composed of 10-20% diatoms with a total cell abundance of 1400-1800 cells L^{-1}. Total phytoplankton abundances were 1629 ± 640 over the ridge and 1615 ± 309 cells L^{-1} in the basin at 10 m and were lower in the DCM and over the ridge 750 ± 482 compared to the basin 924 ± 310 cells L^{-1}. Concentrations of diatoms and dinoflagellates were similar at the DCM over

the ridge and in the basin, but at 10 m, diatom abundance was higher in the basin and dinoflagellates slightly higher over the ridge, although neither were statistically significant (Figure 3.26). NMDS hints at separation of ridge-basin samples but the split is not clear (Figure 3.23).

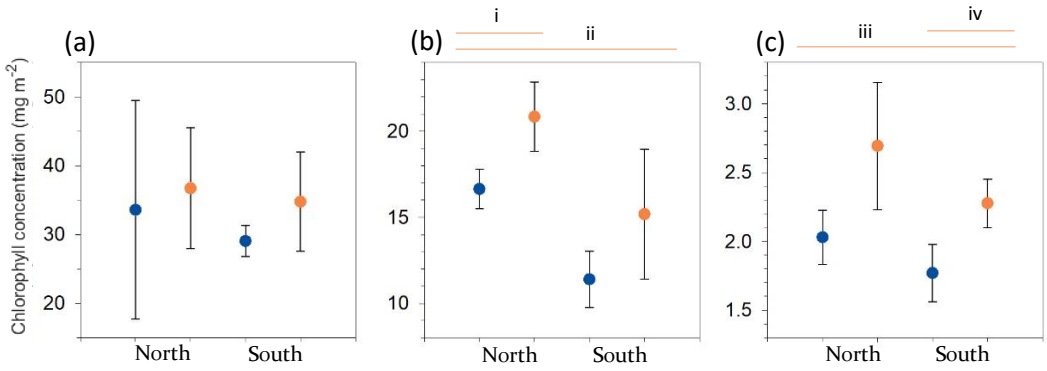

Figure 3.24 Integrated chlorophyll-a for (a) pico-, (b) nano- and (c) micro-phytoplankton, split into North and South stations. Significantly different ridge-basin concentrations (t-test) are (i) nano-north p = 0.035 and (iv) Micro south p = 0.032. Significantly different pair-wise (t-test) comparisons are (ii) nano p = 0.017 and (iii) micro p = 0.022. Mean chlorophyll-a concentration is plotted for each section with standard deviation error bars (n = 3).

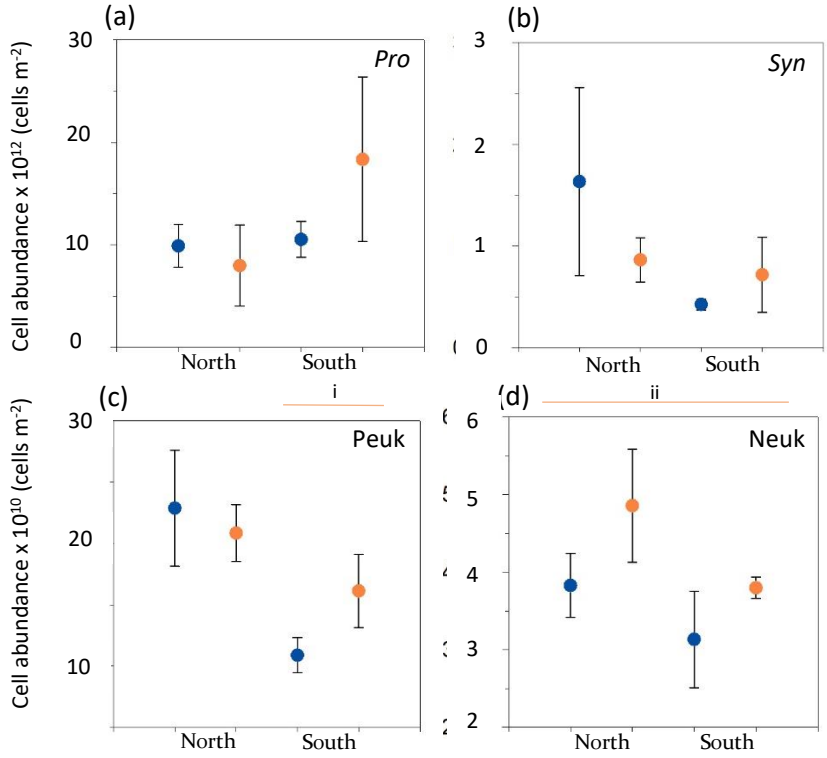

Figure 3.25 Integrated picophytoplankton for (a) Prochlorococcus (Pro), (b) Synechococcus (Syn), (c) picoeukrayotes (Peuk), and (d) nanoeukrayotes (Neuk). Split into north and south stations. Significantly different ridge-basin populations are (ii) nanoeukaryotes pairwise (paired t-test) comparison p = 0.055 and (i) picoeukaryotes in the south p = 0.053 (t-test). Mean cell abundance is plotted for each section with standard deviation error bars (n = 3).

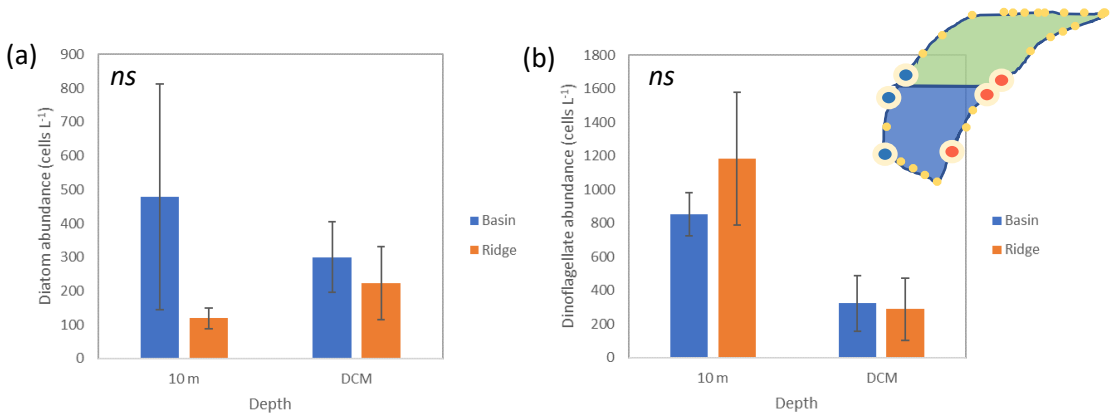

Figure 3.26 Abundance of (a) > 10 µm diatoms and (b) > 10 µm dinoflagellates at 10 m and the DCM off-ridge (blue) and on-ridge (orange). Bars are mean with standard deviation error bars (n = 3). ns = no significant difference between ridge and basin stations was observed at both 10 m and the DCM.

3.3.1.5 Seasonality in the subtropical North Atlantic

Seasonality between October 2015 (AMT25) and June 2016 (RidgeMix) was compared over the Mid-Atlantic Ridge between 23 and 36 °N (Figure 3.27a). Surface waters were warmer during AMT25 (24-26°C) compared to during RidgeMix (20-24°C) causing a stronger thermocline in October 2015 (Figure 3.27b and c). Temperature was similar between cruises at 200m. Salinity was similar during both cruises with waters being more saline in the water column to the south during RidgeMix (Figure 3.27d and e). The difference in temperature between cruises causes different density distribution (Figure 3.27f and g). The mixed layer depth was also similar between cruises, 47 ± 9 m and 41 ± 20 m during AMT25 and RidgeMix respectively. Nitrate concentrations were similar between cruises at 200 m. However, the nitracline was shallower during RidgeMix with higher nitrate concentrations between 100 and 200 m (Figure 3.27h and i). The DCM was shallower during RidgeMix (99 ± 27 m) compared to during AMT25 (124 ± 13 m) and chlorophyll-*a* concentrations on average were lower during Ridgemix (0.32±0.15 mg m^3) compared to AMT25 (0.41±0.13 mg m^3) although are not statistically different.

All chlorophyll-*a* size-fractions have significantly higher chlorophyll-*a* concentrations during RidgeMix (ANOVA, $p < 0.001$, Figure 3.28a). Abundance of *Prochlorococcus*, picoeukaryotes, nanoeukaryotes and coccolithophores were higher and *Synechococcus* lower during RidgeMix (ANOVA, $p < 0.001$, except coccolithophores $p < 0.05$, Figure 3.28b, c and d).

The observed seasonal variation in picophytoplankton groups (95 ± 35%) and size-fractionated total chlorophyll-*a* (74 ± 23%) were larger than observed daily variation (apart from cryptophytes). The average daily variability of total chlorophyll-*a* measured over three days during RidgeMix was 11 ± 13%, or 15 ± 13% for the 0.2-2 µm size fraction, 14 ± 3% for the 2-20 µm size fraction and 34 ± 30% for the > 20 µm size fraction. Total picophytoplankton day-night variation was 31 ± 7% and heterotrophic bacteria 4 ± 3%. *Prochlorococcus* varied by 29 ±

12%, *Synechococcus* by 28 ± 38%, picoeukaryotes 12 ± 10%, nanoeukaryotes 25 ± 32%, coccolithophores 3 ± 4%, and cryptophytes 101 ± 57%.

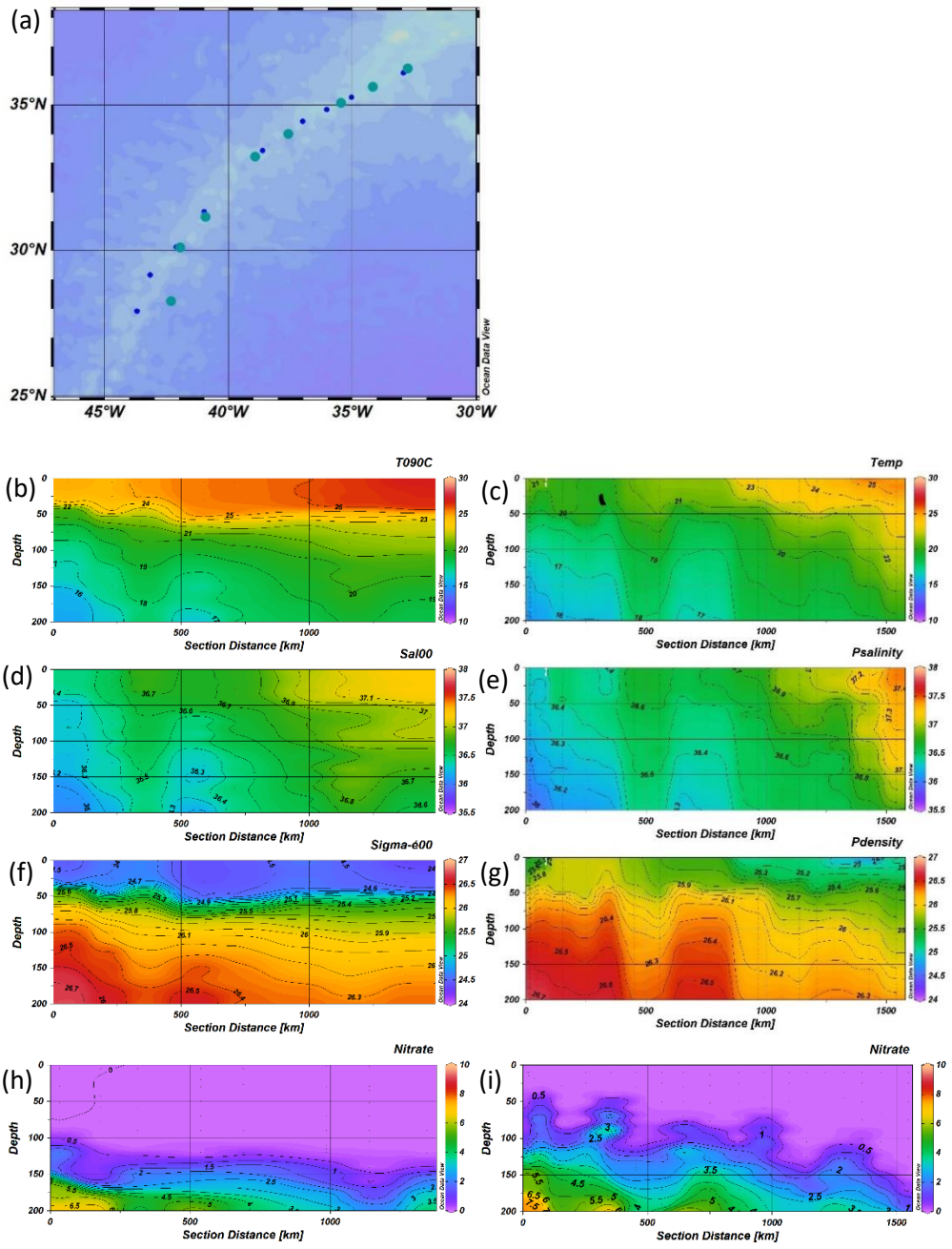

Figure 3.27 Physics and nitrate section plots with depth to 200 m for the stations between 27 and 36°N over the Mid-Atlantic Ridge during AMT25 (October 2015, left column) and RidgeMix (June 2016, right column). (a) Station location during AMT25 (turquoise dots) and RidgeMix (dark blue dots). Section plots (b) and (c) are temperature (°C), (d) and (e) salinity (PSU), (f) and (g) density (kg m^{-3}), and (g) and (i) nitrate (µM) during AMT25 and RidgeMix respectively.

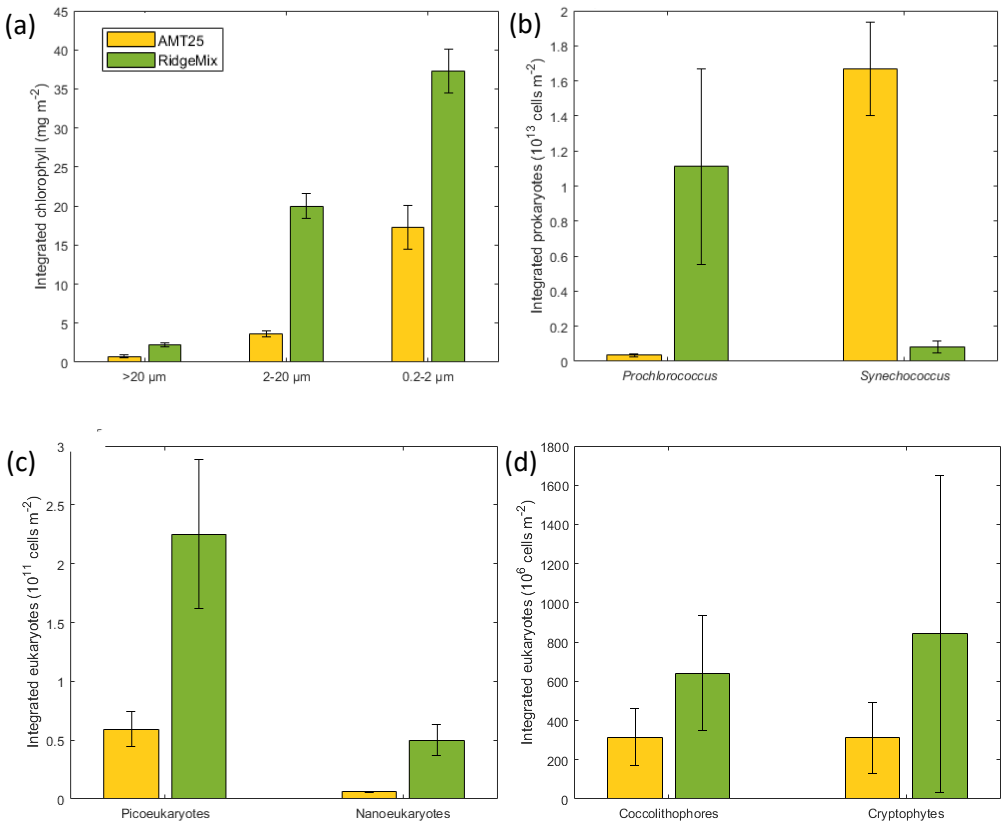

Figure 3.28 (a) Integrated size-fractionated chlorophyll-a and (b, c, d) picophytoplankton cell abundances for 10-180 m during AMT25 and RidgeMix. Bars are mean with standard deviation error bars (n = 8 and 9).

3.3.2 The Sierra Leone and Rio Grande Rise

Two transects southward over two ocean ridges in the Atlantic Ocean were sampled in October 2015. One transect over the Sierra Leone Rise (SL Rise; CTD 39 and 40 Figure 3.29a,c) at ~8°N and the other over the Rio Grande Rise (RG Rise; CTD 71 Figure 3.29b, d) at ~33°S. The thermocline and pycnocline steadily got deeper southward on the transect over the SL Rise (Figure 3.30c and g). Surface temperature was 26 to 28°C (Figure 3.30c) and surface salinity 35.2 to 35.8 PSU (Figure 3.30e). Surface salinity was lower in the top 30 m for the two stations below 6°N (CTD 40 and 41; 35.2-35.3 vs. 35.5, Figure 3.30e). The DCM was at 59 to 68 m with concentrations of 0.72 to 1.2 mg m^{-3} apart from CTD 39 where the DCM was higher at 39 m with concentrations of 2.59 mg m^3. The transect over the RG Rise goes from stratified to a near mixed water column down to 200 m to the south (Figure 3.30d, f, h). Surface temperature ranged from 14 to 19°C (Figure 3.30d) and salinity ranged from 35.4 to 36 (Figure 3.30f).. The DCM depth over the RG Rise gets shallower to the south, from 135 m to 38 m. Chlorophyll-*a* concentrations at the DCM are similar at all stations, 0.42-0.46 mg m^{-3}, but slightly higher at CTDs 70 and 74 (0.57 and 0.65 mg m^{-3}).

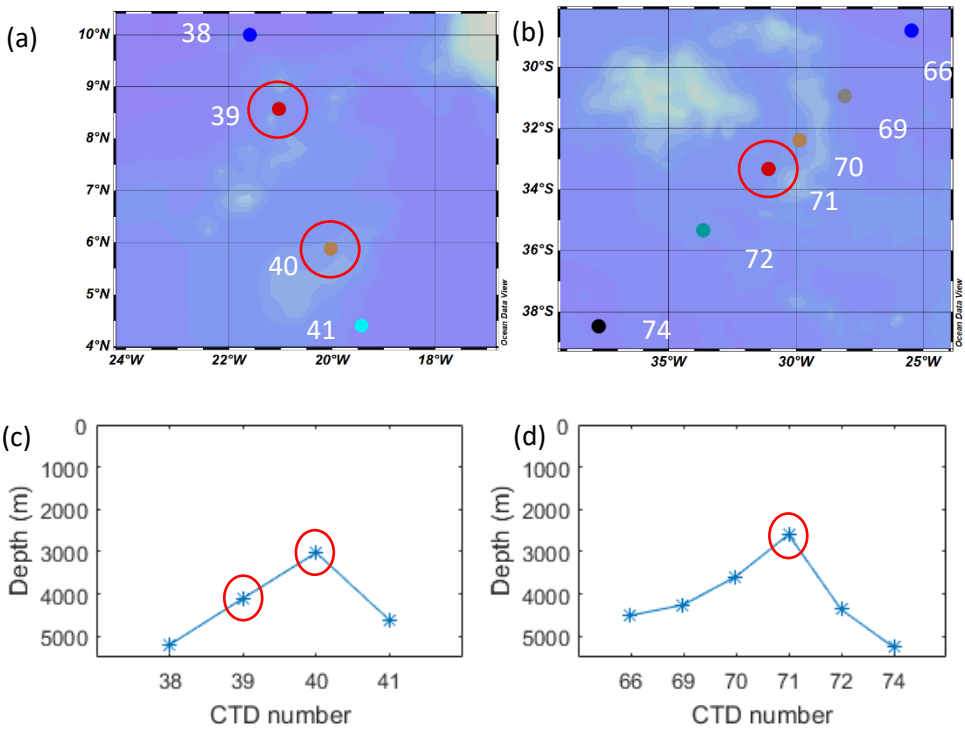

Figure 3.29 Station locations over (a) the Sierra Leonne Rise and (b) the Rio-Grande Rise. Sea floor depth for each of the stations sampled for phytoplankton. (c) Sierra Leone Rise (d) Rio Grande Rise. "Rise" stations circled in red. Sierra Leone Rise CTD 39 was south of a 200 m deep Seamount.

Chlorophyll-*a* concentration in the > 20 µm size fraction increased 2-fold at the stations associated with the ridges (CTD 39 and 71), compared to adjacent stations (5.3 ± 0.4 mg m^{-2} compared to 2.2 ± 0.5 mg m^{-2}, and 14 ± 0.3% of total chlorophyll-*a* compared to 6 ± 2%, Figure 3.31a and b). Over the Sierra Leone Rise, at CTD 39, the 2-20 µm chlorophyll-*a* size-fraction was also higher, 34% compared to 26 ± 3% (Figure 3.31a). Over the Rio Grande Rise, the fraction of chlorophyll-*a* in the 2-20 µm size-fraction increased with increasing latitude south, 15 to 41 % (CTDs 66 to 74) and after CTD 71 integrated chlorophyll-*a* rapidly increased to 55 mg m^{-2} (Figure 3.31b). For picophytoplankton cell abundances, there was higher proportions of *Synechococcus* and picoeukaryotes at CTD 39 and increasing importance of *Synechococcus* and picoeukaryotes south over the RG Rise (Figure 3.31c and d). CTDs 70 and 71 have almost equal *Synechococcus* and picoeukaryotes, but the southern stations have higher contributions from *Synechococcus* and low concentrations of *Prochlorococcus* (Figure 3.31d). Below the RG Rise *Synechococcus* was 13-fold higher (5 x 10^{12} ± 5 x 10^{12}- cells m^{-2} compared to 4 x 10^{11} ± 9 x 10^{10} to the north), whilst *Prochlorococcus* was 6-fold lower (2 x 10^{13} ± 6 x 10^{12} cells m^{-2} compared to 3 x 10^{12} ± 3 x 10^{12} cells m^{-2}). Like *Synechococcus*, there were also increases seen in picoeukaryote (4-fold increase) and nanoeukaryote (2-fold increase) abundance to the south of the RG rise (Figure 3.31d). Total cell abundance over the RG Rise generally decreases to the south, as the fraction of *Prochlorococcus* decreases. However, cell abundance was lowest at CTD 71 (Figure 3.31d). The chlorophyll-*a* concentrations and cell abundances are more variable over the SL rise (Figure 3.31a, c).

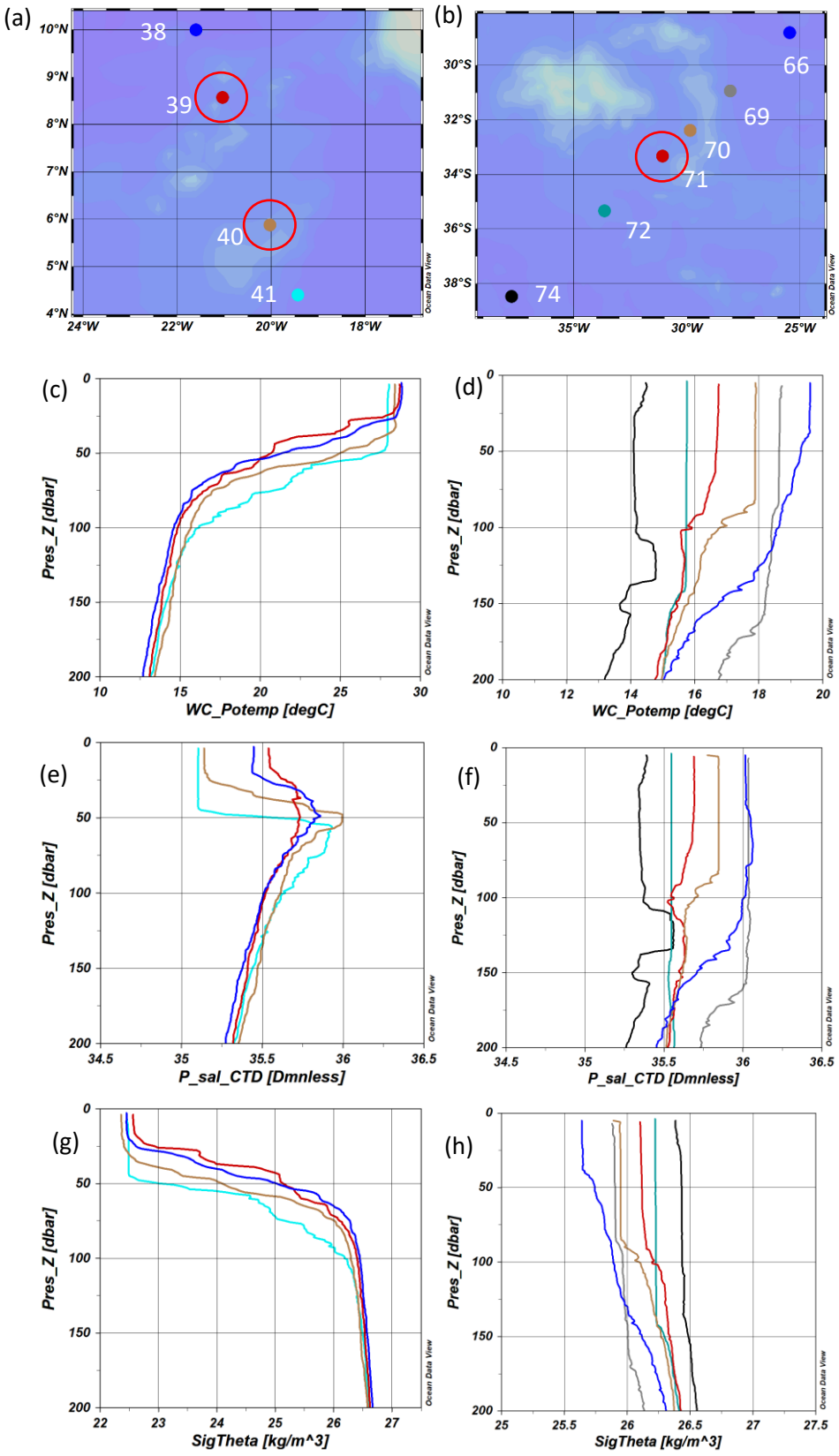

Figure 3.30 Station location and physical properties over (a) Sierra Leonne Rise and (b) Rio-Grande Rise. Stations over the Rises circled in red. Depth profiles of temperature (c) and (d), salinity (e) and (f) and density (g) and (h) for the Sierra Leone Rise (c, e, g) and the Rio-Grande Rise (d, f, h). Station colours for profile plots are show in (a) and (b).

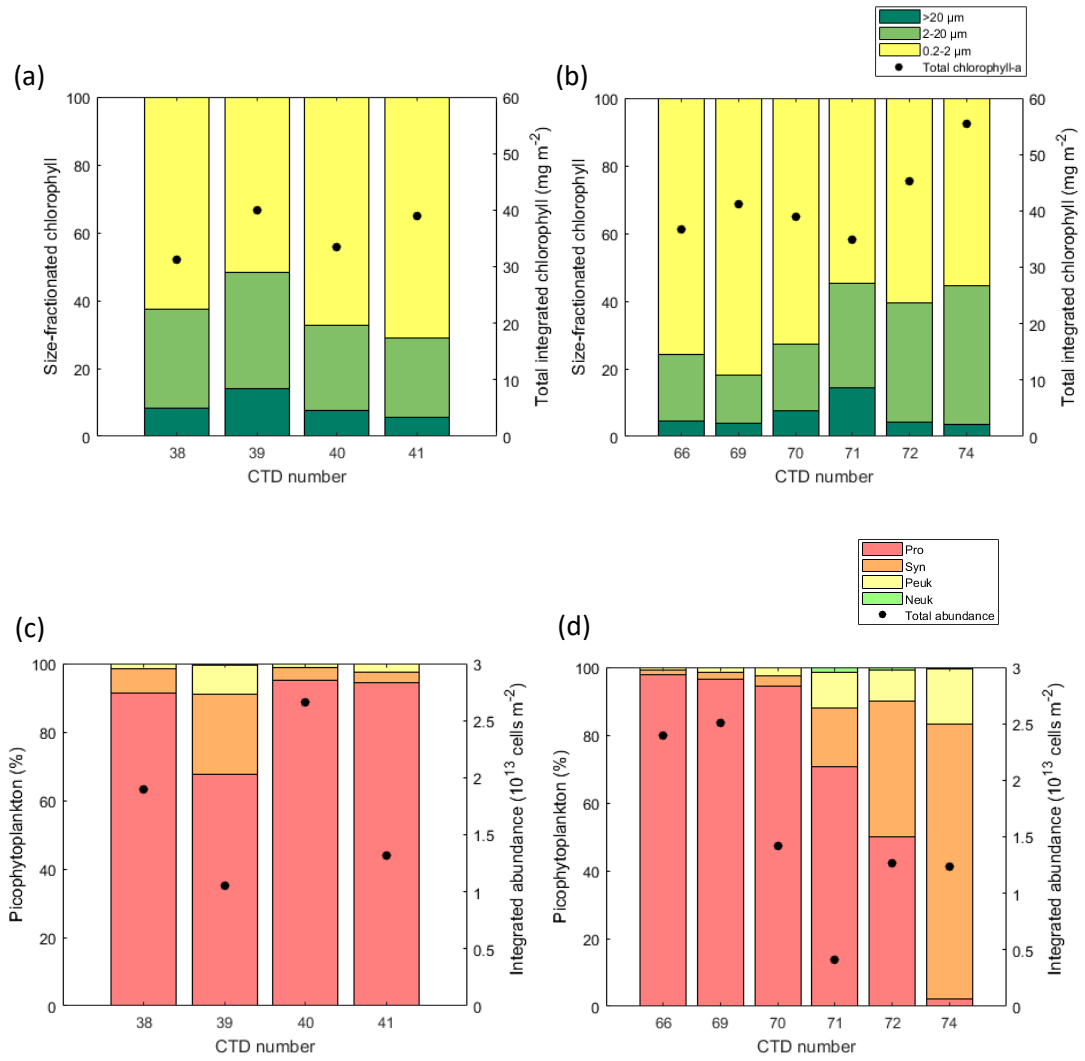

Figure 3.31 Composition and integrated (10-180 m) concentration of (a, b) size-fractionated chlorophyll-a and (c, d) picophytoplankton over the Sierra Leone Rise (a, c) and the Rio Grande Rise (b, d) during AMT25.

3.4 Discussion

3.4.1 Depth distribution of phytoplankton

3.4.1.1 What controls the depth of the DCM?

A combination of bottom-up factors controls the depth of the DCM in the subtropical North Atlantic Ocean: light, nutrients and water column structure (Figure 3.17). Light and nutrients are understood to be principal controls on chlorophyll-*a* distribution, due to their basic control on cell physiology via photosynthesis (Cullen, 1982, 2015; Klausmeier & Litchman, 2001; Acevedo-Trejos et al., 2013, 2015). In this and other studies, the depth of the 1% surface irradiance (PAR) is used as an indicator of the effect of light on the DCM depth (Letelier et al., 2004; Mignot et al., 2014). The depth of the 1% surface irradiance was defined as the physical euphotic zone depth in 1956 by John Ryther (Letelier et al., 2004). The 1% light depth strongly correlates with DCM depth (R^2 = 0.7792, p = 0.01) in our study region, and is in line with

recent studies that have shown the DCM seasonally tracks isolumes (Letelier et al., 2004; Silsbe & Malkin, 2016). The DCM also correlates with the nitrate intercept in this study (R^2 = 0.7324, $p < 0.01$), suggesting the depth of the DCM is controlled by nitrate. However, as the oligotrophic ocean is nutrient limited, it is likely that the depth of the DCM determines the depth of the nitrate intercept due to uptake of nitrate by phytoplankton at the DCM.

The results presented here show that whilst both light and nutrients influence the DCM depth ocean dynamics also influence its modulation (Huete-Ortega et al., 2011). Non-metric multidimensional scaling (NMDS) analysis of environmental variables with the DCM depth found that the 1% light depth, nitracline depth, surface salinity, and density at the DCM were the factors most strongly related to DCM depth in the study area (Figure 3.17). There is a north-south latitudinal gradient in temperature and salinity, therefore density, as well as DCM depth over the study area. As a result, the DCM depth is correlated with sea surface temperature, surface salinity, surface density, and density at the DCM. Water column structure is important in determining the supply of nutrients to phytoplankton communities in surface waters, and is also an important predictor of phytoplankton species and annual phytoplankton variation (Menzel & Ryther, 1961; Mojica et al., 2015).

Isopycnals appear to control the DCM depth on the northern transect (Figure 3.16 sections 1 and 7, isopycnal control). It is thought that whilst PAR controls the depth of the DCM on longer timescales, at shorter timescales the depth of the DCM may be controlled by isopycnal displacement, such as in a dynamic eddy area of the northern transect, 36°N (Letelier et al., 2004; Mignot et al., 2014). The depth of the DCM can also be controlled by a combination of factors not considered in this study, these include: cell physiology, phytoplankton growth, pigment acclimation, phytoplankton swimming and buoyancy behaviours, zooplankton grazing, and other hydrodynamics (Cullen, 2015).

3.4.1.2 Does the chlorophyll-a maximum represent a phytoplankton maximum?

A positive exponential correlation (ρ = 0.737, $p < 0.01$) between chlorophyll-*a* concentration and picophytoplankton abundance was observed at the DCM during RidgeMix. Chlorophyll-*a* is the best indicator of phytoplankton biomass in natural samples (Cullen, 1982). However, the relationship between chlorophyll-*a* and biomass is inconsistent (Cullen, 1982, 2015; Pérez et al., 2006). The chlorophyll-*a* maximum does not always represent the biomass maximum as physiological adaptations – e.g. acclimation, shading, photoinhibition, and production of chlorophyll degradation products - change cell carbon to chlorophyll-*a* ratios (Cullen & Eppley, 1981; Marañón et al., 2000, 2003; Pérez et al., 2006). Chlorophyll-*a* is also generally determined by fluorescence yield, which is not a simple linear function of chlorophyll-*a* concentration (Falkowski & Kiefer, 1985). Whilst fluorescence maxima are usually at the chlorophyll-*a* maxima, the fluorescence yield per mole of chlorophyll-*a* is highly variable with phytoplankton species, cell size, photoinhibition, photoadaptation, nutrient limitation, and

diel rhythms (Cullen & Eppley, 1981; Falkowski & Kiefer, 1985). Despite these limitations, chlorophyll-*a* is still used to provide insights into the biomass of phytoplankton with depth, and is used as a global tracer of primary production via a set of algorithms that utilise ocean colour (Hu et al., 2012). Our findings suggest that the DCM in the subtropical North Atlantic is associated with a higher abundance of cells at this depth. Emerging evidence suggests the DCM in the subtropical ocean could be an important site of new primary production, biomass and carbon export (Letelier et al., 2004; Pérez et al., 2006; Mignot et al., 2014).

3.4.1.3 Depth distribution of picophytoplankton (< 10 µm)

In this study, the highest abundances of *Prochlorococcus* were found just above the DCM and eukaryotes just below. This finding agrees with observations by Latasa et al., (2017) that *Prochlorococcus* occur in the upper part of the DCM and coccolithophores, chlorophytes, and pelagophytes in the deeper layers (Latasa et al., 2016, 2017).

Phytoplankton groups have preferences for different depths within the DCM and are not evenly distributed in the top 200 m (Bidigarel et al., 1990; Latasa et al., 2017). The phytoplankton depth distribution observed here is similar to previous studies in the subtropical and tropical North Atlantic (Marañón et al., 2001; Veldhuis & Kraay, 2004; Pérez et al., 2006) . Picophytoplankton chlorophyll-*a* contribution to total chlorophyll-*a* is highest at the DCM and all picophytoplankton groups exhibit a subsurface abundance maximum which is close to the chlorophyll-*a* maximum. These findings are consistent with past studies in the subtropical and tropical northeast Atlantic (Gin et al., 1999; Mann et al., 2002; Pérez et al., 2006; Moreno-Ostos et al., 2011). Zubkov *et al*. (1998) also found that *Prochlorococcus* dominates the DCM in terms of abundance, chlorophyll-*a* and biomass, and picoeukaryote maximum abundances were always associated with the DCM and contributed substantially to biomass (Li, 1995; Partensky et al., 1996; Veldhuis & Kraay, 2004; Vázquez-Domínguez et al., 2008). It is thought the subsurface maximum in picophytoplankton abundance is due to the competitive advantage small-cells have in low light conditions (Gin et al., 1999; Pérez et al., 2006).

Prokaryotic picoplankton assemblages can shift with depth (Schattenhofer et al., 2009). There is a strong niche partitioning of *Prochlorococcus* and *Synechococcus* depth-wise in the water column, where *Prochlorococcus* is found deeper than *Synechococcus,* as seen here (Olson et al., 1990; Riemann et al., 2011; Casey et al., 2013). This is because *Prochlorococcus* has the competitive advantage in deeper waters where irradiance levels are low, as its light-harvesting antenna is almost twice as efficient as *Synechococcus* at absorbing the blue light found at depth (Morel et al., 1993; Moore et al., 1995; Ting et al., 2002; Heywood et al., 2006). Depth differentiation in *Prochlorococcus* is known to occur due to high stratification during the summer and strong gradients in light, temperature and nutrients (Kashtan et al., 2017). *Prochlorococcus* is known to have two main ecotypes especially adapted for life at different

light levels, the high-light and low-light adapted *Prochlorococcus* (Johnson et al., 2006). Both ecotypes were present here in the subtropical ocean, although enumerated together (Johnson et al., 2006).

3.4.1.4 Depth distribution of > 10 µm phytoplankton

Cell abundance and composition of larger phytoplankton (>10 µm) varied with depth. At 10 m, cell abundances were higher and were dominated by dinoflagellates compared to the DCM, where cell abundance was lower and co-dominated by diatoms and dinoflagellates (and unknown) species. Phytoplankton groups are often found to be different in the DCM and mixed layer due to the different environmental conditions present and phytoplankton ecology (Venrick, 1990; Estrada et al., 2016; Latasa et al., 2017). It is thought that the relatively high abundance of dinoflagellates found in the low nutrient upper euphotic zone of the subtropical ocean may be due to their trophic characteristics, specifically whether they are mixotrophic or heterotrophic, or are able to vertically migrate (Estrada et al., 2016). Dinoflagellates are a very diverse group, with ~50% of dinoflagellate species thought to be obligate heterotrophs (Hoppenrath et al., 2009). Over the past two to three decades, many, if not most, species of dinoflagellates that were previously thought to be autotrophic have been found to be on the mixotrophic spectrum (Jeong et al., 2010; Dagenais-Bellefeuille & Morse, 2013). Mixotrophy and heterotrophy are very hard to identify in Lugol's stained samples. Diatoms on the other hand are obligate autotrophs that can tolerate low and variable light (Key et al., 2010) and are found among the deepest parts of the DCM (Latasa et al., 2017). Diatoms have been observed to dominate the DCM and form extensive DCM blooms in the open ocean of the Sargasso Sea, Pacific and Southern Ocean - thought to be due to the unique nutrient uptake and storage capacity that allows diatoms to outcompete other plankton in regions of episodic nutrient supply, such as the open ocean (Kemp & Villareal, 2018 and references therein).

3.4.2 Spatial distribution of phytoplankton

3.4.2.1 Influence of the Mid-Atlantic Ridge in the subtropical North Atlantic

A comparison of chlorophyll-*a* concentrations and phytoplankton community structure in June 2015 revealed that there was (a) a 30% increase in chlorophyll-*a* concentrations in the 2-20 and >20 µm fractions, (b) a 40% increase in pico- and nanoeukaryote abundance over the mid-Atlantic ridge compared to the adjacent basin. These findings are in line with ecological theory and findings in the shelf sea system. According to Margalef's Mandala, larger-cells are associated with higher levels of turbulence and nutrients, as larger cells have higher nutrient uptake rates and larger nutrient storage capacities, termed k-strategists (Margalef, 1978; Wyatt, 2014; Mouriño-Carballido et al., 2016). At the shelf edge in the Celtic Sea Sharples *et al.* (2009) found larger phytoplankton dominated the shelf edge whilst cyanobacteria *Prochlorococcus* and *Synechococcus* dominated regions away from the shelf edge (Sharples et al., 2007, 2009).

An order of magnitude higher diapycnal nitrate fluxes were observed over the ridge compared to the basin. Tuerena *et al.* (submitted) demonstrates that the ridge-enhanced turbulent mixing, driven by internal tides, account for over half of the diapycnal nitrate flux to the DCM in subtropical oceans, where vertical gradients of all macronutrients (N, P, Si) to the base of the DCM were higher over the ridge than the adjacent basin (Tuerena et al., submitted). With increases in nutrients and turbulence a simplified version of Margalef's mandala predicts the community will be shifted away from a dinoflagellate dominated community and towards a diatom dominated community (Figure 3.32). However, we do not observe any significant difference in either diatom or dinoflagellate abundance at the DCM over the ridge compared to over the basin. In the surface waters (10 m) our findings suggest there may be a reduction in diatoms over the ridge. As nutrients do not reach the surface waters of the oligotrophic ocean, the higher abundances of diatoms over the basin may be due to the presence of diatom nitrogen-fixing symbionts (e.g. *Hemiaulus spp.* with *Richelia* cyanobacteria symbionts) in the tropical surface waters (Villareal, 1994; Capone et al., 2005; Foster et al., 2011). We observe higher numbers of *Hemiaulus spp*. at 10 m in section 4 (Appendix Table 3.2). One of the caveats of the simplified Margalef's Mandala pictured in Figure 3.3.2 is that diatom genera that thrive in subtropical stratified, oligotrophic oceans are not considered (Kemp & Villareal, 2018). Alternately, the lower abundances of diatoms, in the surface waters over the ridge, may be explained by enhanced zooplankton grazing over the Mid-Atlantic Ridge, implying top-down control of biomass. This will be discussed in Chapter 4.

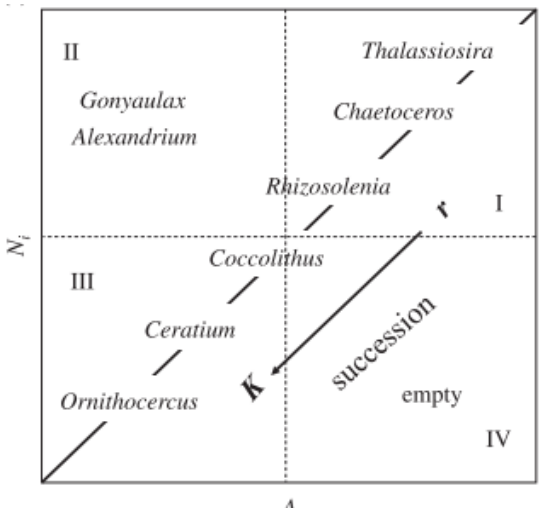

Figure 3.32 Margalefs Mandala (1978) redrawn by Wyatt (2014). x-axis is turbulence (A), y-axis is nutrient concentration (N). The diagonal line shows the main sequence with the r and K strategists. Roman numerals are the four domains.

The results suggest an influence of the Mid-Atlantic ridge on phytoplankton dynamics. Analysis of the phytoplankton community at 10 m and the DCM had the same result as analysis of the whole water column. However, we must be cautious as the results may be an east-west signal rather than ridge-basin signal. Similar to the latitudinal gradient in temperature and salinity, there appears to be a longitudinal gradient in ML depth and water stability (sum BF_{200m}), with waters being more stable over the basin with shallower ML depths than over the ridge.

3.4.2.2 Mesoscale and sub-mesoscale features of the subtropical North Atlantic

Concentrations of *Synechococcus*, picoeukaryotes, nanoeukaryotes, coccolithophores, cryptophytes, and heterotrophic bacteria, as well as the two larger chlorophyll-*a* size-fractions (2-20 and > 20 μm), were on average 20 to 100% higher north of the front at ~31°N, and *Prochlorococcus* 20% lower, compared to south of the front.

3.4.2.2.1 North-South divide

The temperature-salinity relationship identified a front at 31°N, which also corresponded to the north to south contrast in the depth and concentration of the DCM and phytoplankton. In the subtropical North Atlantic, thermal fronts are defined as a change in temperature of 1°C within 10 km (Voorhis & Hersey, 1964). In this study, changes of 1°C in sea surface temperature are observed at the 31°N as well as several locations in the north associated with eddies.

The boundary at 31°N is comparable to Longhurst's biogeographical boundary between the North Atlantic Subtropical Gyral Province (NAST) and the North Atlantic Tropical Gyral Province (NATR) at 25-30°N (Longhurst, 2010; Reygondeau et al., 2013). Longhurst's provinces were classified using surface chlorophyll-*a* images and regional oceanography (mixed layer depth, Brunt-Väisälä frequency, Rossby internal radius of deformation, photic depth, and surface nutrient fields). Longhurst defines the boundary between these two regions as the highly dynamic subtropical convergence (STC) thermal front (Longhurst, 2010). To the north NAST, a transition zone, is bounded by the Azores Current a dynamic eddy region of changing seasonal extent, 40-42°N. To the South NATR is bounded by the North Equatorial Current (NEC, 12-14°N).

A recent study characterised the phytoplankton community through the subtropical and temperate North Atlantic and found the same increase in total chlorophyll-*a* (>50%, in all size-fractions 0.2-2,2-10 and >10 μm) from NATR to NAST, at ~28-32°N ~50°W, as reported here (Cáceres et al., 2016). Like Cáceres *et al*. we observed higher abundances of *Synechococcus*, picoeukaryotes, nanoeukaryotes in NAST (north of 31°N) than NATR (south of 31°N), and homogenous dinoflagellates, but unlike Cáceres *et al*. where diatoms were higher in NAST we observe homogenous distributions of diatoms, except the bloom station to the north of the front (Cáceres et al., 2016). In May 1981, Fasham *et al*., observed the Azores Front between 31-34°N and 28-36°W. In good agreement with the results of this present study, they found two distinct water masses with a deeper DCM to the south (averaging 20 m deeper), and lower chlorophyll-*a* concentrations (50-60% lower) but little evidence for a change in phytoplankton biomass (Fasham et al., 1985). Other studies have observed similar changes in chlorophyll-*a* associated with the Azores Front and thermal fronts of the Subtropical Convergence, 22-35°N (Fernández & Pingree, 1996; Riemann et al., 2011).

3.4.2.2.2 The Azores Current

The southern arm of the summer Azores Current could be a plausible explanation for the north-south divide observed here at 31°N. The Azores current is the meandering southern branch of the Gulf Stream, centred on 34°N, that flows from the division of the Gulf Stream and the North Atlantic Current (Gould, 1985; Klein & Siedler, 1989). During summer, the Azores Current southern arm travels around the corner rise seamounts, ~35°N 50°W, before travelling eastward across the Mid-Atlantic Ridge, the northern arm continues its winter route, see figure 3.33 (Klein & Siedler, 1989).

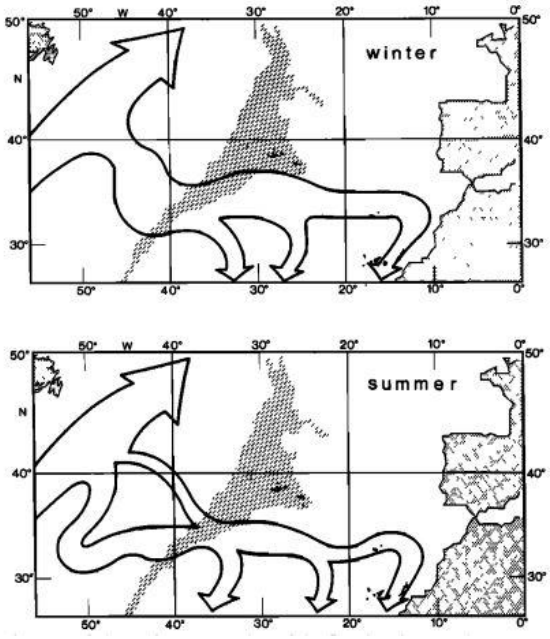

Figure 3.33 Figure 10 from Klein & Siedler, 1989. 'Schematic presentation of the flow in winter and summer. Diagonal shaded areas indicate positions of Mid-Atatnic Ridge.'

The northern arm of the summer Azores Current crosses the northern section of our cruise track (sections 1 and 7 and the top of section 2), following the definition of Gould as where the 15°C isotherm lies above 300 m, which is the same as when the 16°C isotherm rises above 200 m (Gould, 1985; Macedo et al., 2000). The current is particularly visible in the ADT current velocity plot (Figure 3.8), associated with high eddy activity between 32-40°N and 30-47°W, which is in keeping with the suggestion that the Azores front is a baroclinic feature (Fernández & Pingree, 1996).

3.4.2.2.3 Eddies

The Azores current is known to be a dynamic eddy area (Gould, 1985; Alves et al., 2002). This is reflected in the Absolute Dynamic Topography which indicates high eddy activity in northern sections of the study area (Figure 3.8) and the displacement of the thermocline, pycnocline and nitracline in the top 300 m of the water column (Figure 3.5 and 3.7a). High concentrations of larger phytoplankton (> 2 µm) and *Synechococcus,* picoeukaryotes, and nanoeukaryotes were observed at several stations in sections 1, 2 and 7. *Synecococcus*, picoeukaryotes and larger cells are known to thrive in more mesotrophic waters (Zubkov et al., 2000; Latasa et al., 2010). The upwelling of nitrate by eddies is thought to be a large nutrient supply mechanism to the nutrient limited subtropical surface ocean (Benitez-Nelson et al., 2007; McGillicuddy et al., 2007; Mahaffey et al., 2008). The upwelled nutrients of eddies have been observed to stimulate phytoplankton blooms inside both cyclonic and mode-water eddies (McGillicuddy et al., 2007).

We observe a diatom bloom in the northwest corner station (CTD 55, section 6, 36°N), cell concentrations were 42-fold higher at 10 m and two-fold higher at the DCM than the other stations sampled. The presence of a diatom bloom in surface waters of the oligotrophic ocean, where picophytoplankton dominate, suggests eddy influence, as observed by Benitez-Nelson *et al.* (2007) in the subtropical Pacific. Unlike previous studies that observe doming or depression of the pycnocline we do not observe any significant difference in the pycnocline compared to adjacent stations (McGillicuddy et al., 2007). The lack of an uplifted pycnocline but shallower nitracline (~40-60 m shallower) suggests eddy decay, during which time uplifted pycnoclines are relaxed and nutrients moved downward (Benitez-Nelson et al., 2007). Eddy chlorophyll-*a* response depends on the type of eddy and its stage of development, as eddies are constantly changing their biogeochemical conditions (Benitez-Nelson et al., 2004). Mode-water eddies in the subtropical North Atlantic are known to sustain patchy diatom blooms for periods of longer than 3 months (McGillicuddy et al., 2007; Bibby et al., 2008).

3.4.2.3 Temporal change in phytoplankton community

During RidgeMix, three stations were sampled twice over 24 hours, once during the day and once at night, to determine whether the daily differences in phytoplankton community were smaller or larger than differences between seasons. We compared data collected during RidgeMix (June 2016) with data collected during AMT25 (October 2015). Comparing June 2016 and October 2015 there were ~2.8-fold higher chlorophyll-*a*, ~27-fold higher picophytoplankton abundance (*Prochlorococcus* + picoeukaryotes + nanoeukaryotes + coccolithophores + cryptophytes), and ~20-fold lower *Synechococcus* abundance in June 2016. The nitracline was shallower during June 2016 and the DCM, on average, 25 m higher in the water column. Significant phytoplankton seasonality has previously been observed in the subtropical gyres (Zubkov et al., 2000; Poulton et al., 2006) and the Sargasso Sea (Durand et al., 2001; Steinberg et al., 2001), with higher chlorophyll-*a* and carbon fixation during spring. There is a two-fold increase in chlorophyll-*a* concentrations at the Bermuda Atlantic Time Series station in the Sargasso Sea during the spring bloom in early May (Bidigarel et al., 1990). The seasonal expansion and contraction of surface chlorophyll-*a* concentrations in the oligotrophic gyres is consistent with changes in horizontal nitrate supply (Dave et al., 2015). In summer the North Atlantic oligotrophic region (satellite chlorophyll-*a* < 0.1 mg m^{-3}) and subtropical gyre coincide, but in winter the oligotrophic region is greatly reduced to the core of the subtropical gyre (Dave et al., 2015). These authors note that the extent to which the pronounced changes in chlorophyll-*a* are due to photoacclimation or a change in biomass requires further investigation (Behrenfeld et al., 2005; Dave et al., 2015).

It is thought that light influences the seasonal change in DCM depth in the subtropical ocean. In winter the DCM is at its shallowest and during spring it deepens by an estimated 7.5-10 m per month, to reach its deepest depth in summer (Strass & Woodst, 1991; Winn et al., 1995;

Macedo et al., 2000; Letelier et al., 2004; Mignot et al., 2014). This contrasts our observation of a deep DCM depth in October 2015, 124 ± 13 m, and shallower in June 2016, 99 ± 27 m. However, the shallower DCM (by ~25 m) and the changes observed in phytoplankton chlorophyll-*a* and abundance in this study are likely due to the presence of the summer southern arm of the Azores Current reaching down to 31°N during June 2016, see previous section (Fasham et al., 1985; Stramma & Siedler, 1988; Zubkov et al., 2000; Heywood et al., 2006).

The picophytoplankton groups, *Prochlorococcus* and all the eukaryotes were ~27-fold higher during June but *Synechococcus* was ~20-fold higher during October. Picophytoplankton are observed to have both annual and seasonal variation, with *Prochlorococcus* being highest in summer/autumn and picoeukaryotes being highest in spring (Campbell et al., 1997; Liu et al., 2007; Malmstrom et al., 2010). Similar to this study, previous AMT cruises have observed higher *Prochlorococcus* and picoeukaryote standing stocks during spring than autumn (Zubkov et al., 2000). Synechococcus abundance is typically higher in winter-spring when the mixed layer is deep and nutrients are available, such as during the spring bloom (Campbell et al., 1997; Durand et al., 2001; Liu et al., 2007). This is contrary to our findings where *Synechococcus* had higher abundances during autumn (October). Mixed layer depths were similar during October (47 ± 9 m) and June (41 ± 20 m), and nitracline deeper during October, but temperatures were higher and the thermocline stronger (Figure 3.27). Similar to here, higher abundances of *Synechococcus* have been previously observed in autumn (compared to spring) when waters were warmer, in the East Sea, off Korea (Yona et al., 2014). *Synechococcus* is nearly ubiquitous in the marine environment and is adapted to a wide range of environmental conditions due to the presence of numerous clades and ecotypes (Partensky et al., 1999; Dufresne et al., 2008; Ahlgren & Rocap, 2012). The presence of different ecotypes and/or clades could explain why we observe higher abundances of *Synechococcus* in October compared to June.

The finding that seasonal changes in phytoplankton chlorophyll-*a* and abundance are larger than daily change, up to 27-fold compared to up to 30%, is consistent with observations from Dave *et al.*, (2015) that showed that surface chlorophyll-*a* variability is more pronounced seasonally than intra-annually. Picophytoplankton abundance fluctuates with time of day due to synchronisation of the cell cycle with the light-dark cycle, where photosynthesis and carbon fixation takes place during the day and energy is consumed at night with cell division taking place around dusk (Jacquet et al., 2001; Zinser et al., 2009; Ottesen et al., 2013; Ribalet et al., 2015). As a result, *Prochlorococcus* abundance, for example, varied by 29 ± 12% between day and night casts here but can fluctuate daily by as much as two-fold, given it has a doubling time of a day (Ribalet et al., 2015).

3.4.2.4 Sierra Leone Rise and the Rio Grande Rise

Seamounts can deflect currents on large spatial scales, such as around the Corner Rise Seamounts, and on shorter time scales reflect and amplify internal waves, trap topographical waves, amplify tides, amplify turbulent mixing, uplift isotherms and form anticyclonic and cyclonic eddies (Mouriño et al., 2001). Seamounts are known to influence the plankton community in their near vicinity and are considered to be hotspots of pelagic biodiversity (Morato et al., 2010; Mendonça et al., 2012; Santos et al., 2013). However, the effect of seamounts on biological communities is difficult to assess as it is highly sporadic due to the vast range of seamount geometries of differing shape (cuboid to conical), depth (e.g. a summit of 100 m or 2000 m below sea level) and size (Mendonça et al., 2012).

The Sierra Leone Rise (SL Rise) is a discontinuous chain of seamounts that extends away from the southwestern edge of the Guinea plateau, near the coast of west Africa, towards the Mid-Atlantic Ridge (Hékinian et al., 1978). The SL Rise is a stepped plateau around 3500-4000 m deep which is home to seamounts that rise to 200-2000 m (Litvin, 1984). Over the Sierra Leone Rise (SL Rise) a higher proportion of larger phytoplankton (2-20 and > 20 µm), *Synechococcus* and picoeukaryotes were observed. Isotherms gradually deepen to the south, as does a subsurface salinity maximum. The Guinea dome, a permanent quasi-stationary feature centred on 12°N 25°W, is associated with a doming thermocline (Siedler et al., 1992). So, here we may be sampling the southern edge of the dome. Another interesting feature is the low surface salinity at the two southern stations, south of the rise, which is due to a surface current of low salinity flowing eastward across the Atlantic between 5-10°N before looping southward and returning westward between 0-5°N (Figure 3.34a, c). The eastward flowing current is the North Equatorial Counter Current (NECC), which lies between 3 and 10°N, beneath the Intertropical Convergence Zone (ITCZ), is a relatively narrow current that separates the westward flowing north and south equatorial currents (Peterson & Stramma, 1991). The NECC is known to produce upwelling, a shallow thermoclince and low surface temperatures and the Guinea Dome is associated with high, uplifted chlorophyll-*a* concentrations and phytoplankton blooms (Mcclain et al., 1999; Flores et al., 2000). Therefore, with the given data, without further in-depth analysis, it is hard to be certain whether it is topography or currents interacting that cause the larger cells and higher abundances of *Synechococcus* and picoeukaryotes at CTD 39.

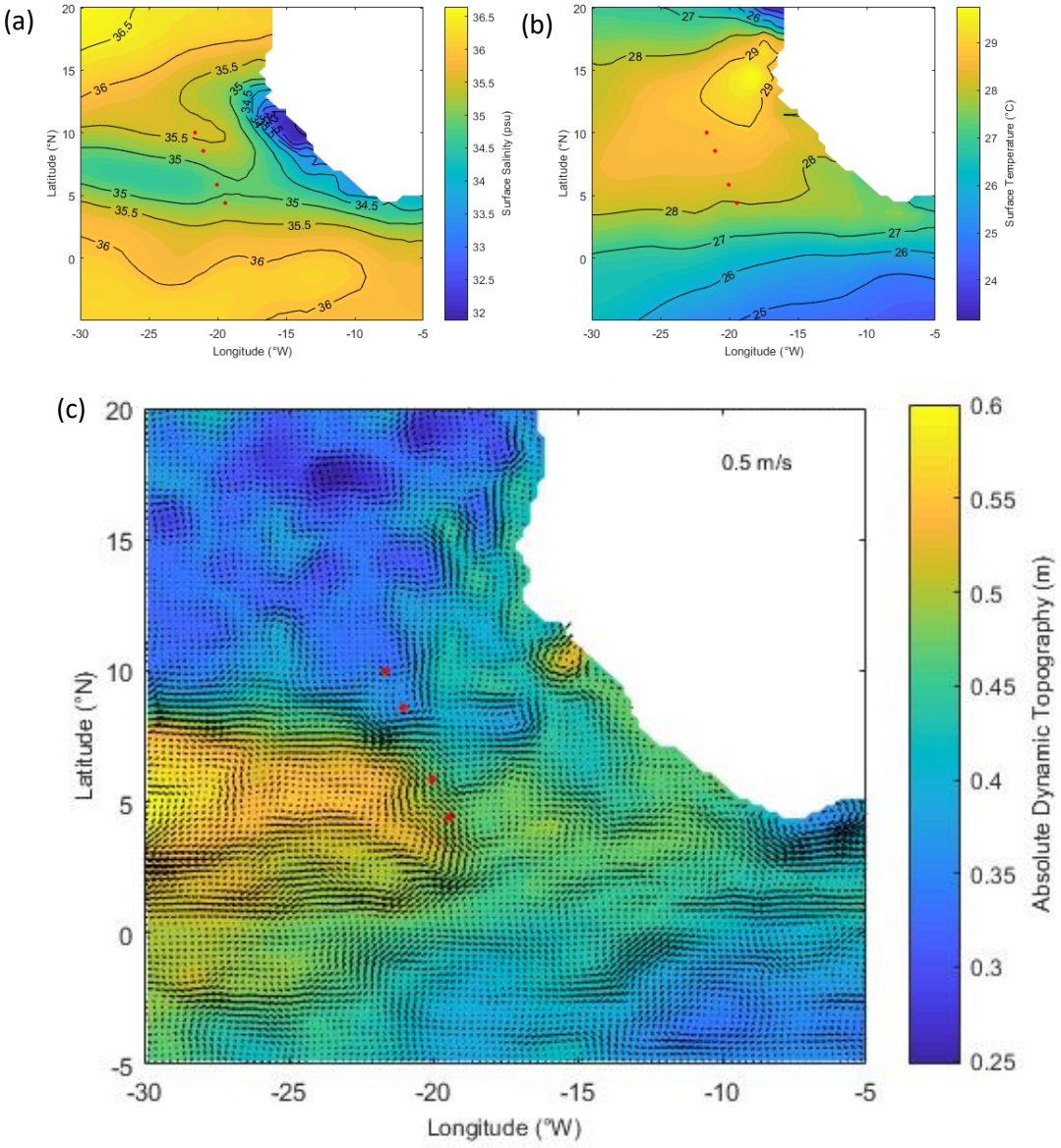

Figure 3.34 (a) Sea surface salinity (b) sea surface temperature (c) Absolute Dynamic Topography and ocean currents (absolute geostrophic velocities u and v) in the Tropical Atlantic Ocean near the Sierra Leone Rise. Red dots are the four CTD stations.

The Rio Grande Rise (RG Rise) is an aseismic ocean ridge, which separates the Santos and Pelotas Basins (Camboa & Rabinowitz, 1984; Sager, 2014). It extends northwest from the South American coast towards the Mid-Atlantic Ridge. The RG Rise is split into western and eastern portions, the western side has an mean depth of 2000 m from which rise guyots and seamounts, less is known about the eastern side which is bounded by fracture zones that parallel the Mid-Atlantic Ridge (Camboa & Rabinowitz, 1984; Sager, 2014). Southward of the RG Rise we observed an abrupt decline in *Prochlorococcus* and an increase in *Synechococcus* and picoeukaryotes (also reflected in the proportions). These findings were observed by Zubkov *et al.* (1998), in October 1996. They found that *Synechococcus* (+picoeukaryotes)

increased locally at the surface near upwelling regions and dramatically between the Rio-Grande Ridge and the Falklands, and *Prochlorococcus* abundance declined dramatically at temperatures below 17°C, above 40°N and below 30°S (Partensky et al., 1996; Zubkov et al., 2000). The water between the Brazil and Falkland currents lacks stratification in the upper 200 m making it a very dynamic region. Cell size also increases to the south of the ridge, over the ridge at CTD 71, there is the largest proportion of >20 µm chlorophyll-*a*.

It is hard to determine whether the underlying topography is the cause of the changes seen, either directly, indirectly or both. As, both CTD 39 and 71 have higher proportions of larger cells, *Synechococcus* and picoeukaryotes which are associated with mixing and higher nitrate input. In addition, the signals seen are similar to those seen over the MAR in the subtropical North Atlantic.

3.4.3 Other controls on phytoplankton distribution

Environmental factors alone are incomplete predictors of phytoplankton community. Subsurface chlorophyll-*a* layers can be formed by a broad range of interacting processes including light and nutrients, local maximum of phytoplankton growth, pigment photoacclimation, swimming and buoyancy behaviours, zooplankton grazing and hydrodynamics (Cullen, 2015). In addition to bottom-up factors explored in this study, there are also top-down factors that control phytoplankton populations, such as grazing, viral lysis, and parasitic symbionts (Lima-Mendez et al., 2015). In this study, heterotrophic bacteria abundance was more than double the picophytoplankton abundance at all stations, so, despite their smaller size of ~0.5 µm, heterotrophic bacteria will have a large impact on ecosystem dynamics. Bacteria interact with the whole ecosystem in a multitude of ways: heterotrophic bacteria and archaea can exclusively access DOM. In addition, they interact/couple with phytoplankton and protists, and are associated with gels, detritus and marine snow (Azam & Malfatti, 2007).

Grazing in the oligotrophic oceans, by herbivorous zooplankton exerts a massive control on phytoplankton populations, where grazing and cell-division can occur at the same rate (Behrenfeld & Boss, 2014). Autotrophic plankton (phytoplankton) are grazed by mixotrophic and heterotrophic plankton, often referred to by size as microzooplankton (< 200 µm) and mesozooplankton (200 - 20,000 µm). Grazers exert top-down pressure on phytoplankton communities and as a result we may not observe hypothesised changes in phytoplankton abundance or biomass (Steinberg & Landry, 2017). Zooplankton dynamics and their potential influence on phytoplankton over the mid-Atlantic Ridge will be discussed in Chapter 4.

Another factor controlling plankton dynamics is mode of life – whether cells are autotrophic, mixotropic or heterotrophic. Mixotrophy, the consumption of inorganic nutrients and organic matter (photosynthesis and hetertrophy), is being found to be more universal than previously

thought, it is particularly high in dinoflagellates and picoeukrayotes and is even present in *Prochlorococcus* and *Synechococcus* (Caron et al., 2016; Stoecker et al., 2016; Yelton et al., 2016). Mixotrophic organisms use a vast variety of strategies to obtain energy. At one end, the mainly phototrophic organisms that occasionally consume prey, at the other, heterotrophs that photosynthesize to survive the absence of food (Caron, 2016). Complete phototrophy appears to be restricted to a few groups, namely the diatoms (Mitra et al., 2014). The extent of cell plasticity to energy source will influence ecosystem dynamics. Mixotrophy is thought to be an advantage in oligotrophic regions where resources are scarce (Zubkov & Tarran, 2008; Barton et al., 2013). Mixotrophy is a factor that is not yet, generally, being considered.

3.5 Summary

Phytoplankton dynamics in the subtropical North Atlantic are subject to light, nutrients, and physical dynamics of the water column. This is not new knowledge. The subtropical North Atlantic gyre between 20-40°N is split into two regions, in terms of biology and water column structure, which concur with Longhurst's tropical and subtropical North Atlantic Provinces and the summer extent of the Azores Current. We note that there appears to be a degree of ambiguity in respect to the naming of ocean currents and fronts in the northern subtropical Atlantic, beneath the subtropical convergence. This is due to seasonal dynamics of the area and a lack of sampling. The large seasonal fluctuations in phytoplankton by as much as 27-fold in the northern subtropical Atlantic are highlighted in this study through comparison of October and June observations.

We also observe a topographical influence on phytoplankton dynamics, with larger-sized cells and a higher abundance of small eukaryotes over the Mid-Atlantic Ridge in addition to a higher abundance of *Synechococcus* over the SL Rise and RG Rise. These findings are consistent with the theory that increased turbulent mixing and nutrients lead to larger cells. However, the sampling regimes during both RidgeMix and AMT25, whilst providing lots of data, are limited. During RidgeMix, sampling occurred to the west of the ridge and above the ridge, so, we cannot know the spatial extent of the 'ridge signal' or the extent to which longitude is an influence. During AMT25, only 4-6 stations were sampled for phytoplankton over each topographical feature. These 'stations-of-opportunity' were of low spatial definition over the features (e.g. one or two stations over the features), with little characterisation of the flow, and with no respect to the underlying topography. In conclusion, here we suggest that abrupt topography does influence the phytoplankton community but advise that further studies are required at a higher spatial resolution, over and around the ridge (3D mesh) with sampling for ocean currents, turbulence, nutrients, phytoplankton community structure, biomass, and growth rates.

3.6 References

Acevedo-Trejos, E., Brandt, G., Bruggeman, J., & Merico, A. (2015). Mechanisms shaping size structure and functional diversity of phytoplankton communities in the ocean. *Scientific Reports*, *5*(8918). https://doi.org/10.1038/srep08918

Acevedo-Trejos, E., Brandt, G., Merico, A., & Smith, S. L. (2013). Biogeographical patterns of phytoplankton community size structure in the oceans. *Global Ecology and Biogeography*, *22*(9), 1060–1070. https://doi.org/10.1111/geb.12071

Ahlgren, N. A., & Rocap, G. (2012). Diversity and distribution of marine Synechococcus: Multiple gene phylogenies for consensus classification and development of qPCR assays for sensitive measurement of clades in the ocean. *Frontiers in Microbiology*, *3*, 1–24. https://doi.org/10.3389/fmicb.2012.00213

Alves, M., Gaillard, F., Sparrow, M., Knoll, M., & Giraud, S. (2002). Circulation patterns and transport of the Azores Front-Current system. *Deep-Sea Research Part II: Topical Studies in Oceanography*, *49*(19), 3983–4002. https://doi.org/10.1016/S0967-0645(02)00138-8

Azam, F., & Malfatti, F. (2007). Microbial structuring of marine ecosystems. *Nature Reviews: Microbiology*, *5*, 782–791. https://doi.org/10.1038/nrmicro1747

Barton, A. D., Pershing, A. J., Litchman, E., Record, N. R., Edwards, K. F., Finkel, Z. V., … Ward, B. A. (2013). The biogeography of marine plankton traits. *Ecology Letters*, *16*(4), 522–534. https://doi.org/10.1111/ele.12063

Behrenfeld, M. J., & Boss, E. S. (2014). Resurrecting the ecological underpinnings of ocean plankton blooms. *Annual Review of Marine Science*, *6*, 167–194. https://doi.org/10.1146/annurev-marine-052913-021325

Behrenfeld, M. J., Boss, E., Siegel, D. A., & Shea, D. M. (2005). Carbon-based ocean productivity and phytoplankton physiology from space. *Global Biogeochemical Cycles*, *19*(1), 1–14. https://doi.org/10.1029/2004GB002299

Benitez-Nelson, C. R., Bidigare, R. R., Dickey, T. D., Landry, M. R., & Leonard, C. L. (2004). Mesoscale Eddies Drive Increased Silica Export in the Subtropical Pacific Ocean. *Science (New York, N.Y.)*, *304*(5669), 408–414. https://doi.org/10.1126/science.1089778

Benitez-Nelson, C. R., Bidigare, R. R., Dickey, T. D., Landry, M. R., Leonard, C. L., Brown, S. L., … Jin Yang, E. (2007). Mesoscale Eddies Drive Increased Silica Export in the Subtropical Pacific Ocean. *Science*, *316*, 1017–1021. https://doi.org/10.1126/science.1140132

Bibby, T. S., Gorbunov, M. Y., Wyman, K. W., & Falkowski, P. G. (2008). Photosynthetic community responses to upwelling in mesoscale eddies in the subtropical North Atlantic and Pacific Oceans. *Deep-Sea Research Part II: Topical Studies in Oceanography*, *55*(10–13), 1310–1320. https://doi.org/10.1016/j.dsr2.2008.01.014

Bidigarel, R. R., Marra, J., Dickey, T. D., Iturriaga, R., Baker, K. S., Smith, R. C., & Pak, H. (1990). Evidence for phytoplankton succession and chromatic adaptation in the Sargasso Sea during spring 1985'. *Marine Ecology Progress Series*, *60*, 113–122.

Brierley, B., Carvalho, L., Davies, S., & Krokowski, J. (2007). *Guidance on the quantitative analysis of phytoplankton in Freshwater Samples. Report to SNIFFER (Project WFD80)*. Edinburgh. Retrieved from http://nora.nerc.ac.uk/id/eprint/5654/1/Phytoplankton_Counting_Guidance_v1_2007_12_05.pdf

Buck, K. R., Chavez, F. P., & Campbell, L. (1996). Basin-wide distributions of living carbon components and the inverted trophic pyramid of the central gyre of the North Atlantic Ocean, summer 1993. *Aquatic Microbial Ecology*, *10*(3), 283–298. https://doi.org/10.3354/ame010283

Cáceres, C., Rivera, A., González, S., & Anadón, R. (2016). Phytoplankton community structure and dynamics in the North Atlantic subtropical gyre. *Progress in Oceanography*, *151*, 177–188. https://doi.org/10.1016/j.pocean.2016.12.003

Camboa, L. A. P., & Rabinowitz, P. D. (1984). The evolution of the Rio Grande Rise in the southwestern Atlantic Ocean. *Marine Geology*, *58*, 35–58.

Campbell, L., Liu, H., Vaulott, D., & Nolla, a. (1997). Annual variability of phytoplankton and bacteria in the subtropical ENS0 event. *Deep Sea Research I*, *44*(2), 167–192.

Campbell, L., Nolla, H. A., & Vaulot, D. (1994). The importance of Prochlorococcus to community structure in the central North Pacific Ocean. *Limnology and Oceanography*, *39*, 954–961.

Campbell, L., & Vaulot, D. (1993). Photosynthetic picoplankton community structure in the subtropical North Pacific Ocean near Hawaii (station ALOHA). *Deep-Sea Research Part I*, *40*(10), 2043–2060. https://doi.org/10.1016/0967-0637(93)90044-4

Capone, D. G., Burns, J. A., Montoya, J. P., Subramaniam, A., Mahaffey, C., Gunderson, T., … Carpenter, E. J. (2005). Nitrogen fixation by Trichodesmium spp.: An important source of new nitrogen to the tropical and subtropical North Atlantic Ocean. *Global Biogeochemical Cycles*, *19*(2), 1–17. https://doi.org/10.1029/2004GB002331

Caron, D. A. (2016). Mixotrophy stirs up our understanding of marine food webs. *Proceedings of the National Academy of Sciences of the United States of America*, *113*(11), 2806–2808. https://doi.org/10.1073/pnas.1600718113

Caron, D. A., Alexander, H., Allen, A. E., Archibald, J. M., Armbrust, E. V., Bachy, C., … Worden, A. Z. (2016). Probing the evolution, ecology and physiology of marine protists using transcriptomics. *Nature Reviews Microbiology*, *15*(1), 6–20. https://doi.org/10.1038/nrmicro.2016.160

Casey, J. R., Aucan, J. P., Goldberg, S. R., & Lomas, M. W. (2013). Changes in partitioning of carbon amongst photosynthetic pico- and nano-plankton groups in the Sargasso Sea in response to changes in the North Atlantic Oscillation. *Deep-Sea Research Part II: Topical Studies in Oceanography*, *93*, 58–70. https://doi.org/10.1016/j.dsr2.2013.02.002

Chen, B., Wang, L., Song, S., Huang, B., Sun, J., & Liu, H. (2011). Comparisons of picophytoplankton abundance, size, and fluorescence between summer and winter in northern South China Sea. *Continental Shelf Research*, *31*(14), 1527–1540. https://doi.org/10.1016/J.CSR.2011.06.018

Cullen, J. J. (1982). The Deep Chlorophyll Maximum: Comparing Vertical Profiles of Chlorophyll *a*. *Canadian Journal of Fisheries and Aquatic Sciences*, *39*(5), 791–803. https://doi.org/10.1139/f82-108

Cullen, J. J. (2015). Subsurface Chlorophyll Maximum Layers: Enduring Enigma or Mystery Solved? *Annual Review of Marine Science*, *7*(1), 207–239. https://doi.org/10.1146/annurev-marine-010213-135111

Cullen, J. J., & Eppley, R. W. (1981). Chlorophyll maximum layers of the Southern California Bight and possible mechanisms of their formation and maintenance. *Oceanologica Acta*, *4*(1), 23–32.

Dagenais-Bellefeuille, S., & Morse, D. (2013). Putting the N in dinoflagellates. *Frontiers in Microbiology*, *4*. https://doi.org/10.3389/fmicb.2013.00369

Dave, A. C., Barton, A. D., Lozier, M. S., & McKinley, G. A. (2015). What drives seasonal change in oligotrophic area in the subtropical North Atlantic? *Journal of Geophysical Research: Oceans*, *120*(6), 3958–3969. https://doi.org/10.1002/2015JC010787

Delgado, M., & Fortuño, J. M. (1991). Atlas de Fitoplancton del Mar Mediterráneo. *Scientia*

Marina, *55*(1), 1–133.

Dufresne, A., Ostrowski, M., Scanlan, D. J., Garczarek, L., Mazard, S., Palenik, B. P., … Partensky, F. (2008). Unravelling the genomic mosaic of a ubiquitous genus of marine cyanobacteria. *Genome Biology*, *9*(5). https://doi.org/10.1186/gb-2008-9-5-r90

Durand, M. D., Olson, R. J., & Chisholm, S. W. (2001). Phytoplankton population dynamics at the Bermuda Atlantic Time-series station in the Sargasso Sea. *Deep-Sea Research Part II: Topical Studies in Oceanography*, *48*(8–9), 1983–2003. https://doi.org/10.1016/S0967-0645(00)00166-1

Durham, W. M., Climent, E., Barry, M., De Lillo, F., Boffetta, G., Cencini, M., & Stocker, R. (2013). Turbulence drives microscale patches of motile phytoplankton. *Nature Communications*, *4*, 2148. https://doi.org/10.1038/ncomms3148

Edler, L., & Elbrächter, M. (2010). *The Utermöhl method for quantitative phytoplankton analysis*. *Microscopic and molecular methods for quantitative phytoplankton analysis*. https://doi.org/10.1016/j.resp.2011.02.009

Estrada, M., Delgado, M., Blasco, D., Latasa, M., Cabello, A. M., Ben??tez-Barrios, V., … Vidal, M. (2016). Phytoplankton across tropical and subtropical regions of the Atlantic, Indian and Pacific oceans. *PLoS ONE*, *11*(3), 1–29. https://doi.org/10.1371/journal.pone.0151699

Falkowski, P. G., & Kiefer, D. a. (1985). Chlorophyll a fluorescence in phytopankton: relationship to photosynthesis and biomass. *Journal of Plankton Research*, *7*(5), 715–731.

Fasham, M. J., Platt, T., Irwin, B., & Jones, K. (1985). Factors Affecting the Spatial Pattern of the Deep Chlorophyll Maximnm in the Region of the Azores Front. *Progress in Oceanography*, *14*, 129–165.

Fernández, E., & Pingree, R. D. (1996). Coupling between physical and biological fields in the North Atlantic subtropical front southeast of the Azores. *Deep-Sea Research Part I: Oceanographic Research Papers*, *43*(9), 1369–1393. https://doi.org/10.1016/S0967-0637(96)00065-9

Finkel, Z. V., Beardall, J., Flynn, K. J., Quigg, A., Rees, T. A. V, & Raven, J. A. (2010). Phytoplankton in a changing world: Cell size and elemental stoichiometry. *Journal of Plankton Research*, *32*(1), 119–137. https://doi.org/10.1093/plankt/fbp098

Flores, J.-A., Bárcena, M. A., & Sierro, F. J. (2000). Ocean-surface and wind dynamics in the Atlantic Ocean off Northwest Africa during the last 140 000 years. *Palaeogeography, Palaeoclimatology, Palaeoecology*, *161*(3–4), 459–478. https://doi.org/10.1016/S0031-0182(00)00099-7

Fofonoff, P., & Millard, R. C. (1983). Algorithms for computation of fundamental properties of seawater. *Unesco Technical Papers in Marine Science*, *44*. Retrieved from http://unesdoc.unesco.org/images/0005/000598/059832eb.pdf

Foster, R. A., Kuypers, M. M. M., Vagner, T., Paerl, R. W., Musat, N., & Zehr, J. P. (2011). Nitrogen fixation and transfer in open ocean diatom–cyanobacterial symbioses. *The ISME Journal*, *5*(9), 1484–1493. https://doi.org/10.1038/ismej.2011.26

Gárate-Lizárraga, I., Muñetón-Gómez, M. D. S., Pérez-Cruz, B., & Díaz-Ortíz, J. A. (2014). Bloom of Gonyaulax spinifera (Dinophyceae: Gonyaulacales) in Ensenada de la Paz lagoon, Gulf of California. *CICIMAR Oceánides*, *29*(1), 11–18.

Gin, K. Y. H., Chisholm, S. W., & Olson, R. J. (1999). Seasonal and depth variation in microbial size spectra at the Bermuda Atlantic time series station. *Deep Sea Research Part I: Oceanographic Research Papers*, *46*(7), 1221–1245. https://doi.org/10.1016/S0967-0637(99)00004-7

Gómez, F., Claustre, H., & Souissi, S. (2008). Rarely reported dinoflagellates of the genera

Ceratium, Gloeodinium, Histioneis, Oxytoxum and Prorocentrum (Dinophyceae) from the open southeast Pacific Ocean. *Revista de Biologia Marina y Oceanografia*, *43*(1), 25–40.

Gould, S. B., Waller, R. F., & Mcfadden, G. I. (2008). Plastid evolution. *Annual Review of Plant Biology*, *59*, 491–517. https://doi.org/10.1146/annurev.arplant.59.032607.092915

Gould, W. J. (1985). Physical Oceanography of the Azores Front. *Progress in Oceanography*, *14*(1972), 167–190.

Gul, S., & Nawaz, M. F. (2014). The Dinoflagellate Genera Protoperidinium and Podolampas from Pakistan's Shelf and Deep Sea Vicinity (North Arabian Sea). *Turkish Journal of Fisheries and Aquatic Science*, *14*, 91–100. https://doi.org/10.4194/1303-2712-v14

Hanada, S. (2016). Anoxygenic Photosynthesis-A Photochemical Reaction That Does Not Contribute to Oxygen Reproduction. *Microbes Environ*, *31*(1), 1–3. https://doi.org/10.1264/jsme2.ME3101rh

Hékinian, R., Bonte, P., Dudley, W., Blanc, P. L., Jehano, C., Labeyrie, L., & Duplessy, J. C. (1978). Volcanics from the Sierra Leone Rise. *Nature*, *275*(5680), 536–538. https://doi.org/10.1038/275536a0

Heywood, J. L., Zubkov, M. V., Tarran, G. A., Fuchs, B. M., & Holligan, P. M. (2006). Prokaryoplankton standing stocks in oligotrophic gyre and equatorial provinces of the Atlantic Ocean: Evaluation of inter-annual variability. *Deep Sea Research Part II: Topical Studies in Oceanography*, *53*(14–16), 1530–1547. https://doi.org/10.1016/j.dsr2.2006.05.005

Holm-Hansen, O., & Riemann, B. (1978). Chlorophyll a determination: improvements in methodology. *Oikos*, *30*, 438–447.

Hoppenrath, M., Elbrächter, M., Drebes, G., & Alfred-Wegener-Institut für Polar- und Meeresforschung. (2009). *Marine phytoplankton : selected microphytoplankton species from the North Sea around Helgoland and Sylt*. E. Schweizerbart'sche Verlagsbuchh.

Hu, C., Lee, Z., & Franz, B. (2012). Chlorophyll a algorithms for oligotrophic oceans: A novel approach based on three-band reflectance difference. *Journal of Geophysical Research: Oceans*, *117*(1), 1–25. https://doi.org/10.1029/2011JC007395

Huete-Ortega, M., Calvo-Díaz, A., Graña, R., Mouriño-Carballido, B., & Marañón, E. (2011). Effect of environmental forcing on the biomass, production and growth rate of size-fractionated phytoplankton in the central Atlantic Ocean. *Journal of Marine Systems*, *88*(2), 203–213. https://doi.org/10.1016/j.jmarsys.2011.04.007

Iwataki, M. (2008). Taxonomy and identification of the armored dinoflagellate genus Heterocapsa (Peridiniales, Dinophyceae). *Plankton & Benthos Research*, *3*, 135–142.

Jacquet, S., Partensky, F., Lennon, J.-F., & Vaulot, D. (2001). Diel patterns of growth and division in marine picoplankton in culture. *Journal of Phycology*, *37*(3), 357. https://doi.org/10.1046/j.1529-8817.2001.037003357.x

Jeong, H. J., Yoo, Y. Du, Kim, J. S., Seong, K. A., Kang, N. S., & Kim, T. H. (2010). Growth, Feeding and Ecological Roles of the Mixotrophic and Heterotrophic Dinoflagellates in Marine Planktonic Food Webs. *Ocean Sci. J*, (2), 65–91. https://doi.org/10.1007/s12601-010-0007-2

Johnson, Z. I., & Martiny, A. C. (2014). Techniques for Quantifying Phytoplankton Biodiversity. *Annual Review of Marine Science*, (September 2014), 1–26. https://doi.org/10.1146/annurev-marine-010814-015902

Johnson, Z. I., Zinser, E. R., Coe, A., McNulty, N. P., Woodward, E. M. S., & Chisholm, S. W. (2006). Niche partitioning among Prochlorococcus ecotypes along ocean-scale environmental gradients. *Science (New York, N.Y.)*, *311*(5768), 1737–1740.

https://doi.org/10.1126/science.1118052

Kashtan, N., Roggensack, S. E., Berta-Thompson, J. W., Grinberg, M., Stepanauskas, R., & Chisholm, S. W. (2017). Fundamental differences in diversity and genomic population structure between Atlantic and Pacific Prochlorococcus. *The ISME Journal*, 1–15. https://doi.org/10.1038/ismej.2017.64

Kemp, A., & Villareal, T., (2018). The case of the diatoms and the muddled mandalas: Time to recognise diatom adaptations to stratified waters. *Progress in Oceanography*, 167, 138-149. https://doi.org/10.1016/j.pocean.2018.08.002

Key, T., McCarthy, A., Campbell, D. a., Six, C., Roy, S., & Finkel, Z. V. (2010). Cell size trade-offs govern light exploitation strategies in marine phytoplankton. *Environmental Microbiology*, *12*(1), 95–104. https://doi.org/10.1111/j.1462-2920.2009.02046.x

Klausmeier, C. A., & Litchman, E. (2001). Algal games: The vertical distribution of phytoplankton in poorly mixed water columns. *Limnology and Oceanography*, *46*(8), 1998–2007. https://doi.org/10.4319/lo.2001.46.8.1998

Klein, B., & Siedler, G. (1989). On the origin of the Azores Current. *Journal of Geophysical Research*, *94*(C5), 6159–6168. https://doi.org/10.1029/JC094iC05p06159

Kraberg, A., Baumann, M., & Dürselen, C.-D. (2010). *Coastal phytoplankton : photo guide for Northern European seas*. Pfeil.

Ku, C., Roettger, M., Zimorski, V., Nelson-Sathi, S., Sousa, F. L., & Martin, W. F. (2014). Plastid origin: Who, when and why? *Acta Societatis Botanicorum Poloniae*, *83*(4), 281–289. https://doi.org/10.5586/asbp.2014.045

Latasa, M., Cabello, A. M., Morán, X. A. G., Massana, R., & Scharek, R. (2017). Distribution of phytoplankton groups within the deep chlorophyll maximum. *Limnology and Oceanography*, *62*(2), 665–685. https://doi.org/10.1002/lno.10452

Latasa, M., Gutiérrez-rodríguez, A., Cabello, A. M., & Scharek, R. (2016). Influence of light and nutrients on the vertical distribution of marine phytoplankton groups in the deep chlorophyll maximum. *Scientia Marina*, *80*(S1), 57–62.

Latasa, M., Scharek, R., Vidal, M., Vila-Reixach, G., Gutiérrez-Rodríguez, A., Emelianov, M., & Gasol, J. M. (2010). Preferences of phytoplankton groups for waters of different trophic status in the northwestern Mediterranean sea. *Marine Ecology Progress Series*, *407*, 27–42. https://doi.org/10.3354/meps08559

Le Bescot, N., Mahé, F., Audic, S., Dimier, C., Garet, M.-J., Poulain, J., … Siano, R. (2016). Global patterns of pelagic dinoflagellate diversity across protist size classes unveiled by metabarcoding. *Environmental Microbiology*, *18*(2), 609–626. https://doi.org/10.1111/1462-2920.13039

Letelier, R. M., Karl, D. M., Abbott, M. R., & Bidigare, R. R. (2004). Light driven seasonal patterns of chlorophyll and nitrate in the lower euphotic zone of the North Pacific Subtropical Gyre. *Limnology and Oceanography*, *49*(2), 508–519. https://doi.org/10.4319/lo.2004.49.2.0508

Li, W. K. (1995). Composition of ultraphytoplankton in the central north Atlantic. *Marine Ecology Progress Series*, *122*(1–3), 1–8. https://doi.org/10.3354/meps122001

Licea, S., Zamudio, M. E., Luna, R., & Soto, J. (2004). Free-living dinoflagellates in the southern Gulf of Mexico: Report of data (1979-2002). *Phycological Research*, *52*(4), 419–428. https://doi.org/10.1111/j.1440-183.2004.00364.x

Lima-Mendez, G., Faust, K., Henry, N., Decelle, J., Colin, S., Carcillo, F., … Raes, J. (2015). Ocean plankton. Determinants of community structure in the global plankton interactome. *Science*, *348*(6237). https://doi.org/10.1126/science.1262073

Litvin, V. M. (Vladimir M. (1984). *The morphostructure of the Atlantic Ocean floor : its development in the Meso-Cenozoic*. D. Reidel.

Liu, H., Chang, J., Wen, L.-S., & Liu, K. K. (2007). Seasonal variability of picoplankton in the Northern South China Sea at the SEATS station. *Deep Sea Research Part II: Topical Studies in Oceanography*, *54*(14–15), 1602–1616. https://doi.org/10.1016/J.DSR2.2007.05.004

Longhurst, A. R. (2010). The Atlantic Ocean. In *Ecological Geography of the Sea* (2nd ed., pp. 131–274). California, USA: Elsevier Academic Press.

Lund, J. W. G., Kipling, C., & Le Cren, E. D. (1958). The inverted microscope method of estimating algal numbers and the statistical basis of estimations by counting. *Hydrobiologia*, *11*(2), 143–170. https://doi.org/10.1007/BF00007865

Macedo, M. F., Duarte, P., Ferreira, J. G., Alves, M., & Costa, V. (2000). Analysis of the deep chlorophyll maximum across the Azores Front. *Hydrobiologia*, *441*, 155–172.

Mahadevan, A. (2016). The Impact of Submesoscale Physics on Primary Productivity of Plankton. *Annual Review of Marine Science*, *8*, 161–184. https://doi.org/10.1146/annurev-marine-010814-015912

Mahaffey, C., Benitez-Nelson, C. R., Bidigare, R. R., Rii, Y., & Karl, D. M. (2008). Nitrogen dynamics within a wind-driven eddy. *Deep Sea Research Part II: Topical Studies in Oceanography*, *55*(10–13), 1398–1411. https://doi.org/10.1016/j.dsr2.2008.02.004

Malmstrom, R. R., Coe, A., Kettler, G. C., Martiny, A. C., Frias-Lopez, J., Zinser, E. R., & Chisholm, S. W. (2010). Temporal dynamics of Prochlorococcus ecotypes in the Atlantic and Pacific oceans. *The ISME Journal*, *4*(10), 1252–1264. https://doi.org/10.1038/ismej.2010.60

Mann, E. L., Ahlgren, N., Moffett, J. W., & Chisholm, S. W. (2002). Copper toxicity and cyanobacterial ecology in the Sargasso Sea. *Limnology and Oceanography*, *47*(4), 976–988.

Marañón, E., Behrenfeld, M. J., González, N., Mouriño, B., & Zubkov, M. V. (2003). High variability of primary production in oligotrophic waters of the Atlantic Ocean: Uncoupling from phytoplankton biomass and size structure. *Marine Ecology Progress Series*, *257*, 1–11. https://doi.org/10.3354/meps257001

Marañón, E., Holligan, P. M., Barciela, R., González, N., Mouriño, B., Pazó, M. J., & Varela, M. (2001). Patterns of phytoplankton size structure and productivity in contrasting open-ocean environments. *Marine Ecology Progress Series*, *216*, 43–56. https://doi.org/10.3354/meps216043

Marañón, E., Holligan, P. M., Varela, M., Mouriño, B., & Bale, A. J. (2000). Basin-scale variability of phytoplankton biomass, production and growth in the Atlantic Ocean. *Deep Sea Research Part I: Oceanographic Research Papers*, *47*(5), 825–857. https://doi.org/10.1016/S0967-0637(99)00087-4

Margalef, R. (1978). Life-forms of phytoplankton as survival alternatives in an unstable environment. *Oceanologica Acta*, *1*, 493–509. https://doi.org/10.1007/BF00202661

Maritorena, S., & Siegel, D. A. (2005). Consistent merging of satellite ocean color data sets using a bio-optical model. *Remote Sensing of Environment*, *94*(4), 429–440. https://doi.org/10.1016/J.RSE.2004.08.014

Martin, S. (2004). *An introduction to ocean remote sensing*. Cambridge: Cambridge University Press.

Massana, R., & Logares, R. (2013). Eukaryotic versus prokaryotic marine picoplankton ecology. *Environmental Microbiology*, *15*(5), 1254–1261. https://doi.org/10.1111/1462-2920.12043

Mcclain, C. R., Murtugudde, R. G., Signorini, S. R., Christian, P. J. R., & Busalacchi, A. J. (1999). Biological and physical signatures in the tropical and subtropical Atlantic. *JOURNAL OF GEOPHYSICAL RESEARCH*, *104*(C8), 367–385. https://doi.org/10.1029/1999JC900134

McGillicuddy, D. J., Anderson, L. a, Bates, N. R., Bibby, T., Buesseler, K. O., Carlson, C. a, … Steinberg, D. K. (2007). Eddy/wind interactions stimulate extraordinary mid-ocean plankton blooms. *Science*, *316*(5827), 1021–1026. https://doi.org/10.1126/science.1136256

Meave-del Castillo, M. E., Zamudio-Resendiz, M. E., & Castillo-Rivera, M. (2012). Riqueza Fitoplanctónica de la Bahía de Acapulco y Zona Costera Aledaña, Guerrero, México. *Acta Botanica Mexicana*, *100*, 405–487.

Mendonça, A., Arístegui, J., Vilas, J. C., Montero, M. F., & Ojeda, A. (2012). Is There a Seamount Effect on Microbial Community Structure and Biomass? The Case Study of Seine and Sedlo Seamounts (Northeast Atlantic). *PLoS ONE*, *7*(1), 29526. https://doi.org/10.1371/journal.pone.0029526

Menzel, D. W., & Ryther, J. H. (1961). Annual variations in primary production of the Sargasso sea off Bermuda. *Deep Sea Research (1953)*, *7*(4), 282–288. https://doi.org/10.1016/0146-6313(61)90046-6

Mignot, A., Claustre, H., Uitz, J., Poteau, A., Ortenzio, F. D., & Xing, X. (2014). Understanding the seasonal dynamics of phytoplankton biomass and the deep chlorophyll maximum in oligotrophic environments: A Bio-Argo float investigation. *Global Biogeochemical Cycles*, (1), 1–21. https://doi.org/10.1002/2013GB004781.Received

Mitra, A., Flynn, K. J., Burkholder, J. M., Berge, T., Calbet, A., Raven, J.A., … Zubkov, M. V. (2014). The role of mixotrophic protists in the biological carbon pump. *Biogeosciences*, 11(4), 995-1005.

Mojica, K. D. A., van de Poll, W. H., Kehoe, M., Huisman, J., Timmermans, K. R., Buma, A. G. J., … Brussaard, C. P. D. (2015). Phytoplankton community structure in relation to vertical stratification along a north-south gradient in the Northeast Atlantic Ocean. *Limnology and Oceanography*, *60*(5), 1498–1521. https://doi.org/10.1002/lno.10113

Moore, L. R., Goericke, R., & Chisholm, S. W. (1995). Comparative physiology of Synechococcus and Prochlorococcus: influence of light and temperature on growth, pigments, fluorescence and absorptive properties. *Marine Ecology Progress Series*, *116*, 259–275. https://doi.org/10.2307/44635011

Morato, T., Hoyle, S. D., Allain, V., & Nicol, S. J. (2010). Seamounts are hotspots of pelagic biodiversity in the open ocean. *PNAS*, *107*(21), 9707–9711. https://doi.org/10.1073/pnas.0910290107

Morel, A., Ahn, Y.-H., Partensky, F., Vaulot, D., & Claustre, H. (1993). <I>Prochlorococcus</I> and <I>Synechococcus</I>: A comparative study of their optical properties in relation to their size and pigmentation. *Journal of Marine Research*, *51*(3), 617–649. https://doi.org/10.1357/0022240933223963

Moreno-Ostos, E., Fernandez, A., Huete-Ortega, M., Mourino-Carballido, B., Calvo-Diaz, A., Moran, X. a G., & Maranon, E. (2011). Size-fractionated phytoplankton biomass and production in the tropical Atlantic. *Scientia Marina*, *75*(2), 379–389. https://doi.org/10.3989/scimar.2011.75n2379

Mouriño-Carballido, B., Hojas, E., Cermeño, P., Chouciño, P., Fernández-Castro, B., Latasa, M., … Vidal, M. (2016). Nutrient supply controls picoplankton community structure during three contrasting seasons in the northwestern Mediterranean Sea. *Marine Ecology Progress Series*, *543*, 1–19. https://doi.org/10.3354/meps11558

Mouriño, B., Fernández, E., Serret, P., Harbour, D., Sinha, B., & Pingree, R. (2001). Variability and seasonality of physical and biological fields at the Great Meteor Tablemount

(subtropical NE Atlantic). *Oceanologica Acta*, *24*(2), 167–185. https://doi.org/10.1016/S0399-1784(00)01138-5

Muciño-Márquez, R. E., Gárate-Lizárraga, I., & López-Cortés, D. J. (2015). Seasonal Variation of the Genus Prorocentrum (Dinophyceae) in Two Tuna Farms in Bahía De La Paz, Mexico. *Acta Biológica Colombiana*, *20*(1), 195–206.

Neilson, J., Durnford, D. (2010). Structural and functional diversification of the light-harvesting complexes in photosynthetic eukaryotes. *Photosynthesis Research*, 106(1-2), 57-71.

Okolodkov, Y. B. (2014). Dinophysiales (Dinophyceae) of the National Park Sistema Arrecifal Veracruzano, Gulf of Mexico, with a key for identification. *Acta Botanica Mexicana*, *106*, 9–71.

Olson, R. J., Chisholm, S. W., Zettler, E. R., Altabet, M. A., & Dusenberry, J. A. (1990). Spatial and temporal distributions of prochlorophyte picoplankton in the North Atlantic Ocean. *Deep Sea Research*, *37*(6), 1033–1051. https://doi.org/10.1016/0198-0149(90)90109-9

Ottesen, E. a, Young, C. R., Eppley, J. M., Ryan, J. P., Chavez, F. P., Scholin, C. a, & DeLong, E. F. (2013). Pattern and synchrony of gene expression among sympatric marine microbial populations. *Proceedings of the National Academy of Sciences of the United States of America*, *110*(6), 488–497. https://doi.org/10.1073/pnas.1222099110

Parker, M. S., Mock, T., & Armbrust, E. V. (2008). Genomic Insights into Marine Microalgae. *Annual Review of Genetics*, *42*, 619–645. https://doi.org/10.1146/annurev.genet.42.110807.091417

Partensky, F., Blanchot, J., Lantoine, F., Neveux, J., & Marie, D. (1996). Vertical structure of picophytoplankton at different trophic sites of the tropical northeastern Atlantic Ocean. *Deep Sea Research Part I: Oceanographic Research Papers*, *43*(8), 1191–1213. https://doi.org/10.1016/0967-0637(96)00056-8

Partensky, F., Blanchot, J., & Vaulot, D. (1999). Differential distribution and ecology of Prochlorococcus and Synechococcus in oceanic waters : a review. *Bulletin de l'Institut Océanographique - Special Issue: Marine Cyanobacteria*, *19*, 457–476.

Pérez, V., Fernández, E., Marañón, E., Morán, X. A. G., & Zubkov, M. V. (2006). Vertical distribution of phytoplankton biomass, production and growth in the Atlantic subtropical gyres. *Deep Sea Research Part I: Oceanographic Research Papers*, *53*(10), 1616–1634. https://doi.org/10.1016/j.dsr.2006.07.008

Peterson, R. G., & Stramma, L. (1991). Upper-level circulation in the South Atlantic Ocean. *Progress in Oceanography*, *26*(1), 1–73. https://doi.org/10.1016/0079-6611(91)90006-8

Poulton, A. J., Holligan, P. M., Hickman, A., Kim, Y. N., Adey, T. R., Stinchcombe, M. C., … Woodward, E. M. S. (2006). Phytoplankton carbon fixation, chlorophyll-biomass and diagnostic pigments in the Atlantic Ocean. *Deep-Sea Research Part II: Topical Studies in Oceanography*, *53*(14–16), 1593–1610. https://doi.org/10.1016/j.dsr2.2006.05.007

Raven, J. A. (1998). The twelfth Tansley Lecture. Small is beautiful: the picophytoplankton. *Functional Ecology*, *12*(4), 503–513. https://doi.org/10.1046/j.1365-2435.1998.00233.x

Reygondeau, G., Longhurst, A., Martinez, E., Beaugrand, G., Antoine, D., & Maury, O. (2013). Dynamic biogeochemical provinces in the global ocean. *Global Biogeochemical Cycles*, *27*(4), 1046–1058. https://doi.org/10.1002/gbc.20089

Ryther, J. H. (1956). Photosynthesis in the ocean as a function of light intensity. *Limnology and Oceanography*, 1, 61-69.

Ribalet, F., Swalwell, J., Clayton, S., Jiménez, V., Sudek, S., Lin, Y., … Armbrust, E. V. (2015). Light-driven synchrony of Prochlorococcus growth and mortality in the subtropical

Pacific gyre. *Proceedings of the National Academy of Sciences of the United States of America*, *112*(26), 8008–8012. https://doi.org/10.1073/pnas.1424279112

Riemann, L., Nielsen, T. G., Kragh, T., Richardson, K., Parner, H., Jakobsen, H. H., & Munk, P. (2011). Distribution and production of plankton communities in the subtropical convergence zone of the Sargasso Sea. I. Phytoplankton and bacterioplankton. *Marine Ecology Progress Series*, *426*, 57–70. https://doi.org/10.3354/meps09001

Rio, M.-H. (2010). Absolute Dynamic Topography from Altimetry: Status and Prospects in the Upcoming GOCE Era. In *Oceanography from Space* (pp. 165–179). Dordrecht: Springer Netherlands. https://doi.org/10.1007/978-90-481-8681-5_10

Sager, W. W. (2014). *Scientific Drilling in the South Atlantic: Rio Grande Rise, Walvis Ridge and surrounding areas*. Rio de Janeiro. Retrieved from www.geomapapp.org

Salas, R., Tillmann, U., & Kavanagh, S. (2014). Morphological and molecular characterization of the small armoured dinoflagellate *Heterocapsa minima* (Peridiniales, Dinophyceae). *European Journal of Phycology*, *49*(4), 413–428. https://doi.org/10.1080/09670262.2014.956800

Santos, M., Moita, M. T., Bashmachnikov, I., Menezes, G. M., Carmo, V., Loureiro, C. M., … Martins, A. (2013). Phytoplankton variability and oceanographic conditions at Condor seamount, Azores (NE Atlantic). *Deep Sea Research Part II: Topical Studies in Oceanography*, *98*, 52–62. https://doi.org/10.1016/j.dsr2.2013.05.037

Schattenhofer, M., Fuchs, B. M., Amann, R., Zubkov, M. V., Tarran, G. A., & Pernthaler, J. (2009). Latitudinal distribution of prokaryotic picoplankton populations in the Atlantic Ocean. *Environmental Microbiology*, *11*(8), 2078–2093. https://doi.org/10.1111/j.1462-2920.2009.01929.x

Sharples, J., Moore, C. M., Hickman, A. E., Holligan, P. M., Tweddle, J. F., Palmer, M. R., & Simpson, J. H. (2009). Internal tidal mixing as a control on continental margin ecosystems. *Geophysical Research Letters*, *36*(23). https://doi.org/10.1029/2009GL040683

Sharples, J., Tweddle, J. F., Green, J. A. M., Palmer, M. R., Kim, Y., Hickman, A. E., … Krivtsov, V. (2007). Spring – neap modulation of internal tide mixing and vertical nitrate fluxes at a shelf edge in summer. *Limnology and Oceanography*, *52*(5), 1735–1747.

Sieburth, J. M. N., Smetacek, V., & Lenz, J. (1978). Pelagic ecosystem structure: Heterotrophic compartments of the plankton and their relationship to plankton size fractions. *Limnology and Oceanography*, *23*(6), 1256–1263. https://doi.org/10.4319/lo.1978.23.6.1256

Siedler, G., Zangenberg, N., Onken, R., & Morligre, A. (1992). Seasonal Changes in the Tropical Atlantic Circulation' Observation and Simulation of the Guinea Dome. *JOURNAL OF GEOPHYSICAL RESEARCH*, *97*(C1), 703–715. https://doi.org/10.1029/91JC02501

Silsbe, G. M., & Malkin, S. Y. (2016). Where Light and Nutrients Collide: The Global Distribution and Activity of Subsurface Chlorophyll Maximum Layers. In P. M. Glibert & T. M. Kana (Eds.), *Aquatic Microbial Ecology and Biogeochemistry: A Dual Perspective* (pp. 141–152). https://doi.org/10.1007/978-3-319-30259-1

Steinberg, D. K., Carlson, C. A., Bates, N. R., Johnson, R. J., Michaels, A. F., & Knap, A. H. (2001). Overview of the US JGOFS Bermuda Atlantic Time-series Study (BATS): a decade-scale look at ocean biology and biogeochemistry. *Deep Sea Research Part II: Topical Studies in Oceanography*, *48*(8–9), 1405–1447. https://doi.org/10.1016/S0967-0645(00)00148-X

Steinberg, D. K., & Landry, M. R. (2017). Zooplankton and the Ocean Carbon Cycle. *Annual Review of Marine Science*, *9*(1), 413–444. https://doi.org/10.1146/annurev-marine-010814-015924

Stoecker, D. K., Hansen, P. J., Caron, D. A., & Mitra, A. (2016). Mixotrophy in the Marine Plankton. *Annual Review of Marine Science*, *9*, 1–25. https://doi.org/10.1146/annurev-marine-010816-060617

Stramma, L., & Siedler, G. (1988). Seasonal changes in the North Atlantic subtropical gyre. *Journal of Geophysical Research*, *93*(C7), 8111–8118. https://doi.org/10.1029/JC093iC07p08111

Strass, V. H., & Woodst, J. D. (1991). New production in the summer revealed by the meridionai slope of the deep chlorophyll maximum. *Deep Sea Research*, *38*(1), 35–56.

Tarran, G. A., Heywood, J. L., & Zubkov, M. V. (2006). Latitudinal changes in the standing stocks of nano- and picoeukaryotic phytoplankton in the Atlantic Ocean. *Deep Sea Research Part II: Topical Studies in Oceanography*, *53*(14–16), 1516–1529. https://doi.org/10.1016/j.dsr2.2006.05.004

Teira, E., Mouriño, B., Marañón, E., Pérez, V., Pazó, M. J., Serret, P., … Fernández, E. (2005). Variability of chlorophyll and primary production in the Eastern North Atlantic Subtropical Gyre: potential factors affecting phytoplankton activity. *Deep Sea Research Part I: Oceanographic Research Papers*, *52*(4), 569–588. https://doi.org/10.1016/j.dsr.2004.11.007

Ting, C. S., Rocap, G., King, J., & Chisholm, S. W. (2002). Cyanobacterial photosynthesis in the oceans: The origins and significance of divergent light-harvesting strategies. *Trends in Microbiology*, *10*(3), 134–142. https://doi.org/10.1016/S0966-842X(02)02319-3

Tomas, C. R. (Ed.). (1997). *Identifying Marine Phytoplankton*. San Diego, California: Academic Press.

Treusch, A. H., Demir-Hilton, E., Vergin, K. L., Worden, A. Z., Carlson, C. a, Donatz, M. G., … Giovannoni, S. J. (2012). Phytoplankton distribution patterns in the northwestern Sargasso Sea revealed by small subunit rRNA genes from plastids. *The ISME Journal*, *6*(3), 481–492. https://doi.org/10.1038/ismej.2011.117

Tuerena, R. E., Williams, R. G., Mahaffey, C., Green, J. A. M., Vic, C., Naveira-Garabato, A., … Sharples, J. (n.d.). Internal tides drive nutrient fluxes into the deep chlorophyll maximum over mid-ocean ridges.

Vázquez-Domínguez, E., Duarte, C. M., Agustí, S., Jürgens, K., Vaqué, D., & Gasol, J. M. (2008). Microbial plankton abundance and heterotrophic activity across the Central Atlantic Ocean. *Progress in Oceanography*, *79*(1), 83–94. https://doi.org/10.1016/j.pocean.2008.08.002

Veldhuis, M. J. W., & Kraay, G. W. (2000). Application of flow cytometry in marine phytoplankton research: current applications and future perspectives. *Scientia Marina*, *64*(2), 121–134. https://doi.org/10.3989/scimar.2000.64n2121

Veldhuis, M. J. W., & Kraay, G. W. (2004). Phytoplankton in the subtropical Atlantic Ocean: Towards a better assessment of biomass and composition. *Deep-Sea Research Part I: Oceanographic Research Papers*, *51*(4), 507–530. https://doi.org/10.1016/j.dsr.2003.12.002

Venrick, E. L. (1990). Mesoscale patterns of chlorophyll a in the Central North Pacific. *Deep Sea Research Part A, Oceanographic Research Papers*, *37*(6), 1017–1031. https://doi.org/10.1016/0198-0149(90)90108-8

Villareal, T. A. (1994). Widespread occurence of the Hemiaulus-cyanobacterial symbiosis in the southwest north Atlantic Ocean. *Bulletin of Marine Science*, *54*(1), 1–7.

Voorhis, A. D., & Hersey, J. B. (1964). Oceanic thermal fronts in the Sargasso Sea. *Journal of Geophysical Research*, *69*(18), 3809–3814. https://doi.org/10.1029/JZ069i018p03809

Wei, Y., Sun, J., Zhang, X., Wang, J., & Huang, K. (2018). Picophytoplankton size and biomass

around equatorial eastern Indian Ocean. *MicrobiologyOpen*. https://doi.org/10.1002/mbo3.629

Williams, O. J., Beckett, R. E., & Maxwell, D. L. (2015). Marine phytoplankton preservation with Lugol's: a comparison of solutions. *Journal of Applied Phycology*, *28*(1705). https://doi.org/10.1007/s10811-015-0704-4

Winn, C. D., Campbell, L., Christian, J. R., Letelier, R. M., Hebel, D. V, Dore, J. E., … Karl, D. M. (1995). Seasonal variability in the phytoplankton community of the North Pacific Subtropical Gyre. *Global Biogeochemical Cycles*, *9*(4), 605–620. https://doi.org/10.1029/95gb02149

Wyatt, T. (2014). Margalef 's mandala and phytoplankton bloom strategies. *Deep Sea Research II*, *101*, 32–49. https://doi.org/10.1016/j.dsr2.2012.12.006

Yelton, A. P., Acinas, S. G., Sunagawa, S., Bork, P., Pedrós-Alió, C., & Chisholm, S. W. (2016). Global genetic capacity for mixotrophy in marine picocyanobacteria. *The ISME Journal*, *10*(12), 2946–2957. https://doi.org/10.1038/ismej.2016.64

Yona, D., Park, M. O., Oh, S. J., & Shin, W. C. (2014). Distribution of Synechococcus and its phycoerythrin pigment in relation to environmental factors in the East Sea, Korea. *Ocean Science Journal*, *49*(4), 367–382. https://doi.org/10.1007/s12601-014-0034-5

Zimorski, V., Ku, C., Martin, W. F., & Gould, S. B. (2014). Endosymbiotic theory for organelle origins. *Current Opinion in Microbiology*, *22*, 38–48. https://doi.org/10.1016/j.mib.2014.09.008

Zinser, E. R., Lindell, D., Johnson, Z. I., Futschik, M. E., Steglich, C., Coleman, M. L., … Chisholm, S. W. (2009). Choreography of the Transcriptome, Photophysiology, and Cell Cycle of a Minimal Photoautotroph, Prochlorococcus. *PLoS ONE*, *4*(4), e5135. https://doi.org/10.1371/journal.pone.0005135

Zubkov, M. V., Sleigh, M. a., Burkill, P. H., & Leakey, R. J. G. (2000). Picoplankton community structure on the Atlantic Meridional Transect: a comparison between seasons. *Progress in Oceanography*, *45*(3–4), 369–386. https://doi.org/10.1016/S0079-6611(00)00008-2

Zubkov, M. V., Sleigh, M. a., Tarran, G. a., Burkill, P. H., & Leakey, R. J. G. (1998). Picoplanktonic community structure on an Atlantic transect from 50°N to 50°S. *Deep-Sea Research Part I: Oceanographic Research Papers*, *45*(8), 1339–1355. https://doi.org/10.1016/S0967-0637(98)00015-6

Zubkov, M. V, & Tarran, G. a. (2008). High bacterivory by the smallest phytoplankton in the North Atlantic Ocean. *Nature*, *455*(7210), 224–226. https://doi.org/10.1038/nature07236

4 Organic matter and zooplankton dynamics in the subtropical North Atlantic: influence of the Mid-Atlantic Ridge

4.1 Introduction

The size of phytoplankton cells plays an important role in dictating how organic carbon is transferred to higher trophic levels or is exported to deep water (Legendre & Rivkin, 2002). Phytoplankton communities dominated by small cells (< 5 μm) regenerate nutrients and carbon within the surface ocean, resulting in low export of organic matter to the deep ocean and low availability of food for higher trophic levels. In contrast, phytoplankton communities dominated by larger cells (> 5 μm) tend to be associated with higher export production by cells sinking directly or via aggregation as well as transfer of organic matter to higher trophic levels and subsequent production of faecal pellets which contribute to export fluxes.

Zooplankton are the primary grazers of phytoplankton. Zooplankton are a morphologically and taxonomically diverse group that includes unicellular, colonial, and multicellular forms, protozoa, protists, vertebrates and invertebrates (Kiørboe, 2011a). They can be classified by taxonomic group, life style, size-distribution, or functional traits (Brun et al., 2017; Castellani & Edwards, 2017). Zooplankton may spend their entire life in the plankton (holoplankton), or part of their life in the plankton (meroplankton) and can be split into picoplankton 0.2-2 μm, nanoplankton 2-20 μm, microplankton 20-200 μm, mesoplankton 200-2000 μm, macroplankton 2-20 cm, and megaplankton 20-200 cm (Table 4.1). Mesozooplankton, which are dominated by copepods, are grazers of larger cells and key players in the export of carbon to depth (Turner, 2004; Kiørboe, 2011b). Zooplankton play a significant role in the biological carbon pump, they 'repackage' phytoplankton into faecal pellets, break up particles 'messy feeding', and export carbon out of the euphotic zone through diel vertical migration (Lampitt et al., 1990; Kobari et al., 2013; Turner, 2015).

In this study, analysis of phytoplankton size and community structure reveals a significant ($p < 0.05$) increase in larger phytoplankton (> 2 μm chlorophyll-*a* size fractions) as well as pico- and nanoeukaryotes ($p < 0.1$) at stations over the Mid-Atlantic Ridge compared to stations in the adjacent basin away from topography (Chapter 3). POC biomass includes living cells, phytodetritus and marine snow (De La Rocha & Passow, 2007; Turner, 2015). With the occurrence of larger cells, due to an increase in volume per cell, we may see increased biomass standing stock and phytodetritus, and increased nucleation of marine snow (De La Rocha & Passow, 2007). Increased availability of larger phytoplankton cells (prey) may increase the concentrations of larger organisms that graze them. Zooplankton biomass is known to significantly correlate with primary production and phytoplankton standing stocks (Madin et al., 2001). The peak zooplankton abundance often coincides with the deep chlorophyll-*a* maximum (Herman, 1983; Eden et al., 2009; Andersen, Neilsen, et al., 2011).

In this chapter, we test the hypotheses that (a) an increase in larger cells will cause an increase in the particulate organic matter standing stock over the Mid-Atlantic Ridge compared to over the abyssal basin and (b) an increase in larger cells will lead to an increase in the abundance of larger zooplankton over the Mid-Atlantic Ridge compared to over the abyssal basin, and facilitate grazing-induced export. These hypotheses were tested by assessing the quantity and quality of particles by determining the distribution of particulate organic carbon and nitrogen (POC and PON, respectively) and lipid composition. Tests on POC blanks and sample variability are also presented. In addition, the abundance, composition and biomass of zooplankton was quantitatively assessed over the entire transect.

Table 4.1 Classification of zooplankton by size and groups (Castellani & Edwards, 2017).

Classification	Size	Groups
Picoplankton	0.2-2 µm	Heterotrophic bacteria
Nanoplankton	2-20 µm	Nanoflagellates
Microplankton	20-200 µm	Protozoans such as ciliates and amoebae (e.g. foraminifera) and some dinoflagellates
Mesoplankton	200-20000 µm (0.2-20 mm)	Dominated by crustacean plankton, in particular copepods
Macroplankton	2-20 cm	Large crustaceans such as euphausids (krill), amphipods, and larger specimens of hydromedusae (jellyfish) and ctenophores (comb jellies) as well as fish larvae
Megaplankton	20-200 cm	Only represented by a few organisms such as chain-forming salps (a tunicate), siphonophores and large jellyfish

4.2 Method

4.2.1 Study location

Samples were collected in the subtropical North Atlantic during RidgeMix (JR15007), June 2016, aboard the RRS James Clark Ross (Figure 4.1). Samples for DOC sorption to POC filters and POC replication experiments were collected in the tropical North and subtropical South Atlantic during AMT25.

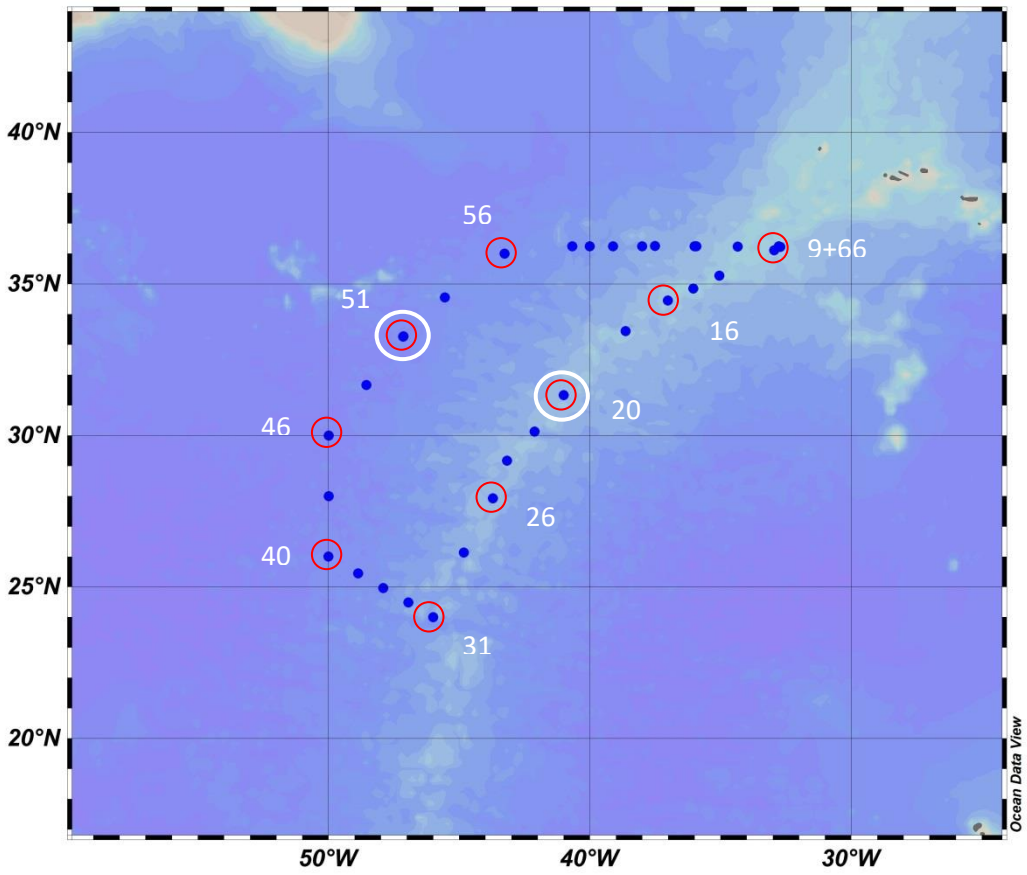

Figure 4.1 Location of stations sampled: blue dots = CTD POC sampling; red circles = stations with zooplankton nets with station number; white circles = two stations where lipid biomarker analysis was conducted.

4.2.2 Particulate organic carbon (POC) analysis

Seawater samples for POC analysis were collected from Niskin bottles during RidgeMix (Figure 4.1). In the top 300m of the water column, seawater was collected at between 6 and 23 depths per station (mean = 15 depths) and typically at the same depths as samples for phytoplankton analysis (chapter 3). Between 250 and 500m, seawater samples for POC analysis were collected every 50m. Samples were collected into triple rinsed 5 L and 10 L plastic bottles after the collection of samples for dissolved oxygen, nutrients and phytoplankton characterisation. Once a week, POC bottles were acid cleaned overnight and triple rinsed with Milli-Q.

In the on-board Chemistry Lab during RidgeMix, 2 to 4 L of seawater was filtered through 0.7 µm pore size GFFs (25 mm, Whatman, pre-ashed 400° C, 12 h). The volume filtered varied depending on the concentrations of material in the water. 2 L was filtered for surface samples (down to ~250 m) and 3 to 4 L was filtered between ~250 m and 500 m. After filtration, filters were placed on foil (350°C, 24 hours) in plastic petri-dishes and left to dry in an oven (60°C). After 12 hours, the petri-dishes were removed from the oven, sealed, placed in double zip-lock plastic bags and stored in the -20°C freezer in polystyrene boxes until transport back to the UK on dry ice (Lorrain et al., 2003; Salter et al., 2007; Turnewitsch et al., 2007).

In the laboratory at the University of Liverpool, samples were analysed for POC and particulate nitrogen (PN) by Sabena Blackbird (see Chapter 2.2.3 for method).

4.2.2.1 POC correction for sorbed DOC

When measuring oceanographic POC, many studies do not include a correction for DOC sorption to filters. DOC sorption was assessed at two stations during AMT25 (CTD37 at 12°22'8.36" N 22°31'56.35" W and CTD 63 at 22°9'28.91" S 25°5'11.9" W using two independent techniques. Firstly, two GFF filters were stacked and 2 L of seawater was filtered from 2 m and 130 m (the deep chlorophyll-*a* maximum) and 500m. Analysis of both top and bottom filters for POC content revealed that the POC blank increased with depth, with the bottom filter representing 30%, 36% and 75% of the top filter at 2m, 130m and 500m, respectively (Appendix Table 4.1). Secondly, filtrate, that is, water that had already passed through a GFF, was re-filtered three times and analysed for POC content (n = 3). The initial POC concentration was 4.09 ± 0.20 µmol L^{-1}. Subsequently POC concentrations from re-filtered seawater were 2.02 ± 0.22 µmol L^{-1}, 1.9 ±.0.37 µmol L^{-1} and 1.84 ± 0.08 µmol L^{-1}, with the final POC concentration representing 47% of the initial POC concentration. These results highlight the need to consider the carbon blank when assessing POC concentrations in the ocean. Given that the contribution of the blank to the initial POC concentration increase with depth, there is potential for over estimation of POC at depth if the blank is not considered.

4.2.2.2 Sample error

To test for POC microscale patchiness within a Niskin bottle, we analysed 3 replicate samples from the surface (2 or 10 m), the chlorophyll-*a* maximum, and from depth (300 or 500 m) during RidgeMix (CTD 66, 36°13'33.54" N 32°42'36.6" W) and AMT25 (See previous section for CTD locations). The replicate samples were taken from the same Niskin bottle. POC concentration variability changed with depth, being 2 to 9 % in surface waters, 10 to 11 % at 500m and 13 to 15 % at the DCM (Table 4.3).

Table 4.2 Niskin bottle POC triplicates (mean ± standard deviation, n = 3) collected during RidgeMix (RM) and AMT25. CV is the coefficient of variation (% variance).

RM	**POC (µmol L^{-1})**	**CV (%)**
CTD 66 - 10 m	2.79 ± 0.06	2
CTD 66 - 102 m	2.69 ± 0.34	13
CTD 66 - 300 m	1.61 ± 0.16	10
AMT25		
CTD 37 - 2 m	4.09 ± 0.20	5
CTD 63 - 2 m	2.59 ± 0.23	9
CTD 63 - 130 m	2.79 ± 0.43	15
CTD 63 - 500 m	1.32 ± 0.14	11

4.2.3 Zooplankton

4.2.3.1 Sample collection and preservation

Zooplankton were collected using the conventional WP-2 200 µm nets at ten stations during RidgeMix (Sameoto et al., 2000; Gallienne & Robins, 2001). Nets were deployed from the aft deck winch, down to 200 m and hauled in at a winch rate of ~10 m/min. Two tows were performed at each station, with zooplankton being captured in a 1 L non-filtering cod end. Samples were collected at night in the dark between 23:00 and 05:00 to account for diurnal migration of zooplankton. Once on deck, the nets were rinsed with seawater and samples were transferred into white buckets. From each tow, 900 mL of sample was fixed with 100 mL of 40% buffered formaldehyde (buffered with sodium tetraborate (borax)) in 1 L wide-necked HDPE bottles. The 1 L samples were stored in black bags in the + 4°C fridge until transport back to the UK.

4.2.3.2 Sample analysis

From each net tow performed at 10 stations, a series of measurements were made at the National Oceanography Centre in Southampton following methods published by Giering et al., (2014), including; total wet weight (> 200 µm); size fractionated dry weight (200-500 µm, 500-1000 µm, 1000-2000 µm and > 2000 µm); and size fractionated zooplankton composition and abundance (200-500 µm, 500-1000 µm, 1000-2000 µm and > 2000 µm).

Preserved 1 L samples were split into quarters using a Folsom's Plankton Sample Divider. One quarter was poured onto a small 200 µm mesh and the excess water removed. The mesh was placed in a petri-dish and the wet weight measured (mesh and petri-dish were pre-weighed) using a METTLER AE240 balance. The sample was then resuspended in 10% formalin and poured through three stacked mesh sieves of size 2000 µm, 1000 um, and 200 µm. The fraction retained on the 200 µm mesh was further split in half using the Folsom Plankton Sample Divider and half was poured through stacked sieves of 500 µm and 200 µm mesh. The organisms on the 2000 µm mesh were picked off with tweezers and placed into a petri-dish containing formalin for counting. The organisms on the 200, 500 and 1000 µm mesh sieves were washed off with formalin and counted using a Bogorov counting chamber for zooplankton. Zooplankton were counted using a MEIJI TECHNO RZ microscope (parallel optical modular stereo microscope with 7.5x to 75x magnification with 10x eyepieces and 1x objective) with digital camera attached (Canon EOS 1000D). The organisms were identified and quantified to group level (see Table 4.4).

Table 4.3 Zooplankton groups identified in this study.

Groups	**Subgroups**
Copepod	Calanoid
	Oithona (Cyclopoida)
	Oncaea (Poecilostomatoida)
	Sapphrinid (Poecilostomatoida)
	Harpacticoida
Amphipod	
Appendicularian (= Larvacean)	
Chaetognath	
Cladoceran (= Branchipoda)	
Foraminifera	
Isopod	
Jelly	Gelatinous organisms (Cnidaria, Ctenophora, and Thaliacae)
	Salp (Thaliacea)
	Siphonophore (Cnidaria: colonial Hydrozoa)
Larvae	
Ostracod	
Phytoplankton	Dinoflagellate: *ceratium spp.*
	Diatom
Polychaete	
Pteropod	
Radiolaria	
Shells (mollusca)	
Shrimp-like (decapods, euphausids, mysids, and Stomatopods)	
Other (eggs, fish larvae)	

After counting, each of the size-fractions was poured onto a 63 µm mesh, rinsed with buffered MilliQ to remove the salt and the organisms were transferred into a pre-weighed muffled foil cups (400°C > 4hrs) using tweezers. The foil cups were then placed in the oven overnight at 40°C. The following day the cups were weighed using a SARTORIOUS ME5 balance. An AD-1683 Static Eliminator was used to remove static from samples prior to weighing. The dry weight was recorded.

To quantify the individuals and biomass per unit volume, the number of individuals and biomass per tow was divided by the volume filtered (m^3). Given a WP-2 net of diameter 0.58 m, towed vertically for 200 m, the total volume of water filtered was 51.0352 m^3.

The relationship between zooplankton abundance, biomass and size-distribution and location (ridge vs. basin and north vs. south of 31°N) was tested using one-way ANOVA tests. The relationship between size-fractionated zooplankton communities and environmental variables were visualised using non-metric multidimensional scaling (NDMS) with Bray-Curtis distance using the metaMDS function of the vegan package in RStudio (Anderson, 2001; Wubet et al., 2012). The goodness of fit statistic, squared correlation coefficient (envfit function), was used to test the significance of environmental variables (north vs. south of front, ridge vs. basin).

4.2.4 Lipid biomarker analysis

At two stations in the subtropical North Atlantic, one over the Mid-Atlantic ridge (CTD 20) the other over the basin (CTD 51), samples were collected for lipid biomarker analysis. Samples were collected using GFF filters (273 mm, pre-ashed, 400° C, 12 h) *in-situ* Stand Alone Pumps (SAPs) from three depths in the water column: the chlorophyll-*a* maximum (DCM), 100 m below the DCM, and 500 m. The SAPs pumps were left to pump for 90 minutes in the water at each specific depth. Lipid samples were analysed using a Thermo Scientific TRACE 1300 series Gas Chromatograph (Split/Splitless injector) coupled with a ISQ-LT single quadrupole mass spectrometer (GCMS). Refer to Chapter 2.2.3 and 2.2.4 for POC and lipid extraction and analysis methods and conditions. Lipid analyses were performed by Izzy Hassall.

4.3 Results

4.3.1 POC and PN

Concentrations of POC and PN (herein [POC] and [PN]) ranged from 3 to 8 µmol L^{-1} POC and 0.5 to 1.1 µmol L^{-1} PN, respectively, with subsurface maxima at nearly all stations in the subtropical North Atlantic (Figure 4.2 and 4.3). Maximum [POC] and [PN] were higher ($p < 0.01$) north of the front at 31°N (sections 1, 2, 6, 7) compared to south of the front (sections 3-5). The highest [POC] and [PN] were at 36°N (sections 1 and 7 and CTD 56 in section 6) as well as at 34.8°N in section 2 (CTD 13). Below the subsurface maximum concentrations decreased gradually to 500 m (Figure 4.3), with the highest variability in [POC] and [PN] measured in the upper 50 m of the water column (Figure 4.3).

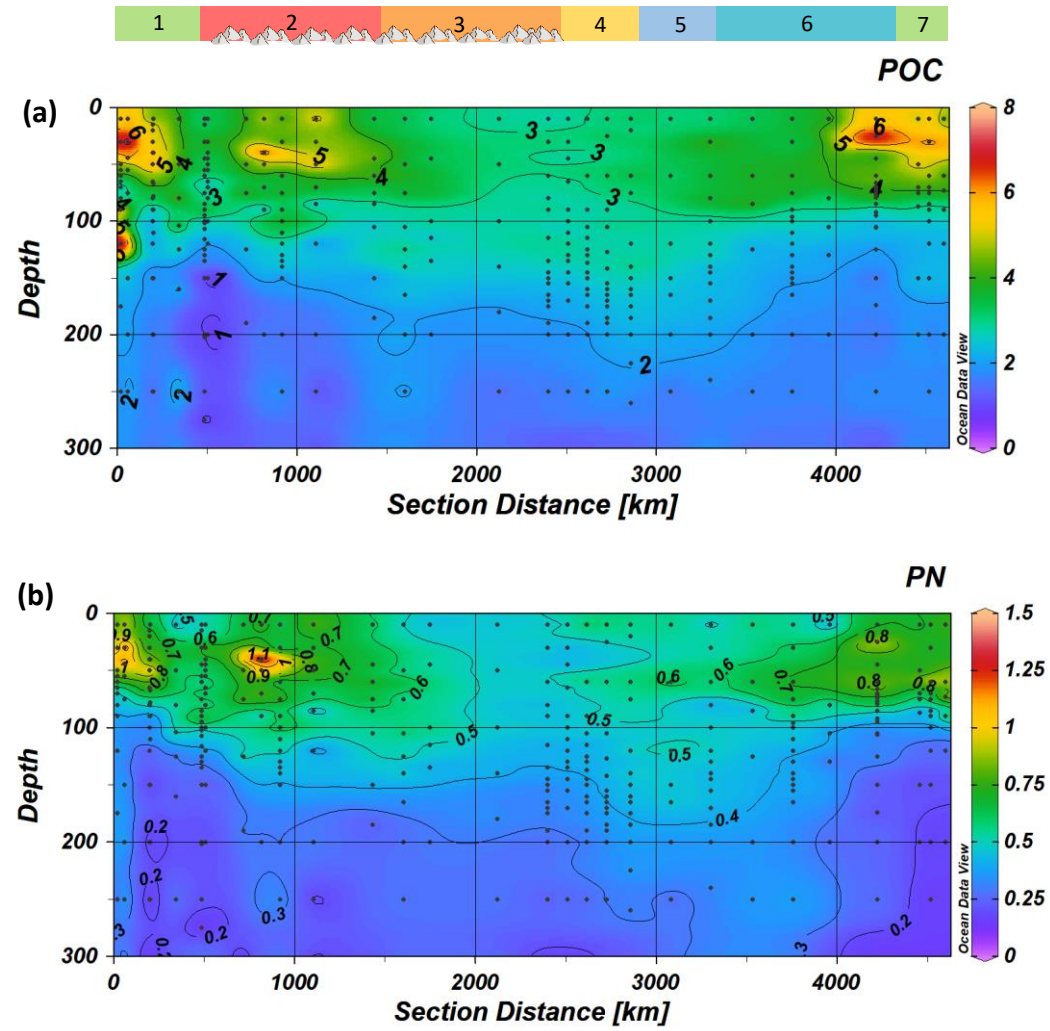

Figure 4.2 (a) Particulate organic carbon (POC, µmol L^{-1}) and (b) particulate nitrogen (PN, µmol L^{-1}) sections with depth from 0 to 300 m. Sections are the same as in Chapter 3 (see Figure 3.6).

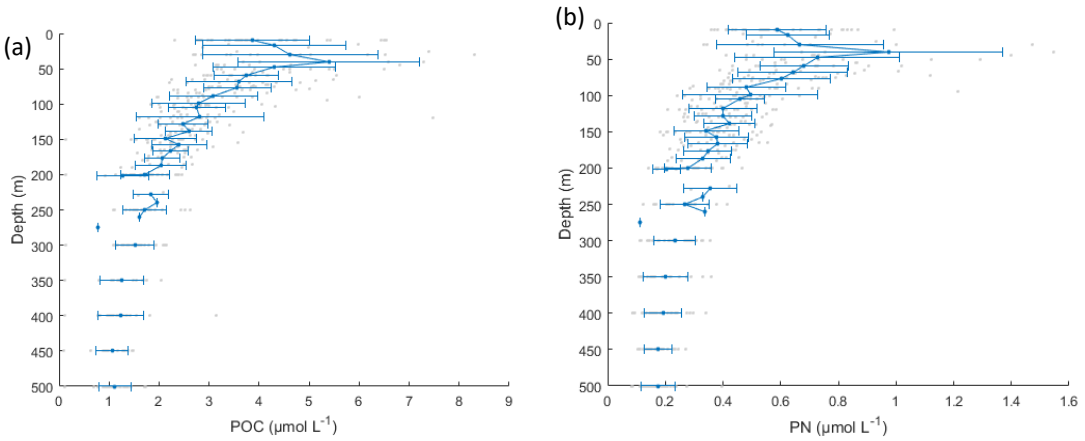

Figure 4.3 Depth variation in (a) POC and (b) PN for all stations from 0 to 500m. Grey dots = data. Blue dots and error bars are average concentrations ± standard deviation at 10 m intervals.

Depth variation in [POC] and [PN] were statistically similar over the ridge and basin (Figure 4.4a, b); depth integrated POC and PN between 0 and 500m and 0 and 200m were

statistically similar over the ridge and basin (t-test, Figure 4.4c, d). Overall, the POC:PN ratio varied from 5.7 to 15.6, with the highest POC:PN ratio observed below 100m at 36°N (Figure 4.5, sections 1 and 7). However, the mean POC:PN ratio was statistically similar over the ridge (6.3 ± 0.6) compared to the basin (5.5 ± 0.5).

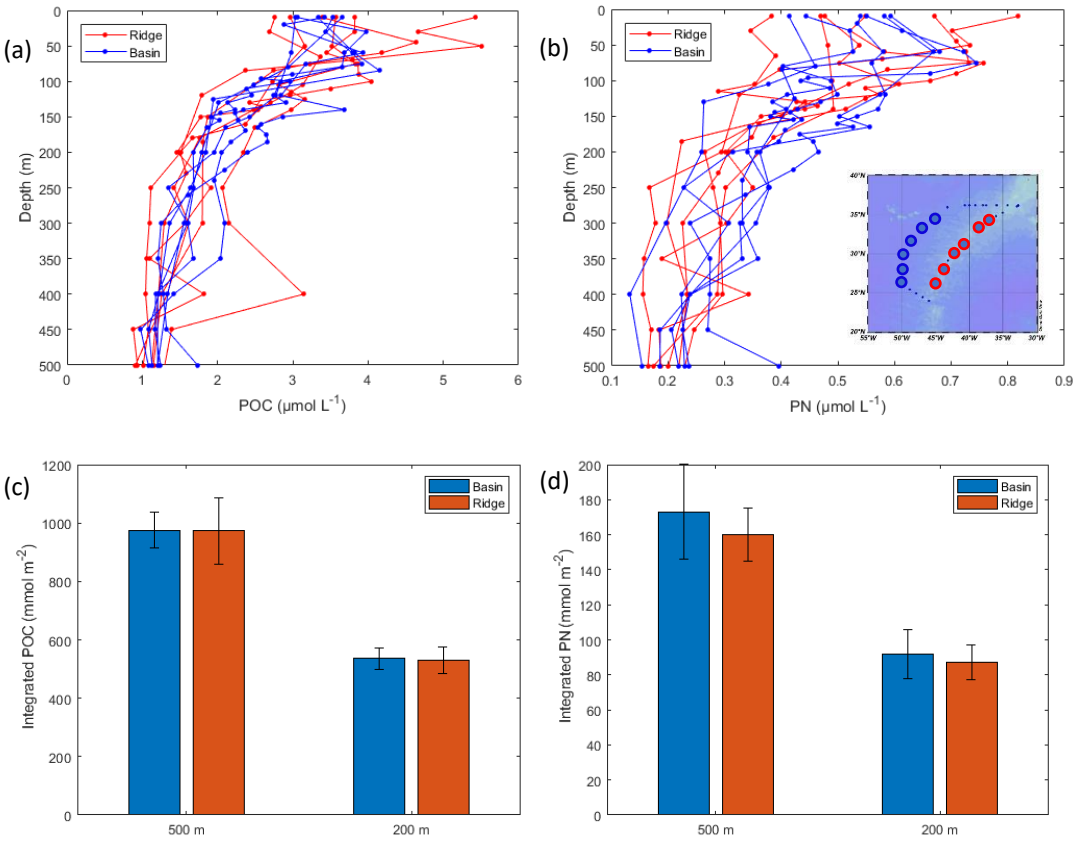

Figure 4.4 Depth variation in (a) POC and (b) PN for ridge (red) and basin (blue) stations. Panel b shows a map of the stations selected for comparison. Water column (c) POC and (d) PN integrated over 500 m and 200 m (n = 6; mean concentration ± standard deviation).

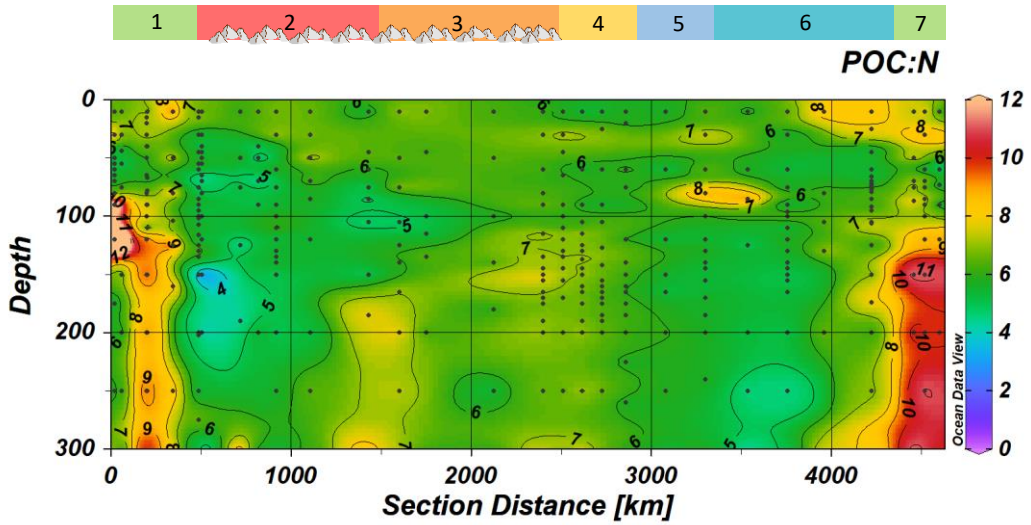

Figure 4.5 Spatial variation in the POC:PN molar ratio.

4.3.2 Zooplankton

The mean (± standard deviation) wet weight for zooplankton was 38 ± 37 mg m^{-3} for all stations. The zooplankton wet weight at 32°N over the ridge (CTD 20) was > 3-fold higher compared to other stations (143 mg m^{-3} compared to 17 to 37 mg m^{-3}) due to the presence of a large salp. The mean (± standard deviation) zooplankton dry weight was 2.0 ± 1.4 mg m^{-3} for all stations. The dry weight of zooplankton at 32°N over the ridge (CTD 20) was double that measured at all other stations (5.5 mg m^{-3} compared to 0.7 to 2.6 mg m^{-3}) due to the presence of > 2000 µm crustaceans. On average, the highest contribution to total dry weight was by the > 2000 µm zooplankton size fraction (41 ± 18%), with the 200-500 µm, 500-1000 µm and 1000-2000 µm size fractions contributing 17 ± 9%, 25 ± 13% and 17 ± 8%, respectively (Figure 4.6). There was a statistically significant increase in the dry weight of the 500-1000 µm size fraction over the ridge (ANOVA, p = 0.005) compared to the stations in the adjacent basin.

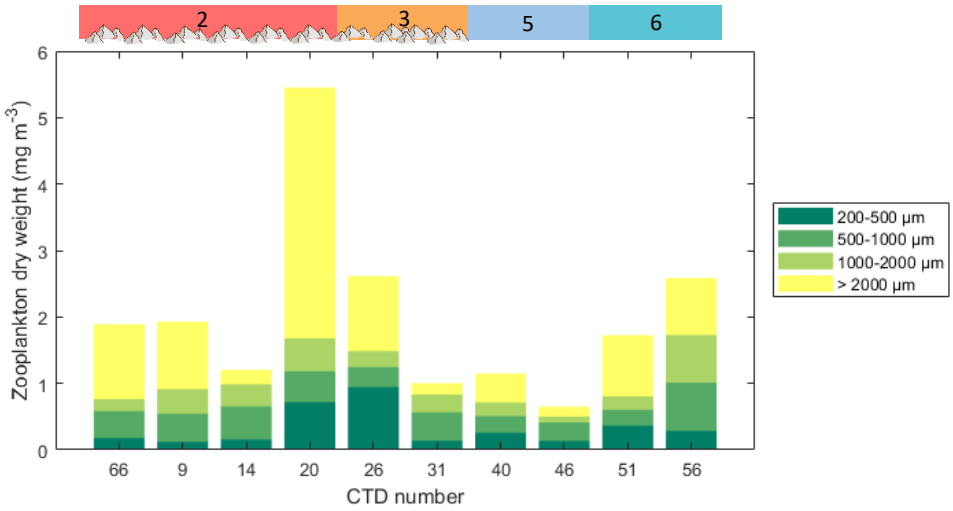

Figure 4.6 Size-fractionated zooplankton dry weight. Sections are as previously stated, with sections 2 and 3 located over the ridge and 5 and 6 over the basin, with north being section 2 and 6 and south sections 3 and 5.

Zooplankton abundance ranged from 37 to 152 individuals per m^3 with CTDs 55 and 20 having the highest abundance (Figure 4.7a). Copepods were the most numerous zooplankton, accounting for 65 ± 12 % of total zooplankton abundance, followed by gelatinous organisms (14 ± 12%) with all other zooplankton groups accounting for less than 8% of zooplankton. The most abundant group of copepods were the Calanoid copepods (70 ± 9%), followed by *Oithona* (16 ± 7%) then Poecilostomatoida (14 ± 5%; Sapphrinid 7 ± 5% and *Oncaea* 6 ± 5%; Figure 4.7b). Harpacticoid contributed less than 1% of copepods.

We observed a large phytoplankton bloom at CTD 56 (see chapter 3) and have removed data from this station from further analysis in order to remove the effect of sub-mesoscale processes such as eddies. Consequently, the abundance of zooplankton was significantly higher (ANOVA, p = 0.038) over the ridge (73 ± 20 indv. m^{-3}) compared to the basin (42 ± 7

indv. m^{-3}). The observed higher zooplankton abundances were due to a higher contribution from calanoid copepods (p = 0.012) over the ridge (35 ± 10 indv. m^{-3}) compared to the basin (17 ± 6 indv. m^{-3}). The abundance of *Oncaea* copepods was also higher at CTDs 66, 9, and 14 in section 2 over the ridge. There were also significantly lower abundances of shells (ANOVA, p = 0.006) over the ridge (0.5 ± 0.08 indv. m^{-3}) compared to the basin (0.9 ± 0.08 indv. m^{-3}).

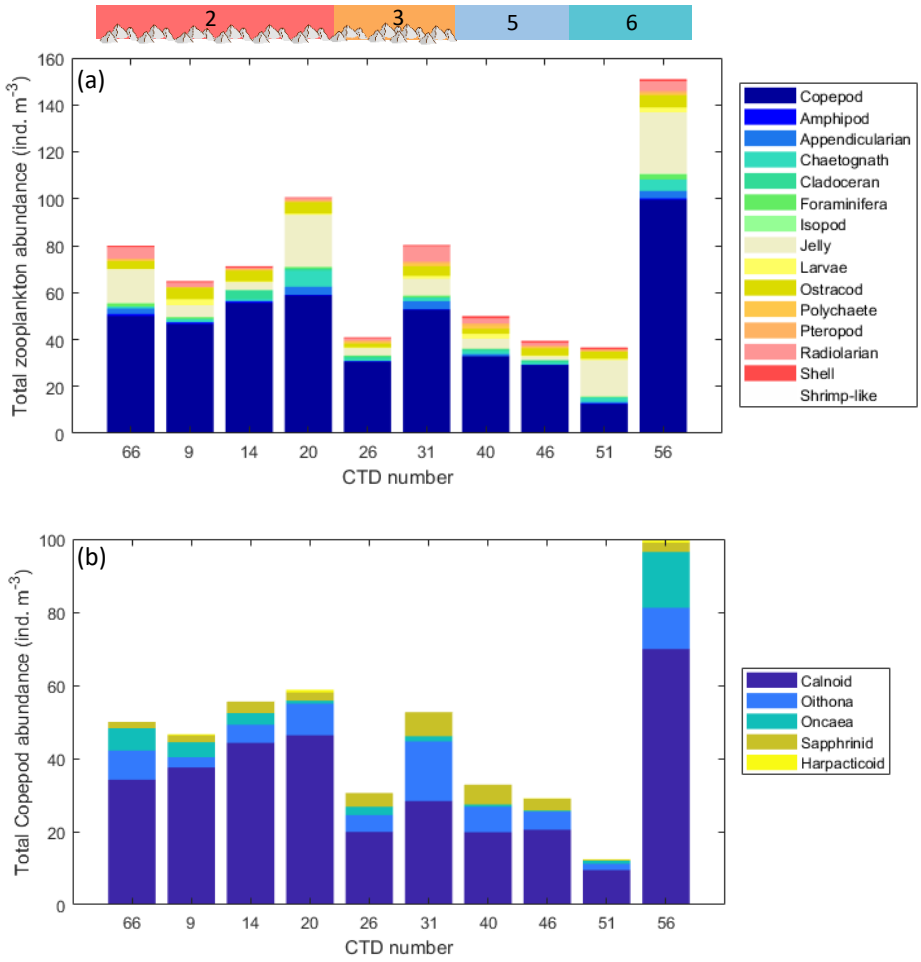

Figure 4.7 (a) Total zooplankton abundance and composition (b) copepod abundance and composition.

In addition to enhancement of zooplankton over the ridge, there was a latitudinal effect with higher abundances (ANOVA) of amphipods (p = 0.019) and isopods (p = 0.034) and a lower abundance of Sapphrinid copepods (p = 0.012) and polychaetes (p = 0.011) to the north of the front at 31°N. There was a 3-fold increase in Sapphrinid copepods between 33°N (~2 indv. m^{-3}) and 24°N (~6 indv. m^{-3}). The copepod group, *Oithona*, was distributed heterogeneously over the study area. The abundance of gelatinous organisms was higher just north of the front at 31°N (CTDs 51 and 20, 15 and 22 indv. m^{-3}) and at 36°N (CTD 56 and 66, 26 and 14 indv. m^{-3}) compared to south of 31°N (2 to 7 indv. m^{-3}; Figure 4.8). The abundance of salps was higher at CTDs 20 and 56 (13 and 10 indv. m^{-3}) compared to the other stations (0.3 ± 0.3 indv. m^{-3}).

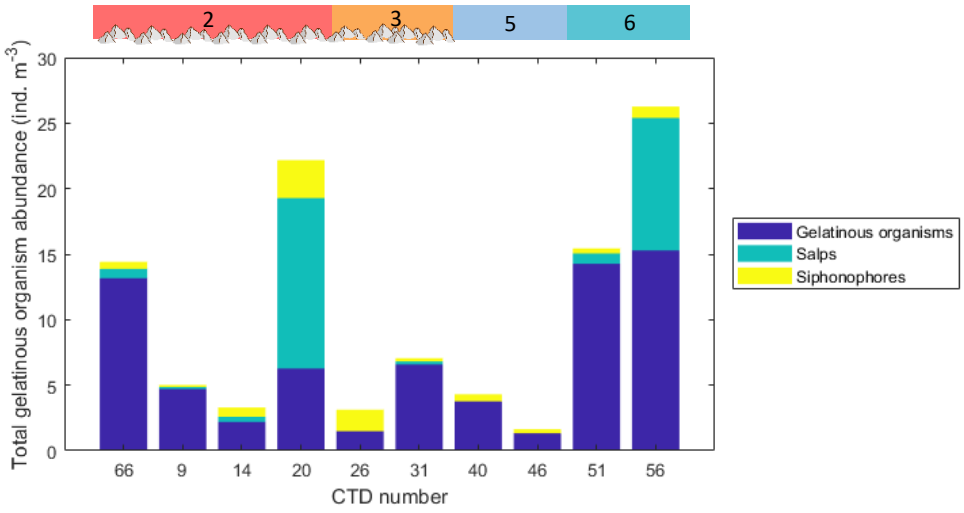

Figure 4.8 Gelatinous organism abundance and composition.

The most abundant mesozooplankton in the subtropical North Atlantic were in the 200-1000 µm size fractions (86 ± 4%) with highest abundances in the 500-1000 µm size-fraction (48 ± 4%), followed by 200-500 µm (38 ± 4%), 1000-2000 µm (10 ± 3%), and then > 2000 µm (3 ± 2%) fractions (Figure 4.9). Copepods were the most numerous mesozooplankton group in the four size fractions (Appendix Table 4.2). Copepods and gelatinous organisms were the most abundant groups in the two smaller size fractions but gelatinous organisms and chaetognaths became relatively more important and copepods less in the two larger size-fractions (Appendix Table 4.2). There were significantly higher zooplankton in the 500-1000 µm size fraction (p = 0.044) over the ridge compared to the adjacent basin. At the 90% significance level, there were significantly higher abundances of zooplankton in both the 200-500 µm and 1000-2000 µm size-fractions over the ridge compared to the adjacent basin (ANOVA, p = 0.053, 0.052).

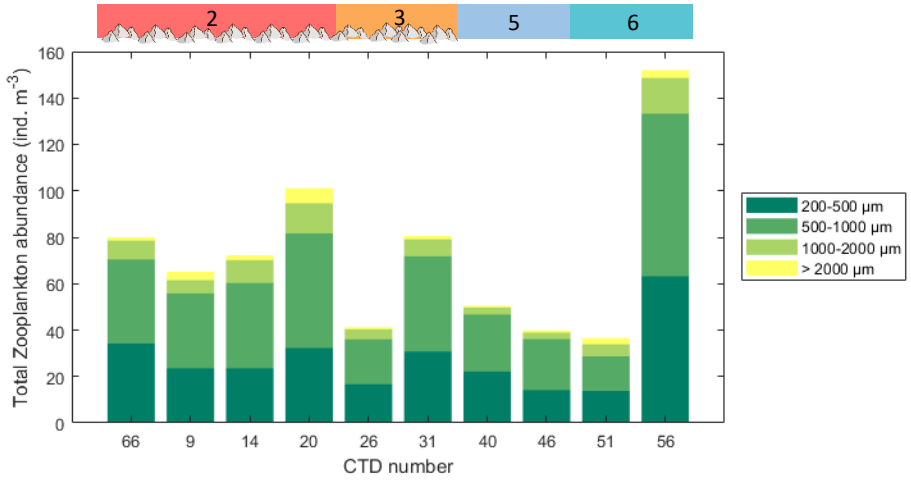

Figure 4.9 Size-fractionation of the zooplankton community.

The NMDS plot allows visualisation of variability in the zooplankton community between ridge and basin and north and south of 31°N stations (Figure 4.10). There was no significant separation between the community over the ridge and basin but there was a significant separation between north (green) and south (black) of the front (p = 0.025; Figure 4.10). However, the clustering is not clearly defined and should be interpreted with caution.

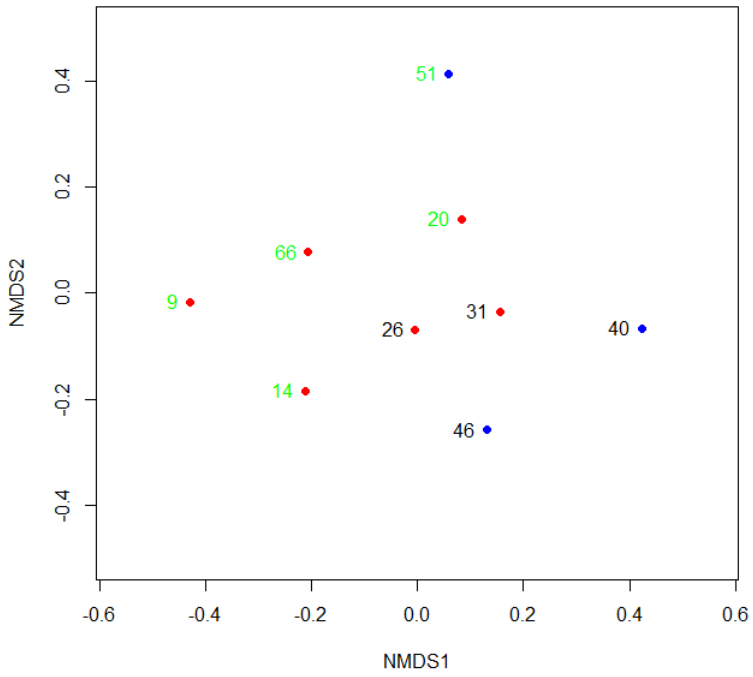

Figure 4.10 Non-metric multidimensional scaling (NMDS) visualisation of dissimilarity between stations in terms of zooplankton community and location. Ridge (red dots) vs. basin (blue dots). North (green text) and south (black text) of 31°N. Numbers are CTD numbers (station).

4.3.3 Lipid biomarkers

Lipid concentrations decreased with depth at both stations sampled (Figure 4.11a, b). In all samples the fatty acids C_{14}, C_{16}, $C_{20:5}$, and $C_{22:6}$ accounted for 61 to 76% of lipids, apart from over the basin at 500 m where they made up 29%. The next most abundant lipids were the fatty acids $C_{16:2(n-6)}$, $C_{16:1(cis-9)}$ $C_{18:3(n-6)}$, $C_{18:4(n-3)}$, $C_{18:1(cis-9)}$, $C_{18:2(cis-9)}$, $C_{18:3(cis-9)}$, and $C_{14\ isomers}$ which, together with the four most abundant fatty acids, constitute 67 to 93% of total lipids. Other lipids present, but at low concentrations (<5% of total lipids), included branched fatty acids (*i*- and *a*-C_{15} and C_{17}, *a*-C_{16}, C_{18} and C_{19}), alcohols (primarily $C_{16\text{-}OH}$ and $C_{18\text{-}OH}$), and sterols (chiefly cholesterol, brassicasterol, cholesta-5,22(*E*)-dien-3ß-ol and cholesta-5,22(*Z*)-dien-3ß-ol, phytadienes; Appendix Table 4.3). There was no significant difference between total lipid concentration over the ridge and basin at any depth (paired t-test).

Table 4.4 Dominant fatty acids in samples, their indicator and mean (± standard deviation) percentage contribution to total lipids in all samples. Phytoplankton fatty acid indicator references: Volkman et al., 1989; Wakeham et al., 1997; Volkman, 2006; Parrish, 2009, 2013.

Fatty acids	Indicator	Mean % contribution
C_{14}	Diatoms, Prymnesionphytes, chlorophytes	8 ± 8
C_{16}	Diatoms, Prymnesionphytes, chlorophytes	15 ± 6
$C_{20:5}$	Diatoms	7 ± 4
$C_{22:6}$	Dinoflagellates	27 ± 21
$C_{16:1(cis-9)}$	Diatoms, Prymnesiophytes	4 ± 4
$C_{16:2(n-6)}$	Chlorophytes?	2 ± 2
$C_{18:3(n-6)}$	Chlorophytes	2 ± 3
$C_{18:4(n-3)}$	Dinoflagellates, Prymnesiophytes	2 ± 3
$C_{18:1(cis-9)}$	Zooplankton derived material	4 ± 2
$C_{18:2(cis-9)}$	Chlorophytes	1 ± 1
C_{14} isomers		13 ± 23

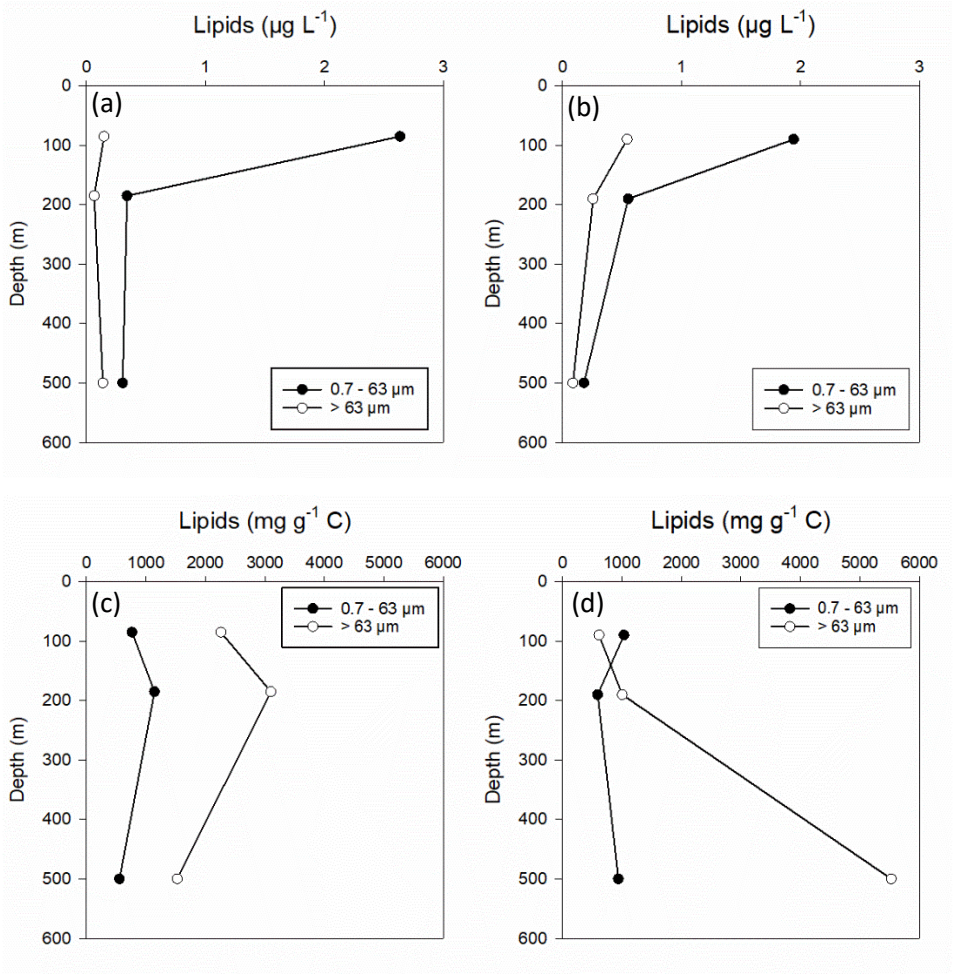

Figure 4.11 Depth variation in lipid concentration (µg L^{-1} and mg g^{-1} C) for (a) a basin station, CTD 51 (b) a ridge station, CTD 20. Lipid concentrations normalised to carbon for (c) basin station and (d) ridge station. Samples were collected using Challenger Stand-Alone Pumps (SAPs) from the DCM, 100 m below the DCM, and 500 m. The filtered water was size-fractionated into > 63 µm (mesh) and 0.7-63 µm (GFF) particles.

Zooplankton biomarkers were present and included monounsaturated fatty acids $C_{18:1(cis-9)}$, $C_{18:1(trans-9)}$ and $C_{20:1(cis-11)}$, fatty alcohols $C_{14\text{-}OH}$, $C_{16\text{-}OH}$ and $C_{18\text{-}OH}$, and C_{27} sterols. Concentrations

of zooplankton biomarkers were highest at the DCM (0.151 ± 0.017 μg L^{-1}) decreasing ~40% by 100 m below the DCM (0.047 ± 0.038 μg L^{-1}). Zooplankton biomarker concentrations at 500 m (0.043 ± 0.004 μg L^{-1}) were similar to those 100 m below the DCM. At 100 m below the DCM all zooplankton biomarkers had lower concentrations over the ridge than over basin but at 500 m there were higher concentrations over the ridge. Consequently, there was a higher percentage increase in zooplankton biomarkers from 100 m below the DCM to 500 m over the ridge compared to the adjacent basin (Figure 4.12). There was a 300-1100% increase in $C_{20:1(cis-11)}$, $C_{14\text{-}OH}$ and $C_{16\text{-}OH}$ from 100 m below the DCM to 500 m. PCA analysis could explain 84.08% of variation between samples using the first two dimensions (Figure 4.13). The DCM were separated from the deeper samples by higher concentrations of C_{27} sterols (including cholesterol), $C_{18:1(cis-9)}$, $C_{18:1(trans-9)}$, and $C_{20:1(cis-11)}$ (dimension 1 with loadings of 16.9-18.0% each). In contrast, dimension 2 had largest loadings from $C_{14\text{-}OH}$ and $C_{16\text{-}OH}$ (46 and 33%) and $C_{18\text{-}OH}$ had a loading of 11%. Thus, 500 m over the ridge has higher concentrations of the fatty alcohols $C_{14\text{-}OH}$ and $C_{16\text{-}OH}$ compared to the basin and all shallower depths.

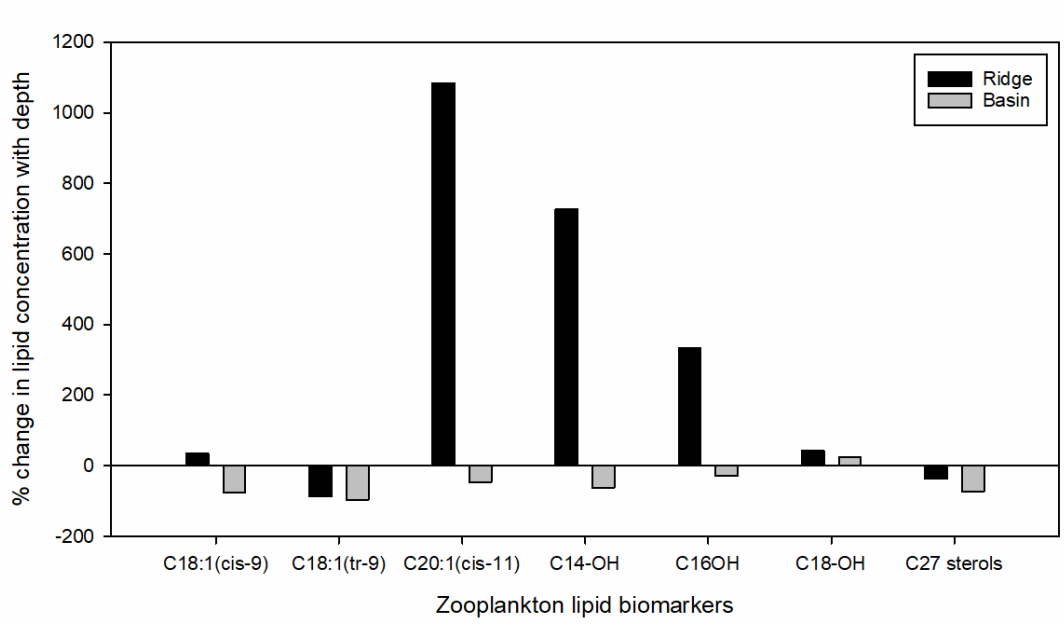

Figure 4.12 Percent change in lipids indicative of zooplankton between 100 m below the DCM and 500 m. Positive percent change shows an increase in lipid concentration with depth. Negative percent change shows a decrease in lipid concentration with depth.

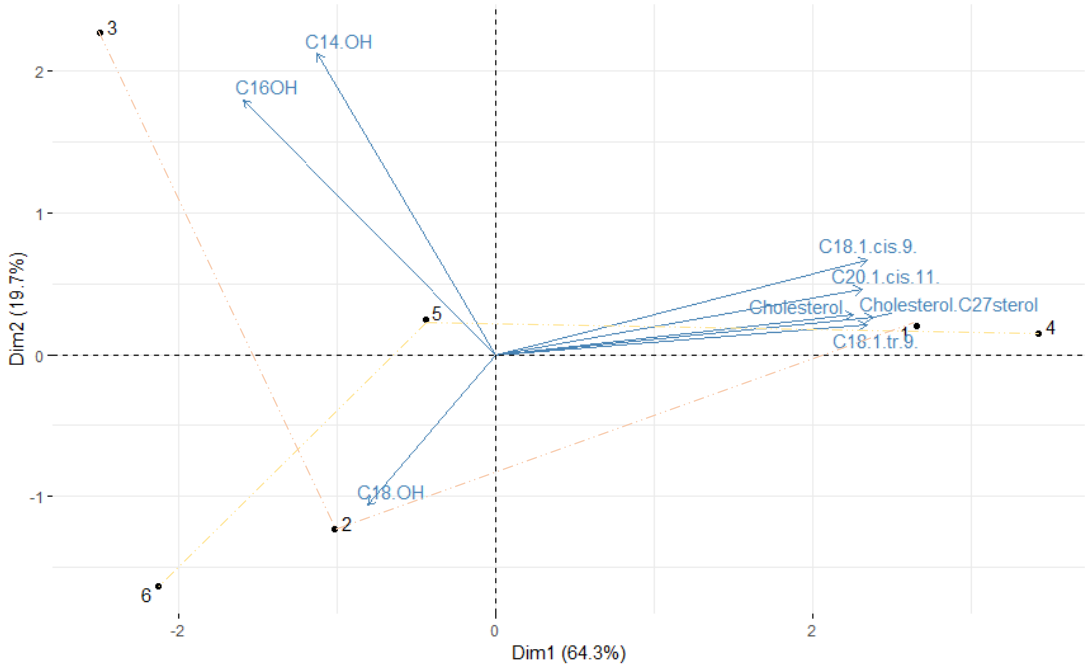

Figure 4.13 Principle Component Analysis (PCA) for zooplankton biomarkers of the two ridge-basin comparison stations. Ridge stations are points 1-3 (pink dashed line) and basin 4-6 (orange dashed line). The three depths at each station were the DCM (points 1 and 4), 100 m below the DCM (points 2 and 5) and 500 m (points 3 and 6).

4.4 Discussion

4.4.1 No change in biomass over the Mid-Atlantic Ridge

There were no significant changes in the integrated biomass (POC or PN) in the top 500 m between stations located over the Mid-Atlantic ridge (974 ± 114 µmol POC m^{-2} and 160 ± 15 µmol PN m^{-2}) and those over the abyssal basin (976 ± 60 µmol POC m^{-2} and 173 ± 27 µmol PN m^{-2}). Subsequently, there was no observable difference in the POC:PN ratio over the ridge (6.3 ± 0.6) compared to the basin (5.5 ± 0.5). [POC] were similar to previous studies in the subtropical Atlantic in summer. During AMT14, [POC] were found to range from 1 to 6 µmol L^{-1} (Poulton et al., 2006). At the Bermuda Atlantic Time Series (BATS), [POC] ranged from 0.83 to 3.33 µmol L^{-1} between 1991 and 1994 (Gundersen et al., 2001).

As changes were observed in phytoplankton composition and size-structure in Chapter 3, it suggests there may be decoupling between phytoplankton, size structure, biomass and primary production in the subtropical Atlantic Ocean as has been observed by Maranon *et al.* (Fasham et al., 1985; Marañón et al., 2001, 2003). Maranon *et al.* found that changes in carbon fixation in the oligotrophic ocean were not accompanied by similar increases in phytoplankton standing stock or change in size-structure. It may also suggest top-down control of biomass by zooplankton grazing. At the Shelf edge in the Celtic Sea, Sharples *et al.* observed a higher proportion of biomass in the larger celled phytoplankton but no increase in total phytoplankton biomass, thought to be due to grazing by fish-larvae (Sharples et al., 2009). In addition, colonisation of marine aggregates by invertebrates has a turnover rate of one to a few

days, which is similar to or faster than colonisation by microorganisms. It is estimated that invertebrate colonisers can degrade 20 to 70% of aggregated carbon before it leaves a 50 m euphotic zone (Kiorboe, 2000). Therefore, grazing on aggregated material by invertebrates, other grazers and microorganisms may degrade most material before it leaves the euphotic zone.

Another consideration is that the POC was sampled from Niskin bottles after collection of water for measurement of other properties (e.g. oxygen, nutrients, and phytoplankton), so large fast sinking particles may have been sampled before POC subsampling. In Chapter 2 Niskin bottle POC was clearly higher than measured from SAPs, which may suffer from particle washout, but lower than MSC. The large-volume bottle, MSC, is split into three particle sinking fractions "suspended", "slow-sinking" and "fast-sinking". However, addition of the "fast-sinking" particle fraction from the Marine Snow Catcher (MSC_{fast}) to Niskin bottle made little difference (< 3%) to total Niskin POC concentrations (refer to Chapter 2 Table 2.5) so, this is unlikely to be the case.

4.4.2 Mesozooplankton composition

Zooplankton, particularly calanoid copepods, were significantly higher over the ridge compared to the adjacent basin when data from CTD56 was omitted. At this latter site, a phytoplankton bloom was observed and was associated with an eddy (see Chapter 3 for details). High zooplankton abundance and biomass have been previously observed within eddies and frontal systems (Clark et al., 2001; Huskin et al., 2001; Goldthwait & Steinberg, 2008; Eden et al., 2009; Andersen et al., 2011). Eddies are characterised by shoaling of isopycnals and higher nutrient fluxes to surface waters which stimulate phytoplankton and zooplankton (Goldthwait & Steinberg, 2008; Landry et al., 2008). However, distinguishing the effect of eddies from ridge-effects is beyond the scope of this study, as both physical features enhance nutrient fluxes and primary production.

Calanoid copepods were the most abundant group of mesozooplankton, they contributed 70 ± 9% to copepods and 43 ± 11% to mesozooplankton. Copepods are the most numerous metazoan in water, here 64 ± 12% of mesozooplankton, they are known to make up between 65 and 99% of mesozooplankton in the epipelagic, of which 62-76% are calanoid copepods (Huskin et al., 2001; López & Anadón, 2008; Steinberg et al., 2008; Andersen et al., 2011; Castellani & Edwards, 2017). Copepod dominance of mesozooplankton in the pelagic ocean may be due to their efficient body build, capability to remotely detect prey and efficiency at finding a mate (Kiørboe, 2011b). There is strong ecological niche differentiation in Calanoid copepods, due to the evolution of a variety of complex life strategies, vertical habitat partitioning and feeding methods, which explains their global distribution (Schnack-Schiel et al., 2010; Litchman et al., 2013; Bode et al., 2015; Brun et al., 2015; Benedetti et al., 2016; Campos et al., 2017). However, as species were not identified in this study, functional analysis

cannot be used to shed further light on the cause of higher calanoid copepods over the ridge. The relative abundance of Copepods reported in this study are similar to previous observations.

Over the ridge, there was an increase in the concentrations of biomarkers associated with zooplankton, specifically storage wax esters ($C_{20:1}$, $C_{14\text{-}OH}$, and $C_{16\text{-}OH}$) between 100 m below the DCM and 500 m (Lee et al., 2006). Zooplankton are thought to play a major role in the transport of organic material out of the mesopelagic zone (from the surface to > 500 m) either as gut content or direct predation at depth (Angel, 1989). The increase in zooplankton associated lipids over the ridge with depth could reflect an increase in transport of material by zooplankton (e.g. faecal pellets) to depth, a change in vertical migration behaviours, or a change in deeper populations of zooplankton.

In a similar manner to patterns in phytoplankton reported in Chapter 3, we observed differences in the zooplankton community to the north and south of a front at 31°N. To the north we found higher abundances of crustacean amphipods and isopods and to the south higher abundances of Sapphrinid copepods and polychaetes (ANOVA, $p < 0.05$). Amphipods can have commensal or parasitic relationships with gelatinous zooplankton, usually medusa, siphonophores, ctenophores, and salps. Although not statistically significant we observe higher abundances of gelatinous organisms to the north of the front (Figure 4.8). At CTD 20 and 56 there were high abundances of the filter feeder salps and at CTDs 20 and 26 the passive ambush carnivores Siphonophores. Salp abundance is known to be positively correlated to primary production (Stone & Steinberg, 2014) and there were higher concentrations of chlorophyll-*a* to the north of 31°N during RidgeMix (ANOVA, $p < 0.01$; refer to Chapter 3).

The other main groups of copepods in marine waters, other than Calanoid, are Cyclopoida and Poecilostomatoida. The Cyclopoida genera *Oithona* is one of the most abundant and ubiquitous cosmopolitan copepods but little is yet known about their biology, ecology and function in marine ecosystems (Gallienne & Robins, 2001). Here we report a heterogenous distribution. The Poecilostomatoida genus *Oncaea* have higher abundances at several stations north of 31°N. *Oncaea* are reported to be well adapted to feeding on surfaces of large non-motile aggregates and gelatinous colonies (Kiørboe, 2011b). Both [POC] and gelantinous organisms were observed to have higher concentrations north of 31°N in this study. The Poecilostomatoida family Sapphirinidae is widely distributed in the tropical and subtropical oceans. Here, we observed an increase in the abundance of Sapphirinidae south of the front. Sapphirinidae are special in that they have two cuticular lenses paired to form a telescope that allows them to visualise the environment, but otherwise little is known about them (Castellani & Edwards, 2017).

In summary, the spatial pattern of mesozooplankton on the Ridgemix transect is similar to that observed for phytoplankton, supporting the tight coupling between these plankton groups. However, the increase in zooplankton associated with the ridge is more pronounced than the change in the phytoplankton community, as is the north-south contrast in zooplankton relative to the front at ~ 31°N. There may also be changes in copepod species (not identified in this study) as well as vertical distribution and migration patterns associated with the ridge and the different water masses (Angel, 1989).

4.4.3 Mesozooplankton size-distribution

There was a significant increase in the 500-1000 μm zooplankton size fraction over the ridge compared to the adjacent basin, as well as significant increase in biomass in the 500-1000 μm (ANOVA, $p < 0.05$) as well as the 200-500 μm and 1000-2000 μm size-fractions (ANOVA, $p < 0.1$). Coupling between phytoplankton abundance and the smaller size fractions of zooplankton have been previously observed. At the ALOHA station in summer, a disproportionate increase in smaller copepods (150-500 μm) occurs due to the presence of nitrogen-fixing phytoplankton (Landry et al., 2001). In the long-lived diatom blooms in the Sargasso Sea, there are increases in the < 2000 μm zooplankton (Goldthwait & Steinberg, 2008). In both studies, an increase in phytoplankton was sustained for sufficient time to allow mesozooplankton to respond to the increase in the food source, which is typically on a timescale of weeks to months relating to zooplankton growth and reproduction. Therefore, we speculate that the enhanced diapycnal flux of nutrients over the ridge are sustained for a sufficient amount of time to support phytoplankton growth and to elicit a response in the zooplankton community.

It is well documented that the small zooplankton dominate the size structure in subtropical and tropical regions (Huskin et al., 2001; Woodd-Walker, 2001; Paffenhofer & Mazzocchi, 2003; Schnack-Schiel et al., 2010). Small (200-500 μm) calanoid copepodites, *Clausocalanus* spp., *Oncaea* spp., *Corycaeus* spp., and *Oithona similis*, accounted for 60% of total abundance around the Azores (Huskin et al., 2001). Additionally, it is well known that the traditional WP-2 nets, used in this study, under-represent smaller organisms such as *Oithona*, *Oncaea* and copepod nauplii (López & Anadón, 2008). Gallienne and Robins (2001) estimate that the conventional WP-2 nets substantially under-capture mesozooplankton leading to underestimates of abundance by ~90% and biomass by a third in the subtropical oligotrophic Atlantic Ocean. Therefore, we may be under-representing the 200-500 μm size-fraction substantially, which may explain why at all stations we find higher abundances of mesozooplankton in the 500-1000 μm than the 200-500 μm size fraction.

4.4.4 Zooplankton grazing (micro- and mesozooplankton)

The most numerous mesozooplankton observed in this study were copepods and gelatinuous organisms which made up 65 ± 12% and 14 ± 12% of total mesozooplankton abundance respectively. Gelatinous organisms are a broad group that includes cnidarian medusa (jellyfish), ctenophores (comb jellies) and pelagic tunicates, characterised by similarities in body design, planktonic lifestyle, and rapid numerical growth and swarming tendencies, they range from non-selective filter feeders that consume bacteria, phytoplankton and microzooplankton (e.g. salps) to passive ambush predators that consume copepods, amphipods, ostracods, molluscs, chaetognths, euphausiids, larvae, and fish eggs and larvae (e.g. Siphonophores and hydrozoan; Condon et al., 2012; Castellani & Edwards, 2017). Gelatinous organisms were more abundant North of the front compared to south of the front, which may be due to higher concentrations of chlorophyll-*a* (2-fold higher, refer to chapter 3.3.1.1) and higher abundances of crustaceans (copepods, amphipods, isopods, ANOVA, $p < 0.05$). Like gelatinous organisms, copepods are a diverse group which can be herbivorous, omnivorous or carnivorous, although most are omnivorous or carnivorous (Bode et al., 2015). Their diet ranges from phytoplankton, microzooplankton, other copepods, marine snow, and detritus and they feed by either, or both, ambush feeding (motile prey; cyclopoid and calanoid copepods) and filter-current feeding (motile and non-motie prey; calanoid copepods; Kiørboe, 2011b; Castellani & Edwards, 2017). It has recently been recognised that small copepods, particularly *Oncaea* colonise and feed on marine snow (Kiørboe, 2011b). Calanoid copepods were more abundant over the ridge and *Oncaea* copepods in the north over the ridge. However, without copepod species identification and improved understanding of species feeding habits there is a limited amount we can draw from group copepod (particularly Calanoid copepod) and gelatinous organism counts due to the wide diversity of species and traits.

Copepods primarily graze on cells > 20 µm (Calbet & Landry, 1999) and consume particles in a particular narrow size-range, approximately 18:1 of their body size (Hansen et al., 1994), followed by the most abundant particles (Kiørboe, 2008). The smallest zooplankton collected here was ~200 µm and the largest > 2000 µm which means their prey size is ~11 to 111 µm in size. Zooplankton grazing may explain the lower abundance of diatoms over the ridge compared to the basin and similarity in abundance of > 10 µm phytoplankton cell counts, as higher abundances of small (500-1000 µm) copepods were observed over the ridge (refer to section 3.3.1.4 for phytoplankton results).

As has been observed in other studies, there was no significant correlation between integrated chlorophyll-*a* concentrations and zooplankton abundance here (Roman et al., 2002; Goldthwait & Steinberg, 2008; Appendix Figure 4.1). As copepods consume protozoa (generally microzooplankton) and detritus, chlorophyll-*a* and phytoplankton are only a

fraction of the food available to them (Roman et al., 2002). In the Subtropical Convergence Zone, in the Sargasso Sea, athecate dinoflagellates and ciliates are the most important grazers of phytoplankton with grazing rates several times higher than copepods (Andersen et al., 2011). Dinoflagellates and ciliates, in turn, are the most likely prey of copepods (Andersen, Neilsen, et al., 2011). In chapter 3 we report potentially lower diatom concentrations and higher dinoflagellate concentrations in the surface waters at 10 m over the ridge. As ciliates and dinoflagellates (protozoa) have been suggested to be the most likely grazers of diatoms (Brown et al., 2008; Landry et al., 2008), the lower abundance of diatoms over the ridge may be explained by top-down control from protozoan grazing which are in turn grazed on by mesozooplankton (> 200 μm).

Another important group are nanoflagellates, a group responsible for repackaging picoplankton into larger more accessible aggregates (Vázquez-Domínguez et al., 2008; Andersen et al., 2011). It is likely that we did not count heterotrophic nanoflagellates with flow cytometry, which relies on cell fluorescence, and microscopy which doesn't preserve flagellates well or allow easy identification of trophic mode. Bacteria and nanozooplankton make up most of the heterotrophic carbon (~70%) in the photic zone of the Sargasso Sea (Roman et al., 1995). As the phytoplankton are predominantly pico- sized (< 2 μm) in the subtropical ocean it is likely that a large fraction of mesozooplankton diet is made up of heterotrophic prey (e.g. nanoflagellates, dinoflagellates and ciliates) that feed on pico- and nanophytoplankton. Lessard & Murrellt (1996) found that < 5 μm herbivorous flagellates are the most important group of herbivores in the Sargasso Sea during spring, clearing 50% of the water per day. These small herbivorous cells have similar generation times to phytoplankton so limit the picophytoplankton population. Larger herbivorous metazoans, such as copepods, have longer generation times of weeks to months, allowing large cells to bloom following nutrient injection due to lag time in growth of the predators (Acevedo-Trejos et al., 2015).

4.5 Summary

[POC] and [PN] were similar at all stations over the Mid-Atlantic ridge and the adjacent basin in the subtropical north Atlantic. However, there was enhanced zooplankton abundance, particularly calanoid copepods over the ridge and higher abundance and biomass in the 500-1000 μm size fraction. Increases in small zooplankton could reflect enhanced prey over the ridge of either phytoplankton or protozoa, the latter increasing in response to the change in phytoplankton community towards larger cells, observed in chapter 3. Lipid analysis reveals higher quantities of zooplankton biomarkers at 500 m over the ridge suggesting either enhancement of transport of material to depth or a change in vertical position and migrations of zooplankton. As seen in the phytoplankton data there is also a difference between community composition north and south of the front at ~ 31°N and inside the eddies sampled

in the northwest corner of the Ridgemix transect. Overall, our results provide evidence for modification of the zooplankton community in response to enhanced nutrient fluxes and thus phytoplankton growth over the ridge compared to the adjacent oligotrophic basin. An increase in zooplankton will likely facilitate export production via repackaging of phytoplankton cells into faecal pellets and rapid sinking of these particles, thus suggesting that regions of enhanced topography may be hot spots for export production. This needs to be tested in future studies.

4.6 References

Acevedo-Trejos, E., Brandt, G., Bruggeman, J., & Merico, A. (2015). Mechanisms shaping size structure and functional diversity of phytoplankton communities in the ocean. *Scientific Reports*, *5*(8918). https://doi.org/10.1038/srep08918

Andersen, N. G., Neilsen, G. T., Jakobsen, H. H., Munk, P., & Riemann, L. (2011). Distribution and production of plankton communities in the subtropical convergence zone of the Sargasso Sea. II. Protozooplankton and copepods. *Marine Ecology Progress Series*, *426*, 71–86. https://doi.org/10.3354/meps09001

Anderson, M. J. (2001). A new method for non-parametric multivariate analysis of variance, *26*(2001), 32–46.

Angel, M. V. (1989). Vertical profiles of pelagic communities in the vicinity of the Azores Front and their implications to deep ocean ecology. *Progress in Oceanography*, *22*(1), 1–46. https://doi.org/10.1016/0079-6611(89)90009-8

Benedetti, F., Gasparini, P., Sakina-Dorothé, A., & Ayata, E. (2016). Identifying copepod functional groups from species functional traits. *J. Plankton Res*, *38*(1), 159–166. https://doi.org/10.1093/plankt/fbv096

Bode, M., Hagen, W., Schukat, A., Teuber, L., Fonseca-Batista, D., Dehairs, F., & Auel, H. (2015). Feeding strategies of tropical and subtropical calanoid copepods throughout the eastern Atlantic Ocean - Latitudinal and bathymetric aspects. *Progress in Oceanography*, *138*, 268–282. https://doi.org/10.1016/j.pocean.2015.10.002

Brown, S. L., Landry, M. R., Selph, K. E., Yang, E. J., Rii, Y. M., & Bidigare, R. R. (2008). Diatoms in the desert: Plankton community response to a mesoscale eddy in the subtropical North Pacific. https://doi.org/10.1016/j.dsr2.2008.02.012

Brun, P., Payne, M. R., & Kiørboe, T. (2017). A trait database for marine copepods. *Earth Syst. Sci. Data*, *9*, 99–113. https://doi.org/10.5194/essd-9-99-2017

Brun, P., Vogt, M., Payne, M. R., Gruber, N., O'Brien, C. J., Buitenhuis, E. T., … Luo, Y.-W. (2015). Ecological niches of open ocean phytoplankton taxa. *Limnology and Oceanography*, *60*, 1020–1038. https://doi.org/10.1002/lno.10074

Calbet, A., & Landry, M. R. (1999). influences on the microbial food web : Direct and indirect trophic Mesozooplankton in the oligotrophic interactions open ocean. *Limnology and Oceanography*, *44*(6), 1370–1380.

Campos, C. C., Garcia, T. M., Neumann-Leitão, S., & Soares, M. O. (2017). Ecological indicators and functional groups of copepod assemblages. *Ecological Indicators*, *83*, 416–426. https://doi.org/10.1016/j.ecolind.2017.08.018

Castellani, C., & Edwards, M. (Eds.). (2017). *Marine Plankton: A Practical Guide to Ecology, Methodology, and Taxonomy* (1st ed.). Oxford: Oxford University Press.

Clark, D. R., Aazem, K. V., & Hays, G. C. (2001). Zooplankton Abundance and Community Structure Over a 4000 km Transect in the North-east Atlantic. *Journal of Plankton Research*, *23*(4), 365–372. https://doi.org/10.1093/plankt/23.4.365

Condon, R. H., Graham, W. M., Duarte, C. M., Pitt, K. A., Lucas, C. H., Haddock, S. H. D., … Madin, L. P. (2012). Questioning the Rise of Gelatinous Zooplankton in the World's Oceans. *BioScience*, *62*(2), 160–169. https://doi.org/10.1525/bio.2012.62.2.9

De La Rocha, C. L., & Passow, U. (2007). Factors influencing the sinking of POC and the efficiency of the biological carbon pump. *Deep-Sea Research Part II: Topical Studies in Oceanography*, *54*, 639–658. https://doi.org/10.1016/j.dsr2.2007.01.004

Eden, B. R., Steinberg, D. K., Goldthwait, S. A., & Mcgillicuddy, D. J. (2009). Zooplankton

community structure in a cyclonic and mode-water eddy in the Sargasso Sea. *Deep-Sea Research Part I*, *56*, 1757–1776. https://doi.org/10.1016/j.dsr.2009.05.005

Fasham, M. J., Platt, T., Irwin, B., & Jones, K. (1985). Factors Affecting the Spatial Pattern of the Deep Chlorophyll Maximnm in the Region of the Azores Front. *Progress in Oceanography*, *14*, 129–165.

Gallienne, C. P., & Robins, D. B. (2001). Is Oithona the most important copepod in the world's oceans? *Journal of Plankton Research*, *23*(12), 1421–1432. https://doi.org/10.1093/plankt/23.12.1421

Giering, S. L. C., Sanders, R., Lampitt, R. S., Anderson, T. R., Tamburini, C., Boutrif, M., … Mayor, D. J. (2014). Reconciliation of the carbon budget in the ocean's twilight zone. *Nature*, *507*. https://doi.org/10.1038/nature13123

Goldthwait, S. A., & Steinberg, D. K. (2008). Elevated biomass of mesozooplankton and enhanced fecal pellet flux in cyclonic and mode-water eddies in the Sargasso Sea. *Deep-Sea Research II*, *55*, 1360–1377. https://doi.org/10.1016/j.dsr2.2008.01.003

Gundersen, K., Orcutt, K. M., Purdie, D. A., Michaels, A. F., & Knap, A. H. (2001). Particulate organic carbon mass distribution at the Bermuda Atlantic Time-series Study (BATS) site. *Deep-Sea Research Part II: Topical Studies in Oceanography*, *48*(8–9), 1697–1718. https://doi.org/10.1016/S0967-0645(00)00156-9

Hansen, B., Bjornsen, P. K., Hansen, P. J. (1994). The size ratio between planktonic predators and their prey. *Limnology and Oceanography*, 39(2), 395-403.

Herman, A. W. (1983). Vertical distribution patterns of copepods, chlorophyll, and production in northeastern Baffin Bay. *Limnology and Oceanography*, *28*(4), 709–719. https://doi.org/10.4319/lo.1983.28.4.0709

Huskin, I., Anadon, R., Medina, G., Head, R. N., & Harris, R. P. (2001). Mesozooplankton distribution and copepod grazing in the subtropical Atlantic near the Azores: influence of mesoscale structures. *Journal of Plankton Research*, *23*(7), 671–691. https://doi.org/10.1093/plankt/23.7.671

Kiørboe, T. (2008). *A mechanistic approach to plankton ecology*. Princeton, NJ: Princeton University Press.

Kiørboe, T. (2011a). How zooplankton feed: mechanisms, traits and trade-offs. *Biological Reviews*, *86*(2), 311–339. https://doi.org/10.1111/j.1469-185X.2010.00148.x

Kiørboe, T. (2011b). What makes pelagic copepods so successful? *Journal of Plankton Research*, *33*(5), 677–685. https://doi.org/10.1093/plankt/fbq159

Kobari, T., Kitamura, M., Minowa, M., Isami, H., Akamatsu, H., Kawakami, H., … Honda, M. C. (2013). Impacts of the wintertime mesozooplankton community to downward carbon flux in the subarctic and subtropical Pacific Oceans. *Deep-Sea Research Part I: Oceanographic Research Papers*, *81*, 78–88. https://doi.org/10.1016/j.dsr.2013.07.003

Lampitt, R. S., Noji, T., & von Bodungen, B. (1990). What happens to zooplankton faecal pellets? Implications for material flux. *Marine Biology*, *104*(1), 15–23. https://doi.org/10.1007/BF01313152

Landry, M. R., Al-Mutairi, H., Selph, K. E., Christensen, S., Nunnery, S., & Landry, M. R. (2001). Seasonal patterns of mesozooplankton abundance and biomass at Station ALOHA. *Deep-Sea Research II*, *48*, 2037–2061.

Landry, M. R., Brown, S. L., Rii, Y. M., Selph, K. E., Bidigare, R. R., Yang, E. J., & Simmons, M. P. (2008). Depth-stratified phytoplankton dynamics in Cyclone Opal, a subtropical mesoscale eddy. *Deep Sea Research II*, *55*, 1348–1359. https://doi.org/10.1016/j.dsr2.2008.02.001

Lee, R. F., Hagen, W., & Kattner, G. (2006). Lipid storage in marine zooplankton. *Marine Ecology Progress Series*, *307*(1863), 273–306. https://doi.org/Doi 10.3354/Meps307273

Legendre, L., & Rivkin, R. B. (2002). Fluxes of carbon in the upper ocean: Regulation by food-web control nodes. *Marine Ecology Progress Series*, *242*, 95–109. https://doi.org/10.3354/meps242095

Lessard, E. J., & Murrellt, M. C. (1996). Distribution, abundance and size composition of heterotrophic dinoflagellates and ciliates in the Sargasso Sea near Bermuda. *DeepSea Research I*, *43*(7), 1045–1065.

Litchman, E., Ohman, M. D., & Kiørboe, T. (2013). Trait-based approaches to zooplankton communities. *J. Plankton Res*, *35*(3), 473–484. https://doi.org/10.1093/plankt/fbt019

López, E., & Anadón, R. (2008). Copepod communities along an Atlantic Meridional Transect: Abundance, size structure, and grazing rates. *Deep-Sea Research Part I: Oceanographic Research Papers*, *55*(10), 1375–1391. https://doi.org/10.1016/j.dsr.2008.05.012

Lorrain, A., Savoye, N., Chauvaud, L., Paulet, Y. M., & Naulet, N. (2003). Decarbonation and preservation method for the analysis of organic C and N contents and stable isotope ratios of low-carbonated suspended particulate material. *Analytica Chimica Acta*, *491*(2), 125–133. https://doi.org/10.1016/S0003-2670(03)00815-8

Madin, L. P., Horgan, E. F., & Steinberg, D. K. (2001). Zooplankton at the Bermuda Atlantic Time-series Study (BATS) station: diel, seasonal and interannual variation in biomass, 1994-1998. *Deep-Sea Research II*, *48*, 2063–2082.

Marañón, E., Behrenfeld, M. J., González, N., Mouriño, B., & Zubkov, M. V. (2003). High variability of primary production in oligotrophic waters of the Atlantic Ocean: Uncoupling from phytoplankton biomass and size structure. *Marine Ecology Progress Series*, *257*, 1–11. https://doi.org/10.3354/meps257001

Marañón, E., Holligan, P. M., Barciela, R., González, N., Mouriño, B., Pazó, M. J., & Varela, M. (2001). Patterns of phytoplankton size structure and productivity in contrasting open-ocean environments. *Marine Ecology Progress Series*, *216*, 43–56. https://doi.org/10.3354/meps216043

Paffenhofer, G.-A., & Mazzocchi, M. G. (2003). Vertical distribution of subtropical epiplanktonic copepods. *Journal of Plankton Research*, *25*(9), 1139–1156. https://doi.org/10.1093/plankt/25.9.1139

Parrish, C. C. (2009). Essential fatty acids in aquatic food webs. In *Lipids in Aquatic Ecosystems* (pp. 309–326). New York, NY: Springer New York. https://doi.org/10.1007/978-0-387-89366-2_13

Parrish, C. C. (2013). Lipids in Marine Ecosystems. *ISRN Oceanography*, *2013*, 1–16. https://doi.org/10.5402/2013/604045

Poulton, A. J., Sanders, R., Holligan, P. M., Stinchcombe, M. C., Adey, T. R., Brown, L., & Chamberlain, K. (2006). Phytoplankton mineralization in the tropical and subtropical Atlantic Ocean. *Global Biogeochemical Cycles*, *20*(4), 1–10. https://doi.org/10.1029/2006GB002712

Roman, M. R., Adolf, H. A., Landry, M. R., Madin, L. P., Steinberg, D. K., & Zhang, X. (2002). Estimates of oceanic mesozooplankton production: a comparison using the Bermuda and Hawaii time-series data. *Deep-Sea Research II*, *49*, 175–192.

Roman, M. R., Caron, D. A., Kremer, P., Lessard, E. J., Madin, L. P., Malone, T. C., … Youngbluth, M. J. (1995). Spatial and temporal changes in the partitioning of organic carbon in the plankton community of the Sargasso Sea off Bermuda. *Deep-Sea Research Part I*, *42*(6), 973–992. https://doi.org/10.1016/0967-0637(95)00028-5

Salter, I., Lampitt, R. S., Sanders, R., Poulton, A., Kemp, A. E. S., Boorman, B., … Pearce, R. (2007). Estimating carbon, silica and diatom export from a naturally fertilised phytoplankton bloom in the Southern Ocean using PELAGRA: A novel drifting sediment trap. *Deep-Sea Research Part II: Topical Studies in Oceanography*, *54*(18–20), 2233–2259. https://doi.org/10.1016/j.dsr2.2007.06.008

Sameoto, D., Wiebe, P., Runge, J., Postel, L., Dunn, J., Miller, C., & Coombs, S. (2000). Collecting zooplankton. In R. P. Harris, P. . Wiebe, J. Lenz, H. R. Skjoldal, & M. Huntley (Eds.), *ICES Zooplankton Methodology Manual* (pp. 55–81). San Diego: Academic Press. https://doi.org/10.1016/B978-012327645-2/50004-9

Schnack-Schiel, S. B., Mizdalski, E., & Cornils, A. (2010). Copepod abundance and species composition in the Eastern subtropical/tropical Atlantic. *Deep-Sea Research Part II: Topical Studies in Oceanography*, *57*(24–26), 2064–2075. https://doi.org/10.1016/j.dsr2.2010.09.010

Sharples, J., Moore, C. M., Hickman, A. E., Holligan, P. M., Tweddle, J. F., Palmer, M. R., & Simpson, J. H. (2009). Internal tidal mixing as a control on continental margin ecosystems. *Geophysical Research Letters*, *36*(23). https://doi.org/10.1029/2009GL040683

Steinberg, D. K., Cope, J. S., Wilson, S. E., & Kobari, T. (2008). A comparison of mesopelagic mesozooplankton community structure in the subtropical and subarctic North Pacific Ocean. *Deep-Sea Research II*, *55*, 1615–1635. https://doi.org/10.1016/j.dsr2.2008.04.025

Stone, J. P., & Steinberg, D. K. (2014). Long-term time-series study of salp population dynamics in the Sargasso Sea. *Marine Ecology Progress Series*, *510*, 111–127. https://doi.org/10.3354/meps10985

Turner, J. T. (2004). The Importance of Small Planktonic Copepods and Their Roles in Pelagic Marine Food Webs. *Zoological Studies*, *43*(2), 255–266. Retrieved from http://www.sinica.edu.tw/zool/zoolstud/43.2/255.pdf

Turner, J. T. (2015). Zooplankton fecal pellets, marine snow, phytodetritus and the ocean's biological pump. *Progress in Oceanography*, *130*, 205–248. https://doi.org/10.1016/j.pocean.2014.08.005

Turnewitsch, R., Springer, B. M., Kiriakoulakis, K., Vilas, J. C., Arístegui, J., Wolff, G., … Waniek, J. J. (2007). Determination of particulate organic carbon (POC) in seawater: The relative methodological importance of artificial gains and losses in two glass-fiber-filter-based techniques. *Marine Chemistry*, *105*(3–4), 208–228. https://doi.org/10.1016/j.marchem.2007.01.017

Vázquez-Domínguez, E., Duarte, C. M., Agustí, S., Jürgens, K., Vaqué, D., & Gasol, J. M. (2008). Microbial plankton abundance and heterotrophic activity across the Central Atlantic Ocean. *Progress in Oceanography*, *79*(1), 83–94. https://doi.org/10.1016/j.pocean.2008.08.002

Volkman, J. K. (2006). Lipid Markers for Marine Organic Matter. In J. K. Volkman (Ed.), *Marine Organic Matter: Biomarkers, Isotopes and DNA* (pp. 27–70). Berlin/Heidelberg: Springer-Verlag. https://doi.org/10.1007/698_2_002

Volkman, J. K., Jeffrey, S. W., Nichols, P. D., Rogers, G. I., & Garland, C. D. (1989). Fatty acid and lipid composition of 10 species of microalgae used in mariculture. *Journal of Experimental Marine Biology and Ecology*, *128*(3), 219–240. https://doi.org/10.1016/0022-0981(89)90029-4

Wakeham, S. G., Hedge, J. I., Lee, C., Peterson, M. L., & Hernest, P. J. (1997). Compositions and transport of lipid biomarkers through the water column and surficial sediments of the equatorial Pacific Ocean. *Deep Sea Research Part II: Topical Studies in OceanographySea Research*, *44*, 2131–2162.

Woodd-Walker, R. S. (2001). Spatial distributions of copepod genera along the Atlantic Meridional Transect. *Hydrobiologia*, *453/454*, 161–170.

Wubet, T., Christ, S., Schö Ning, I., Boch, S., Gawlich, M., Schnabel, B., … Buscot, F. (2012). Differences in Soil Fungal Communities between European Beech (Fagus sylvatica L.) Dominated Forests Are Related to Soil and Understory Vegetation. *PLoS ONE*, *7*(10), 1–14. https://doi.org/10.1371/journal.pone.0047500

5 Synthesis

In this study I set out to determine whether the Mid-Atlantic Ridge affects plankton dynamics in the subtropical North Atlantic and whether three commonly used marine particle collection techniques collect the same pool of particles. To conclude I shall outline the hypotheses and major findings presented in each chapter, discuss the wider implications of results and suggest areas for future research.

5.1 Summary of key findings

In Chapter 2, three marine particle collection techniques were compared: Niskin bottles, the Marine Snow Catcher (MSC), and Stand Alone Pump (SAP), to examine whether they collect the same quantity and composition of particles. Samples were collected from the oligotrophic subtropical North Atlantic (RidgeMix, JR15007) and the Celtic Shelf Sea (DY026, DY029, DY033). I conclude that the three techniques do not collect entirely the same particles. Both the quantity and composition of particles varied between techniques while the composition of particles in the Celtic Sea varied with technique and physical conditions at each station.

In Chapter 3 the controls of phytoplankton distribution in the subtropical North Atlantic (RidgeMix, JR15007) and the influence of ocean ridges on the phytoplankton community were assessed. This section set out to determine the effects on the phytoplankton community of an order of magnitude higher diapycnal nitrate flux into the base of the DCM, due to enhanced turbulent mixing and a steeper nitrate gradient, over the Mid-Atlantic Ridge compared to the adjacent basin (Tuerena et al., submitted; Vic et al., 2018). I hypothesised that an increased nitrate flux over the ridge would enhance local phytoplankton abundance and shift the community towards larger cells, such as diatoms. Higher concentrations of chlorophyll-*a* in the two larger phytoplankton size-fractions (2-20 µm and > 20 µm) and enhanced abundances of picoeukaryotes (~2.9 µm) and nanoeukaryotes (~4.6 µm) were observed over the ridge, but there was no difference in > 10 µm phytoplankton microscopy counts compared to over the basin. Therefore, we can partially accept the hypothesis; whilst there were no significant differences in phytoplankton abundance and diatom concentrations over the ridge there were higher concentrations of larger cells. Similar observations were made comparing the open ocean and the Celtic Shelf Sea; higher mixing over the shelf increased the abundance of smaller picoeukaryotes compared to the open ocean, but not larger phytoplankton cells such as diatoms as observed at the shelf edge, due to the lower degree of mixing on-shelf (Sharples et al., 2009). This is a novel finding that suggests ocean ridges impact phytoplankton communities via ridge-enhanced nitrate fluxes resulting in a response similar to that seen on-shelf in the Celtic Sea. This has large implications for the cycling and export of carbon in regions over ocean ridges, where a shift towards larger cells and potentially higher growth

rates will increase the abundance of zooplankton and enhance fish productivity, and ultimately enhance carbon export (Legendre & Rivkin, 2002; Sharples et al., 2009; Siegel et al., 2014). Over the ridge, the decoupling observed between phytoplankton abundance and cell size is likely due to the interaction of bottom-up and top-down controls on the phytoplankton community. We postulate that, higher nitrate fluxes enhance the rate of primary production and increase the abundance of larger celled species (e.g. picoeukaryotes and diatoms) but enhanced zooplankton productivity limits phytoplankton abundance through increased grazing pressure (Margalef, 1978; Legendre & Rivkin, 2002; Sharples et al., 2009; see Chapter 4).

Higher abundances of phytoplankton were also observed to the north of 31°N, associated with the Azores current, its eddies, and the transition of oligotrophic gyre waters to temperate waters. Comparison of phytoplankton abundances between October and June over the Mid-Atlantic Ridge saw seasonality in phytoplankton abundance and composition, thought to be due to variation in Azores current flow (the edge of the subtropical gyre).

In Chapter 4, the hypothesis that the changes in phytoplankton communities reported in Chapter 3 would influence POM and zooplankton quantity and composition over the ridge was tested. Hence, the larger cells over the ridge would increase the standing stock of organic material and the abundance of large zooplankton that graze on them (Legendre & Rivkin, 2002). Concentrations of POC (and PN) were similar over the ridge and basin but there were higher zooplankton abundances over the ridge, particularly of small (500-1000 μm) calanoid copepods. In support of this finding, there was also a higher signal for zooplankton wax esters (lipid storage compounds) at 500 m over the ridge. Enhanced abundance of zooplankton over the ridge has implications for increased carbon export through rapidly sinking faecal pellets and diurnal migration of zooplankton (Lampitt et al., 1990; Kobari et al., 2013; Turner, 2015). The lack of change in the standing stock of POM over the ridge is likely due to both limitation of phytoplankton abundance by zooplankton grazing and zooplankton grazing on aggregates (Roman, 1984; Legendre & Rivkin, 2002). Similarly to the phytoplankton, there were higher abundances of particulate organic material and zooplankton to the north of 31°N and associated with the Azores current and eddies.

5.2 Wider implications, limitations and future directions

The subtropical oligotrophic ocean is viewed as an area of low primary production which is supported by regenerated nutrients (Azam et al., 1983; Azam & Malfatti, 2007; Longhurst, 2010). The results presented in this study suggest that the subtropical oligotrophic ocean is not as homogeneous as previously thought. Firstly, the northern edge of the subtropical North Atlantic gyre exhibits seasonal differences and strong eddy mixing which both influence

plankton composition and biomass. Secondly, there appears to be a "ridge effect", where enhanced vertical turbulent mixing and nitrate fluxes over the Mid-Atlantic ridge shift the community towards larger phytoplankton cells and higher abundances of zooplankton. This shift in plankton community may lead to a change in how carbon is cycled and the magnitude of carbon export from surface waters over the ridge compared to the adjacent basin, where larger ungrazed cells have been suggested to determine the magnitude of POC export to the ocean interior (Boyd & Newton, 1999). It is possible that increased particle flux and change in quality will influence the benthic community at and near to areas of abrupt topography (Turnewitsch et al., 2016). Carbon export flux and cycling were not quantified in this study and are an area for further research. The shift in plankton community over the ridge may also drive changes in higher trophic levels in the pelagic ocean; around seamounts predator diversity is known to peak and species of tuna and shark have been observed to catch more fish (Worm et al., 2003; Morato et al., 2010).

The wider implications of a ridge 'effect' (a shift in the phytoplankton community towards larger cells, a higher abundance of zooplankton and a potential change in carbon export) on the ocean are large due to vast spatial extent of both the subtropical oceans, which make up 60% of the global ocean (Emerson et al., 1997), and the global occurrence of mid-ocean ridges in all of these regions. A "ridge effect" is thought to be particularly significant in the subtropical oceans due to the limited nutrient supply to these regions (Williams & Follows, 1998). In the subtropical ocean, phytoplankton carbon fixation drives about half of the ocean's biological removal of carbon from the atmosphere (5-6 Gt C yr^{-1} of 10-11 Gt C yr^{-1}; Emerson et al., 1997; Sanders et al., 2014) but with the inclusion of a ridge effect, this value may be higher. The findings of the current study highlight the importance of considering bottom topography in studies of plankton and carbon cycling as well as joint consideration of bottom-up and top-down control on communities. However, the limitations of the cruise track must be considered, namely that sampling only occurred over the ridge and to the west of the ridge over the adjacent basin, and the northern waters were influenced by the Azores current and its eddies. To ascertain the ridge effect in this location, it is recommended that further study occur on multiple transects over the ridge to create a 3D picture of the local plankton community along with analysis of ocean current flow, water masses and nitrate fluxes.

This study unveils the tip of the iceberg on the effect of ocean ridges on plankton dynamics. Further studies of high spatial resolution (both horizontally and vertically) of the plankton community are required for a full understanding of the influence of the MAR on plankton dynamics. Future research of plankton (phytoplankton and zooplankton) composition at the species level and the influence of heterotrophy should be undertaken and analysis of microzooplankton, nanoflagellates and hetertrophic bacteria should be considered, given that the microbial loop is of high importance in subtropical oceans (Vázquez-Domínguez et al.,

2008). It is suggested that further study is undertaken where, in addition to community abundance, species composition and size distribution analysed in the present study, primary production and phytoplankton growth rates also be considered to help determine whether there is a change in cycling and uptake of carbon. It is also suggested that trophic interactions be quantified to help elucidate any ecosystem changes that may result from a change in phytoplankton species composition due to increased nutrients over the ridge compared to the adjacent basin. There is also a need for a better spatial and temporal understanding of plankton community dynamics in the oligotrophic ocean (species composition, interactions, variability), before we can accurately understand the biological structure of plankton change over ocean ridges in these regions.

The study of particle collection techniques here builds upon previous research into the substantial differences in particle quantity collected by SAPs and Niskin bottles. The additional comparison of lipid composition in this study and the inclusion of the MSC highlights that not only do techniques collect different quantities of particles, but the particles have hugely varying compositions, depending on physical conditions. The consequences for our understanding of the ocean could potentially be large considering we don't understand how or why the techniques vary in the particle pool they collect. Therefore, we do not know which technique, if any, is most representative of water column particle concentration and therefore whether, for example, carbon export fluxes are accurate. The differences observed between techniques highlight the need to consider how representative the sampling methods are and to be conservative when extrapolating regional results from a specific physical regime to the global scale. There is a need to identify which fraction of the particle pool each technique collects, for more information on how this pool varies with physical conditions, and a call for development of new techniques that do not alter water column particle composition upon collection.

5.3 References

Azam, F., Fenchel, T., Field, J., Gray, J., Meyer-Reil, L., & Thingstad, F. (1983). The Ecological Role of Water-Column Microbes in the Sea. *Marine Ecology Progress Series*, *10*, 257–263. https://doi.org/10.3354/meps010257

Azam, F., & Malfatti, F. (2007). Microbial structuring of marine ecosystems. *Nature Reviews: Microbiology*, *5*, 782–791. https://doi.org/10.1038/nrmicro1747

Boyd, P. W., & Newton, P. P. (1999). Does planktonic community structure determine downward particulate organic carbon flux in different oceanic provinces? *Deep-Sea Research Part I: Oceanographic Research Papers*, *46*(1), 63–91. https://doi.org/10.1016/S0967-0637(98)00066-1

Emerson, S., Quay, P., Karl, D., Winn, C., & Tupas, L. (1997). Experimental determination of the organic carbon flux from open-ocean surface waters. *Nature*, *389*, 951–954.

Kobari, T., Kitamura, M., Minowa, M., Isami, H., Akamatsu, H., Kawakami, H., … Honda, M. C. (2013). Impacts of the wintertime mesozooplankton community to downward carbon flux in the subarctic and subtropical Pacific Oceans. *Deep-Sea Research Part I: Oceanographic Research Papers*, *81*, 78–88. https://doi.org/10.1016/j.dsr.2013.07.003

Lampitt, R. S., Noji, T., & von Bodungen, B. (1990). What happens to zooplankton faecal pellets? Implications for material flux. *Marine Biology*, *104*(1), 15–23. https://doi.org/10.1007/BF01313152

Legendre, L., & Rivkin, R. B. (2002). Fluxes of carbon in the upper ocean: Regulation by food-web control nodes. *Marine Ecology Progress Series*, *242*, 95–109. https://doi.org/10.3354/meps242095

Longhurst, A. R. (2010). The Atlantic Ocean. In *Ecological Geography of the Sea* (2nd ed., pp. 131–274). California, USA: Elsevier Academic Press.

Margalef, R. (1978). Life-forms of phytoplankton as survival alternatives in an unstable environment. *Oceanologica Acta*, *1*, 493–509. https://doi.org/10.1007/BF00202661

Morato, T., Hoyle, S. D., Allain, V., & Nicol, S. J. (2010). Seamounts are hotspots of pelagic biodiversity in the open ocean. *PNAS*, *107*(21), 9707–9711. https://doi.org/10.1073/pnas.0910290107

Roman, M. R. (1984). Ingestion of detritus and microheterotrophs by pelagic marine zooplankton. *Bulletin of Marine Science*, *35*(3), 477–494.

Sanders, R., Henson, S. a., Koski, M., De La Rocha, C. L., Painter, S. C., Poulton, A. J., … Martin, A. P. (2014). The Biological Carbon Pump in the North Atlantic. *Progress in Oceanography*, *129*, 200–218. https://doi.org/10.1016/j.pocean.2014.05.005

Sharples, J., Moore, C. M., Hickman, A. E., Holligan, P. M., Tweddle, J. F., Palmer, M. R., & Simpson, J. H. (2009). Internal tidal mixing as a control on continental margin ecosystems. *Geophysical Research Letters*, *36*(23). https://doi.org/10.1029/2009GL040683

Siegel, D. A., Buesseler, K. O., Doney, S. C., Sailley, S. F., Behrenfeld, M. J., & Boyd, P. W. (2014). Global assessment of ocean carbon export by combining satellite observations and food-web models. *Global Biogeochemical Cycles*, *28*, 181–196. https://doi.org/10.1002/2013GB004743.Received

Tuerena, R. E., Williams, R. G., Mahaffey, C., Green, J. A. M., Vic, C., Naveira-Garabato, A., … Sharples, J. (n.d.). Internal tides drive nutrient fluxes into the deep chlorophyll maximum over mid-ocean ridges.

Turner, J. T. (2015). Zooplankton fecal pellets, marine snow, phytodetritus and the ocean's biological pump. *Progress in Oceanography*, *130*, 205–248.

https://doi.org/10.1016/j.pocean.2014.08.005

Turnewitsch, R., Dumont, M., Kiriakoulakis, K., Legg, S., Mohn, C., Peine, F., & Wolff, G. (2016). Tidal influence on particulate organic carbon export fluxes around a tall seamount. *Progress in Oceanography*, *149*, 189–213. https://doi.org/10.1016/j.pocean.2016.10.009

Vázquez-Domínguez, E., Duarte, C. M., Agustí, S., Jürgens, K., Vaqué, D., & Gasol, J. M. (2008). Microbial plankton abundance and heterotrophic activity across the Central Atlantic Ocean. *Progress in Oceanography*, *79*(1), 83–94. https://doi.org/10.1016/j.pocean.2008.08.002

Vic, C., Naveira Garabato, A. C., Green, J. A. M., Spingys, C., Forryan, A., Zhao, Z., … Sharples, J. (2018). The Lifecycle of Semidiurnal Internal Tides over the Northern Mid-Atlantic Ridge. *Journal of Physical Oceanography*, *48*(1), 61–80. https://doi.org/10.1175/JPO-D-17-0121.1

Williams, R. G., & Follows, M. J. (1998). *The Ekman transfer of nutrients and maintenance of new production over the North Atlantic*. *Deep-Sea Research I* (Vol. 45). Retrieved from http://citeseerx.ist.psu.edu/viewdoc/download?doi=10.1.1.538.8325&rep=rep1&type=pdf

Worm, B., Lotze, H. K., & Myers, R. A. (2003). Predator diversity hotspots in the blue ocean. *Proceedings of the National Academy of Sciences*, *100*(17), 9884–9888. https://doi.org/10.1073/pnas.1333941100

6 Appendix

Appendix 1

Table 1.1 RidgeMix station location, identifier and sampling activity. Physical properties (e.g. temperature, salinity, fluorescence, PAR) from sensors and nutrient sampling from Niskin bottles on the CTD rosette (CTD), phytoplankton sampling from Niskin bottles on the CTD rosette (phyto), zooplankton vertical net tows (zoop), and Stand Alone Pump deployment (SAPs).

CTD	Station	Latitude decimal°	Longitude decimal°	Date	Time (GMT)	Activity	Notes
2	N1	36.246967	-40.007267	03/06/2016	05:13	CTD Phyto	
3	N2	36.247	-39.007	03/06/2016	15:08	CTD	
4	N3	36.247	-37.996733	04/06/2016	00:56	CTD Phyto	
5	N4	36.247	-37.005	04/06/2016	09:30	CTD	
6	N5	36.24155	-35.99225	04/06/2016	17:21	CTD Phyto	
7	N6	36.247	-34.997	04/06/2016	23:23	CTD	
8	N7	36.230	-33.902	05/06/2016	07:29	CTD	
9	R1	36.221367	-32.762917	05/06/2015	23;16	CTD Phyto Zoop	Ridge Mooring super station
10	R1	36.114233	-32.950033	07/06/2016	09:17	CTD Phyto Zoop SAPs	Ridge Mooring super station
11	R2	35.677	-34.116	08/06/2016	02:30	CTD	
12	R3	35.275717	-35.042183	08/06/2016	08:56	CTD Phyto	Ridge
13	R4	34.85195	-36.044167	08/06/2016	16:15	CTD Phyto	Ridge
14	R5	34.450017	-37.013533	09/06/2016	02:00	Zoop SAPs	Ridge
15	R5	34.450017	-37.013533	09/06/2016	07:11	CTD Phyto	Ridge
16	R6	34.000	-38.000	09/06/2016	14:00	CTD	Ridge
17	R7	33.440983	-38.632583	09/06/2016	21:14	CTD Phyto	Ridge
18	R8	32.717	-39.411	10/06/2016	05:30	CTD	Ridge
19	R9	31.991	-40.271	10/06/2016	12:55	CTD	Ridge
20	R10	31.33565	-40.998667	10/06/2016	20:35	CTD Phyto Zoop SAPs	Ridge
21	R11	30.668	-41.752	11/06/2016	11:20	CTD	Ridge
22	R12	30.125017	-42.117783	11/06/2016	16:31	CTD Phyto	Ridge
23	R12a	30.125017	-42.117783	11/06/2016	22:45	CTD	Ridge
24	R13	29.169683	-43.172533	12/04/2016	05:48	CTD Phyto	Ridge
25	R14	28.517	-43.347	12/06/2016	13:25	CTD	Ridge
26	R15	27.93015	-43.708417	12/06/2016	19:20	CTD Phyto Zoop SAPs	Ridge
27	R17	27.038	-44.218	13/06/2016	09:30	CTD	Ridge
28	R19	26.136933	-44.826883	13/06/2016	21:35	CTD Phyto	Ridge
29	R21	25.280	-45.240	14/06/2016	06:15	CTD	Ridge
30	R22a	24.640	-45.620	14/06/2016	14:25	CTD	Ridge
31	R 24	24.000067	-45.999717	14/06/2016	21:07	CTD Phyto Zoop SAPs	Ridge
32	R24	24.000067	-45.999717	14/06/2016	21:52	CTD	
34	S6	24.487633	-46.93945	15/06/2016	12:55	CTD	

						Phyto	
35	S6	24.487633	-46.93945	15/06/2016	12:55	CTD	
36	S4	24.963117	-47.907933	16/06/2016	00:12	CTD Phyto	
37	S4	24.96934	-47.90446	16/06/2016	02:20	CTD	
38	S2	25.446767	-48.86545	16/06/2016	12:28	CTD Phyto	
39	S2	25.446767	-48.86545	16/06/2016	12:12	CTD Phyto	
40	D18	26.00075	-50.001233	17/06/2016	00:08	CTD Phyto Zoop SAPs	Basin
41	D18	25.99582	-50.00146	17/06/2016	05:40	CTD	Basin
42	D16	26.99978	-49.999349	17/06/2016	17:00	CTD	
43	D14	27.99645	-49.9954	18/06/2016	00:34	CTD Phyto	Basin
44	D13	29.0006	-49.999829	18/06/2016	10:25	CTD	Basin
45	D12	32.48664	-47.82664	18/06/2016	18:18	CTD	
46	D11	29.99815	-49.9918	18/06/2016	18:01	CTD Phyto Zoop SAPs	Basin
47	D10	30.830	-49.298	19/06/2018	10:20	CTD	Basin
48	D9	31.665717	-48.545883	19/06/2016	18:22	CTD Phyto	Basin
49	D8	32.48664	-47.82664	20/06/2016	04:35	CTD	Basin
50	D7	33.264567	-47.142283	20/06/2016	13:35	CTD	Basin
51	D7	33.264567	-47.142283	20/06/2016	22:07	CTD Phyto Zoop SAPs	Basin
52	D6	34.000	-46.490	21/06/2016	09:58	CTD	Basin
53	D5	34.5547	-45.54665	21/06/2016	17:26	CTD Phyto	Basin
54	D4	35.235	-44.418	22/06/2016	04:39	CTD	Basin
55	D3	36.0046	-43.267483	22/06/2016	13:29	CTD Phyto	Basin
56	D3	36.000717	-43.262567	23/06/2016	21:41	CTD Phyto Zoop SAPs	Basin Open Ocean super station
57	D2	36.261	-42.264	24/06/2016	11:18	CTD	
58	N1a	36.247567	-40.675383	24/06/2016	23:01	CTD Phyto	
59	N2a	36.243383	-39.115533	26/06/2016	04:20	CTD Phyto	
60	N3a	36.2505	-37.506983	26/06/2016	15:53	CTD Phyto	
61	N4a	36.24345	-35.924617	27/06/2016	03:37	CTD Phyto	
62	N5a	36.235367	-34.344583	27/06/2016	14:37	CTD Phyto	
63	N5a	36.235367	-34.344583	27/06/2016	20:55	CTD	
64	R1	36.218567	-32.7099	28/06/2016	01:27	CTD	
65	R1	36.218567	-32.7099	28/06/2016	20:10	CTD Phyto	
66	R1	36.225983	-32.710167	28/06/2016	23:45	CTD Phyto Zoop SAPs	Ridge Mooring Super-station
67	R1	36.244067	-32.777133	01/07/2016	09:59	CTD Phyto Zoop SAPs	Ridge Mooring Super-station

Appendix 2

Table 2.1 RidgeMix in-situ pump (SAP) and Niskin bottle particulate organic carbon (POC), particulate nitrogen (PN) and carbon:nitrogen ratio (C:N) results. Samples were collected from the chlorophyll-a maximum, 100 m below and 500 m. Stations 10, 56 and 66 also had a surface sample at 15 m. tSAPs is the sum of the two SAPs size-fractions. The smaller size-fraction of the SAPs has a "blank" (bottom filter) subtracted from it.

Station	Depth	POC (x 10^{-3} µM)				PN (x 10^{-3} µM)				C:N	
		0.7-53 µm SAPS – Blank	>53 µm SAPS	tSAPS	CTD	0.7-53 µm SAPS – Blank	>53 µm SAPS	tSAPS	CTD	SAPS	CTD
10	15	354	14	368	441	44	2	46	81	8.0	5.4
	60	2535	169	2704	3292	403	28	431	619	6.3	5.3
	160	311	36	346	1087	53	8	61	204	5.7	5.3
	500	94	23	117	778	19	4	23	172	5.0	4.5
13	75	2719	16	2735	3202	359	2	361	799	7.5	4.5
	175	333	3	337	1771	56	1	57	297	5.7	4.0
	500	97	3	100	965	26	1	26	166	3.9	6.0
20	85	2166	239	2404	2745	320	61	381	587	6.3	4.7
	185	447	63	510	1806	59	25	85	224	6.0	8.0
	500	208	27	234	1148	27	20	47	201	5.0	5.7
26	130	1617	9	1626	2708	238	18	256	442	6.7	6.1
	230	246	3	249	1586	54	9	62	289	4.5	5.5
	500	105	2	107	1127	25	7	31	220	4.2	5.1
31	150	94	78	172	2721	157	12	169	286	7.1	9.5
	250	16	31	47	1532	24	7	31	214	7.2	7.2
	500	9	24	33	1099	24	8	31	128	4.4	8.6
40	160	949	8	958	2584	155	17	172	498	6.1	5.2
	260	165	3	169	1605	25	8	33	337	6.2	4.8
	500	45	3	48	1735	13	7	19	396	4.3	4.4
46	140	1365	12	1377	2341	184	2	185	428	7.3	5.5
	240	187	4	191	1957	41	1	41	331	4.8	5.9
	500	52	2	54	1081	3	0	2	186	28.1	5.8
51	90	2285	243	2528	3000	333	79	411	663	6.1	4.5
	190	332	80	412	1676	49	31	80	341	5.1	4.9
	500	204	54	259	1243	68	40	108	237	2.4	5.2
56	15	5650	1289	6940	6543	540	179	719	868	9.7	7.5
	75	2619	230	2849	3898	416	41	456	721	6.2	5.4
	175	272	66	338	1787	46	11	57	216	5.9	8.3
	500	224	55	279	1134	32	14	47	129	6.0	8.8
66	15	188	157	345	2759	309	25	333	474	7.2	5.8
	100	171	110	281	2295	371	18	389	470	5.6	4.9
	200	22	66	88	1636	61	14	76	239	4.3	6.9
	500	11	39	50	1740	57	13	70	275	2.4	6.3

Table 2.2 For lipid concentrations during DY026 in the Celtic Sea see attached electronic appendix.

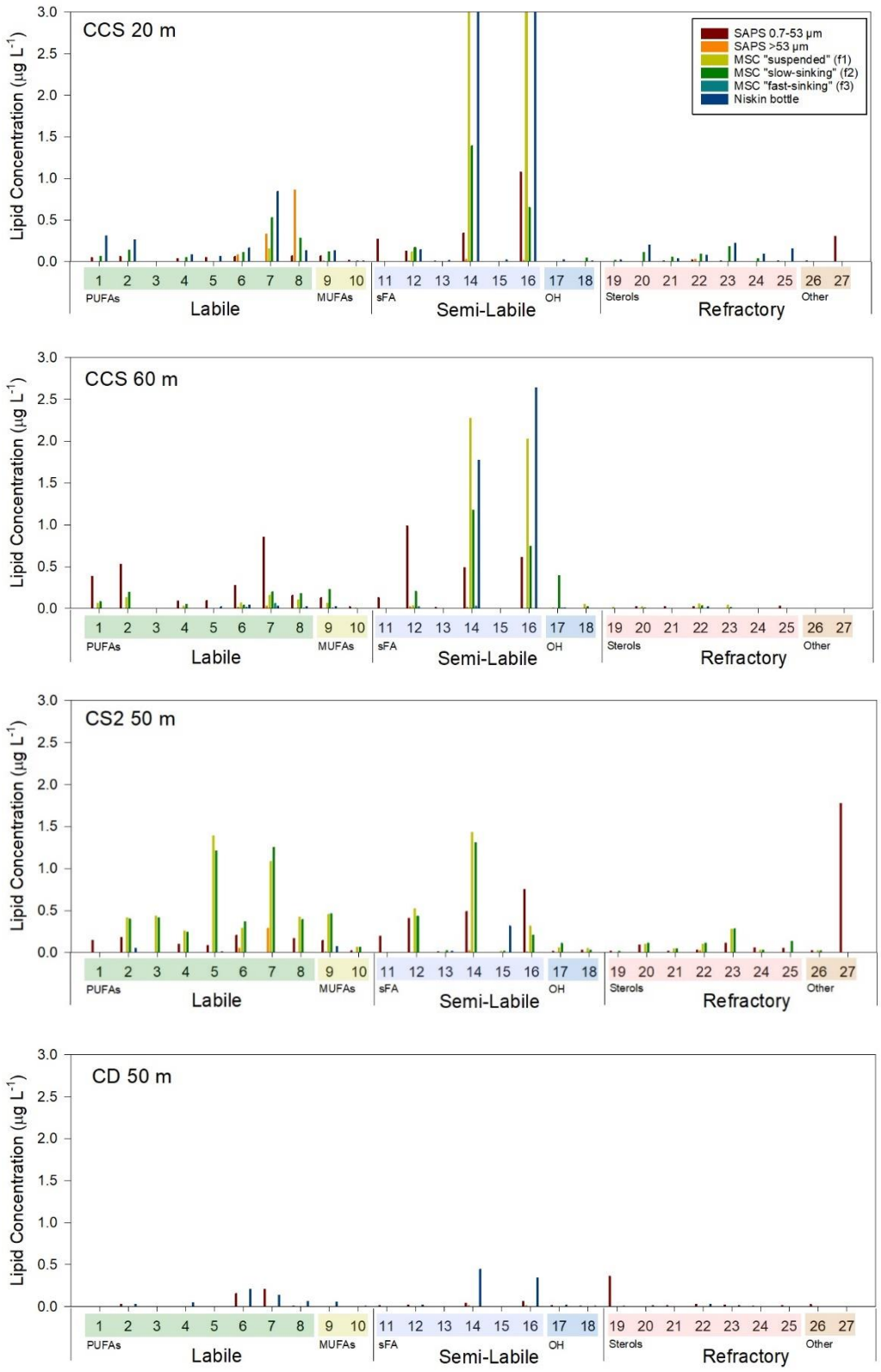

Figure 2.1 The most abundant biomarkers in each technique for each of the four stations during DY026 in the CelticSea. The lipids are split into labile, semi-labile and refractory and within those groups polyunsaturated fatty acids (PUFAs), monounsaturated fatty acids (MUFAs), saturated fatty acids (sFA), alcohols (OH), sterols and other. The numbers correspond to specific biomarkers. (1) 18:5ω3. (2) 18:4ω3. (3) 18:3ω6. (4) 18:2ω6. (5) 18:3ω3. (6) 20:5ω3. (7) 22:6ω3. (8) 16:1w7. (9) 18:1(cis-9). (10) 18:1(tr-9). (11) C12. (12) C14. (13) C15. (14) C16. (15) C17. (16) C18. (17) 16-OH. (18) 18-OH. (19) $C_{26\Delta5,22}$. (20) $C_{27\Delta5,22}$. (21) $C_{27\Delta5,22}$. (22) $C_{27\Delta5,}$ Cholesterol. (23) $C_{28\Delta5,22}$, Brassicasterol. (24) $C_{29\Delta5,22E}$, Stigmasterol. (25) β-sitosterol trimethyl ether. (26) Phytodiene isomer. (27) Unknown compound. In CCS 20 m, MSC susp is 14 ng L^{-1} for C_{16} and 14.2 for C_{18}, and for MSC fast is 10.8 ng L^{-1} for C_{16} and 13.6 ng L^{-1} for C_{18}.

Table 2.3 List of common key lipids in samples their alternative notations, IUPAC and common names (if applicable).

Key Lipids	Alternative notation	IUPAC name	Common Name
C_{12} FAME		Dodecanoic acid	Lauric acid
C_{14} FAME		Tetradecanoic acid	Myristic acid
C_{15} FAME		Pentadecanoic acid	
C_{16} FAME		Hexadecanoic acid	Palmitic acid
C_{18} FAME		Octadecanoic acid	Stearic acid
$C_{16:1\omega7}$	$C_{16:1(n-7)}$ or $C_{16:1(cis-9)}$	(Z)-hexadec-9-enoic acid	Palmitoleic acid
$C_{18:4\omega3}$	$C_{18:4(n-3)}$ or $C_{18:4(cis-6)}$	(6Z,9Z,12Z,15Z)-octadec-6,9,12,15-tetraenoic acid	Stearidonic acid (SDA)
$C_{18:3\omega6}$	$C_{18:3(n-6)}$ or $C_{18:3(cis-6)}$	(6Z,9Z,12Z)-octadec-6,9,12-trienoic acid	*Gamma*-linolenic acid (GLA)
$C_{18:2\omega6}$	$C_{18:2(n-6)}$ or $C_{18:2(cis-9)}$	(9Z,12Z)-octadec-9,12-dienoic acid	Linoleic acid
$C_{18:3\omega3}$	$C_{18:3(n-3)}$ or $C_{18:3(cis-9)}$	(9Z,12Z,15Z)-octadec-9,12,15-trienoic acid	*Alpha*-linolenic acid (ALA)
$C_{18:1\omega9}$	$C_{18:1(n-9)}$ or $C_{18:1(cis-9)}$	(Z)-octadec-9-enoic acid	Oleic acid
$C_{18:1\omega9}$	$C_{18:1(n-9)}$ or $C_{18:1(trans-9)}$	(E)-octadec-9-enoic acid	Elaidic acid
$C_{20:5\omega3}$	$C_{20:5(n-3)}$ or $C_{20:5(cis-8)}$	(5Z,8Z,11Z,14Z,17Z)-icosa-5,8,11,14,17-pentaenoic acid	Eicosapentarnoic acid (EPA)
$C_{22:6\omega3}$	$C_{22:6(n-3)}$ or $C_{22:6(cis-9)}$	(4Z,7Z,10Z,13Z,16Z,19Z)-docosa-4,7,10,13,16,19-hexaenoic acid	Docosahexaenoic acid (DHA)
$C_{16\text{-}OH}$		1-Hexadecanol	
$C_{18\text{-}OH}$		1-Octadecanol	
$C_{26\Delta5,22}$		26-norcholesta-5,22-dien-3β-ol	
$C_{27\Delta5,22}$		Cholesta-5,22(E)-dien-3β-ol	Cholesta-5,22E-3β-ol
$C_{27\Delta5,22}$		Cholesta-5,22(Z)-dien-3β-ol	Cholesta-5,22Z-3β-ol
$C_{27\Delta5}$		Cholest-5-en-3β-ol	Cholesterol
$C_{28\Delta5,22}$		24-methylcholesta-5,22-dien-3β-ol	Brassicasterol
$C_{29\Delta5,22}$		24-ethylcholesta-5,22-dien-3β-ol	Stigmasterol

Appendix 3

Table 3.1 Replication of size-fractionated chlorophyll-a results. AMT25 shows replicate Niskin bottles at 130 m (n = 2). RidgeMix shows replicate samples from the same Niskin bottle (n = 3).

Cruise	Depth	Total chlorophyll-a (mg m^{-3})	> 20 µm (mg m^{-3})	2-20 µm (mg m^{-3})	0.2-2 µm (mg m^{-3})
AMT25 CTD 17	130 m	0.19 ± 0.08	0.005 ± 0.003	0.03 ± 0.008	0.16 ± 0.07
	CV (%)	41	70	31	44
RidgeMix CTD 66	10 m	0.09 ± 0.01	0.008 ± 0.002	0.01 ± 0.002	0.04 ± 0.01
	CV (%)	13	37	5	33
	102 m	0.7 ± 0.03	0.03 ± 0.001	0.1 ± 0.03	0.5 ± 0.007
	CV (%)	5	4	25	1
	300 m	0.01 ± 0.003	0.002 ± 0.0007	0.007 ± 0.001	0.003 ± 0.0005
	CV (%)	22	35	20	19

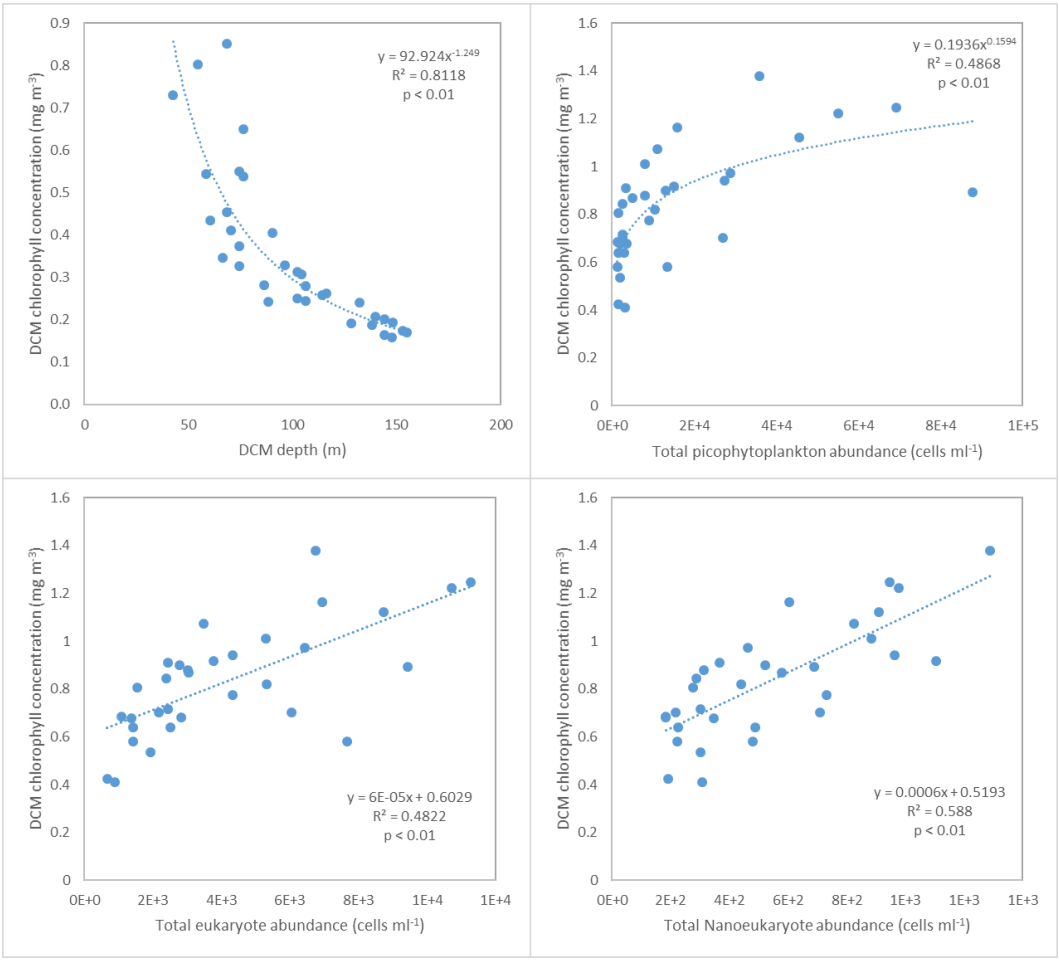

Figure 3.2 Correlations between DCM depth, DCM concentration and picophytoplankton abundance at the DCM.

Table 3.2 Phytoplankton > 10 µm (cells L^{-1}). Phytoplankton identified to genus level. Unidentifiable species were grouped by size and group (10-20 µm and > 20 µm diatom, dinoflagellate, flagellate and unknown). Five pennate diatoms species were unidentifiable but labelled by distinct physical characteristics i.e. sticks.

	10 m									DCM								
CTD	66	10	20	22	28	40	46	48	56	66	10	20	22	28	40	46	48	56
Centric diatoms																		
Asteromphalus spp.		1					19		1	1								
Bacteriastrum spp.																	1	
Chaetoceros spp.	1	17	2		1	6			2432	1	99	14	1	29	13	2	3	29
Corethron spp.								2		1	2	1	1			1		
Guinardia spp.									255									1
Hemiaulus spp.		1	21	1	1	13	29	55	634	2	1						1	24
Leptocylindrus spp.		43					1		16715	2	4	3	1	11	10			186
Planktoniella spp.										2	5	1		1	2	2		2
Proboscia spp.		26							87	1	7			1		1		9
Rhizosolenia spp.	2	9	6				1	9	36	1	5		1	1	4	5		13
Roperia spp.													1			1		
Thalassiosira spp.																1	1	
Round unknown spp.	5	72	4	1		2		3	2	100	164	173	13	17	19	9	21	215
Pennate diatoms																		
Asteroplanus spp.							4			10			5	1	10	9		1
Asterionellopsis spp.																2		
Bacillaria spp.													1			2		
Cylindrotheca spp.		1										2	3				11	
Pseudo-nitzschia spp.		1	1			1			2432	11	30		10		4	12	16	151
Thalassionema spp.													3			6		31
Sticks sp.	53	15	108	73	108	58	544	564	279	87	41	61	19	155	81	6	107	34
2 sticks sp.					1			1		10	12	8	1	4	66	21	5	11
*Triangle*2 sp.*					1			1		17	11	5		8	42	66	8	3
*Triangle*2 w sticks sp.*		5							56	9	4					3	8	
Long bow shaped diatom sp.		34								3	7							
Dinoflagellates																		
Akashiwo spp.			1	1		3		13									13	
Alexandrium spp.				32				7										
Amphidinium spp.	21	86	41	21	9	7	1	12	238	7	1	21	3	5	6	3		
Amphisolenia spp.		1		3									1		2	1	1	1
Ceratium spp.	20	13	21	19	15	23	20	19	21	3	3	6	1	1	1	1	8	8
Cladopyxis spp.	3		3	1				1	1						1			
Corythodinium spp.													1					
Dictyocha spp.			7	1						1	3	139	36	10	16	12	1	10
Gonyaulax spp.	1	5	2	4	4	9	1	1				1				2	1	
Gymnodinium spp.			13	17	1		42	3								4	1	
Heterocapsa spp.	115	65	489	222	115	108	114	108	197	22	9	16	9	13	10	13	19	3
Histioneis spp.	2	2	2	4	1	2			1	1		3	1	2	1			

	10 m									DCM								
CTD	66	10	20	22	28	40	46	48	56	66	10	20	22	28	40	46	48	56
Dinoflagellates continued…																		
Karenia spp.	16			3				3						3				
Mesoporos spp.			9				9	25						4			9	
Ornithocercus spp.	1		1	1	1		1		1							1		
Oxytoxum spp.	47	79	100	66	11	15	36	68	15	11	11	13	8	9	3	16	19	9
Podolampas spp.	1	8	6	14	9	6	2	7	11	1	3	3	1	3	4	2	3	2
Phalacroma spp.		1		1	1			1	28	1		1		1	1	3	1	
Prorocentrum spp.	7	46	8	57		3	21		17	2		4	10	3				13
Protoceratium spp.	1											9	3				6	
Protonotiluca spp.				1														
Protoperidinium spp.	5	9	7	7	3	2	8	3	11	4	2	6	2	3		1	4	7
Phaeocystis spp.			2															
Pterosperma spp.													1					
Pyrophacus spp.									2									
Pyrocystis spp.									1									
Scripsiella spp.	48	105	39	54	32	83	51	3	112	4			1	5	34		1	1
Takayama spp.				9									7				3	
Torodinium spp.													1					
> 20 um unidentified diatom spp.	11	55	6	2	5	3	7	19	12	49	45	26	9	26	89	58	38	194
10-20 unidentified diatom spp.	19	60	3	13		9	60	22	7714	51	85	19	35		79	19	35	66
> 20 um unidentified dinoflagellate spp.	30	62	8	7	30	35	10	30	158	23	19	29	8	10	23	4	14	23
10-20 unidentified dinoflagellate spp.	759	813	880	367	772	671	399	579	3913	294	130	250	120	82	158	136	405	449
> 20 um unidentified flagellate spp.	21	22	27	3	7	11	7	21	33	11	14	151	6	19	25	13	24	18
10-20 unidentified flagellate spp.	174	85	313	9	130	117	6	304	643	85	38	19	3	3	73	32	114	177
> 20 um unidentified spp.	18	22	45	1	13	19	5	19	213	46	20	37	17	32	28	17	30	77
10-20 unidentified spp.	209	313	142	57	203	203	63	66	2795	158	307	282	85	60	168	101	269	513

Appendix 4

Table 4.1 POC blank analysis at 2 m, 130 m (chlorophyll-a maximum) and 500 m. Double filters were used to assess the "DOC blank" – the bottom filter.

CTD	Top filter POC (µmol L^{-1})	Bottom filter POC (µmol L^{-1})	%
37 – 2 m	4.14	0.86	21
63 – 2 m 1	2.72	0.81	30
63 – 2 m 2	2.32	0.71	31
63 – 130 m 1	2.57	0.98	38
63 – 130 m 2	2.50	0.90	36
63 – 500 m 1	1.33	0.92	69
63 – 500 m 2	1.17	0.96	82

Table 4.2 Size-fractionated zooplankton group abundance and contribution of each group to total zooplankton abundance for each station. The last two columns are average and standard deviation of contribution of each group during RidgeMix.

		Abundance (individuals m^{-3})										% of total zooplankton abundance											
	Related CTD	**62**	**3**	**9**	**16**	**26**	**33**	**37**	**44**	**51**	**55**	**62**	**3**	**9**	**16**	**26**	**33**	**37**	**44**	**51**	**55**	**Av**	**Stdev**
200-500 um	Copepod	19.28	16.93	16.77	21.01	10.97	14.58	12.23	8.31	3.61	43.42	56	72	71	65	66	47	55	59	26	69	**59**	**14**
	Amphipod	0.00	0.00	0.16	0.00	0.00	0.00	0.00	0.00	0.00	0.00	0	0	1	0	0	0	0	0	0	0	**0**	**0**
	Appendicularian	1.41	0.00	0.00	1.57	0.08	2.04	0.31	0.00	0.00	1.25	4	0	0	5	0	7	1	0	0	2	**2**	**2**
	Chaetognath	0.00	0.16	0.00	1.25	0.08	0.00	0.00	0.47	0.31	0.16	0	1	0	4	0	0	0	3	2	0	**1**	**2**
	Cladoceran	0.00	0.16	2.82	0.63	1.10	0.31	0.78	0.94	0.00	0.00	0	1	12	2	7	1	4	7	0	0	**3**	**4**
	Foraminifera	1.10	0.63	0.00	0.47	0.39	0.63	0.00	0.00	0.31	2.04	3	3	0	1	2	2	0	0	2	3	**2**	**1**
	Isopod	0.00	0.00	0.00	0.00	0.00	0.00	0.00	0.00	0.00	0.00	0	0	0	0	0	0	0	0	0	0	**0**	**0**
	Jelly	7.99	1.72	0.47	4.55	0.94	2.51	1.88	0.00	6.90	8.78	23	7	2	14	6	8	9	0	50	14	**13**	**15**
	Larvae	0.00	1.57	0.31	0.00	0.24	0.94	1.57	0.31	0.00	0.78	0	7	1	0	1	3	7	2	0	1	**2**	**3**
	Ostracod	2.04	1.88	2.04	2.04	1.25	2.66	1.41	2.19	2.19	3.45	6	8	9	6	8	9	6	16	16	5	**9**	**4**
	Polychaete	0.31	0.00	0.16	0.00	0.24	0.31	0.00	0.16	0.00	0.16	1	0	1	0	1	1	0	1	0	0	**1**	**1**
	Pteropod	0.16	0.00	0.00	0.31	0.16	0.47	0.63	0.16	0.31	0.16	0	0	0	1	1	2	3	1	2	0	**1**	**1**
	Radiolarian	1.57	0.31	0.31	0.31	0.86	5.64	2.19	0.94	0.00	2.66	5	1	1	1	5	18	10	7	0	4	**5**	**6**
	Shell	0.31	0.16	0.47	0.16	0.39	0.47	0.94	0.63	0.16	0.31	1	1	2	0	2	2	4	4	1	0	**2**	**1**
	Shrimp-like	0.00	0.00	0.00	0.00	0.00	0.16	0.16	0.00	0.00	0.00	0	0	0	0	0	1	1	0	0	0	**0**	**0**
	Total zoop	34.17	23.51	23.51	32.29	16.69	30.72	22.10	14.11	13.79	63.17												
500-1000 um	Copepod	25.24	24.45	31.19	31.19	17.09	32.60	19.44	18.42	6.58	48.44	70	76	85	63	89	79	79	84	44	69	**74**	**13**
	Amphipod	0.16	0.31	0.24	0.16	0.08	0.00	0.00	0.08	0.31	0.16	0	1	1	0	0	0	0	0	2	0	**1**	**1**
	Appendicularian	0.78	0.00	0.08	1.72	0.00	0.94	0.63	0.00	0.16	1.41	2	0	0	3	0	2	3	0	1	2	**1**	**1**
	Chaetognath	0.00	0.00	0.00	1.41	0.16	0.63	0.47	0.08	0.78	2.04	0	0	0	3	1	2	2	0	5	3	**2**	**2**
	Cladoceran	0.00	0.00	0.71	0.31	0.00	0.00	0.00	0.08	0.00	0.00	0	0	2	1	0	0	0	0	0	0	**0**	**1**
	Foraminifera	0.16	0.00	0.00	0.16	0.00	0.00	0.16	0.00	0.00	0.00	0	0	0	0	0	0	1	0	0	0	**0**	**0**
	Isopod	0.00	0.00	0.00	0.00	0.00	0.16	0.00	0.00	0.16	0.00	0	0	0	0	0	0	0	0	1	0	**0**	**0**
	Jelly	4.86	1.88	1.49	10.35	1.10	3.29	1.57	1.18	5.17	12.38	13	6	4	21	6	8	6	5	35	18	**12**	**10**
	Larvae	0.00	0.94	0.00	0.31	0.00	0.31	0.31	0.00	0.16	0.94	0	3	0	1	0	1	1	0	1	1	**1**	**1**
	Ostracod	1.25	2.66	2.35	2.51	0.31	1.41	0.63	0.86	0.47	1.41	3	8	6	5	2	3	3	4	3	2	**4**	**2**
	Polychaete	0.16	0.16	0.16	0.16	0.31	0.47	1.25	0.31	0.16	0.31	0	0	0	0	2	1	5	1	1	0	**1**	**1**
	Pteropod	0.16	0.00	0.00	0.31	0.00	0.16	0.16	0.24	0.16	0.78	0	0	0	1	0	0	1	1	1	1	**1**	**0**

		Abundance (individuals m^{-3})										% of total zooplankton abundance											
	Related CTD	**62**	**3**	**9**	**16**	**26**	**33**	**37**	**44**	**51**	**55**	**62**	**3**	**9**	**16**	**26**	**33**	**37**	**44**	**51**	**55**	**Av**	**Stdev**
Continued…	Radiolarian	3.29	1.57	0.08	0.47	0.08	0.94	0.00	0.24	0.16	1.41	9	5	0	1	0	2	0	1	1	2	**2**	**3**
	Shell	0.16	0.31	0.16	0.16	0.08	0.00	0.00	0.16	0.63	0.47	0	1	0	0	0	0	0	1	4	1	**1**	**1**
	Shrimp-like	0.00	0.00	0.31	0.16	0.08	0.16	0.00	0.39	0.00	0.31	0	0	1	0	0	0	0	2	0	0	**0**	**1**
	Total zoop	**36.21**	**32.29**	**36.76**	**49.38**	**19.28**	**41.07**	**24.61**	**22.02**	**14.89**	**70.07**												
1000-2000 um	Copepod	4.78	3.76	6.82	4.23	2.27	4.78	1.02	1.88	1.65	6.43	59	66	69	33	52	66	34	69	32	42	**52**	**16**
	Amphipod	0.47	0.00	0.08	0.08	0.08	0.24	0.00	0.00	0.00	0.31	6	0	1	1	2	3	0	0	0	2	**1**	**2**
	Appendicularian	0.16	0.16	0.24	0.16	0.00	0.31	0.00	0.00	0.47	0.39	2	3	2	1	0	4	0	0	9	3	**2**	**3**
	Chaetognath	0.71	0.31	0.47	2.43	0.24	0.63	0.55	0.31	0.39	2.19	9	5	5	19	5	9	18	11	8	14	**10**	**5**
	Cladoceran	0.00	0.08	0.16	0.00	0.00	0.00	0.00	0.00	0.00	0.00	0	1	2	0	0	0	0	0	0	0	**0**	**1**
	Foraminifera	0.00	0.00	0.00	0.00	0.00	0.00	0.00	0.00	0.00	0.08	0	0	0	0	0	0	0	0	0	1	**0**	**0**
	Isopod	0.08	0.00	0.00	0.08	0.00	0.00	0.00	0.00	0.00	0.16	1	0	0	1	0	0	0	0	0	1	**0**	**0**
	Jelly	1.41	0.86	0.94	5.17	1.02	0.78	0.71	0.31	2.19	3.92	17	15	10	40	23	11	24	11	42	26	**22**	**12**
	Larvae	0.08	0.00	0.00	0.00	0.00	0.00	0.16	0.00	0.16	0.31	1	0	0	0	0	0	5	0	3	2	**1**	**2**
	Ostracod	0.08	0.16	0.16	0.31	0.08	0.08	0.08	0.00	0.24	0.39	1	3	2	2	2	1	3	0	5	3	**2**	**1**
	Polychaete	0.08	0.08	0.08	0.08	0.24	0.39	0.16	0.08	0.00	0.31	1	1	1	1	5	5	5	3	0	2	**2**	**2**
	Pteropod	0.08	0.08	0.31	0.08	0.31	0.08	0.00	0.08	0.08	0.08	1	1	3	1	7	1	0	3	2	1	**2**	**2**
	Radiolarian	0.08	0.08	0.00	0.00	0.00	0.00	0.00	0.00	0.00	0.08	1	1	0	0	0	0	0	0	0	1	**0**	**1**
	Shell	0.16	0.08	0.08	0.00	0.00	0.00	0.00	0.08	0.00	0.08	2	1	1	0	0	0	0	3	0	1	**1**	**1**
	Shrimp-like	0.00	0.08	0.55	0.31	0.16	0.00	0.31	0.00	0.00	0.63	0	1	6	2	4	0	11	0	0	4	**3**	**3**
	Total zoop	**8.15**	**5.72**	**9.88**	**12.93**	**4.39**	**7.29**	**2.98**	**2.74**	**5.17**	**15.36**												
>2000 um	Copepod	0.71	1.49	0.78	2.35	0.24	0.71	0.16	0.47	0.63	1.33	47	41	38	36	27	47	20	46	23	40	**37**	**10**
	Amphipod	0.24	0.31	0.16	0.00	0.00	0.00	0.00	0.00	0.00	0.08	16	9	8	0	0	0	0	0	0	2	**3**	**5**
	Appendicularian	0.00	0.00	0.00	0.00	0.00	0.16	0.00	0.16	0.00	0.08	0	0	0	0	0	11	0	15	0	2	**3**	**6**
	Chaetognath	0.16	0.71	0.31	1.72	0.39	0.08	0.31	0.00	0.39	0.55	11	20	15	26	45	5	40	0	14	16	**19**	**14**
	Cladoceran	0.00	0.00	0.00	0.00	0.00	0.00	0.00	0.00	0.00	0.00	0	0	0	0	0	0	0	0	0	0	**0**	**0**
	Foraminifera	0.00	0.00	0.00	0.00	0.00	0.00	0.00	0.00	0.00	0.00	0	0	0	0	0	0	0	0	0	0	**0**	**0**
	Isopod	0.08	0.16	0.16	0.00	0.00	0.00	0.00	0.00	0.00	0.08	5	4	8	0	0	0	0	0	0	2	**2**	**3**
	Jelly	0.16	0.55	0.39	2.12	0.08	0.47	0.16	0.16	1.18	1.18	11	15	19	32	9	32	20	15	43	35	**23**	**11**
	Larvae	0.08	0.00	0.00	0.24	0.08	0.00	0.00	0.00	0.31	0.00	5	0	0	4	9	0	0	0	11	0	**3**	**4**
	Ostracod	0.00	0.24	0.08	0.00	0.00	0.00	0.00	0.00	0.08	0.00	0	7	4	0	0	0	0	0	3	0	**1**	**2**

		Abundance (individuals m^{-3})										% of total zooplankton abundance											
	Related CTD	**62**	**3**	**9**	**16**	**26**	**33**	**37**	**44**	**51**	**55**	**62**	**3**	**9**	**16**	**26**	**33**	**37**	**44**	**51**	**55**	**Av**	**Stdev**
Continued…	Polychaete	0.00	0.00	0.08	0.08	0.00	0.08	0.16	0.08	0.08	0.00	0	0	4	1	0	5	20	8	3	0	**4**	**6**
	Pteropod	0.08	0.00	0.00	0.00	0.08	0.00	0.00	0.00	0.08	0.00	5	0	0	0	9	0	0	0	3	0	**2**	**3**
	Radiolarian	0.00	0.00	0.00	0.00	0.00	0.00	0.00	0.08	0.00	0.00	0	0	0	0	0	0	0	8	0	0	**1**	**2**
	Shell	0.00	0.00	0.00	0.00	0.00	0.00	0.00	0.00	0.00	0.00	0	0	0	0	0	0	0	0	0	0	**0**	**0**
	Shrimp-like	0.00	0.16	0.08	0.08	0.00	0.00	0.00	0.08	0.00	0.08	0	4	4	1	0	0	0	8	0	2	**2**	**3**
	Total zoop	**1.49**	**3.61**	**2.04**	**6.58**	**0.86**	**1.49**	**0.78**	**1.02**	**2.74**	**3.37**												

Table 4.3 To see lipid concentrations from the SAPs 0.7-53 µm and > 53 µm fractions over the ridge (CTD 20) and basin (CTD 51) see attached electronic appendix.

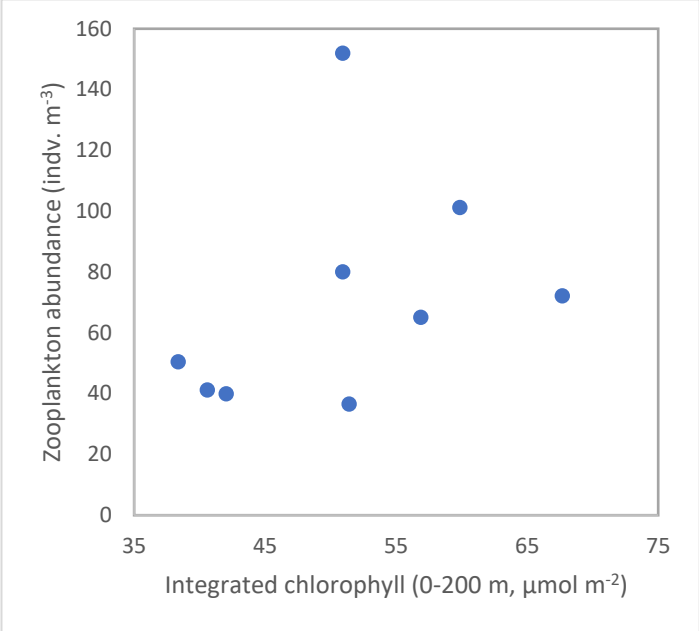

Figure 4.3 Integrated chlorophyll-a concentration against zooplankton abundance in the top 200 m of the water column.